DISSERTATION

Titel der Dissertation

„Grafted PLGA-Microparticles: Functionalization, Release Kinetics, and Epithelial/Endothelial Inter-action under Flow Conditions "

Verfasserin

Mag. pharm. Xue-Yan WANG

angestrebter akademischer Grad

Doktorin der Naturwissenschaften (Dr. rer. nat.)

Wien, 2014

To my parents,

Thank you for everything.

献给我的父亲母亲

Contents

Part I

PREFIX

AUTHORS CONTRIBUTIONS

I hereby declare that I have significantly contributed to the realization of the studies included in the present thesis.

For the publications *"Lectin-coated PLGA microparticles: Thermoresponsive release and in vitro evidence for enhanced cell interation*, International Journal of Pharmaceutics, 436:738-743, 2012" and *"Lectin-grafted PLGA microcarriers loaded with fluorescent model drugs: characteristics, release profiles and cytoadhesion studies*, Scientia Pharmaceutica, in press" [1.2.1 (i) (ii)] I designed and performed the experiments, analyzed and interpreted the data and wrote the manuscript.
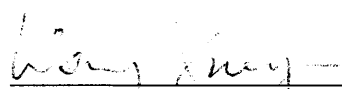
I conceived the experimental set-up, analyzed the data and authored the manuscript for *"Influence of stabilizers and preparation procedures on ligand density of PLGA-microparticles"* [1.2.2].

The review article "Use of lectin-functionalized *particles for oral immunotherapy*, Therapeutic Delivery, 3:277-290, 2012" [1.2.3] was written in collaboration with the other authors.

In case of the papers *"A multichannel acoustically driven microfluidic chip to study particle-cell interactions*, Biomicrofluidics, 7:044127, 2013" and *"A novel cell-based microfluidic multichannel setup – impact of hydrodynamics and surface characteristics on the bioadhesion of polystyrene microspheres*, Colloids and Surfaces B: Biointerfaces, 102:849-856, 2013" [2.2.1 (i) (ii)] I contributed to the study design, analyzed and interpreted the data and wrote the manuscripts.

Concerning the manuscripts *"Lectin-mediated biorecognition: Glycosylation pattern of human endothelial cells and blood cell-agglutinating effects of wheat germ agglutinin"* [2.2.2] and *"Permeation of nanoparticles across cell monolayers in vitro – Impact of growth support"* [2.2.3] I contributed to the design and elaboration of the chip set-up. Moreover, I planned and partially performed the experiments, analyzed and interpreted the data and contributed to writing the papers.

Vienna, March 2014

Xue Yan WANG

ABSTRACT

Nowadays, the potential use of micro- and nanoparticles for drug delivery purposes is intensively investigated. Different molecules can be loaded into particles by selected techniques and even the surface of the drug carriers can be structurally modified. This allows for prolonged residence time of micro- and nanoparticles in the circulation increasing bioavailability and can moreover facilitate targeting diseased cells and tissues specifically.

Accordingly, the first part of the present thesis deals with preparation parameters and their impact on microparticle characteristics. Experiments with biocompatible and biodegradable PLGA microparticles loaded with hydrophilic, amphotheric, or lipophilic fluorescent model drugs revealed that selection of the preparation technique, the size, the loading as well as the release profile is basically dependent on the lipophilicity of the matrix and the entrapped drugs. Matching lipophilicity yielded best results. Interestingly, only hydrophilic fluorescein-sodium as a payload was released in a thermo-responsive manner as indicated by < 0.23% cumulative release at 4°C as opposed to > 80% at 37°C after 48h. In terms of surface modification of particles for site-specific delivery, particles prepared in presence of the alternative stabilizer poly(ethylene-*alt*-maleic acid), which contains additional reactive carboxylic end groups, yielded the highest coupling rate of bioadhesive wheat germ agglutinin and consequently strongest interaction with Caco-2 cells as compared with particles prepared in presence of the commonly used stabilizers polyvinylalcohol and poloxamer 188 by solvent evaporation techniques. Furthermore, it is most likely that the hydrodynamic flow under physiological conditions and associated hydrodynamic forces will affect the interaction between particles and tissues. In the second part of present work, a multi-channel acoustically driven microfluidic system based on surface acoustic wave technology (SAW) was developed further in terms of parallelization. This device with four channels operated in parallel offered high reproducibility as well as versatility, and was further employed to mimic physiological conditions *in vitro*. As a proof-of-concept, the SAW-driven microfluidic device was applied to investigate the adhesion of positively and negatively charged polystyrene microspheres to endothelial and epithelial cell monolayers in the presence of hydrodynamic drag. Under flow conditions charge of 1 μm particles exerted negligible influence on epithelial and endothelial binding at average shear rates between 0.5 s^{-1} and 2.25 s^{-1} but biorecognitive lectin-particles yielded higher adhesion rates at the mean.

Moreover, as a step further towards lectin-mediated drug delivery for

parenteral administration, the glycosylation pattern of human endothelial cells of micro- and macrovascular origin before and after inflammation was elucidated by lectin screening. Wheat germ agglutinin (WGA) revealed the highest binding rates to endothelial monolayers especially in case of inflamed primary cells. Interestingly, up to a concentration of 15.88 µg mL^{-1} WGA exerted no agglutinating effects on blood cells. This finding represents a paradigm shift and will open new perspectives for glycotargeting in pharmaceutics.

Finally, transport studies of nanoparticles across artificial intestinal epithelia clearly demonstrated that commonly applied filter membranes as a growth support act as an additional barrier against particle transport and fluorophore leakage results in arbitrary higher transport rates. As a more reliable alternative, metal grids with a mesh width of 25 µm as a growth support and ultracentrifugation as a method for removal of free nanoparticle were proposed.

All in all, in this thesis some key parameters issues basically influencing the preparation techniques, surface functionalization, and endothelial as well as epithelial *in vitro* models have been elucidated and described in detail in an effort to extend the scope of applicability of targeted drug delivery systems.

Zusammenfassung

Derzeit stehen Mikro-und Nanopartikel als Drug Delivery Systeme im Mittelpunkt des Interesses von Forschung und Entwicklung im pharmazeutischen Bereich. Sie bieten viele Vorteile wie die Verfügbarkeit unterschiedlicher Herstellungstechniken und damit die Anpassungsfähigkeit an die Eigenschaften des Wirkstoffes. Darüber hinaus kann die Oberfläche der partikulären Wirkstoffträger strukturell modifiziert werden, sodass einerseits die Verweildauer der Mikro-und Nanopartikel im Körper verlängert und damit die Bioverfügbarkeit des Wirkstoffes erhöht wird. Andererseits können durch Strukturierung der Oberfläche mit biorekognitiven Liganden dem Partikel Eigenschaften verliehen werden, nur mit spezifischen Zelltypen und Zielgeweben zu interagieren, wodurch die Dosis und die Nebenwirkungsrate von Formulierungen gesenkt werden kann.

Der erste Teil der vorliegenden Arbeit beleuchtet Aspekte der Funktionalisierung von Mikropartikeln, die aus dem biokompatiblen und bioabbaubaren Polyester Poly (D,L-laktid-*co*-glykolid) hergestellt werden. Die Oberflächenmodifikation mit bioadhäsivem Weizenlektin bewirkt, dass im Gegensatz zum freien Arzneistoff erst der inkorporierte hydrophile Wirkstoff in Dünndarmzellen aufgenommen wird. Interessanterweise wird der hydrophile Modellarzneistoff nur bei Körpertemperatur freigesetzt. Andererseits steigt der erreichbare Beladungsgrad der Mikropartikel mit der Lipophilie des Wirkstoffes. Zusätzlich wird Poly (Ethylen-*alt*- Maleinsäure) (PEMA) als Stabilisator bei der Herstellung von Mikropartikeln vorgestellt, der im Gegensatz zu den etablierten Stabilisatoren eine wesentlich höhere Ligandendichte an der Partikeloberfläche ermöglicht. In einem Review wird die Anwendung von Lektin-modifizierten Mikrosphären zur Behandlung von Allergien beschrieben.

Der zweite Teil dieser Arbeit ist dem hydrodynamischen Fluss in Blutgefäßen und Dünndarm gewidmet, der die Wechselwirkung von Partikeln mit Zellen enorm beeinflusst, jedoch in der Literatur bisher kaum berücksichtigt wurde. Zur Simulation des Flusses wird ein mikrofluidisches, auf Oberflächen-akustischen Wellen basierendes und bereits etabliertes System in Richtung Parallelisierung weiterentwickelt. Interessanterweise üben Scherraten zwischen 0,5 s^{-1} und 2,25 s^{-1} keinen nenenswerten Einfluss auf die Adhäsion von negativ oder positiv geladenen Mikropartikeln aus. Weizenlektin-modifizierte Mikropartikel zeigen im bewegten system eine höhere Bindungsrate an artifizielles Dünndarmepithel. Zur Etablierung eines *in-vitro* Modelles für Blutgefäße werden erstmals Endothelzellen im mikrofluidisch bewegten System erfolgreich kultiviert, die Verträglichkeit mit Erythrozyten untersucht und ein für beide Zelltypen geeignetes

Puffersystem etabliert. Zusätzlich wird dieses Modell auf entzündetes Endothel erweitert. Obwohl nach derzeitigem Stand des Wissens die parenterale Applikation durch die Lektin-bedingte Agglutination von Erythrozyten ausgeschlossen wird, ist i.v.-Gabe dennoch denkbar, da <15,88 µg mL^{-1} Weizenlektin keine Haemagglutination auslösen. Schließlich zeigen Permeationsstudien von Nanopartikeln im zellbasierten *in-vitro* Modell, dass die Filterschicht des Systems eine stärkere Barriere darstellt als die Zellschicht. Als Alternative wird die Verwendung von Metallgittern mit einer Maschenweite von 25 µm vorgeschlagen. Zusätzlich wird darauf hingewiesen, dass markierte Partikel das Fluorophor freisetzen können und dadurch scheinbar höhere Transportraten bestimmt werden.

Insgesamt konnten im Rahmen der vorliegenden Dissertation wesentliche Beiträge zum Verständnis der Wechselwirkung zwischen Polymer und Wirkstoff, zwischen Partikeloberfläche und Ligand sowie zwischen Partikeln und Zellen sowohl unter statischen als auch dynamischen Bedingungen geleistet werden. Somit stehen weitere Bausteine zur Realisierung des Konzeptes von zielorientierten Arzneiformen zur Verfügung.

Part II

MAIN SECTION

INTRODUCTION

Nowadays, micro- and nanotechnology grows by leaps and bounds, undergoing explosive developments and delivering technological breakthroughs. The progress in this multidisciplinary research area creates a myriad of new opportunities in medical sciences, including diagnostics, drug delivery systems, and therapy regimens [1]. Considerable research efforts are focused on micro- and nanoparticles for administration as drug delivery systems. Using a proper technique, the drug of interest can be adsorbed, covalently linked or loaded into micro- and nanoparticles. Hence, the active pharmaceutical ingredient (API) is protected from enzymatic degradation (protease, nuclease), metabolism, and premature loss of activity on the way to the desired site of action [2, 3]. Furthermore, site-specific drug delivery is a broad and emerging field of application. For that purpose the surface of micro- and nanocarriers is grafted with certain ligands in order to specifically target diseased cells and tissues and/or to prolong the residence time of formulations [3-5]. A wide array of drug delivery systems has been developed for this applications such as liposomes, dendrimers, magnetic particles, ceramic carriers and polymeric particles [2, 3, 5, 6]. Among the polymeric carriers, biodegradable and biocompatible poly (D,L-lactide-*co*-glycolide) (PLGA) formulations are the most extensively studied as drug delivery systems, which are applied for sustained, targeted, and localized delivery of different agents [3, 7].

Thus, a focus of the present thesis is shedding some light on surface functionalized PLGA-microparticles for drug delivery. Since PLGA is currently the most attractive polymer for fabrication of various devices for drug delivery, at the beginning of this chapter a fundamental description of PLGA will summarize the characteristics, the preparation techniques of drug carriers, and the surface functionalization strategies as well as examples of various applications. *(1.1)*

In the specific section, the influence of hydrophilicity of model drugs on the properties of PLGA-microparticles such as size, stability, payload, release profile, and cytoadhesive properties will be described. For that purpose, three different fluorescent model drugs, representing hydrophilic, amphoteric and lipophilic APIs were prepared and their surface has been functionalized. *(1.2.1)*

Solvent evaporation technique is the most frequently used method to prepare PLGA-particles. However, stabilizers are inevitable necessary to yield particles that can counteract covalent surface functionalization of microcarriers [8-10]. Thus, the effect of traditional and newly introduced stabilizers on efficacy of covalent conjugation of ligands will be examined in comparison with microparticles prepared without

stabilizer. *(1.2.2)*

Regarding to the numerous applications of PLGA micro- and nanoparticles, biomimetic particulate vaccines represent a promising approach for the therapy of various immunologically mediated diseases [11]. Thus, in the last section of the first chapter, a review about oral immunotherapy will be presented. It focuses on the characteristics and advantages of polymeric PLGA-particles as well as the lectin-mediated improvement of intestinal uptake. *(1.2.3)*

Upon administration in humans, either perorally or parenterally, particles will interact in a different manner with the organism as opposed to conventional drug formulations. In particular, the hydrodynamic flow in the gastrointestine or circulation and the associated hydrodynamic forces will affect the interaction of particles with cells and tissues. Microfluidic systems represent a promising platform for studying the influence of hydrodynamics on the bioadhesive properties of particulate carriers. Therefore, the second aim of the present thesis is the investigation of particle-cell interactions under flow conditions. For this purpose, an acoustically-driven microfluidic system based on surface acoustic waves (SAW) has already been established in our group [12]. In the introductory section, fundamental knowledge about surface acoustic waves and its applications will be described. *(2.1)*

In the specific section, a multi-channel acoustically driven microfluidic platform will be further developed towards parallelization and is based on the formerly developed device. Furthermore, in order to mimic the circulatory system, human endothelial cells will be cultivated inside the microchannels of this device. Finally, a proof-of-concept will be presented by studying the adhesion of microspheres to endothelial monolayers under hydrodynamic conditions *(2.2.1 (i))*. In the subsequent section, the characteristics of electrostatic interactions between tissues and particles will be elucidated. Negatively charged polystyrene microparticles will be electrostatically coated with cationic polyelectrolyte. Since the membrane of mammalian cells is generally negatively charged [13], it is assumed that positively charged drug carriers strongly interact with cells. Using the multi-channel microfluidic device, the interaction between coated particles and intestinal epithelial cells will be investigated under hydrodynamic flow *(2.2.1 (ii))*.

The circulatory system might be simulated *in vitro* using the multi-channel microfluidic platform. As a first step to put this idea into practice, six fluorescein-labeled plant lectins with different carbohydrate specificity will be used to elucidate the glycosylation pattern of endothelial cells before and after inflammation. Moreover, in order to evaluate the possibility of the development of lectin-grafted

drug delivery carriers for parenteral administration, the effect of wheat germ agglutinin on agglutination of blood cells will be investigated. *(2.2.2)*

Most commonly filter membranes are used to investigate the permeation of novel drug carriers such as nano- and microparticles across cultivated cell layers. However, the properties of such transport systems (*e.g.* pore sizes, pore densities) might considerably influence the results. The last section of this thesis is focused on the estimation of the impact of commercially available filter membranes as growth supports for cell layers on the transport rates of particles. Finally, a set-up based on stainless steel grids is presented as a potential alternative to conventional filter materials. *(2.2.3)*

REFERENCES

[1] Sahoo SK, Parveen S, Panda JJ. The present and future of nanotechnology in human health care. *Nanomedicine.* **2007** 3(1):20-31.

[2] Sahoo SK, Labhasetwar V. Nanotech approaches to drug delivery and imaging. *Drug Discov Today.* **2003** 8(24):1112-20.

[3] Panyam J, Labhasetwar V. Biodegradable nanoparticles for drug and gene delivery to cells and tissue. *Adv Drug Deliv Rev.* 2003 55(3):329-47.

[4] Moghimi SM, Hunter AC, Murray JC. Long-circulating and target-specific nanoparticles: theory to practice. *Pharmacol Rev.* **2001** 53(2):283-318.

[5] Brigger I, Dubernet C, Couvreur P. Nanoparticles in cancer therapy and diagnosis. *Adv Drug Deliv Rev*. **2002** 54(5):631-51.

[6] Lamprecht A, Ubrich N, Yamamoto H, Schäfer U, Takeuchi H, Maincent P, Kawashima Y, Lehr CM. Biodegradable nanoparticles for targeted drug delivery in treatment of inflammatory bowel disease. *J Pharmacol Exp Ther.* **2001** 299(2):775-81.

[7] Ratzinger G, Fillafer C, Kerleta V, Wirth M, Gabor F, The role of surface functionalization in the design of PLGA micro- and nanoparticles, *Crit Rev Ther Drug.* **2010** 27(1):1-83.

[8] Ratzinger G, Länger U, Neutsch L, Pittner F, Wirth M, Gabor F. Surface modification of PLGA particles: the interplay between stabilizer, ligand size, and hydrophobic interactions. *Langmuir.* **2010** 26(3):1855-9.

[9] Keegan ME, Falcone JL, Leung TC, Saltzman WM. Biodegradable microspheres with enhanced capacity fo covalently bound surface ligands. *Macromolecules.* **2004** 37:9779-9784.

[10] McCarron PA, Marouf WM, Donnelly RF, Scott CJ. Enhanced surface attachment of protein-type targeting ligands to poly(lactide-co-glycolide) nanoparticles using variable express. *Biomed Mater Res.* **2008** 87(4):873–884.

[11] Keegan ME, Whittum-Hudson JA, Mark Saltzman W. Biomimetic design in microparticulate vaccines. *Biomaterials.* **2003** 24(24):4435-43.

[12] Fillafer C, Ratzinger G, Neumann J, Guttenberg Z, Dissauer S, Lichtscheidl IK, Wirth M, Gabor F, Schneider MF. An acoustically-driven biochip - impact of flow on the cell-association of targeted drug carriers. *Lab Chip.* **2009** 9(19):2782-8.

[13] Mehrishi JN, Bauer J. Electrophoresis of cells and the biological relevance of surface charge. *Electrophoresis.* **2002** 23(13):1984-94.

1

FUNCTIONALIZED PLGA-MICROPARTICLES FOR DRUG DELIVERY

1.1 BACKGROUND

Within the past two decades, poly(lactide-*co*-glycolide) (PLGA) emerged as one of the most successfully applied polymers to fabricate devices for drug delivery and tissue engineering purposes [1, 2]. Due to its attractive properties (Figure 1), PLGA has been extremely intensively investigated as delivery vehicles for drugs, proteins and various other macromolecules such as DNA, RNA and peptides [3-5].
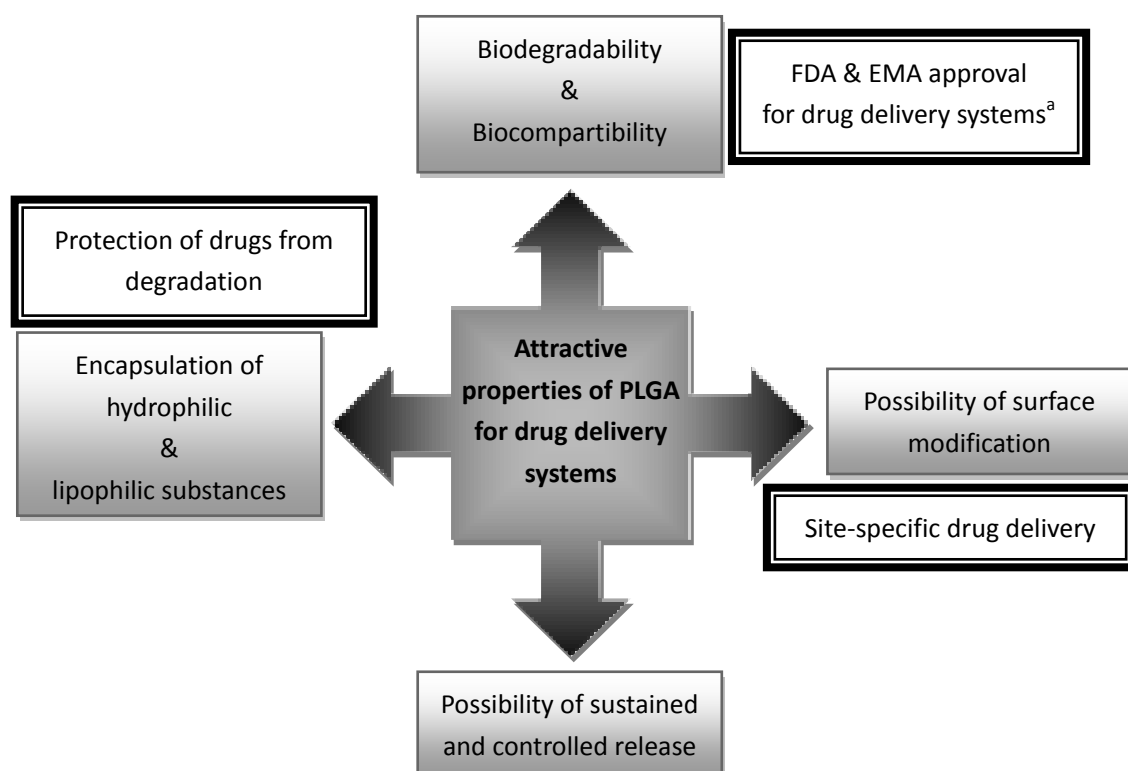
Figure 1. Attractive properties of PLGA for drug delivery systems [2] FDA: abbreviation for US Food and Drug Administration; EMA: abbreviation for European Medicines Agency.
[a] according to S. Nimesh. Gene Therapy: Potential Applications of Nanotechnology. Woodhead Pulishing Limited (UK). 2013.

Basic characteristics of PLGA

PLGA is a copolyester of lactic acid and glycolic acid (Figure 2). Due to the asymmetric α-carbon of lactide yielding a D- or L-stereomer, PLGA is correctly termed as poly(D,L-lactide-*co*-glycolide) [1]. The L-enantiomer of poly lactic acid is semicrystalline, whereas the mix of the D- and L-stereoisomers is completely amorphous due to disordered polymer chains. In comparison with lactide, the glycolide lacks one methyl group which increases hydrophilicity and crystallinity [6, 7]. At present, commercially available GMP-grades of PLGA are Medisorb®

(Alkermes, Cambridge, USA), Lactel® (Durect Corporation, AL, USA), Purasorb® (Purac resp. CSM, Netherland), and Resomer® (Evonik, Essen, Germany) [8]. The PLGA-copolymer is synthesized at large scale by ring-opening polymerization of the cyclic dimeric anhydrides with Zn or Zn-lactate as a catalyst [9]. When lactic acid is added to stop the polymerization process, uncapped PLGA (so-called "H-type") is yielded containing free carboxylic end groups [8]. This type of PLGA polymer is the basis for covalent or ionic surface modification of particulate delivery vehicles made from this polymer. A wide range of solvents can be used to dissolve PLGA, for instance, chlorinated solvents (*e.g.* dichloromethane), tetrahydofuran, acetone or ethyl acetate [10, 11]. Since the glass transition temperature of PLGA copolymers is slightly higher than the body temperature of 37°C, the polymer is in a hard and brittle state under physiological conditions and causes high mechanical strength of drug delivery vehicles [6, 12]. Furthermore, due to the influence of the molecular weight of PLGA-chains, the intrinsic viscosity related to the molecular weights is usually indicated in commercially available products [6]. PLGA shows a non-linear and dose-dependent profile in pharmacokinetics and biodistribution in humans [13]. Moreover, although mild local tissue reactions at the site of application can occur [14, 15], PLGA has been generally recognized as a safe polymer for macro-, micro- and nanoparticulate systems.

Figure 2. Metabolism and excretion of PLGA

Biodegradation of PLGA

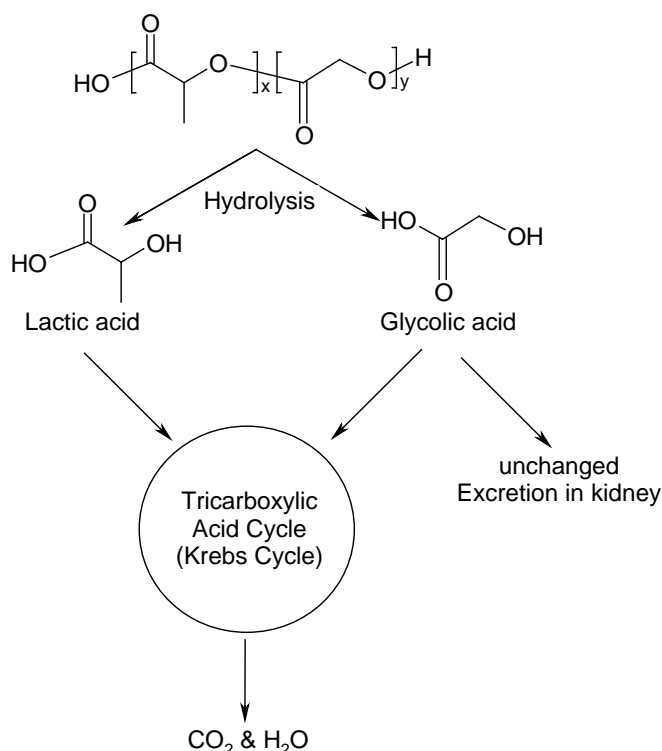In aqueous environment, swelling of the matrix is followed by degradation of PLGA. The backbone ester linkages of the copolymer are cleaved hydrolytically into oligomers, and finally into monomers [1, 6, 12, 16-18]. Consequently, this degradation process is termed hydrolytic degradation or biodegradation [19]. This biodegradation process can comprise surface diffusion, bulk diffusion, surface erosion and bulk erosion and has been discussed controversially [1].

Nowadays it is generally accepted that particles < 300 μm are degraded by homogenous or bulk degradation. Degradation of the matrix starts with adsorption of water at the surface and swelling of the matrix. Then a three-phase mechanism is proposed: (i) random chain scission of the polymer backbone resulting in decrease of the molecular weight of the polymer, however, without total weight loss and formation of soluble monomers; (ii) rapid loss of molecular weight of polymer chains and of total mass accompanied by formation of water-soluble oligomers and monomers of < 5200 Da, which is the beginning of erosion; (iii) further formation of water-soluble monomers from oligomeric fragments until the complete solubilization of polymers [20]. Such biodegradation process of PLGA polymer is mainly through bulk degradation at uniform rate [6, 18] with random hydrolytic chain scissions [21], as well as the autocatalytic effect of the carboxylic end groups formed during hydrolysis [6, 12]. The copolymer PLGA is degraded into its monomers lactic and glycolic acids [6, 12, 16]. Entering the tricarboxylic acid cycle, lactic acid is metabolized and finally eliminated as carbon dioxide and water from body [6, 7, 12, 16]. In contrast, glycolic acid can be eliminated unchanged via the kidneys or is oxidized to yield glyoxlic acid which can be further metabolized to yield serine, glycin or pyruvate (Figure 2) [6].

Several characteristics of the polymer can affect the biodegradation process of PLGA. The polymer composition, especially the molar ratio of the individual monomer components in the polymer chains, is the most important factor influencing the degradation rate. Since the amount and arrangement of glycolic acid blocks is a critical parameter determining the hydrophilicity of the matrix, generally the increase of glycolic blocks results in accelerated degradation of the copolymer [1]. For instance, PLGA 65:35 (lactide:glycolide) degrades faster than PLGA 75:25 and PLGA 85:15 [22]. Interestingly, an equimolar amount of monomers (PLGA 50:50) provokes the fastest degradation and increasing either the one or the other monomer results in delayed hydrolysis [12, 17]. Furthermore, the crystallinity of PLGA polymer affects the biodegradation rate, the mechanical strength, and the swelling behavior of copolymer. However, there are still contradictory reports about the influence on the degradation rate [23]. The average

molecular weight of PLGA copolymer is indicative for the polymer chain length, and directly affects the degradation rate. Generally, polymers of higher molecular weight composed of longer polymer chains exhibit a lower degradation rate [24]. Additionally, the shape of the matrix and the pH value of the aqueous environment also affect the biodegradation process of PLGA [1]. At this, a higher ratio of surface area to volume of the matrix corresponding to smaller particles and alkaline as well as strongly acidic media accelerate the polymer degradation [1, 25]. Interestingly, the role of enzymes in the biodegradation of PLGA is still controversially discussed. Although most of the literature reports that degradation of PLGA is solely by hydrolysis [5], differences of the degradation rates between *in vitro* and *in vivo* have been observed which suggests contribution of enzymes to degradation of PLGA in the body [12].

Preparation of functionalized PLGA particulate drug delivery systems

PLGA copolymer based particulate drug delivery systems can be fabricated by different techniques. Among these, three important basic methods are currently most popular, solvent evaporation techniques, phase separation (coacervation) methods and spray drying. In case of the solvent evaporation technique, the active pharmaceutical ingredient (API) is dissolved according to its hydrophilicity either in an organic solution of PLGA (single emulsion technique) or in an aqueous solution and emulsified in the organic PLGA phase (double emulsion technique). The organic solution or the water-in-oil emulsion is then emulsified in a high volume of outer aqueous phase, which results in the formation of an oil-in-water single emulsion or a water-in-oil-in-water double emulsion, respectively. Subsequently, the organic solvent is allowed to evaporate and the liquid droplets become denser and harden to yield finally solid particles. In contrast to solvent evaporation technique based on the solvent extraction, phase separation techniques are based on the addition of a non-solvent [4, 26]. After dispersing the drug in the PLGA-solution addition of the non-solvent reduces the solubility of the polymer resulting in formation of a coacervate at the interface [8]. Finally, spray drying technique is a rapid, convenient process suitable for the industrial upscaling and GMP-conform production [1]. At this, the API-containing PLGA-solution is atomized into a turbulent stream of warm air, the solvent of the liquid droplets is evaporated by the air stream and finally the dry particles are deposited by a cyclone and collected [19, 26].

The aim of targeted drug delivery, sometimes also termed as smart drug delivery, is to deliver APIs most exclusively to cells and tissues of interest [27, 28]. Thus, surface functionalization of PLGA particles by grafting with selected biorecognitive ligands for certain cell-associated

structural moieties is a most promising approach towards site specific drug delivery [8]. Considering the type of interaction two basic strategies of drug targeting are distinguished, passive and active targeting. In the case of passive targeting, the natural biodistribution pattern is utilized for selective accumulation of the drug delivery system at a certain region of the body [29]. For instance, the enhanced permeation and retention effect (EPR) relies on the increased capillary permeability in rapidly proliferating tumors or inflamed tissue. In case of active targeting, tissue or cell-specific accumulation of the carrier is due to specific biorecognitive interactions with the target-tissue. The soluble or solid drug-loaded carrier system is decorated with a ligand, the so-called "homing device", that guides the formulation to certain structures on the cell surface or tissue of interest and exclusively releases its payload at the desired site of action [28].

As mentioned above, uncapped PLGA of the "H-type" with free carboxylic acid groups at the end of polymer chains offers versatile opportunities for surface functionalization of particles. Covalent modification and surface coating via ionic interactions are the two most important pathways for stable surface functionalization. Furthermore, amphiphile molecules and proteins can be adsorbed on the surface of particulate drug carriers exploiting hydrophobic interactions with hydrophobic regions of PLGA, which is independent from the type of PLGA [8]. As carbodiimide coupling represents a versatile approach towards surface functionalization of PLGA nano- and microcarriers, this technique will be discussed in detail:

Carbodiimide Method

Carbodiimides are the most popular zero-length cross-linkers. They mediate the formation of amid linkages between carboxylic and primary amine groups or phosphoramidate linkages between phosphates and amines. However, due to the relatively weak nucleophilic characteristics of the PLGA-carboxylates in an aqueous medium, the successful conjugation via nucleophilic addition is sometimes limited. Upon reaction of carboxylic groups with N-substituted carbodiimides a highly active O-acylisourea intermediate is formed, which can further react with a nucleophile such as a primary amine to form a stable amide bond yielding isourea as a by-product (Figure 3). Considering the mild working conditions of this method within a pH range of 4.5 to 7.5 is most favorable for sensitive ligands such as proteins, peptides and easily degradable molecules. The water-soluble 1-ethyl-3-(3-dimethylaminopropyl) carbodiimide (EDAC) is the one of the most popular carbodiimides. However, there are several disadvantages of using only EDAC for coupling. Firstly, the EDAC-solution must be prepared freshly and used immediately to
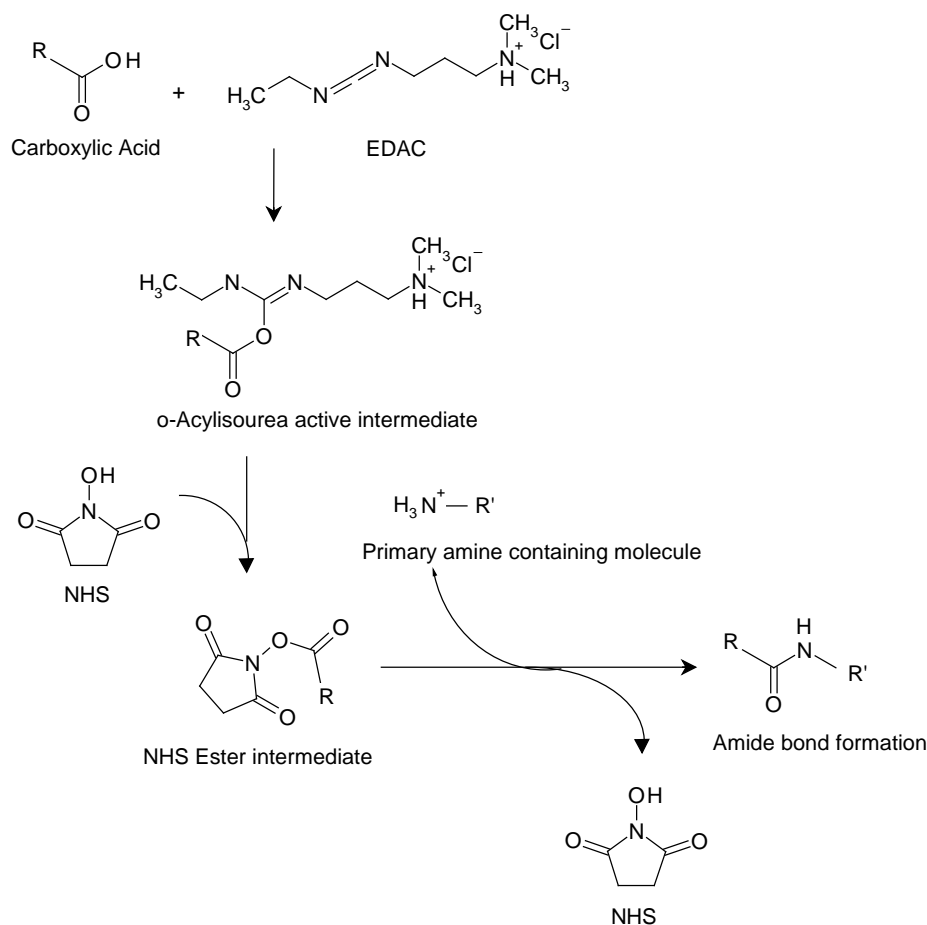
Figure 3. Reaction scheme of the carbodiimide method using EDAC and NHS

prevent extensive loss of activity. Secondly, the active intermediate O-acylisourea is rapidly hydrolyzed in aqueous environment. To overcome these pitfalls, EDAC is combined with N-Hydroxysuccinimide (NHS) or water-soluble N-Hydroxysulfosuccinimide (sulfo-NHS). The hydroxyl group of NHS or sulfo-NHS can easily react with the active-ester to form a more stable NHS-ester intermediate with a longer half-life in the range of some hours. This intermediate preferably reacts with amines than with hydroxyls and improves the coupling efficiency (Figure 3). Furthermore, due to the enhanced stability of intermediate, the reaction can be done in two-steps: The first step comprises the activation of carboxylic groups of PLGA by EDAC/NHS, and during the second step a stable amide bond is generated with primary amine groups of the ligands. Most importantly and advantageously, between the two steps excess of reagent can be removed by dialysis, centrifugation or size exclusion chromatography. This multi-step procedure helps to prevent cross-linking of proteins, which usually occurs in a one-step procedure when the reactants contain both, carboxylic and primary amine groups [30]. Alternatively,

when the ligand of interest contains no functional groups for coupling with the carboxylic groups of PLGA, the latter might be modified with spacers such as diamines, polyamines or dihydrazides [31]. Such spacers not only make covalent linkage possible but also accessibility of cell-bound targets and thus bioactivity might be improved due to antennary exposure of the ligand. Additionally, the ligand density might be improved by using homofunctional branched spacers with multiple binding sites. [8].

Applications of PLGA-particles

Due to the numerous advantages of PLGA, nano- and microparticles made thereof have been intensively investigated for drug delivery purposes in various biomedical areas, such as vaccination, cancer, inflammation, cardiovascular diseases, infectious diseases and others [2]. Besides the research activities focused on such new delivery vehicles in lab scale, several pharmaceuticals based on PLGA-particles are already available on the market to date (Table 1) [8, 26].

In terms of drug targeting via functionalized PLGA drug carriers, the lectin-mediated biorecognition is an attractive concept to achieve a site-specific delivery. H.J. Gabius defines a lectin as a (glycol)protein different from immunoglobulins which bind carbohydrate, however do not biochemically modify the sugar structure [32]. The concept of lectin-mediated drug targeting exploits the specificity of protein-sugar interactions. The target of "glycotargeting" is the highly glycosylated dense layer coating the outer surface of all mammalian cells, the so-called glycocalyx [33]. It contains a myriad of different glycans as binding sites for lectins [34]. H.J. Gabius called the diversity of glycosylation as "sugar code", encoding biological information in 1.44×10^{15} different hexasacchrides [35]. Since the glycocalxy varies between species, biological organizations, and also between different tissue and cell types as well as even healthy and diseased tissue within the same organism [33], certain lectins can target specifically different biological sites. Moreover, the binding of some lectins to carbohydrate-containing receptors at the cell surface can trigger vesicular transport processes such as clathrin or caveolin-mediated endocytosis which mediate uptake of lectin-decorated drug delivery carriers into the cell and sometimes exocytosis at the basolateral face so that the delivery system can even cross polarized epithelial cells [34].

Among the numerous common known plant lectins, wheat germ agglutinin (WGA) from *Triticum vulgare* (also known as *T.aestivum*) is a very attractive candidate as a vehicle for lectin-mediated drug targeting approaches, especially for peroral administration. WGA is a dimeric protein with two identical subunits of 171 amino acid residues and

contains four repetitive hevein domains comprising a sequence of 43 amino acids which function as binding pockets for carbohydrates. WGA can specifically bind to sialic acid and N-acetylglucosamine of the glycocaylx on the cell surfaces and its binding site can be inhibited by the competitive carbohydrate N-acetylchitotriose [36]. Interestingly, the glycosylated extracellular domain 3 of the epidermal growth factor (EGF) receptor is involved in WGA-binding. Due to the up-regulated expression of EGF-receptors in some tumors, this approach might also be applicable in cancer therapy. The cellular uptake of WGA is an active energy-dependent process. At 4°C, the lectin only binds to the cell surface, while at 37°C lectin binding to the cell surface is followed by internalization. It is suggested that at least 60% of WGA enter the lysosomal degradative pathway after uptake by the cells [37].

Table 1. Approved pharmaceuticals available on the market. Data are modified from [8, 25]. Most of the pharmaceuticals are marketed as powders for reconstitution and suspension i.v. administration.
 # available as periodontal insert.
* indicates drug formulations available in Austria according to the database of the Austrian Agency for Health and Food Safety (AGES) https://aspregister.basg.gv.at/aspregister/.

	Active pharmaceutical ingredient (API)	Marketed product	Company	Application
Peptides and Proteins	Buserelin acetate	Suprecur® Depot*	Sanofi-Aventis	Endometriosis
	Lanreotide acetate	Somatuline® -Depot, -LA*	Ipsen Pharma	Acromegaly
	Leuprolide acetate	Lupron Depot® , Depot-PED®	AbbVie	Endometriosis, Prostate cancer, Fibroids, Center precocious puberty
		Lutrate ®Depot*	GP Pharm	Prostate cancer
		Enantone®*	Takeda	Prostate cancer, Center precocious puberty
	Octreotide acetate	Sandostatin LAR®*	Novartis Pharma	Acromegaly
	Somatropin (rDNA origin)	Nutropin AQ®	Genentech	Pediatric growth hormone deficiency
	Triptorelin acetate	Gonapeptyl Depot®	Ferring	Prostate cancer
		Decapeptyl Depot®*	FERRING	Endometriosis, Prostate cancer, Center precocious puberty
	Triptorelin embonate	Moapar®	Debiopharm	Prostate cancer Prostate cancer; severe sexual deviation (e.g. paedophilia)
	Triptorelin pamoate	Pamorelin LA®* Trelstar®	Ipsen Pharma Actavis	Prostate cancer Prostate cancer
Small Molecules	Minocycline hydrochloride	Arestin®*#	OraPharma	Periodontal disease peridontal insert
	Naltrexone	Vivitrol®	Alkermes	Alcohol dependence
	Risperidone	Risperdal Consta®*	HaematoPharm, Janssen-Cilag	Antipsychotic

REFERENCES

[1] Makadia HK, Siegel SJ. Poly Lactic-co-Glycolic Acid (PLGA) as Biodegradable Controlled Drug Delivery Carrier. *Polymers (Basel).* **2011** 3:1377-1397.

[2] Danhier F, Ansorena E, Silva JM, Coco R, Le Breton A, Préat V. PLGA-based nanoparticles: an overview of biomedical applications. *J Control Release.* **2012** 161:505-522.

[3] Bouissou C, Rouse JJ, Price R, van der Walle CF. The influence of surfactant on PLGA microsphere glass transition and water sorption: Remodeling the surface morphology to attenuate the burst release. *Pharm Res*. **2006** 23:1295–1305.

[4] Jain RA. The manufacturing techniques of various drug loaded biodegradable poly(lactide coglycolide) (PLGA) devices. *Biomaterials.* **2000** 21:2475–2490.

[5] Ruhe PQ, Hedberg EL, Padron NT, Spauwen PH, Jansen JA, Mikos AG. rhBMP-2 release from injectable poly (DL-lactic-co-glycolic acid)/calcium-phosphate cement composites. *J Bone Jt Surg.* **2003** 85:75–81.

[6] Wu XS. Synthesis and properties of biodegradable lactic/glycolic acid polymers. In: Wise et al., editors. Encyclopedic Handbook of Biomaterials and Bioengineering. New York: Marcel Dekker, **1995.** p. 1015-1054.

[7] Tice TR, Cowsar DR. Biodegradable controlled-release parenteral systems. *Pharm Technol* **1984** 11:26-35.

[8] Ratzinger G, Fillafer C, Kerleta V, Wirth M, Gabor F, The role of surface functionalization in the design of PLGA micro- and nanoparticles, *Crit Rev Ther Drug.* **2010** 27:1-83.

[9] Gilding DK, Reed AM. Biodegradable polymers for use in surgery: polyglycolic/poly(lactic acid) homo- and copolymers. *Polymer.* **1979** 20:137–143.

[10] Uhrich KE, Cannizzaro SM, Langer RS, Shakesheff KM. Polymeric systems for controlled drug release. *Chem Rev.* **1999** 99:3181–3198.

[11] Wu XS, Wang N. Synthesis, characterization, biodegradation, and drug delivery application of biodegradable lactic/glycolic acid polymers. Part II: Biodegradation. *J Biomater Sci Polym Ed.* **2001** 12:21–34.

[12] Lewis DH. Controlled release of bioactive agents from lactide/glycolide polymers. In: Chasin M, Langer R, editors. Biodegradable polymers as drug delivery systems. New York: Marcel Dekker, **1990.** p. 1-41.

[13] Yang YY, Chung TS, Ng NP. Morphology, drug distribution, and in vitro release profiles of biodegradable polymeric microspheres containing protein fabricated by double-emulsion solvent extraction/evaporation method. *Biomaterials.* **2001** 22:231–241.

[14] Dailey L, Jekel N, Fink L, Gessler T, Schmehl T, Wittmar M, Kissel T, Seeger W.

Investigation of the proinflammatory potential of biodegradable nanoparticle drug delivery systems in the lung. *Toxicol Appl Pharmacol.* **2006** 215:100–108.

[15] Sundback CA, Shyu JY, Wang Y, Faquin WC, Langer RS, Vacanti JP, Hadlock TA. Biocompatibility analysis of poly(glycerol sebacate) as a nerve guide material. *Biomaterials.* **2005** 26:5454–5464.

[16] Jalil R, Nixon JR. Biodegradable poly(lactic acid) and poly(lactide-*co*-glycolide) microcapsules: problems associated with preparative techniques and release properties. *J Microencapsulation* **1990** 7:297-325.

[17] Kitchell JP, Wise DL. Poly(lactic/glycolic acid) biodegradable drug-polymermatrix systems. *Methods Enzymol* **1985** 112:436-448.

[18] Cohen S, Alonso MJ, Langer R. Novel approaches to controlledrelease antigen delivery. *Int J Technol Assessment Health Care* **1994** 10:121-30.

[19] Jain RA. The manufacturing techniques of various drug loaded biodegradable poly(lactide-co-glycolide) (PLGA) devices. *Biomaterials.* **2000** 21:2475-2490.

[20] Raghuvanshi RS, Singh M, Talwar GP. Biodegradable delivery system for single step immunization with tetanus toxoid. *Int J Pharm* **1993** 93:R1-5.

[21] Thies C, Bissery MC. Biodegradable microspheres for parenteral administration. In: Lim F, editor. Biomedical applications of microencapsulation. Boca Raton, FL: CRC Press, **1984.** p. 53-74.

[22] Park TG. Degradation of poly(lactic- co-glycolic acid) microspheres: Effect of copolymer composition. *Biomaterials.* **1995** 16:1123–1130.

[23] Alexis F. Factors affecting the degradation and drug-release mechanism of poly (lactic acid) and poly [(lactic acid)-co-(glycolic acid)]. *Polym Int.* **2005** 54:36–46.

[24] Park TG. Degradation of poly (D,L-lactic acid) microspheres: Effect of molecular weight. *J Control Release.* **1994** 30:161–173.

[25] Holy C. In vitro degradation of a novel poly(lactide-co-glycolide) 75/25 foam. *Biomaterials.* **1999** 20:1177–1185.

[26] Mundargi RC, Babu VR, Rangaswamy V, Patel P, Aminabhavi TM. Nano/micro technologies for delivering macromolecular therapeutics using poly (D,L-lactide-co-glycolide) and its derivatives. *J. Control. Rel.* **2008** 125:193 – 209.

[27] Couvreur P, Vauthier C. Nanotechnology: Intelligent design to treat complex disease, *Pharmaceutical Research.* **2006** 23:1417 – 1450.

[28] Sahoo SK, Labhasetwar V. Nanotech approaches to drug delivery and imaging, *Drug Discovery Today.* **2003** 8:1112 – 1120.

[29] Davis SS. Biomedical applications of nanotechnology--implications for drug targeting and gene therapy. *Trends Biotechnol.* **1997** 15:217-24.

[30] Hermanson GT. Bioconjugate Techniques. Academic Press, San Diego, 1996.

[31] Sharon JL, Puleo DA. The use of n-terminal immobilization of pth(1-34) on plga to enhance bioactivity. *Biomaterials.* **2008** 29:3137–3142.

[32] Rüdiger H, Gabius HJ. Plant lectins: occurrence, biochemistry, functions and applications. *Gyconj J.* **2001** 18: 589-613.

[33] Gagneux P, Varki A. Evolutionary considerations in relating oligosaccharide diversity to biological function, *Glycobiology.* **1999** 9: 747-755.

[34] Bies C, Lehr CM, Woodley JF. Lectin-mediated drug targeting: history and applications. *Adv Drug Deliv Rev.* **2004** 56:425-435.

[35] Gabius HJ. Biological information transfer beyond the genetic code: the sugar code, *Naturwissenschaften.* **2000** 87: 108-121.

[36] Van Damme EJM, Peumans WJ, Pusztai A, Bardocz S. Handbook of plant lectins: properties and biomedical applications. 1st ed. Chichester (UK): John Wiley & Sons. **1997.**

[37] Gabor F, Wirth M. Lectin-mediated drug delivery: fundamentals and perspectives, *STP. Pharma. Sciences.* **2003** 13: 3-16.

1.2 SPECIFIC TOPICS

1.2.1 Encapsulation of hydrophilic and lipophilic model drugs

Lectin-coated PLGA microparticles: Thermoresponsive release and *in vitro* evidence for enhanced cell interation

Xue-Yan Wang, Romana Koller, Michael Wirth, Franz Gabor

Faculty of Life Sciences, Department of Pharmaceutical Technology and Biopharmaceutics, University of Vienna, Vienna A-1090, Austria

1. FUNCTIONALIZED PLGA-MICROPARTICLES FOR DRUG DELIVERY

Contents lists available at SciVerse ScienceDirect

International Journal of Pharmaceutics

journal homepage: www.elsevier.com/locate/ijpharm

Lectin-coated PLGA microparticles: Thermoresponsive release and in vitro evidence for enhanced cell interaction

Xue-Yan Wang, Romana Koller, Michael Wirth, Franz Gabor *

Department of Pharmaceutical Technology and Biopharmaceutics, University of Vienna, Vienna, Austria

ARTICLE INFO

ABSTRACT

PLGA-microparticles with 4.7 μm in diameter were prepared by the double emulsion technique and loaded with 1.7 μg fluorescein/mg PLGA mimicking a hydrophilic API. In an effort to further elucidate the release and bioadhesive characteristics of lectin-grafted formulations in vitro, the particles were coated with wheat germ agglutinin. The microparticles exhibited thermo-responsive release since no free fluorescein was detected at 4 °C or room temperature. At body temperature, however, more than 80% of the payload was released within 48 h. The adhesion of lectin-grafted particles to Caco-2 monolayers, which were applied as a model for the human intestinal epithelium, exceeded that of plain ones 1.5-fold as also observed by fluorescence microscopy. Furthermore, the amount of model drug bound and taken up into the cells was 5.8-fold higher after incubation for 4 h at 37 °C as compared to fluorescein in solution. According to fluorescence imaging a considerable amount of the total fluorescein payload was accumulated intracellularily after incubation for 5 h at 37 °C. These findings not only confirm the utility of bioadhesives of the second generation for improved absorption of low molecular weight hydrophilic compounds but also indicate storage stability of such suspensions at 4 °C and room temperature without any premature loss of API.

1. Introduction

Nowadays, particulate formulations are intensively investigated as drug delivery systems. They offer lots of advantages such as feasibility of encapsulation of different drugs especially sensitive APIs, sustained drug delivery from the particle matrix, and protection of the payload against unfavorable conditions in the body. Among the polymers in use, Poly (lactic-*co*-glycolic acid) (PLGA) is most popular because it is biodegradable and biocompatible and generally recognized as safe by the FDA (Anon., 2012). In order to develop long-term active formulations, in which sensitive drugs could be delivered to their target without degradation, a variety of APIs has been encapsulated into PLGA micro- and nanoparticles (Mundargi et al., 2008), for example, recombinant human growth factor (Rafi et al., 2010), swine insulin (Bao et al., 2006), recombinant glycosylated glial cell-line derived neurotrophic factor (Garbayo et al., 2008), and HIV peptides (Manocha et al., 2005). One of the methods most commonly used to encapsulate hydrophilic drugs within particles is the water/oil/water or double emulsion technique based

on solvent evaporation (Ye et al., 2010). Since the release profile of the payload depends on the degradation characteristics of the polymer and the particle size, microspheres offer the advantage of sustained release kinetics and higher payload (Florence, 2005). In order to transport drugs as close as possible to the site of action, microcarriers can be targeted with different ligands. In particular, the lectin-mediated targeting is well known as a variant of the bioadhesion concept, which is not only applicable for gastrointestinal targeting, but also for other biological barriers (Bies et al., 2004; Wirth et al., 2002). Among these sugar-binding proteins, wheat germ agglutinin (WGA) from *Triticum vulgare*, which specifically binds to sialic acid and N-acetyl-D-glucosamine, possesses cytoadhesive and cytoinvasive characteristics. Furthermore, due to WGA-mediated biorecognition of the glycosylated structures in the intestine, we have already published several drug delivery systems grafted with WGA for GI-targeting (Ratzinger et al., 2010a, 2010b; Roth-Walter et al., 2005; Weissenböck et al., 2004).

The aim of the present work was to develop a WGA-targeted PLGA microparticulate delivery system loaded with fluorescein sodium as a model drug. Fluorescein sodium was chosen because of its excellent water solubility, low molecular weight and fluorescent properties facilitating detection. Lectin was immobilized to the surface of PLGA microparticles using the carbodiimid method. As already reported by Keegan's group, PLGA particles are usually prepared by solvent evaporation using polyvinylalcohol (PVA)

 * Corresponding author at: Department of Pharmaceutical Technology and Biopharmaceutics, University of Vienna, Althanstraße 14, 1090 Vienna, Austria.
Tel.: +43 1 4277 55406; fax: +43 1 4277 9554.
 E-mail address: franz.gabor@univie.ac.at (F. Gabor).

as stabilizer. Despite thoroughly washing, however, the PVA still resides on the surface of particles and leads to decreased ligand coupling efficiency (Keegan et al., 2006). Therefore, poly(ethylene-alt-maleic acid) (PEMA) was applied as a new stabilizer during the preparation process because its carboxylate groups can increase the coupling rate (Keegan et al., 2004). The resulting particulate drug delivery system was examined in terms of particle size, stability, payload, and release profile of encapsulated fluorescein sodium. In order to elucidate the impact of the bioadhesive coating, assays were performed using Caco-2 monolayers which represent a well-established model of the human intestinal epithelium. Besides imaging techniques quantitative protocols such as pulse-chase incubations were pursued to simulate the situation in the human intestine. Moreover, the characteristics of the microspheres were compared with an aqueous solution of free model drug to figure out the advantages of the bioadhesive microparticles.

2. Materials and methods

2.1. Materials

PLGA (poly(D,L-lactide-co-glycolide), Resomer RG503H, 50:50 lactide/glycolide) was obtained from Boehringer Ingelheim (Ingelheim, Germany). Poly (ethylene-*alt*-maleic anhydride) (PEMA) and fluorescein sodium were bought from Sigma Aldrich (Vienna, Austria). Wheat germ agglutinin (WGA) from *T. vulgare* was purchased from Vector Laboratories (Burlingame, USA). Hoechst 33342 trihydrochloride trihydrate was obtained from Invitrogen (Vienna, Austria). All other chemicals used were of analytical purity.

2.2. Preparation of fluorescein-loaded PLGA microparticles

Fluorescein loaded PLGA microparticles were prepared by a water-in-oil-in-water solvent-evaporation technique. 400 μL aqueous solution of fluorescein sodium (7.5 mg/mL) were emulsified with a solution containing 400 mg PLGA in 2.4 g ethyl acetate by sonication for 2 min (sonifier: Bandelin electronic UW70/HD70; tip: MS 72/D; Berlin, Germany). After adding 8 mL of a 0.5% aqueous solution of PEMA the emulsion was sonicated again for 2 min yielding the (w/o)/w emulsion which was poured into 100 mL of a 0.25% aqueous solution of PEMA. After mechanical stirring at 600 rpm for 1 h at room temperature, residual ethyl acetate was removed under reduced pressure. In order to remove non-encapsulated fluorescein sodium, the microparticles were washed three times with 120 mL 20 mM HEPES/NaOH-buffer pH 7.0. Finally the particles were resuspended in 100 mL of the same buffer. The PLGA content of lyophilized aliquots was determined gravimetrically after dialysis against distilled water. The particle size distribution was determined using a Malvern Mastersizer 2000 laser particle size analyzer (Malvern Instruments, Malvern, UK).

2.3. Preparation of wheat germ agglutinin functionalized microparticles

WGA was covalently coupled to the carboxylate-groups at the surface of PLGA microparticles according to a modified carbodiimide method (Ertl et al., 2000). Briefly, 5 mL of the PLGA microparticles suspension in 20 mM HEPES/NaOH-buffer pH 7.0 containing 0.1% Pluronic® F-68 were activated by adding 5 mL of a freshly prepared solution containing 1-ethyl-3(3-dimethylaminopropyl) carbodiimide (EDAC, 1400 mg) and N-hydroxysuccinimide (NHS, 59 mg) in the same buffer. After end-over-end incubation for 30 min at room temperature the microparticles were washed by dilution with 15 mL 20 mM HEPES/NaOH-buffer pH 7.4 containing 0.1% Pluronic® F-68 and centrifugation (3200 rpm, 10 min, 4 °C) to remove the excess reagents.

After resuspending the microparticles in 10 mL of the same buffer 500 μL of an aqueous solution of WGA (5 mg/mL) were added followed by end-over-end incubation for 1 h at room temperature. Unreacted binding sites were saturated by incubation with 2.4 mL glycine solution (100 mg/mL in buffer) for 30 min at room temperature. Subsequently, the microparticles were washed twice by centrifugation (3200 rpm, 10 min, 4 °C) with 15 mL buffer each as above. Finally, the particles were resuspended in 10 mL buffer and stored at −80 °C until use. As a reference, plain PLGA microparticles were treated as above but adding solely buffer instead of the EDAC, NHS, WGA and glycine.

2.4. Determination of the fluorescein sodium content of the microparticles

Aliquots (300 μL) of the microparticle suspensions were hydrolyzed by addition of 100 μL 4 M NaOH in triplicate. The fluorescein content of 100 μL aliquots was determined in 96-well plates at 485/525 nm (exc./em.) using a fluorescence microplate reader (Infinite M200, Tecan, Grödig, Austria). The amount of encapsulated label was calculated from a calibration curve established with fluorescein sodium in 1 M NaOH.

2.5. Release of the fluorescein sodium from the microparticles

To assess the release of encapsulated fluorescein sodium, 500 μL suspension containing either plain or surface modified particles were incubated with 20 mM HEPES/NaOH-buffer pH 7.4 containing 0.1% Pluronic® F-68 at 4 °C, 37 °C, and room temperature. At certain time intervals, the respective supernatants were collected by centrifugation (14,000 rpm, 5 min, 4 °C) and the amount of liberated fluorescein sodium was determined in each sample fluorimetrically at 485/525 nm. Finally, the percentage of the released fluorescein was calculated with reference to the encapsulated fluorescein content.

2.6. Cell culture

Caco-2 cells were purchased from the German collection of microorganisms and cell culture (DSMZ, Braunschweig, Germany). Cells were cultivated in RPMI 1640 cell culture medium containing 10% fetal calf serum, 4 mM L-glutamine and 150 mg/mL gentamycine in a humidified 5% CO_2/95% air atmosphere at 37 °C and were subcultured by TrypLE® select. Tissue culture reagents were obtained from Sigma Aldrich (St. Louis, USA) and Gibco Life Technologies Ltd. (Invitrogen Corp., Carlsbad, USA). Cells between passage 63 and 73 were used for the present study. For cell experiments following a pulse-chase protocol and fluorescence microscopy, 1.7×10^4 Caco-2 single cells were seeded per well using 96-well microplates or glass cover slips combined with the flexiPERM micro 12 system, respectively. Cells were cultivated under standard cell culture conditions until a confluent monolayer has been formed.

2.7. Pulse-chase studies of the particle–cell interaction and comparison with free fluorescein in aqueous solution

In order to evaluate the particle–cell interactions, fluorescein loaded microparticles were incubated with Caco-2 monolayers under different conditions following a pulse-chase protocol. At this, the microparticle suspension was diluted with isotonic 20 mM HEPES/NaOH-buffer pH 7.4 to yield a concentration of 200 μg particles/mL. For comparison, a solution of fluorescein in the same buffer containing equal amounts to that of the microparticles was applied (0.35 μg/mL). After washing confluent Caco-2 monolayers with isotonic 20 mM HEPES/NaOH-buffer pH 7.4 (100 μL/well), the

cells were incubated with 100 μL/well of the microparticle suspension or the aqueous fluorescein solution for 30 min at 4 °C and 37 °C, respectively (pulse phase). After removal of unbound microparticles or free fluorescein by washing twice with 100 μL 20 mM HEPES/NaOH-buffer pH 7.4, the relative cell-associated fluorescence intensity was determined at 485/525 nm. Subsequently, the cell layers were incubated up to 4 h at 37 °C (chase phase), followed by a further washing step as above. Again, the relative fluorescence intensities were determined before and after this final washing step at 485/525 nm.

2.8. Fluorescence microscopy

Caco-2 monolayers grown on glass cover slips in the flex-iPERM micro 12 system were used for fluorescence microscopy. After removing the cell culture medium, the nuclei of the living cells were stained by incubation with Hoechst 33342 (5 μg/mL RPMI medium; 50 μL/well) for 30 min at 37 °C. Excessive dye was removed by washing the monolayers twice with 100 μL isotonic 20 mM HEPES/NaOH-buffer pH 7.4 each. After incubation with 100 μL microparticle suspension (200 μg/mL isotonic 20 mM HEPES/NaOH-buffer pH 7.4) at 37 °C for 1, 3 and 5 h, respectively, the Caco-2 layers were washed with 100 μL isotonic 20 mM HEPES/NaOH-buffer pH 7.4 to remove any unbound particles and fluorescein released into the supernatant. Without any further preparation images of the cell layers were acquired using a Zeiss Axio Observer.Z1 microscopy system equipped with LED illumination system "Colibri" (Göttingen, Germany).

3. Results and discussion

3.1. Characterization of fluorescein-loaded PLGA-microparticles

With respect to the size of particulate drug delivery systems for intestinal delivery of hydrophilic APIs, among others, some issues remain to be considered: (i) Desai et al. (1997) reported that particles in the lowest micrometer range rather remain in the intestinal lumen than to be taken up by the cells. (ii) Microparticles provide a higher payload of hydrophilic APIs than submicron particles (Florence, 2005). (iii) Smallest microparticles provide a surface area large enough for modification with targeters. Thus, PLGA-microparticles with a mean diameter of 4.7 ± 0.75 μm loaded with fluorescein sodium as a model for hydrophilic APIs were prepared by the double emulsion solvent-evaporation technique. The amount of encapsulated fluorescein sodium was 1.75 ± 0.02 μg and 1.77 ± 0.01 μg fluorescein sodium per mg PLGA with and without WGA conjugation, respectively. Microscopic inspection of the particles revealed homogenous distribution of fluorescence throughout the particle matrix. According to Keegan et al. (2004, 2006), the use of PEMA instead of the traditional stabilizer poly(vinyl alcohol) enhances the conjugation efficiency with amine-containing ligands due to adhesion of the carboxylated surfactant at the surface of the microspheres. Accordingly, the amount of WGA coupled to the surface of PLGA-microparticles using PEMA as surfactant was about 1.3-fold higher in comparison to the PVA stabilized particles (data not shown). In spite of replacement of PVA by PEMA, the plain and surface grafted particles were fully redispersible and stable upon storage for at least one month at 4 °C.

3.2. Release profile of fluorescein sodium from PLGA microparticles

Most probably due to purification of the microparticles immediately after preparation the first burst release associated with
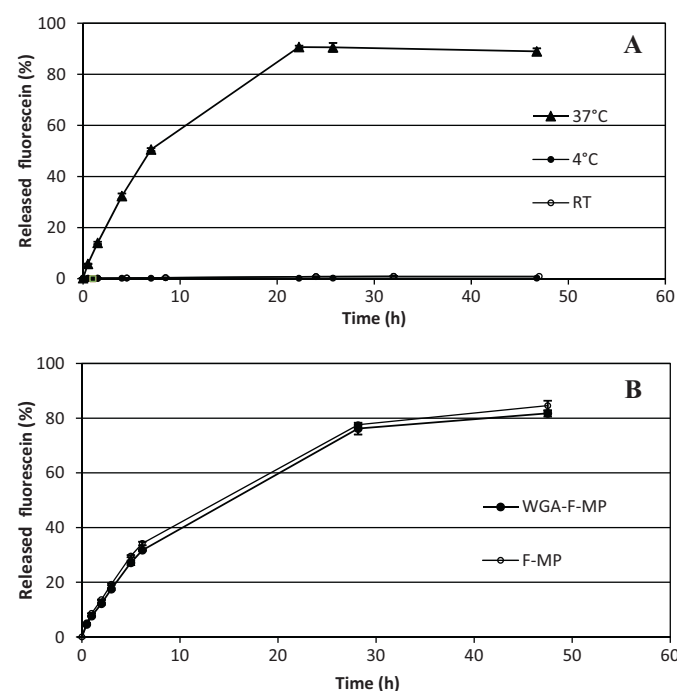

Fig. 1. Release of fluorescein sodium from PLGA microparticles. (A) depicts the release profile from microparticles before WGA conjugation at three different temperature levels (4 °C, 37 °C, and room temperature (RT)). (B) shows the liberation at 37 °C before (Fluorescein sodium-microparticles, F-MP) and after WGA conjugation (WGA-fluorescein sodium-microparticles, WGA-F-MP) (SD ≤ 2.16, n = 3).

dissolution of surface-bound hydrophilic label was not observed (Fig. 1). Interestingly, the drug model substance was released at a fairly constant rate even over 23 h corresponding to the second and third slower continuous release phase (Faisant et al., 2006). This amount corresponds to the maximum release rate of 88.9 ± 0.23% since no further release of model drug was observed upon prolonged incubation. In case of thermo-responsive release it was reported that temperatures higher than 37 °C alter the first burst phase due to morphological changes of the microparticles such as surface pore closing and geometry change but the post-burst release phases remain unaltered (Zolnik et al., 2006). However, no information is available about the situation at temperatures below 37 °C. To date it is generally accepted that PLGA microspheres smaller than 300 μm undergo homogenous or bulk degradation where the degradation rate of the surface is equivalent to that of the core (Anderson and Shive, 1997). The temperature-dependent parameters governing the release from 4.7 μm PLGA spheres comprise the solubility and diffusion of the label as well as the mobility and degradation rate of PLGA-chains. Since fluorescein sodium is highly soluble independent from temperature and the difference in release rate between room temperature and 37 °C is quite higher than that between 4 °C and room temperature, the physicochemical properties of the model drug are supposed to be of minor influence. Additionally, the release profile of entrapped fluorescein was almost the same independent from surface modification of the microparticles with lectin. Thus it might be concluded that the enhanced release at body temperature is solely due to the hydrophobic PLGA-matrix. Such thermo-responsive release characteristics go along with storage stability at 4 °C and room temperature, but with release of the API from the formulation as soon as reaching body temperature. This might be of high interest not only for formulation of unstable low molecular weight biotech drugs but also for surface modification of drug loaded particulate matter.
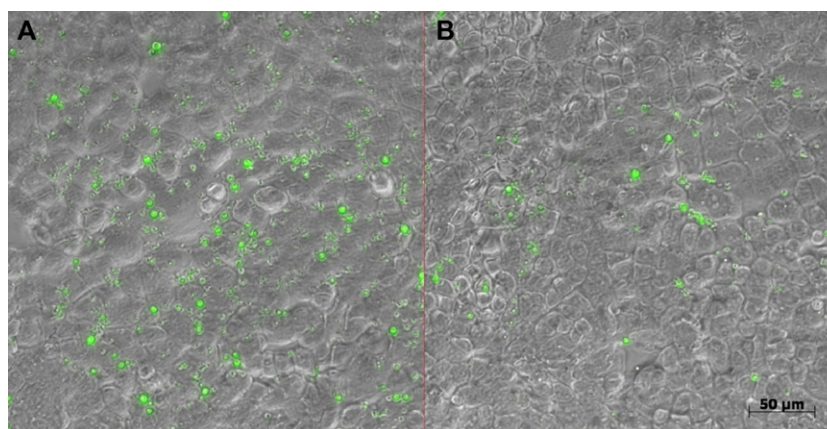
Fig. 2. Overlay of differential interference contrast and fluorescence images of Caco-2 monolayers incubated with WGA-grafted fluorescein-loaded PLGA microparticles (A) and the same particles without WGA grafting (B) for 30 min at 4 °C followed by two washing steps.

3.3. Cytoadhesion studies

In order to elucidate the effects of grafting the microparticles with WGA, Caco-2 monolayers were incubated with particles for 30 min at 4 °C and examined qualitatively as well as quantitatively after removal of unbound microparticles. Even microscopic inspection revealed a considerably higher number of cell-bound microparticles in case of lectin-modification as compared to plain particles, which confirms successful coupling of the lectin (Fig. 2). In accordance with the release studies at 4 °C, staining of cells by released dye was not observed. Performing the same experiment in 96-well plates and fluorescence reading revealed that about 1.5-fold more microparticles had bound to the cell-membrane upon surface modification with the biorecognitive lectin (Data not shown). The enhanced bioadhesion of the WGA-grafted particles derives from the strong interaction of the lectin with sialic- or N-acetyl-D-glucosamine moieties of the artificial intestinal epithelium, which resists even the washing procedure (Gabius, 2009). As depicted by the images, intracellular uptake of the lectinized particles does not occur since the incubation temperature of 4 °C suppresses energy-dependent transport processes and the size of the particles exceeds by far that of vesicles generated during receptor-mediated endocytosis which represents the mechanism of WGA-mediated cytoinvasion (Gabor and Wirth, 2003).

3.4. Elucidation of the microparticle–cell interaction following a pulse-chase protocol in comparison to free fluorescein

To investigate the mechanism of the interaction between Caco-2 monolayers and WGA-grafted fluorescein-loaded microparticles in a quantitative way, pulse-chase experiments were performed (Fig. 3). Firstly, after removing the medium, the Caco-2 cell monolayers were pulse-incubated with the particle suspension for 30 min at 4 °C or 37 °C. Since fluorescein is not released at 4 °C and unbound particles were removed by washing, the RFI (relative fluorescence intensity) at 4 °C represents the amount of cell-bound microparticles or cell-bound encapsulated model drug. In contrast, because of release of encapsulated fluorescein at 37 °C, the cell-associated RFI of 37 °C pulse incubation represents the sum of cell-bound microparticle-entrapped and cell-associated released dye. When the same amount of free fluorescein was added as the payload of the microparticles (0.35 μg/mL), the amount of cell-associated model drug (180 ± 2 RFI) was fourfold higher as compared to non-grafted microparticles (47 ± 9 RFI) but only 2.7-fold higher as compared to bioadhesive microparticles (66 ± 7 RFI)

after pulse incubation at 4 °C (Fig. 3A). Due to higher diffusional uptake of free fluorescein, this difference slightly increases to 4.7-fold or 3.2-fold, respectively, in case of 37% pulse incubation (Fig. 3B). Obviously, the difference in cell-associated RFI between the solution of the model drug and the microparticles mainly derives from quench of the label by the microparticles' matrix. At both temperature levels of the pulse incubation, however, the cell-associated RFI of WGA-grafted microparticles exceeded that of plain particles by about 40% at the mean. In accordance with the cytoadhesion studies (Section 3.3), this again confirms successful covalent modification of the microparticles and their enhanced bioadhesivity as compared to lectin-free microparticles.

Secondly, after 4 h of chase incubation at 37 °C following pulse incubation at both temperature levels, the total fluorescence intensities were determined omitting a washing step (Fig. 3, chase total). Thus, they represent the sum of the fluorescence intensities referred to both, released fluorescein present in the supernatant and taken up into the cell as well as cell-bound microencapsulated model drug. In case of the microparticles, the high RFI values point to extraordinarily high thermoresponsive release of model drug which was entrapped and quenched by the PLGA matrix before. Again, the total release from lectinised-microparticles exceeded by far that from non-coated ones due to the fact that a considerably higher number of WGA-coated particles containing quenched model drug adhered to the cells as already observed (see Fig. 2). In case of the fluorescein solution, no change in RFI was observed after chase incubation. Altogether, the microparticle approach is favorable since less than 10% of the model drug were finally detected when applied as a solution.

Thirdly, after removal of non-cell-associated fluorescein, the determined relative fluorescence intensity represents cell-associated fluorescein deriving from intracellularily accumulated fluorescein and microparticle-entrapped cell-bound dye (Fig. 3). After pulse incubation at 4 °C and chase incubation at 37 °C the amount of cell-associated model drug was 2.9-fold higher when applied as microparticles and further increased to 4.2-fold in case of WGA-grafted microparticles as compared to the solution. Upon incubation at body temperature the percentage of model drug delivered to the cells exceeded that of the solution 4.4-fold (non-coated microparticles) or 5.8-fold (WGA-coated microparticles). These results again confirm the superiority of the microparticle approach, which is further improved by surface modification of the particles with cytoadhesive WGA.

To visualize the course of release of the model drug from lectin-coated microparticles, preloaded Caco-2 monolayers were
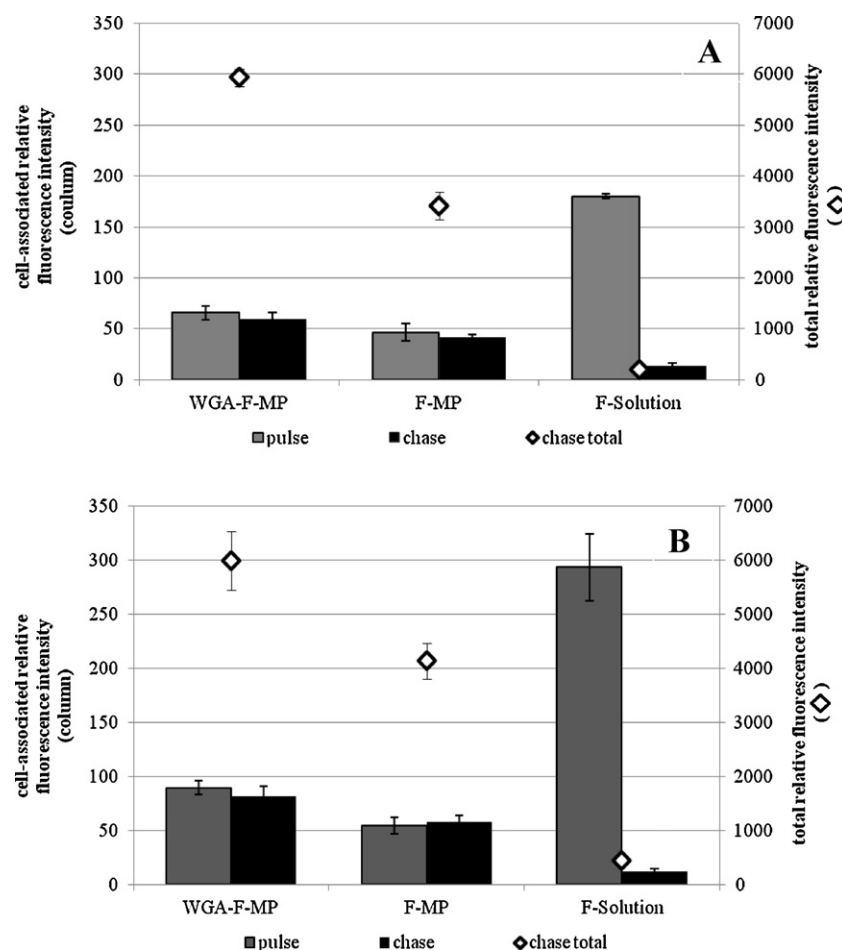
Fig. 3. Comparison between WGA-grafted fluorescein-loaded microparticles (WGA-F-MP; 200 μg/ml), fluorescein-loaded microparticles (F-MP; 200 μg/ml) and fluorescein in aqueous solution (F-Solution; 0.35 μg/ml) after pulse incubation at 4 °C for 30 min and chase incubation at 37 °C for 4 h (A) or pulse incubation at 37 °C for 30 min and chase incubation at 37 °C for 4 h (B). The grey columns (pulse incubation) and black columns (chase incubation) refer to the y-axis at the left, which represents the cell-associated relative fluorescence intensity after pulse or chase incubation after removal of free fluorescein. The diamonds (chase total) refer to the y-axis at the right, which represents the total relative fluorescence intensity after chase incubation without washing.

incubated for different time intervals at 37 °C (Fig. 4). After 1 h the fluorescent particles were still bound to the cells and cellular enrichment of released dye was hardly detectable. After further 2 h of incubation, however, the released model drug is already taken up locally by the cells as indicated by appearance of a diffuse fluorescent corona around the microparticles in the underlying cells. Finally, after 5 h of incubation at body temperature, most of the microparticles lost their label and are sparsely visible, but the majority of cells is stained by the released dye. Consequently, this set of fluorescence photos demonstrates that the presented micro-formulation is cytoadhesive due to the lectin coat and delivers the entrapped model API directly into the underlying cells in a sustained manner.

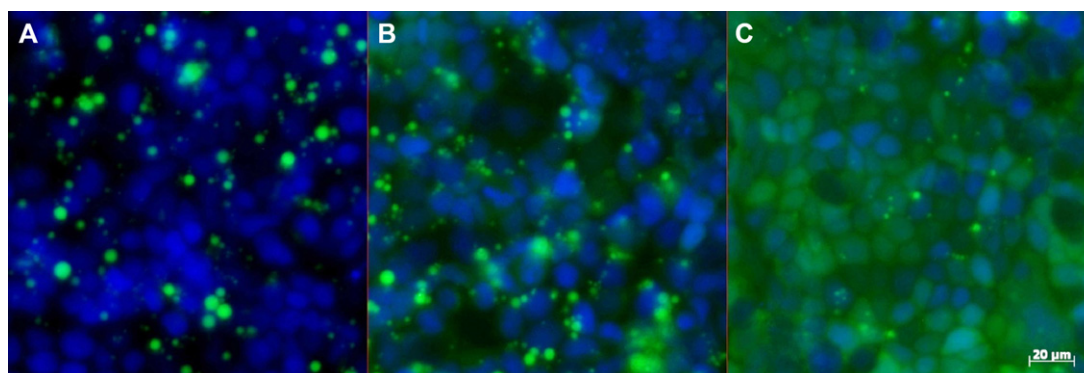**Fig. 4.** Fluorescence microscopic images of the Caco-2-binding of WGA-grafted fluorescein-loaded microparticles followed by release and cellular-uptake of encapsulated fluorescein sodium (green) at 37 °C after 1 h (A), 3 h (B) and 5 h (C). The nuclei of the cells were stained in blue by Hoechst 33342. (For interpretation of the references to colour in this figure legend, the reader is referred to the web version of the article.)

4. Conclusion

Biodegradable PLGA microparticles with 4.7 μm in diameter were prepared by a w/o/w solvent evaporation technique using PEMA instead of a traditional stabilizer, which 1.3-fold increases the number of modifiable carboxylate groups at the particle surface. The particles were rendered cytoadhesive by covalent coupling of WGA and loaded with fluorescein sodium as a model API yielding a payload of 1.7 μg/mg polymer independent from surface modification. The comparison with free model API and non-coated microparticles using Caco-2 monolayer assays revealed two notable characteristics of WGA-grafted microparticles: Firstly, the model API was only released from the microparticles at body temperature. Although the genuine mechanism remains to be elucidated, this property implies storage stability of the drug-loaded microparticle suspension at both, 4 °C and room temperature, which is suggested to be beneficial for drug candidates with poor storage stability. Secondly, as confirmed by fluorescence microscopy, the WGA-coat made the particles bioadhesive resulting in 1.5-fold enhanced cell-binding as compared to non-modified ones. The close vicinity of the particles to the absorptive enterocytes shortened the diffusional pathway of the drug into the cell and concurrently increased the gradient between the lumen and the cytoplasm so that enhanced intracellular uptake of the hydrophilic model drug was observed. According to quantitative pulse-chase experiments, lectin-mediated cytoadhesion increased the cellular accumulation 5.8-fold as compared to the API-solution. This confirms utility of the lectin-approach for enhanced and sustained intestinal cellular uptake of hydrophilic drugs from microparticles. Since WGA also binds to sialic acid moieties of the mucus (Wirth et al., 2002), these lectin coated particles representing bioadhesives of the second generation are expected to be firmly fixed to the absorptive epithelium in vivo due to double anchoring. As this concept would not only be useful for delivery of hydrophilic low MW, but also other poorly absorbable low and high MW drugs from the biotech pipeline, the feasibility of this approach will be tested with other active compounds in future.

References

Anderson, J.M., Shive, M.S., 1997. Biodegradation and biocompatibility of PLA and PLGA microspheres. Adv. Drug Del. Rev. 28, 5–24.

http://www.fda.gov/Food/FoodIngredientsPackaging/ucm084292.htm.

Bao, W., Zhou, J., Luo, J., et al., 2006. PLGA microspheres with high drug loading and high encapsulation efficiency prepared by a novel solvent evaporation technique. J. Microencapsul. 23, 471–479.

Bies, C., Lehr, C.-M., Woodley, J.F., 2004. Lectin-mediated drug targeting: history and applications. Adv. Drug Del. Rev. 56, 425–435.

Desai, M.P., Labhasetwar, V., Walter, E., et al., 1997. The mechanism of uptake o biodegradable microparticles in Caco-2 cells is size dependent. Pharm. Res. 14, 1568–1573.

Ertl, B., Heigl, F., Wirth, M., Gabor, F., 2000. Lectin-mediated bioadhesion: preparation, stability and Caco-2 binding of wheat germ agglutinin-functionalized poly(D,L-lactic-co-glycolic acid)-microspheres. J. Drug Targeting 8, 173–184.

Faisant, N., Akiki, J., Siepmann, F., et al., 2006. Effects of the type of release medium on drug release from PLGA-based microparticles: Experiment and theory. Int. J. Pharm. 314, 189–197.

Florence, A.T., 2005. Nanoparticle uptake by the oral route: Fulfilling its potential? Drug Discov. Today 2, 75–81.

Gabius, H.-J., 2009. The Sugar Code, first ed. Wiley-VCH, Weinheim.

Gabor, F., Wirth, M., 2003. Lectin-mediated drug delivery: fundamentals and perspectives. STP Pharma Sci. 13, 3–16.

Garbayo, E., Ansorena, E., Lanciego, J.L., et al., 2008. Sustained release of bioactive glycosylated glial cell-line derived neurotrophic factor from biodegradable polymeric microspheres. Eur. J. Pharm. Biopharm. 69, 844–851.

Keegan, M.E., Falcone, J.L., Leung, T.C., et al., 2004. Biodegradable microspheres with enhanced capacity for covalently bound surface ligands. Macromolecules 37, 9779–9784.

Keegan, M.E., Royce, S.M., Fahmy, T., et al., 2006. In vitro evaluation of biodegradable microspheres with surface-bound ligands. J. Control. Release 110, 574–580.

Manocha, M., Pal, P.C., Chitralekha, K.T., et al., 2005. Enhanced mucosal and systemic immune response with intranasal immunization of mice with HIV peptides entrapped in PLG microparticles in combination with Ulex Europaeus-I lectin as M cell target. Vaccine 23, 5599–5617.

Mundargi, R.C., Babu, V.R., Rangaswany, V., et al., 2008. Nano/micro technologies for delivering macromolecular therapeutics using poly(D,L-lactide-co-glycolide) and its derivatives. J. Control. Release 125, 193–209.

Rafi, M., Singh, S.M., Kanchan, V., et al., 2010. Controlled release of bioactive recombinant human growth hormone from PLGA microparticles. J. Microencapsul. 27, 552–560.

Ratzinger, G., Agrawal, P., Körner, W., et al., 2010a. Surface modification of PLGA nanospheres with Gd-DTPA and Gd-DOTA for high-relaxivity MRI contrast agents. Biomaterials 31, 8716–8723.

Ratzinger, G., Wang, X., Wirth, M., et al., 2010b. Targeted PLGA microparticles as a novel concept for treatment of lactose intolerance. J. Control. Release 147, 187–192.

Roth-Walter, F., Schöll, I., Untersmayr, E., et al., 2005. Mucosal targeting of allergen-loaded microspheres by Aleuria aurantia lectin. Vaccine 23, 2703–2710.

Weissenböck, A., Wirth, M., Gabor, F., 2004. WGA-grafted PLGA-nanospheres: Preparation and association with Caco-2 single cells. J. Control. Release 99, 383–392.

Wirth, M., Gerhardt, K., Wurm, C., et al., 2002. Lectin-mediated drug delivery: influence of mucin on cytoadhesion of plant lectins in vitro. J. Control. Release 79, 183–191.

Ye, M., Kim, S., Park, K., 2010. Issues in long-term protein delivery using biodegradable microparticles. J. Control. Release 146, 241–260.

Zolnik, B.S., Leary, P.E., Burgess, D.J., 2006. Elevated temperature accelerated release testing of PLGA microspheres. J. Control. Release 112, 293–200.

1.2.1 Encapsulation of hydrophilic and lipophilic model drugs

Lectin-grafted PLGA microcarriers loaded with fluorescent model drugs: characteristics, release profiles, and cytoadhesion studies

Xue-Yan Wang, Romana Koller, Michael Wirth, Franz Gabor

Faculty of Life Sciences, Department of Pharmaceutical Technology and Biopharmaceutics, University of Vienna, Vienna A-1090, Austria

1. FUNCTIONALIZED PLGA-MICROPARTICLES FOR DRUG DELIVERY

Scientia Pharmaceutica

Research article

Lectin-Grafted PLGA Microcarriers Loaded with Fluorescent Model Drugs: Characteristics, Release Profiles, and Cytoadhesion Studies

Xue-Yan WANG, Romana KOLLER, Michael WIRTH, Franz GABOR *

Department of Pharmaceutical Technology and Biopharmaceutics, University of Vienna, Althanstrasse 14, 1090, Vienna, Austria.

* Corresponding author. E-mail: franz.gabor@univie.ac.at (F. Gabor)

This article is available from: http://dx.doi.org/10.3797/scipharm.1312-08

Abstract

PLGA microparticles loaded with three different fluorescent model drugs, fluorescein sodium (hydrophilic), sulforhodamine (amphoteric), and boron-dipyrromethene (BODIPY® 493/503, lipophilic), were prepared by the solvent evaporation technique. Due to varying hydrophilicity, the diameters of the microparticles ranged between 4.1 and 4.7 µm. According to fluorimetric analysis, the loading varied from 0.06 to 2.25 µg of the model drug per mg PLGA. In terms of the release profile, the fluorescein sodium-entrapped formulation exhibited thermo-responsive release kinetics. In the case of sulforhodamine- and BODIPY® 493/503-loaded particles, almost no release was observed, neither at 4°C nor 37°C during the first 50 hours. Furthermore, to estimate the bioadhesive properties of such drug delivery systems, the surface of the loaded particles was grafted with wheat germ agglutinin by applying the carbodiimide method. Cytoadhesion studies with Caco-2 monolayers revealed an up to 1.9-fold and 3.6-fold increase in the bioadhesion of the lectin-functionalized, model drug-loaded particles as compared to the albumin- and non-grafted microcarriers, respectively. All in all, the results clearly indicated that the lipophilicity of the polymer matching that of the drug favored entrapment, whereas mismatching impeded loading into the PLGA-microparticles. Even in the case of low loading, these delivery systems might be useful for the fluorescent detections and microscopic imaging of cellular interactions due to their fluorescent properties and lack of dye leakage. Moreover, lectin grafting can mediate bioadhesive properties to such particulate drug carriers which could be a promising approach to improve drug delivery.

X.-Y. Wang *et al.*:

Keywords

Caco-2 • Cytoadhesion • Microparticles • PLGA • Wheat Germ Agglutinin (WGA)

Introduction

As is nowadays generally accepted, the administration of polymeric micro- and nano-carriers as particulate drug formulations offers numerous advantages in comparison to conventional approaches, such as the protection of encapsulated active pharmaceutical ingredients (APIs) against the harmful gastrointestinal environment, the possibility of encapsulating hydrophilic as well as lipophilic drugs, the controlled release of loaded APIs, the feasibility of different physicochemical targeting approaches, as well as the improvement of bioavailability [1]. Because of these reasons, the characteristics of numerous polymeric drug carriers have been intensively studied. Among these polymers, the most commonly investigated one is PLGA (poly(lactic-co-glycolic acid)) due to its biocompatibility and biodegradability, its ability to modify the release profiles by use of different polymerization grades, as well as its long-time use in humans resulting in being "generally recognized as safe" by the FDA [2–6]. In terms of encapsulation of APIs with poor biopharmaceutic and pharmacokinetic properties, a wide variety of drugs has been successfully applied in particulate delivery [2], such as the antioxidants coenzyme Q10 [7] and curcumin [8], the anti-leishmanial agent amphotericin B [9], the immunosuppressant cyclosporine [10], the anti-cancer agent doxorubicin [11], and others. In the case of surface modification for drug targeting, the uncapped types of PLGA with terminal carboxylate groups provoked interest due to the feasibility of functionalization with a number of ligands, especially proteins and peptides. In particular, the surface modification of particles with lectins is a promising approach for gastrointestinal targeting [12]. In order to prolong the residence time in the GI tract by improving mucoadhesion, immobilization of wheat germ agglutinin (WGA) from *Triticum vulgare* might be useful. Due to its specific interaction with sialic acid and the N-acetyl-D-glucosamine moieties of the glycocalyx of enterocytes [13], several drug delivery systems functionalized with WGA have been developed in our group for intestinal targeting [14–17].

In the present work, three different fluorescent dyes were entrapped into PLGA microparticles. Fluorescein sodium, sulforhodamine, and 4,4-difluoro-1,3,5,7,8-penta-methyl-4-bora-3a,4a-diaza-*s*-indacene (BOD; BODIPY® 493/503) were chosen as model drugs due to their differing solubilities being hydrophilic, amphoteric [18], and lipophilic, respectively. PLGA-microcarriers were prepared using the solvent evaporation technique either as water-in-oil-in-water (double emulsions) or as oil-in-water (single emulsion) methods according to the lipophilicity of the loaded fluorescent dyes. Moreover, the surface of the microparticles was modified with ligands (e.g. WGA) by the carbodiimide method, which mediates the formation of amid linkages between carboxylic and primary amine groups. Therefore, instead of the commonly used stabilizer polyvinylalcohol (PVA), poly(ethylene-*alt*-maleic acid) (PEMA) was applied. Due to its carboxylate content PEMA might enhance the coupling efficiency as described by Keegan et al. [19]. Subsequently, the size, stability, payload, and release profile of the loaded model drugs of the prepared microparticles were analyzed. Additionally, the surface of the microcarriers was modified to mediate specific bioadhesive properties. In comparison to the albumin- and non-grafted drug carriers, the impact of this functionalization was examined *in vitro* with Caco-2 cell monolayers, which is a generally accepted and well-established epithelial cell model [20].

Results and Discussion

Characterization of the Model Drug-Loaded PLGA-Microparticles

Tab. 1. Characteristics of the fluorescent model drug-loaded PLGA-microparticles

Type / Loading of microspheres	Preparation technique	Characteristic of dye	Mean diameter (µm)	Dye loading (µg/mg PLGA)	Encapsul. efficiency (%)
Fluorescein-Na entrapped particles / Fluorescein - Na	(w/o)w double emulsion	hydrophilic	4.5 ± 1.2	1.75 ± 0.03	46.7
Sulforhodamine entrapped particles / Sulforhodamine	(w/o)w double emulsion	amphoteric	4.7 ± 1.5	0.06 ± 0.01	0.8
BOD entrapped particles / BODIPY® 493/503	o/w single emulsion	hydrophobic	4.1 ± 1.4	2.25 ± 0.07	59.9

Due to its hydrophobic characteristics, BODIPY®493/503 was entrapped into micro-particles via the single emulsion (o/w) method, whereas fluorescein sodium as well as sulforhodamine were encapsulated applying the (w/o/w) double emulsion technique. As illustrated in Table 1, independent from the type of loaded model drug, the particles possess a comparable mean diameter of about 4.4 µm. There are some reasons rendering this size range appropriate for the intestinal drug delivery: first, in contrast to nanoparticles, the total API-loading is higher. Second, at the same weight, particles of low micron size provide a larger surface area for functionalization with targeters than larger particles. Third, according to Desai et al. [21], particles in the low micrometer size range are not likely to be taken up by the cells, but rather remain in the intestinal lumen. Therefore, such particles could facilitate a long-term drug release in a controlled manner. Furthermore, in order to enhance the capability of later covalent conjugation with primary amine-bearing protein ligands to the particle surface by carbodiimide chemistry, PEMA (poly(ethylene-*alt*-maleic acid)) as a new stabilizer instead of the traditional one poly(vinyl alcohol) (PVA) was applied by the solvent-evaporation technique [19].

Among all microparticle preparations, the BOD-loaded microparticles exhibited the smallest mean particle size, the highest model drug loading, and the highest encapsulation efficiency (Table 1). This might be due to the lipophilicity of both, the dye and the polymeric matrix, which results in high affinity between both components. As a result of these prevailing strong hydrophobic interactions, the fluorescent dye preferentially remains in the oily phase together with PLGA during the emulsification step as reflected by the high dye loading and also yields tighter and smaller microparticles by the single emulsion technique [22, 23]. In contrast, the dye loading of fluorescein sodium-loaded microcarriers was 22% lower. This result is due to low affinity between the hydrophilic dye and the hydrophobic polymer. Consequently, in the case of the double emulsion technique, hydrophilic drugs can easily distribute from the inner aqueous phase to outer aqueous medium during the emulsification process, which considerably reduces the loading

efficiency. Interestingly, although the fluorescein sodium and sulforhodamine-loaded particles were prepared by the same technique, and equimolar amounts of dyes were applied, the encapsulation efficiency of these two model drugs varied considerably. As demonstrated in Table 1, the entrapped amount of fluorescein sodium was approximately 1.75 µg per mg PLGA, in contrast to 0.06 µg per mg PLGA in the case of sulforhodamine. This might be due to the amphoteric character of sulforhodamine, which allowed the red fluorescent substance to accumulate inside the aqueous phase as well as inside the oil phase during the first emulsification step. Therefore, after the addition of the second aqueous phase, sulforhodamine might have been distributed into this external phase and washed out during the subsequent purification step.

Furthermore, after the surface modifications with the targeters, all the microparticles were homogenously dispersible in buffer, and stored stably at −80°C for at least one month until further experiments.

Release Kinetics of the Entrapped Fluorescent Model Drugs from PLGA Microparticles

The release studies of the entrapped fluorescent model drugs were performed before the surface modification of the microparticles at 4°C as well as 37°C and after the surface functionalization with WGA at 37°C. As demonstrated in Figure 1, in contrast to the literature [24, 25], the three types of particles exhibited no signs of first burst release which might be due to the purification steps after preparation. Interestingly, a thermo-responsive release profile of entrapped fluorescein sodium from PLGA microparticles was observed (Figure 1A) [26]. At this rate, less than 0.23% of the entrapped model drug was released from the particulate formulation after nearly 50 h incubation at 4°C in contrast to more than 90% at 37°C. However, in Figure 1B and 1C it is shown that such a thermo-responsive release from sulforhodamine- or BOD-entrapped PLGA-microparticles was not observed. According to Shive et. al. [4], PLGA microparticles smaller than 300 µm in diameter were degraded in a homogenous manner with an equivalent degradation rate at the surface and in the core. Thus, such different release profiles might be governed predominantly by two parameters: (i) the solubility of the entrapped model drugs in buffer; (ii) the diffusion velocity of the fluorescein sodium from the PLGA-matrix into the buffer. Since the inner texture of PLGA-microparticles is porous, water can easily penetrate such small holes to get contact with the encapsulated dye molecules. However, among the three types of fluorescent dyes investigated, only fluorescein sodium was excellently soluble in water and dissolved in aqueous buffer solution independently from the temperature. Therefore, the first entrapped and then dissolved fluorescein sodium easily diffused from the particle's matrix into the surrounding medium. For the sulforhodamine-loaded microspheres, the fairly lower encapsulated amount might have led to a lower detection sensitivity of the liberated dye, and according to its amphiphilic character, its aqueous solubility was lower than that of fluorescein sodium. Finally, in the case of the BOD-loaded microspheres, the hydrophobic character of BOD favored the model drug to remain inside the hydrophobic PLGA-matrix and not to partition into the surrounding aqueous buffer. In addition, independent from the model drug, microparticles with or without WGA-grafted surfaces displayed the same release kinetics of the entrapped model drug at the same conditions.
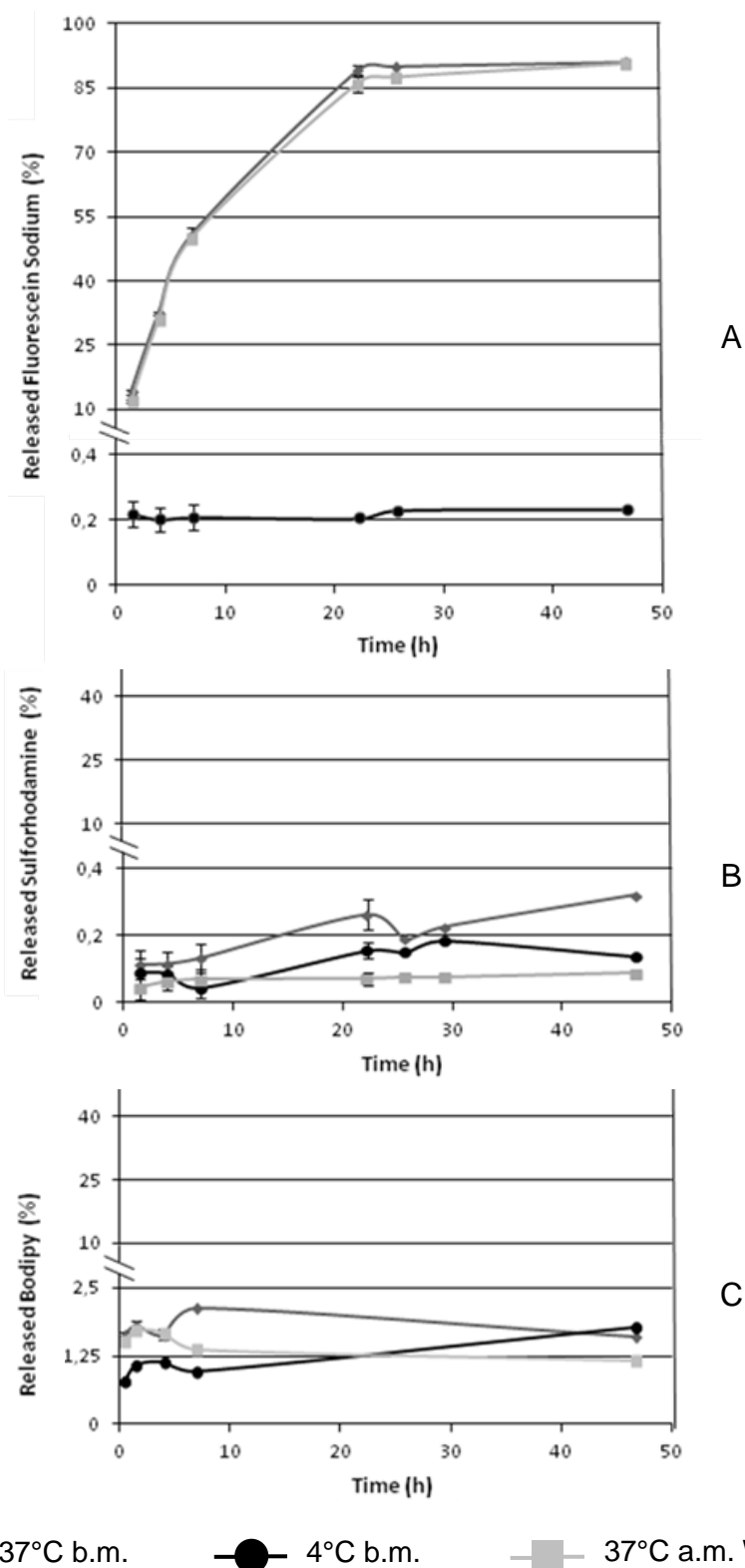
Fig. 1. Release profiles of entrapped fluorescein sodium (A), sulforhodamine (B), and BOD (C) from PLGA microparticles. The release studies were either performed before surface modification (b.m.) at two different temperatures (4°C and 37°C), or after surface modification with WGA at 37°C (a.m. WGA) (SD ≤ 2.03, n=3).

In conclusion, due to the different properties of entrapped fluorescent model drugs as well as the influence of temperature on the PLGA-matrix, the three different types of microspheres exhibited different release profiles. In addition, particle surface modification with lectin did not affect the liberation kinetics of the entrapped model drugs.

Cytoadhesion Studies
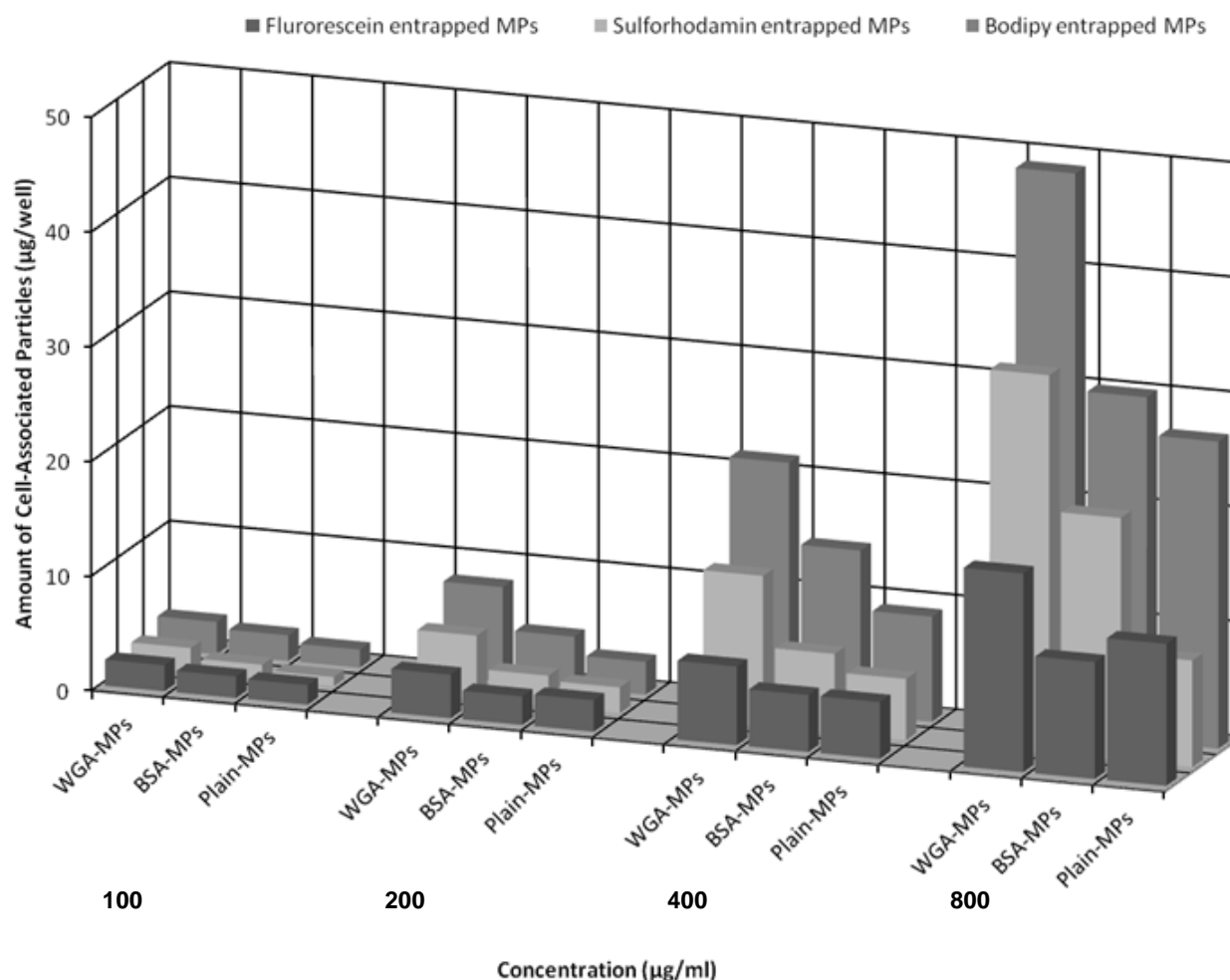
Fig. 2.   Cytoadhesion studies of fluorescein sodium, sulforhodamine, and BOD-loaded PLGA-microparticles with Caco-2 monolayers at concentrations of 100, 200, 400, and 800 µg/mL after 30 min incubation at 4°C. The surfaces of the particles were modified with WGA-, BSA-, or non-modified, abbreviated as WGA-MPs, BSA-MPs, and Plain-MPs, respectively (n = 3, SD ≤1.07).

In order to study the cytoadhesive properties of the targeted particulate formulations, Caco-2 cell monolayers were incubated with the respective particle suspension for 30 min at 4°C. After two washing steps, the cell-associated relative fluorescence intensity was quantified. WGA is a lectin with biorecognitive properties that interacts with glycosylated structures in the intestine, which increases the bioadhesion to epithelial cells [12]. Thus, the lectin-grafted microparticles served as targeted formulations, whereas BSA- and non-grafted particles served as controls.
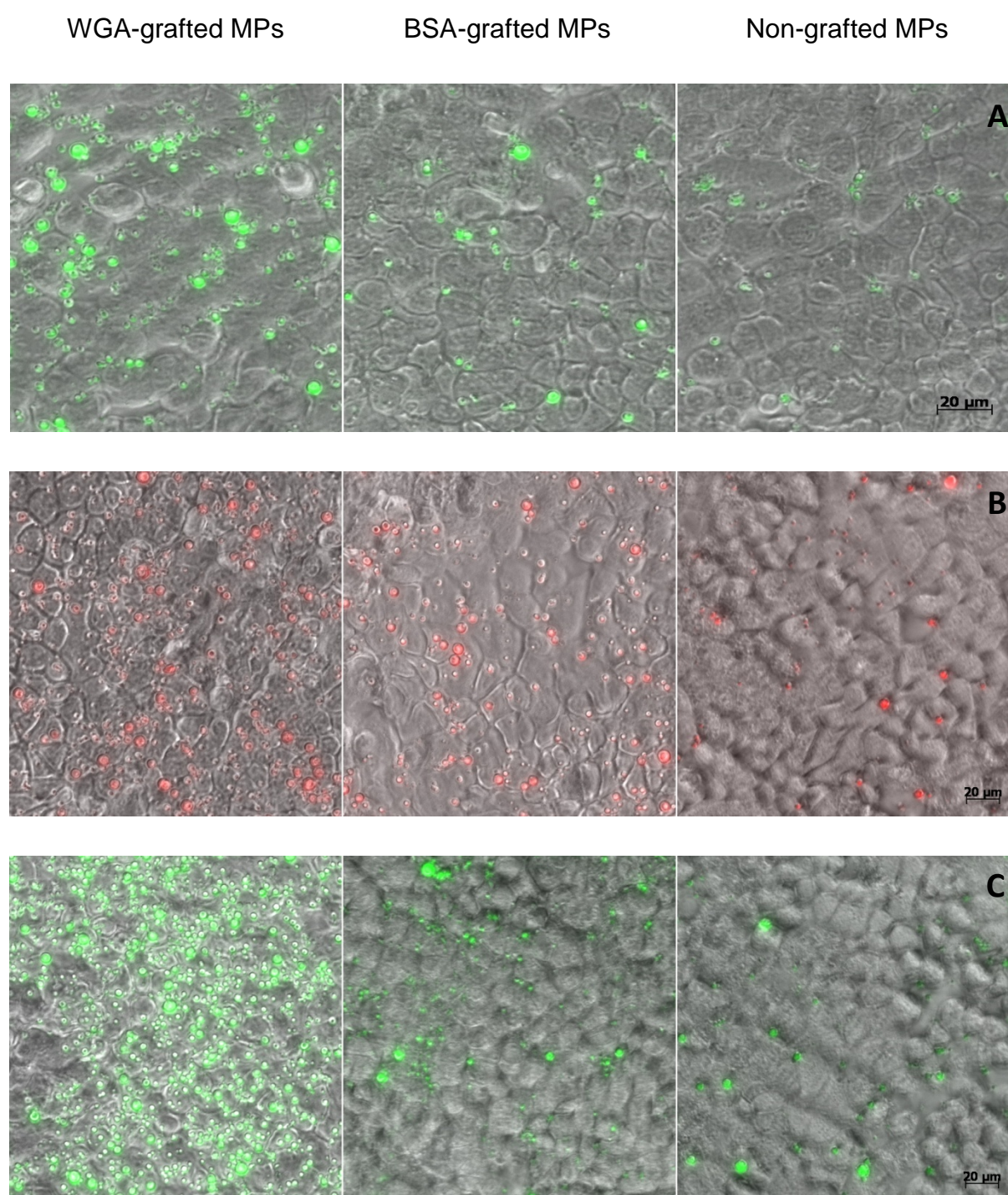
Fig. 3.   Overlay of differential interference contrast and fluorescence images of Caco-2 monolayers incubated with fluorescein sodium- (A), sulforhodamine- (B), and BOD- (C) entrapped PLGA microparticles for 30 min at 4°C followed by two washing steps (concentration of PLGA-MPs: 200 µg/mL).

As illustrated in Figure 2, independent from the type of the entrapped model drugs as well as concentrations of the applied particle suspension, the highest amount of cell-associated particles was observed in the case of the WGA-grafted microparticles exceeding that of the BSA-grafted ones up to 1.9-fold and non-grafted drug carriers 3.6-fold, respectively. These specific binding effects of WGA-functionalized particles to Caco-2 cells were also confirmed by microscopy (Figure 3). As depicted by the images, intracellular uptake of the particulate formulations was not observed. This might be due to the incubation temperature of 4°C, which inhibits energy-dependent transport mechanisms, as well as the size of the particles being too large to undergo receptor-mediated endocytosis [21]. Additionally, the amount of cell-associated particles per well increased with the concentration of applied particle suspension (Figure 2). A comparison of the surface-modified particles revealed that the BOD-entrapped microcarriers yielded the highest binding efficiency at all concentration levels, whereas fluorescein sodium-loaded particles exhibited the lowest rate of cytoadhesion. For example, the amount of cell-associated WGA-grafted, fluorescein sodium-loaded carriers ranged between 2.3±0.14 and 17.3±1.01 µg/well with a concentration of particles from 100 µg/mL to 800 µg/mL. This result corresponds to only 80–35% of that of the cell-associated BOD-entrapped microparticles at the same concentration. It should also be considered that due to the hydrophobic character of BOD as well as the amphoteric properties of sulforhodamine, which resist purification by washing with water, non-encapsulated dye might remain non-specifically adsorbed at the surface of the particles. Furthermore, such surface-anchored model drugs might detach from particles during incubation with cells to bind to the cell membrane. Importantly, such loosely bound and detached fluorescent dyes emit higher fluorescent signals in comparison to entrapped fluorescent substances inside of the particle-matrix due to quenching phenomena. Since such free fluorescent dyes can strongly contribute to the signal intensity and are also calculated as cell-bound particles, the measured amount of the cell-associated BOD- and sulforhodamine-entrapped particles might be higher than the truly cell-bound amount. Since the hydrophilicity of fluorescein anticipates the complete removal of particle-bound dye from the surface during several washing steps with aqueous buffer, such a confusing effect can be excluded. Because of this reason, the calculated amount of cell-associated fluorescein sodium particles was lower than that of the other two formulations. Interestingly, the BSA-grafted microparticles exhibited a slightly higher binding efficiency to the cell monolayer as compared to the non-grafted particles, which might be due to the nonspecific protein-protein interactions between albumin and the cell membrane.

Conclusion

In this study, three fluorescent model drugs were microencapsulated in a hydrophobic matrix using modifications of the solvent evaporation technique according to the differing hydrophilicity of the entrapped drugs. In the case of similar hydrophobicity of both model drugs BOD and PLGA, the single emulsion technique yielded microparticles of the smallest size and highest encapsulation efficiency, but almost no release presumably due to strong hydrophobic interactions. In the case of hydrophilic fluorescein sodium and amphoteric sulforhodamine, however, only the double emulsion technique yielded microparticles. These were of larger size and lower drug loading due to the differing hydrophobicity of the drug and polymer. As amphoteric drugs and hydrophobic polymers also intensely interact, almost no release was observed from the sulforhodamine-loaded

PLGA carriers. In contrast, mismatching characteristics of the drug and polymer facilitated release as indicated by the thermoresponsive release of fluorescein sodium. Consequently, the choice of the preparation technique, size, loading, as well as the release profile was basically guided by the solubility characteristics of the matrix and the entrapped drug. Moreover, non-releasing microparticles with a high quantum yield, such as the BOD-PLGA microcarriers, represent a useful tool to elucidate the interaction with cells quantitatively by fluorescence reading and qualitatively by microscopic imaging as confirmed by the Caco-2 monolayer experiments.

Experimental

Materials

PLGA (poly(lactic-*co*-glycolic acid), Resomer® RG503H, 50:50 lactide/glycolide) was obtained from Boehringer Ingelheim (Ingelheim, Germany). PEMA (poly(ethylene-alt-maleic anhydride)), fluorescein sodium salt, sulforhodamine 101, and albumin bovine fraction V (BSA) were bought from Sigma Aldrich (Vienna, Austria). Wheat germ agglutinin (WGA) from *Triticum vulgare* was purchased from Vector laboratories (Burlingame, USA). BODIPY® 493/503 (4,4-difluoro-1,3,5,7,8-pentamethyl-4-bora-3a,4a-diaza-*s*-indacene) was from Invitrogen (Eugene, USA). All other chemicals were of analytical purity.

Preparation of Fluorescent Model Drugs Loaded with PLGA Microparticles

Sulforhodamine- and fluorescein sodium-loaded PLGA microparticles were prepared by a water-in-oil-in-water solvent-evaporation technique. For that purpose, 400 µL of an aqueous solution containing fluorescein sodium (3.75 mg/mL) or sulforhodamine (7.5 mg/mL) were emulsified with a solution containing 400 mg PLGA in 2.4 g of ethyl acetate by sonication for 2 min (sonifier: Bandelin electronic UW70/HD70; tip, MS 72/D, Berlin, Germany). After adding 8 mL of an aqueous solution of PEMA (0.5%), the emulsion was sonicated again for 2 min yielding the (w/o)/w emulsion that was poured into 100 mL of 0.25% aqueous solution of PEMA. For the BOD-entrapped microparticles, an oil-in-water solvent-evaporation technique was applied. A solution containing 400 mg PLGA and 1.5 mg BOD in 2.8 g ethyl acetate was emulsified with 8 mL of an aqueous solution of PEMA (0.5%) by sonication for 2 min yielding an o/w emulsion which was poured into 100 mL of a 0.25% aqueous solution of PEMA. After mechanical stirring at 600 rpm for 1 h at room temperature, residual ethyl acetate was removed under reduced pressure. In order to remove the non-entrapped fluorescent dyes, the microparticles were washed three times with 120 mL 20 mM HEPES/NaOH pH 7.4 each and resuspended finally in 100 mL of the same buffer. The PLGA content was determined gravimetrically from lyophilized aliquots after exhaustive dialysis against distilled water. The particle size distribution was determined by laser light scattering (Mastersizer 2000 laser particle size analyzer,Malvern Instruments, Malvern, UK).

Surface Modification of Microparticles with Wheat Germ Agglutinin or Bovine Serum Albumin

Wheat germ agglutinin (WGA) or bovine serum albumin (BSA) was covalently bound to the surface of the PLGA microparticles following the carbodiimde method. Briefly, the surface carboxylate groups of the 5 mL PLGA microparticle suspension in 20 mM HEPES/NaOH pH 7.0 containing 0.1% Pluronic® F-68 were activated by the addition of 5 mL of freshly

prepared solution of 1-ethyl-3(3-dimethylaminopropyl) carbodiimide (EDAC, 1400 mg) and N-hydroxysuccinimide (NHS, 59 mg) in the same buffer. After end-over-end incubation for 30 min at room temperature, the microparticles were washed once by dilution with 15 mL of 20 mM HEPES/NaOH pH 7.4 containing 0.1% Pluronic® F-68 and centrifuged (3200 rpm, 10 min, 4°C) to remove the excess reagents. For coupling, the activated microparticles were resuspended in 10 mL of the same buffer and mixed with either 500 µL aqueous solution of WGA (5 mg/mL) or 458 µL aqueous solution of BSA (10 mg/mL) by end-over-end incubation for 1 h at room temperature. Non-reacted binding sites were saturated by incubation with 2.4 mL glycine solution (100 mg/mL) in 20 mM HEPES/NaOH pH 7.4 containing 0.1% Pluronic® F-68 for 30 min at room temperature. Subsequently, the microparticles were washed twice by centrifugation (3200 rpm, 10 min, 4°C) with 15 mL buffer each. Finally, the particles were resuspended in 10 mL buffer and stored at −80°C until use. As a reference, the non-grafted PLGA microparticles were treated as stated above, but by solely adding buffer instead of EDAC, NHS, WGA, BSA, and glycine.

Determination of the Amount of Loaded Fluorescent Model Drugs

To quantify the entrapped fluorescein sodium or sulforhodamine, 300 µL aliquots of the microparticle suspensions were hydrolyzed by the addition of 100 µL 4 M NaOH and the fluorescence intensity of the 100 µL aliquots was measured at 485/525 nm (exc./em.) and 580/615 nm (exc./em.) for fluorescein sodium and sulforhodamine, respectively. The amount of the model drug was calculated from a calibration curve established with fluorescein sodium or sulforhodamine in 1 M NaOH.

To determine the amount of entrapped BOD, 150 µL aliquots of the microparticle suspensions were hydrolyzed with 50 µL of 4 M NaOH and diluted 10-fold with a mixture of DMSO and 20 mM HEPES/NaOH pH 7.4 containing 0.1% Pluronic® F-68 (1+8). In 96-well microplates, 100 µL samples were analyzed at 485/525 nm (exc./em.) and the amount of the entrapped BOD was calculated from a calibration curve of BOD in a mixture of DMSO and 20 mM HEPES/NaOH pH 7.4 containing 0.1% Pluronic® F-68 (1+9).

All assays were done at least in triplicate.

Release of the Fluorescent Model Drugs from the Microparticles

To study the release kinetics of the entrapped model drugs, 500 µL suspensions in 20 mM HEPES/NaOH pH 7.4 supplemented with 0.1% Pluronic® F-68, containing either plain- or surface-functionalized particles, were incubated at 4°C and 37°C. At certain time intervals, the supernatants were collected by centrifugation (14000 rpm, 5 min, 4°C) and the amount of released fluorescent dyes was determined fluorimetrically at 485/525 nm (fluorescein sodium and BOD) or at 580/615 nm (sulforhodamine). The percentage of released model drug was calculated with reference to the total dye content of the microparticles.

Cell Cultures

The Caco-2 cell line was purchased from the German collection of microorganisms and cell cultures (DSMZ, Braunschweig, Germany). Cells were cultivated in RPMI 1640 cell culture medium containing 10% fetal calf serum, 4 mM L-glutamine, and 150 mg/mL gentamycine in a humidified 5% CO_2/95% air atmosphere at 37°C and were subcultured by TrypLE® select. Tissue culture reagents were obtained from Sigma Aldrich (St. Louis, USA) and Gibco Life Technologies Ltd. (Invitrogen Corp., Carlsbad, USA). Cells between

passage 60 and 71 were used for the present study. For cell experiments and fluorescence microscopy, 1.7×10^4 Caco-2 single cells were seeded per well using 96-well microplates. Cells were cultivated under standard cell culture conditions for one week to obtain a confluent monolayer.

Cytoadhesion Studies

In order to evaluate the cytoadhesive properties of the microparticles, the particle suspensions were diluted with isotonic 20 mM HEPES/NaOH pH 7.4 to yield 100, 200, 400, and 800 µg particles/mL. After washing the confluent Caco-2 monolayers once with isotonic 20 mM HEPES/NaOH pH 7.4 (100 µL/well), the cells were incubated with 100 µL/well of the microparticle suspension for 30 min at 4°C. After removing the unbound microparticles by washing twice with isotonic 20 mM HEPES/NaOH pH 7.4 (100 µL/well), the relative fluorescence intensities were determined at 485/525 nm for fluorescein sodium and BOD or at 580/615 nm for sulforhodamine. Finally, the amount of the cell-associated particles was calculated from a calibration curve established with the particle suspensions.

Fluorescence Microscopy

Caco-2 monolayers cultivated in 96-well microplates as described above were used for fluorescence microscopy. After washing the confluent Caco-2 monolayers once with isotonic 20 mM HEPES/NaOH pH 7.4 (100 µL/well), the cells were incubated with 100 µL of the microparticle suspension (200 µg particles/mL in isotonic 20 mM HEPES/NaOH pH 7.4) at 4°C for 30 min. Unbound particles were removed by washing the Caco-2 layers twice with isotonic 20 mM HEPES/NaOH pH 7.4 (100 µL/well). Without any further preparations, images of the cell layers were acquired using a Zeiss Axio Observer.Z1 microscopy system equipped with an LED illumination system "Colibri" (Göttingen, Germany).

Authors' Statement

Competing Interests

The authors declare no conflict of interest.

References

[1]   Grama CN, Ankola DD, Ravi Kumar MNV.
       Poly(lactide-co-glycolide) nanoparticles for peroral delivery of bioactives.
       Curr Opin Colloid Interface Sci. 2011; 16: 238–245.
       http://dx.doi.org/10.1016/j.cocis.2010.11.005

[2]   http://www.accessdata.fda.gov/scripts/cder/iig/index.cfm

[3]   Bala I, Hariharan S, Kumar MNVR.
       PLGA nanoparticles in drug delivery: the state of the art.
       Crit Rev Ther Drug Carrier Syst. 2004; 21: 387–422.
       http://dx.doi.org/10.1615/CritRevTherDrugCarrierSyst.v21.i5.20

[4]   Shive MS, Anderson JM.
       Biodegradation and biocompatibility of PLA and PLGA microspheres.
       Adv Drug Deliv Rev. 1997; 28: 5–24.
       http://dx.doi.org/10.1016/S0169-409X(97)00048-3

[5]   Mohamed F, Van der Walle CF.
        Engineering biodegradable polyester particles with specific drug targeting and drug release properties.
        J Pharm Sci. 2008; 97: 71–87.
        http://dx.doi.org/10.1002/jps.21082

[6]   Kumari A, Yadav SK, Yadav SC.
        Biodegradable polymeric nanoparticles based drug delivery systems.
        Colloids Surf B Biointerfaces. 2010; 1: 1–18.
        http://dx.doi.org/10.1016/j.colsurfb.2009.09.001

[7]   Swarnakar NK, Jain AK, Singh RP, Godugu C, Das M, Jain S.
        Oral bioavailability, therapeutic efficacy and reactive oxygen species scavenging properties of
        coenzyme Q10-loaded polymeric nanoparticles.
        Biomaterials. 2011; 32: 6860–6874.
        http://dx.doi.org/10.1016/j.biomaterials.2011.05.079

[8]   Song Z, Feng R, Sun M, Guo C, Gao Y, Li L, Zhai G.
        Curcumin-loaded PLGA-PEG-PLGA triblock copolymeric micelles: Preparation, pharmacokinetics and
        distribution in vivo.
        J Colloid Interf Sci. 2011; 354: 116–123.
        http://dx.doi.org/10.1016/j.jcis.2010.10.024

[9]   Choi KC, Bang JY, Kim PI, Kim C, Song CE.
        Amphotericin B-incorporated polymeric micelles composed of poly(d,l-lactide-co-glycolide)/dextran
        graft copolymer.
        Int J Pharm. 2008; 355: 224–230.
        http://dx.doi.org/10.1016/j.ijpharm.2007.12.011

[10]   Jain S, Mittal A, Jain AK, Mahajan RR, Singh D.
        Cyclosporin a loaded PLGA nanoparticle: Preparation, optimization, In-Vitro characterization and
        stability studies.
        Curr Nanosci. 2010; 6: 422–431.
        http://dx.doi.org/10.2174/157341310791658937

[11]   Betancourt T, Brown B, Brannon-Peppas L.
        Doxorubicin-loaded PLGA nanoparticles by nanoprecipitation: Preparation, characterization and in
        vitro evaluation.
        Nanomedicine (London). 2007; 2: 219–232.
        http://dx.doi.org/10.2217/17435889.2.2.219

[12]   Bies C, Lehr CM, Woodley JF.
        Lectin-mediated drug targeting: history and applications.
        Adv Drug Del Rev. 2004; 56: 425–435.
        http://dx.doi.org/10.1016/j.addr.2003.10.030

[13]   Wirth M, Gerhardt K, Wurm C, Gabor F.
        Lectin-mediated drug delivery: influence of mucin on cytoadhesion of plant lectins in vitro.
        J Control Release. 2002; 79: 183–191.
        http://dx.doi.org/10.1016/S0168-3659(01)00538-7

[14]   Ratzinger G, Agrawal P, Körner W, Lonkai J, Sanders HMHF, Terreno E, Wirth M, Strijkers GJ,
        Nicolay K, Gabor F.
        Surface modification of PLGA nanospheres with Gd-DTPA and Gd-DOTA for high-relaxivity MRI
        contrast agents.
        Biomaterials. 2010; 34: 8716–8723.
        http://dx.doi.org/10.1016/j.biomaterials.2010.07.095

[15]   Ratzinger G, Wang X, M. Wirth M, Gabor F.
        Targeted PLGA microparticles as a novel concept for treatment of lactose intolerance.
        J Control Release. 2010; 147: 187–192.
        http://dx.doi.org/10.1016/j.jconrel.2010.04.017

[16] Roth-Walter F, Schöll I, Untersmayr E, Ellinger A, Boltz-Nitulescu G, Scheiner O, Gabor F, Jensen-Jarolim E.
Mucosal targeting of allergen-loaded microspheres by Aleuria aurantia lectin.
Vaccine. 2005; 23: 2703–2710.
http://dx.doi.org/10.1016/j.vaccine.2004.11.052

[17] Weissenböck A, Wirth M, Gabor F.
WGA-grafted PLGA-nanospheres: Preparation and association with Caco-2 single cells.
J Control Release. 2004; 99: 383–392.
http://dx.doi.org/10.1016/j.jconrel.2004.07.025

[18] Kang J, Kang N, Yu Y, Zhang J, Petersen N, Tian Gf, Nedergaard M.
Sulforhodamine 101 induces long-term potentiation of intrinsic excitability and synaptic efficacy in hippocampal ca1 pyramidal neurons.
Neuroscience. 2010; 169: 1601–1609.
http://dx.doi.org/10.1016/j.neuroscience.2010.06.020

[19] Keegan ME, Falcone JL, Leung TC, Saltzman WM.
Biodegradable microspheres with enhanced capacity for covalently bound surface ligands.
Macromolecules. 2004; 37: 9779–9784.
http://dx.doi.org/10.1021/ma049470u

[20] Gabor F, Stangl M, Wirth M.
Lectin-mediated bioadhesion: binding characteristics of plant lectins on the enterocyte-like cell lines Caco-2, HT-29 and HCT-8.
J Control Release. 1998; 55: 131–142.
http://dx.doi.org/10.1016/S0168-3659(98)00043-1

[21] Desai MP, Labhasetwar V, Walter E, Levy RJ, Amidon GL.
The mechanism of uptake biodegradable microparticles in Caco-2 cells is size dependent.
Pharm Res. 1997; 14: 1568–1573.
http://dx.doi.org/10.1023/A:1012126301290

[22] Shi M, Yang Y-Y, Chaw C-S, Goh S-H, Moochhala SM, Ng S, Heller J.
Double walled POE/PLGA microspheres: encapsulation of water-soluble and water-insoluble proteins and their release properties.
J Control Release. 2003; 89: 167–177.
http://dx.doi.org/10.1016/S0168-3659(02)00493-5

[23] Barichello JM, Morishita M, Takayama K, Nagai T.
Encapsulation of hydrophilic and lipophili drugs in PLGA nanoparticles by the nanoprecipitation method.
Drug Dev Ind Pharm. 1999; 25: 471–476.
http://dx.doi.org/10.1081/DDC-100102197

[24] Faisant N, Siepmann J, Benoit JP.
PLGA-based microparticles: elucidation of mechanisms and a new, simple mathematical model quantifying drug release.
Eur J Pharm Sci. 2002; 15: 355–366.
http://dx.doi.org/10.1016/S0928-0987(02)00023-4

[25] Faisant N, Akiki J, Siepmann F, Benoit JP, Siepmann J.
Effects of the type of release medium on drug release from PLGA-based microparticles: Experiment and theory.
Int J Pharm. 2006; 314: 189–197.
http://dx.doi.org/10.1016/j.ijpharm.2005.07.030

[26] Wang X-Y, Koller R, Wirth M, Gabor F.
Lectin-coated PLGA microparticles: thermoresponsive release and in vitro evidence for enhanced cell interaction.
Int J Pharm. 2012; 436: 738–743.
http://dx.doi.org/10.1016/j.ijpharm.2012.07.025

1.2.2 Impact of stabilizers on surface modification

Influence of stabilizers and preparation procedures on ligand density of PLGA-microparticles

Xue-Yan Wang, Sandra Kubin, Michael Wirth, Franz Gabor

Faculty of Life Sciences, Department of Pharmaceutical Technology and Biopharmaceutics, University of Vienna, Vienna A-1090, Austria

To be submitted to Science of Advanced Materials

Corresponding author:
Franz Gabor
Faculty of Life Sciences, Department of Pharmaceutical Technology and Biopharmaceutics, University of Vienna, Vienna A-1090, Austria
Phone: +43-1-4277-55406
Fax: +43-1-4277-9554
Email: franz.gabor@univie.ac.at

1. FUNCTIONALIZED PLGA-MICROPARTICLES FOR DRUG DELIVERY

Abstract

Targeted drug delivery requires administration of stable surface-functionalized particles but grafting might be counteracted by presence of stabilizers. To elucidate the influence of polyvinylalcohol (PVA), Pluronic® F-68 (PL), and poly(ethylene-*alt*-maleic acid) (PEMA) on ligand density after immobilization, the energy input during solvent evaporation was modified to yield particles in a comparable size range of about 3.5 µm in terms of the surface area mean. The cytoadhesive fluorescent-labeled wheat germ agglutinin was covalently coupled to the carboxylate groups of the PLGA matrix via carbodiimide. Calculation of the ligand density from the surface area mean and fluorescence intensity of immobilized lectin revealed that in case of solvent evaporation in presence of stabilizers the number of immobilized ligand molecules per microparticle followed the order PEMA (21%) > PVA 4 kDa (17%) > PL (13%) > PVA 40 kDa (8%) as compared with spray dried particles prepared without any stabilizer (100%). Cytoadhesion studies with Caco-2 monolayers confirmed retained biorecognitivity of the immobilized targeter and the cell binding rate followed the same ranking as above except for the two types of PVA which changed their places. All in all, PEMA emerged as an alternative stabilizer preferable over well established PVA and PL because it offers additional reactive carboxylates for grafting as well as sufficient stabilization of the microparticles especially in case of hydrophilic drugs as a payload.

Keywords

Introduction

Currently great efforts are focused on the development of micro- and nanoscaled particulate drug delivery systems offering potential benefits such as protection of the API against harmful environment, prolonged release and enhanced solubility of poorly bioavailable drugs. Additionally, different preparation techniques ranging from the lab to the industrial scale enable entrapment of hydrophilic as well as hydrophobic drugs of different molecular weight. An intensively investigated future trend of this concept is the development of site-specific drug delivery systems by structural modification of the surface. Ideally the grafting with biorecognitive ligands would allow specific targeting of cells and tissues, which is supposed to ultimately result in increased efficacy at reduced dosage concurrent with minimized side effects for the patient [1, 2].

For preparation of surface-modified particles, two approaches are currently pursued, either a one step procedure using fully functionalized polymers as a starting material or a two step procedure by surface modification of previously prepared particles. In the latter case, surface functionalization might be counteracted by the presence of stabilizers. On the one hand, stabilizers are inevitably necessary to prevent aggregation, on the other hand they are adsorbed at the surface shielding functional groups required for covalent linkage of ligands.

In order to approach this problem, microparticles are prepared from the copolyester Poly (D,L-lactide-*co*-glycolide) (PLGA), which is most widely used for the preparation of particulate drug delivery systems for oral [3], parenteral [4], dermatological [5], pulmonary [6], nasal [7], and ocular [8] routes as well as diagnostics [9] due to biocompatibility and biodegradability [10]. Among the numerous methods developed for preparation of PLGA-particles, spray drying and solvent evaporation techniques are most frequently applied. In case of spray drying, the droplets of an atomized PLGA solution are dried in a stream of warm air [11. 12]. In case of the solvent evaporation technique, a lipophilic API is dissolved in the organic solution of PLGA (single emulsion technique) whereas a hydrophilic API is dissolved in an aqueous phase and emulsified in an organic PLGA phase (double emulsion technique). The organic solution or emulsion is then emulsified in an outer aqueous phase, which results in the formation of an oil-in-water single emulsion or a water-in-oil-in-water double emulsion, respectively. Subsequently, the organic solvent is evaporated and the liquid droplets increase in density to yield finally solid particles. Both methods, however, require a stabilizer to prevent emulsion breaking and aggregation. Polyvinylalcohol (PVA) and poloxamers, especially poloxamer 188 (Pluronic® F-68), are most frequently applied and they are reported to be incorporated on the particle surface during

preparation, which can affect size, zeta potential, mucoadhesion [13, 14] and particularly surface functionalization.

As potential binding sites are required for functionalisation, the H-type of PLGA is used, which contains free carboxylate groups, and the carbodiimde technique [15] is applied for covalent conjugation of bioadhesive wheat germ agglutinin. Use of the fluorescein-labeled bioadhesive analogue (F-WGA) as a ligand enables both, determination of the coupling efficiency by fluorimetry and estimation of retained biorecognition by cytoadhesion assays using Caco-2 monolayer representing a well-established model of the human intestinal epithelium.

In the present study, PLGA-microparticles are prepared by the double emulsion solvent evaporation technique. Three types of surfactants are used as stabilizers, namely polyvinylalcohol (PVA), poloxamer 188 (Pluronic® F-68) and poly(ethylene-*alt*-maleic acid) (PEMA). According to McCarron et al [16] PVA reduced the coupling rate of polyclonal antibodies to PLGA-nanoparticles by 50%. Additionally, it should be considered that the commonly applied PVA exhibits a molecular weight <100,000 Dalton and represents a heterogeneous mixture of polymer chains with different length [17-19] which influences the properties of formed particles. Therefore, PVA of 31,000 Dalton and 205,000 Dalton and nearly identical polymer components were used in this study. In order to increase the density of carboxylic acid groups on the surface of particles as well as to stabilize the particles, PEMA was also included [20, 21]. For comparison of the influence of stabilizers on the ligand density at the particle surface, spray-dried PLGA-microparticles were also functionalized without any stabilizer [3].

Materials and Methods

Materials

PLGA (poly(D,L-lactide-*co*-glycolide), Resomer® RG503H, 50:50 lactide/glycolide) was bought from Boehringer Ingelheim (Ingelheim, Germany). Poly (ethylene-*alt*-maleic anhydride), Pluronic® F-86, Polyvinyl alcohol 40-88 (PVA 40-88, MW 205,000), and Polyvinyl alcohol 4-88 (PVA 4-88, MW 31,000) were obtained from Sigma Aldrich (Vienna, Austria). Fluorescein-labeled Wheat Germ Agglutinin (F-WGA, molar ratio fluorescein/protein=2.9) from *Triticum vulgare* was purchased from Vector laboratories (Burlingame, USA). All other chemicals were of analytical purity.

Preparation of PLGA-microparticles

PLGA-microparticles were prepared by the water-in-oil-in-water solvent evaporation technique. Briefly, 400 µL distilled water were emulsified with a solution containing 400 mg PLGA in 2.4 g ethyl acetate by sonication. After adding 8 mL 0.5% aqueous solution of different tensides, the emulsion was homogenized again by different procedures in order to prepare particles in a comparable size range: In case of Poly (ethylene-*alt*-maleic acid)(PEMA), which was prepared from Poly (ethylene-*alt*-maleic anhydride) by hydrolysis with 0.2M NaOH [22], the emulsion was sonified (Bandelin electronic UW70/HD70; tip: MS 72/D; Berlin, Germany) for 2 min at 40% intensity. In case of all other surfactants high speed homogenization (ULTRA - TURRAX® T8, IKA, Staufen, Germany) was applied for 6 min at about 25,000rpm (Pluronic F-86®; position #6) or 22,000 rpm (PVA 40-88 and PVA 4-88; position #5). After pouring the (w/o)/w emulsion into 100 mL 0.25% aqueous solution of the corresponding tenside, the particle suspension was stirred at 600 rpm over night at room temperature to evaporate residual ethyl acetate. Finally, the microparticles were washed three times with 120 mL 20mM HEPES/NaOH pH 7.0 and resuspended in 100 mL of the same buffer.

Spray-dried PLGA microparticles were prepared and fractionated according to their size as previously described [3, 23, 24]. Briefly, a 6.5% (w/v) PLGA solution in methylene chloride was spray-dried (Mini Spray Dryer B-191, Buechi Labortechnik AG, Flawil, Switzerland). For size fractionation 100 mg dry particles were dispersed in 10 mL distilled water by sonication and centrifuged at 400 rpm for 2 min. The pellet containing too large particles was discarded and the supernatant was again centrifuged for 10 min at 3200 rpm for 10 min. The supernatant containing mainly nanoscaled particles was discarded and the pellet was re-suspended in 5 mL 20mM HEPES/NaOH 7.0.

The PLGA content of lyophilized aliquots was determined gravimetrically after exhaustive dialysis against distilled water. The particle size distribution was determined using a Malvern Mastersizer 2000 laser particle size analyzer (Malvern Instruments, Malvern, UK).

Surface modification with fluorescein-labeled wheat germ agglutinin

F-WGA was covalently linked to the carboxylate groups on the surface of PLGA-microparticles using a modified carbodiimide method [25]. In brief, a dispersion of 5 mL PLGA-microparticles in 20 mM HEPES/NaOH pH 7.0 was incubated end-over-end for 2 h at room temperature with 2.5 mL of a freshly prepared solution containing 1400 mg 1-ethyl-3(3-dimethylaminopropyl) carbodiimide and 59 mg N-hydroxysuccinimide in the same buffer. The beads containing activated carboxylic groups were washed three times with 20 mM HEPES/NaOH pH 7.4 to remove the excess reagents. After resuspending the microparticles in 5 mL of the same buffer, 500 µL aqueous solution of F-WGA (5 mg/mL) were added followed by end-over-end incubation overnight at room temperature. Non-reacted binding sites were saturated by subsequent incubation with 1.8 mL glycine solution (200 mg/mL in buffer) for 5 h at room temperature. Finally, the microparticles were washed three times by centrifugation to remove excessive reagents, resuspended in 5 mL buffer and stored at -80 °C until use. The mass of modified PLGA-particles was determined gravimetrically as mentioned above.

Quantification of particle-immobilized F-WGA

The amount of surface-bound F-WGA was determined by quantification of the label after dissolving the microparticles. For that purpose, 500 µL suspension containing F-WGA-modified particles were firstly spun down at 3200 rpm for 15 min. and the pellet was hydrolyzed with 500 µL 0.1 M NaOH for 3 days. The relative fluorescence intensities (RFI) of hydrolyzed samples were determined at 485/525 nm using a Tecan Infinite® 200 fluorescence reader (Grödig, Austria) and the amount of immobilized WGA was calculated from the calibration curve of F-WGA.

Calculation of the WGA-density at the particle surface

The surface area A [m^2] and volume V [m^3] of a spherical particle with radius r [m] is calculated according to equation 1.1 and 1.2, respectively:

$$A = 4r^2\pi \tag{1.1}$$

$$V = \frac{4r^3\pi}{3} \tag{1.2}$$

Consequently, the mass of a single particle m [kg] can be calculated from equation 1.3 with ρ [$kg\ m^{-3}$] as the density of the polymer.

$$m = \rho V \tag{1.3}$$

Therefore, the total number of particles N and total surface area A_{total} [m^2] each milligram particles is calculated from equation 1.4 and 1.5, respectively:

$$N = \frac{10^{-6}}{m} \tag{1.4}$$

$$A_{total} = NA \qquad (1.5)$$

Finally, after substitution, the simplified expression is presented by 1.6:

$$A_{total} = \frac{3 \times 10^{-6}}{\rho r} \qquad (1.6)$$

with ρ is 1280 kg m^{-3} in the case of PLGA and r is the Sauter mean diameter D[3,2]. Since the molecular weight of WGA is 36kDa, the number of coupled WGA-molecules per m^2 N_{WGA/m^2} can be calculated from equation 1.7.,

$$N_{WGA/m^2} = \frac{Avagadro's\ number * p * 10^{-6}}{A_{total} * 36000} \qquad (1.7)$$

where p is the ratio of conjugated WGA to PLGA-microparticles [µg/mg] and Avagadro's number is 6.022x10^{23}.

Furthermore, the number of coupled WGA-molecules each PLGA-microparticle ($N_{WGA/MP}$) as another parameter describing the coupling efficiency is calculated according to expression 1.8.:

$$N_{WGA/MP} = \frac{Avagadro's\ number * p * 10^{-6}}{N * 36000} \qquad (1.8)$$

Cell culture

Caco-2 cells were purchased from the German collection of microorganisms and cells (DSMZ, Braunschweig, Germany). Cells were cultivated in RPMI 1640 cell culture medium containing 10% fetal calf serum, 4 mM L-glutamine and 150 mg/mL gentamycine in a humidified 5% CO_2/95% air atmosphere at 37°C and were subcultured by treatment with TrypLE® select. Cells between passage 56 and 87 were used in the present study. For cytoadhesion studies, 1.7 x 10^4 Caco-2 single cells/well were seeded in 96-well microplates. Cells were cultivated under standard cell culture conditions for one week until a confluent monolayer has been formed.

Cytoadhesion Studies

In order to evaluate the particle-cell interactions, PLGA-microparticles were incubated with Caco-2 monolayers. After washing the confluent Caco-2 monolayer once with isotonic 20 mM HEPES/NaOH pH 7.4, the cells were incubated with 100 µL per well of the microparticle suspension (20 µg microparticles) for 30 min at 4 °C. Unbound microparticles were removed by washing twice with the same buffer, and the RFI of the monolayer was determined at 485/525 nm. The amount of the cell-associated particles was calculated from a calibration curve established with F-WGA microparticle suspensions.

Scanning electron microscopy (SEM)

The dry particles were placed on sample holders and coated with gold using Q150R ES rotary-pumped sputter coater (Queorum, UK) at 0.1 mbar and 60 mA for 60 sec. The samples were imaged in high vacuum using a Hitachi Tabletop Microsocpe TM-1000 (Krefeld, Germany).

Results and Discussion

Characterization of PLGA-microparticles

In order to elucidate the influence of stabilizers on the ligand density and subsequently the cytoadhesive properties, PLGA-microparticles were prepared by solvent evaporation in presence and spray drying in absence of a stabilizer. As the surface area is a key parameter the energy input had to be adjusted to obtain particles within a comparable size range. Although the concentration of the stabilizers was kept constant, the characteristics inherent to the stabilizer additionally determine the droplet size when the solvent evaporation technique is applied. Whereas PEMA required highest energy input by ultrasonication to yield particles in the micrometer range, for use of PVA or PL lower dispersing energy by ULTRA - TURRAX® was sufficient (Table 1). Interestingly, emulsification of PVA-containing batches at speed setting #4 yielded larger microparticles, but nanoparticles were obtained at setting #6. Consequently, setting #5 corresponding to about 22,000 rpm was chosen for preparation of both types of PVA-MPs. In case of PL as a stabilizer only a high dispersing energy corresponding to 25,000 rpm resulted in formation of microparticles in desired size range. Such different effects of poloxamer and polyvinyalcohol on particle size are also reported in the literature by different groups. Applying similar preparation techniques, particles using poloxamer 188 as stabilizer were bigger than those prepared with PVA even in the case of nanoparticles [19] and microparticles [18]. The different procedures yielded microparticles in the size range between 2.96 to 7.11 µm (Table 1). As described by Ratzinger et al [3, 27], spray-dried PLGA-particles are highly hydrophobic resulting in formation of aggregates upon dispersion and thus a broader size distribution. In an effort to limit the size distribution, the spray-dried particles were roughly fractionated by centrifugation yielding higher uniformity. In contrast, particles prepared by solvent evaporation were smaller with lower uniformity (Table 1) corresponding to a narrower size distribution. Among the microparticles prepared by solvent evaporation, PVA 4-88 as stabilizer (PVA 4-MPs) yielded the biggest particles that was followed by the order: poly(ethylene-*alt*-maleic acid) particles (PEMA-MPs) > Pluronic® F-68 particles (PL-MPs) > PVA 40-88 particles (PVA 40-MPs). Interstingly the size of PVA 4-MPs exceeded that of PVA 40-MPs. This is might be due to the high molecular weight and an approximately 2-fold higher viscosity of PVA 40-88 as compared to PVA 4-88, which provoked formation of tighter and smaller oily droplets during the second emulsification step and thus yielded smaller particles. SEM images (Figure 1) confirmed these results and displayed smooth particle surfaces.

Usually, the particle size determined by laser diffraction is presented as volume moment mean or De Broukerer mean diameter D[4,3] relying on the volume as a basis for calculation the particle size [28]. However,

for evaluation of the variation of ligand density at the surface due to different stabilizers, the surface area mean or Sauter mean diameter D[3,2] is relevant, since it represents the particle distribution calculated from the surface area [28]. Interestingly, the spray-dried particles exhibited a difference of about 3.2 µm between D[4,3] and D[3,2]. This indicates a broad size distribution with several big particles or aggregates larger than 4 µm, which contribute essentially to D[4,3]. However, most of the batches contained particles around 4 µm contributing strongly to D[3,2]. This result was also confirmed by the uniformity values and SEM images (Figure 1A). Thus, the surface area of particles was meaningful for our purpose and D[3,2] was used as diameter of different PLGA-microparticles for further discussion. Accordingly, the PLGA-microparticles either prepared by solvent evaporation or spray drying yielded a diameter around 3.5 µm in terms of the surface area mean (Table 1).

Quantification of immobilized wheat germ agglutinin on the surface of PLGA-microparticles

The amount of fluorescein-labeled wheat germ agglutinin (F-WGA) immobilized at the surface of PLGA-MPs was quantified fluorimetrically. In order to consider any loss of PLGA-particles during the process, the weight of the modified particles was also determined. The ratios between functionalized WGA and PLGA-particles on a weight basis (p [µg/mg]) are presented in Table 2. The spray-dried microparticles prepared without surfactant yielded the highest amount of WGA per particle, which was more than 2-fold higher than that of particles fabricated by solvent evaporation in presence of stabilizer. Among the particles prepared by the double emulsion technique, the weight ratios between WGA and PLGA-MPs followed the order: PVA 40-MPs > PEMA-MPs > PL-MPs >PVA 4-MPs. Such a weight-related ranking, however, is not reliable for comparison of the stabilizer induced variation of ligand density since the particles possess different size and consequently surface area.

Considering the surface area for calculation of the number of immobilized WGA molecules according to the equations given above revealed that again spray-dried particles contained the highest number of coupled lectin molecules (Table 2). Since the spray-dried particles are characterized by a high ratio p as well as a rather smaller total surface area, which both exert a positive effect on calculation of N_{WGA/m^2}, undoubtedly an excellent coupling efficiency is obtained. However, since PEMA-MPs exceeded PVA 40-MPs, the order of stabilized particles varied now as follows: PEMA-MPs > PVA 40-MPs > PL-MPs >PVA 4-MPs. This alteration in coupling efficiency might be due to the difference in particle size corresponding to the total surface area. At a certain total weight of particles, a larger total surface area is associated with a smaller mean diameter of the particles. According to expression 1.7, the number of coupled lectin/m^2 is proportional to p

however inversely proportional to A_{total}. Therefore, although PVA 40-MPs exhibit a higher coupling ratio p, a lower number of WGA-molecules is immobilized at the surface due to a larger total surface area as compared with PEMA-MPs. Additionally, the difference between MPs prepared in presence and in absence of stabilizer increased concurrently. For instance, the ratio p of PEMA-MPs was 62% lower than that of sprayed-dried particles compared to 70% difference of the value N_{WGA/m^2}. In case of PVA 40-MPs, the difference to surfactant-free particles was 65% for the ratio p and 74% for the value N_{WGA/m^2}. This pronounced decrease in coupling efficiency of particles prepared by the solvent evaporation technique according to the calculation mode might again be due to the same reason as mentioned above.

For further refinement and reliability in describing the ligand density, the number of particles is taken into account. According to expression 1.8, the number of coupled WGA molecules each particle is strongly dependent on the number of MPs (N) of certain weight. Moreover, since all particles were made from PLGA, N is inversely proportional to the diameter r of the particles according to the expressions 1.2 - 1.4. Thus, it is concluded that, the bigger the particles, the smaller is the N which vice versa means that a larger particle can bind more ligands than a smaller one. As expected, among all types of PLGA-MPs, spray-dried particles with the biggest mean diameter yielded the highest amount of WGA functionalized on their surface, whereas PVA 40-MPs possessing the smallest particle size exhibited the lowest lectin-density. Interestingly, although the size of PEMA-MPs was at the upper end of particles prepared by solvent evaporation, the lectin density per particle $N_{WGA/MP}$ was the highest and about 20% higher than that of PVA 4-MPs with the largest mean diameter.

Among all types of particles, the spray-dried particles possessed the highest lectin density since surface exposed carboxylate groups of PLGA were not shielded by stabilizers and were freely accessible for activation and coupling. In case of solvent evaporation, however, stabilizers are necessary to prevent coalescence of the emulsion droplets. Adhesion at the particle surface or even incorporation nearby the surface of might shield the carboxylic end groups of PLGA-chains and decrease the coupling efficiency. As reported by Scholes et al, PVA could not be complete removed even by repeated washings and they suggested physical incorporation of PVA into the nanoparticle surface due to hydrophobic interactions or hydrogen bonding as a reason [13]. Pluronic F-68® is triblock copolymer consisting of a hydrophobic poly(propylene glycol) (PPO) backbone grafted with two hydrophilic poly(ethylene glycol) (PEO) chains. The PEO chains protrude towards the aqueous medium, whereas the PPO moiety adsorbs at the hydrophobic surface of the particles [27, 29]. Depending on the amount of adsorbed Pluronic F-68®, a 'mushroom-like' or 'brush-like' layer is formed [29] with 6 nm in thickness according to Backer et al [30]

or >20 nm as reported by Santander-Ortega et al [31]. Thus, such a surfactant-layer limits access of carboxylic groups of PLGA and counteracts coupling efficiency. In contrast, PEMA offers additional reactive carboxylate groups instead of non-reactive hydroxyls in the case of PVA and Pluronic F-68®. Consequently, PEMA-MPs exhibited the highest ligand density of all particles prepared by solvent evaporation. Moreover, as reported by Keegan et al, the immobilized ligand still remains on the particle surface even after the release of encapsulated proteins. This supports the assumption that during bulk erosion of PLGA-MPs the particle surface is not destroyed immediately and the stabilizer conjugated ligands remain bioreactive at least for a certain period [20]. In accordance with Keegan et al. the results reveal that the use of PEMA is a better choice for preparation of biodegradable particles with functionalized surface and high ligand density than the well established stabilizers PVA and Pluronic®. Nevertheless, it should be considered that the number of coupled ligands on the surface of PEMA-MPs was about a fifth of surfactant-free particles, most likely due to the fact that only part of the carboxylic acid chains of PEMA is accessible for conjugation so that PEMA still exhibits a considerable blocking effect as compared to spray-dried particles. Contrariwise, particles prepared by spray-drying suffer from a broad size distribution, which requires size fractionation associated with low recovery. Additionally, different stabilizers can influence other particle characteristics such as size and biological properties. Particles prepared with PVA for stabilization are usually small and rather uniform in size [32]. Pluronic®-contained particulate carriers possess enhanced mucoadhesive properties [33] and can activate the complement system [34]. Thus, the preparation technique as well as the choice of stabilizer for a certain microparticulate drug delivery system strongly depends on the aim of application.

Evaluation of particle-cell interactions

In order to assess the relationship between WGA-density at the particle surface and bioadhesion, cytoadhesion studies using Caco-2 monolayers as an ex-vivo model were performed. For that purpose, the amount of cell-associated particles referring to the cell-bound RFI is given as percentage of the amount of added particles. After repeated washings the highest binding of microcarriers to the monolayer was observed in case of stabilizer free spray-dried microparticles amounting to 44 ± 8.3 % (Figure 2). In case of PEMA-MPs it roughly halved decreasing to 23 ± 1.5 %. PVA 4-MPs revealed the lowest binding rate to the cell layer, whereas PL-MPs and PVA 40-MPs interacted with the cells to a similar extent. However it should be considered that cytoadhesion depends on both, number of conjugated lectin and the particle size. Generally, big particles possess a large surface area allowing immobilization of a higher number of cytoadhesive ligands and offer a larger contact area to the glycocalyx

of the cells than smaller ones. Contrariwise, big particles need a higher coupling density to survive the strong shear stress during repeated washings. Consequently, comparing the WGA-density at the surface and the percentage of bound particles, PEMA-MPs bind strong enough to the cell surface to withstand detachment by washing. In case of spray dried MPs, a quite higher ligand density is required to remain attached. Although the lectin density of PVA 4-MPs is higher than that of PVA 40-MPs, lower cell-adhesion was observed. Probably the lectin-mediated interaction was too weak so that they were easily washed away. Interestingly, in case of PVA 40-MPs the amount of cell-bound microcarriers is higher than expected as indicated by the lectin-density. Probably, strong non-specific interactions contribute to binding rendering these particles problematic for targeting purposes. All in all, the cytoadhesion studies additionally confirm that PEMA is a stabilizer preferable for site specific microparticles.

Conclusion

Targeted particulate drug delivery requires high ligand density at the surface to enable strong biorecognitive interactions with the intended site of action. Usually first the drug-loaded particles are prepared and their surface is decorated in a second step. Upon covalent immobilization of ligands using reactive groups of the matrix, spray drying is the method of first choice since no stabilizer is required and the particles offer the advantage of non-restricted access for modification provided that the particles do not agglomerate in aqueous dispersion. In case of high hydrophilicity or thermosensitivity of the payload such as drugs from the biotech pipeline, however, the double emulsion technique is an alternative preparation method. Basically, this technique requires stabilizers to yield particles but conversely functional groups are shielded resulting in reduced ligand density. In this study, the carboxylate-rich polymer PEMA was found to fulfill both tasks, sufficient stabilization and thus narrow size distribution of the particles as well as sufficient reactive moieties for functionalization with biorecognitive ligands. The ligand density significantly exceeded that of microparticles prepared with well-established PVA or Pluronic®. Although the minimum ligand density required to accomplish biorecognitive interactions is still unknown, PEMA is proposed as a useful stabilizer even for active targeting of particles.

Acknowledgement

References

[1] O. M. Koo, I. Rubinstein, and H. Onyuksel, Nanomedicine, 1, 193, **(2005)**

[2] I. Brigger, C. Dubernet, and P. Couvreur, Adv. Drug Delivery Rev. 54, 631, **(2002)**

[3] G. Ratzinger, X. WANG, M. Wirth, and F. Gabor, J. Control. Release, 147, 187 **(2010)**

[4] G.S. Das, G.H.R. Rao, R.F. Wilson, and T. Chandy, Drug Delivery 7, 129, **(2000)**

[5] E.G. De Galon, M.J. Blanco-Prieto, P. Ygartua, and S. Santoyo, J. Control. Release 75, 191, **(2001)**

[6] R.M. Seguin, and N. Ferrari, Expert Opin. Investig. Drugs 18, 1505, **(2009)**

[7] N. Csaba, A. Sanchez, and M.J. Alonso, J. Control. Release 113, 164, **(2006)**

[8] T. Moritera, Y. Ogura, N. Yoshimura, Y. Honda, R. Wada, S. Hyon, and Y. Ikada, Invest. Ophthalmol. Vis. Sci. 33, 3125, **(1992)**

[9] G. Ratzinger, P. Agrawal, W. Körner, J. Lonkai, H.M.H.F. Sanders, E. Terreno, M. Wirth, G.J. Strijkers, K. Nicolay, and F. Gabor, Biomaterials 31, 8716, **(2010)**

[10] J.M. Anderson, and M.S. Shive, M.S., Adv. Drug Delivery Rev. 28, 5, **(1997)**

[11] R.C. Mundargi, V.R. Babu, V. Rangaswamy, P. Patel, and T.M. Aminabhavi TM, J. Control. Release 125, 193, **(2008)**

[12] R.A. Jain, Biomaterials 21, 2475, **(2000)**

[13] P.D. Scholes, A.G.A. Coombes, L. Illum, S.S. Davis, J.F. Watts, C. Ustariz, M. Vert, and M.C. Davis, Int. J. Pharm. 59, 261, **(1999)**

[14] S. Feng, and G. Huang, J. Control. Release 71, 53, **(2001)**

[15] G.T. Hermanson, Editor, *Bioconjugate Techniques*. Academic Press, San Diego, **(1996)**

[16] P.A. McCarron, W.M. Marouf, R.F. Donnelly, and C.J. Scott, Biomed. Mater. Res. 87, 873, **(2008)**

[17] J. Vanderwoort, and A. Ludwig, Int. J. Pharm. 238, 77, **(2002)**

[18] T. Feczko, J. Toth, and J. Gyenis, Colloid. Surface. A 319, 188, **(2008)**

[19] K.C. Song, H.S. Lee, I.Y. Choung, K.I. Cho, Y. Ahn, and E.J. Choi, Colloid. Surface. A 276, 162, **(2006)**

[20] M.E. Keegan, J.L. Falcone, T.C. Leung, and W.M. Saltzman, Macromolecules, 37, 9779, **(2004)**

[21] M.E. Keegan, S.M. Royce, T. Fahmy, and W.M. Saltzman, J. Control. Release 110, 572, **(2006)**

[22] B.L. Rivas, S.A. Pooley, E. Pereira, E.Montoya, and R. Cid, J. Appl. Polym. Sci. 101, 2057, **(2006)**

[23] C. Fillafer, G. Ratzinger, J. Neumann, Z. Guttenberg, S. Dissauer, I.K. Lichtscheidl, M. Wirth, F. Gabor, and M.F. Schneider, Lab Chip 9, 2782, **(2009)**

[24] B. Ertl, F. Heigl, M. Wirth, and F. Gabor, J. Drug. Target. 8, 173, **(2000)**

[25] X.-Y. Wang, R. Kollar, M. Wirth, and F. Gabor, Int. J. Pharm. 436, 738, **(2012)**

[26] M.P. Desai,V. Labhasetwar, E. Walter, R.J. Levy, and G.L. Amidon, Pharm Res.

14, 1568, **(1997)**

[27] G. Ratzinger, U. Länger, L. Neutsch, F. Pittner, M. Wirth and F. Gabor, Langmuir 26, 1855 **(2010)**

[28] A. Rawle, *Basic principles of particle size analysis*, Malvern Instruments Limited, Worcestershire, UK. from www.malvern.co.uk

[29] J.-T. Li, K. Caldwell, and N. Rapoport, Langmuir 10, 4475, **(1994)**

[30] J. A. Baker, and J. C. Berg, Langmuir 4, 1055, **(1988)**

[31] M.J. Santander-Ortega, A.B. Jodar-Reyes, N. Csaba, D. Bastos-Gonzalez, and J.L. Ortega-Vinuesa, Colloid Interface Sci. 302, 522, **(2006)**

[32] J. Panyam, and V. Labhasetwar, Adv. Drug Deliver. Rev. 55, 329, **(2003)**

[33] A. Zimmer, P. Chetoni, M. Saettone, H. Zerbe, and J. Kreuter, J. Control. Release, 33, 31, **(1995)**

[34] S. M. Moghimi, A. C. Hunter, C. M. Dadswell, S. Savay, C. R. Alving, and J. Szebeni, Biochimica et Biophysica, 1689, 103, **(2004)**

PLGA-microparticles	Type of surfactants as stabilizers	Molecular weight of surfacant	Preparation technique	D [4,3] Volume moment mean (µm)	D [3, 2] Surface area mean (µm)	Uniformity
PEMA-MPs	poly(ethylene-alt-maleic acid) (PEMA)	100000 - 500000	(w/o)w double emulsion Sonifier with intensity 40%	4.7 ± 0.01	3.2 ± 0.01	0.46
PL-MPs	Pluronic® F-68 (poloxamer 188)	8350	(w/o)w double emulsion ULTRA-TURAXX® #6	3.8 ± 0.08	2.9 ± 0.08	0.40
PVA 40-MPs	polyvinylalcohol (PVA) 40-88	205000	(w/o)w double emulsion ULTRA-TURAXX® #5	2.9 ± 0.01	2.2 ± 0.01	0.47
PVA 4-MPs	polyvinylalcohol (PVA) 4-88	31000	(w/o)w double emulsion ULTRA-TURAXX® #5	5.6 ± 0.01	3.4 ± 0.01	0.51
spray-dried MPs	-	-	Spray drying	7.1 ± 0.02	3.9 ± 0.01	0.73

Table 1. Characteristics of the PLGA-microparticle prepared by different methods.

PLGA-microparticles	Particle surface area (m^2/mg) (A_{total})	µg WGA/ mg PLGA-MPs $(p)(\%)^a$	number of WGA- molecule/m^2 $(N_{WGA/m^2})(\%)^a$	number of WGA- molecule each PLGA-MP $(N_{WGA/MP})(\%)^a$
PEMA-MPs	1.4×10^{-3}	0.6 ± 0.02 (38%)	6.4×10^{15} (30%)	2.2×10^5 (21%)
PL-MPs	1.6×10^{-3}	0.5 ± 0.01 (35%)	5.5×10^{15} (26%)	1.4×10^5 (13%)
PVA 40-MPs	2.1×10^{-3}	0.7 ± 0.01 (47%)	5.6×10^{15} (27%)	0.8×10^5 (8%)
PVA 4-MPs	1.4×10^{-3}	0.4 ± 0.01 (30%)	5.3×10^{15} (25%)	1.8×10^5 (17%)
spray-dried MPs	1.2×10^{-3}	1.5 ± 0.01 (100%)	20.9×10^{15} (100%)	10.4×10^5 (100%)

Table 2 Characteristics of the fluorescence-labeled wheat germ agglutinin (WGA) functionalized PLGA-microparticle.

[a] presented in % related to covalent coupling in the absence of stabilizer by spray drying.
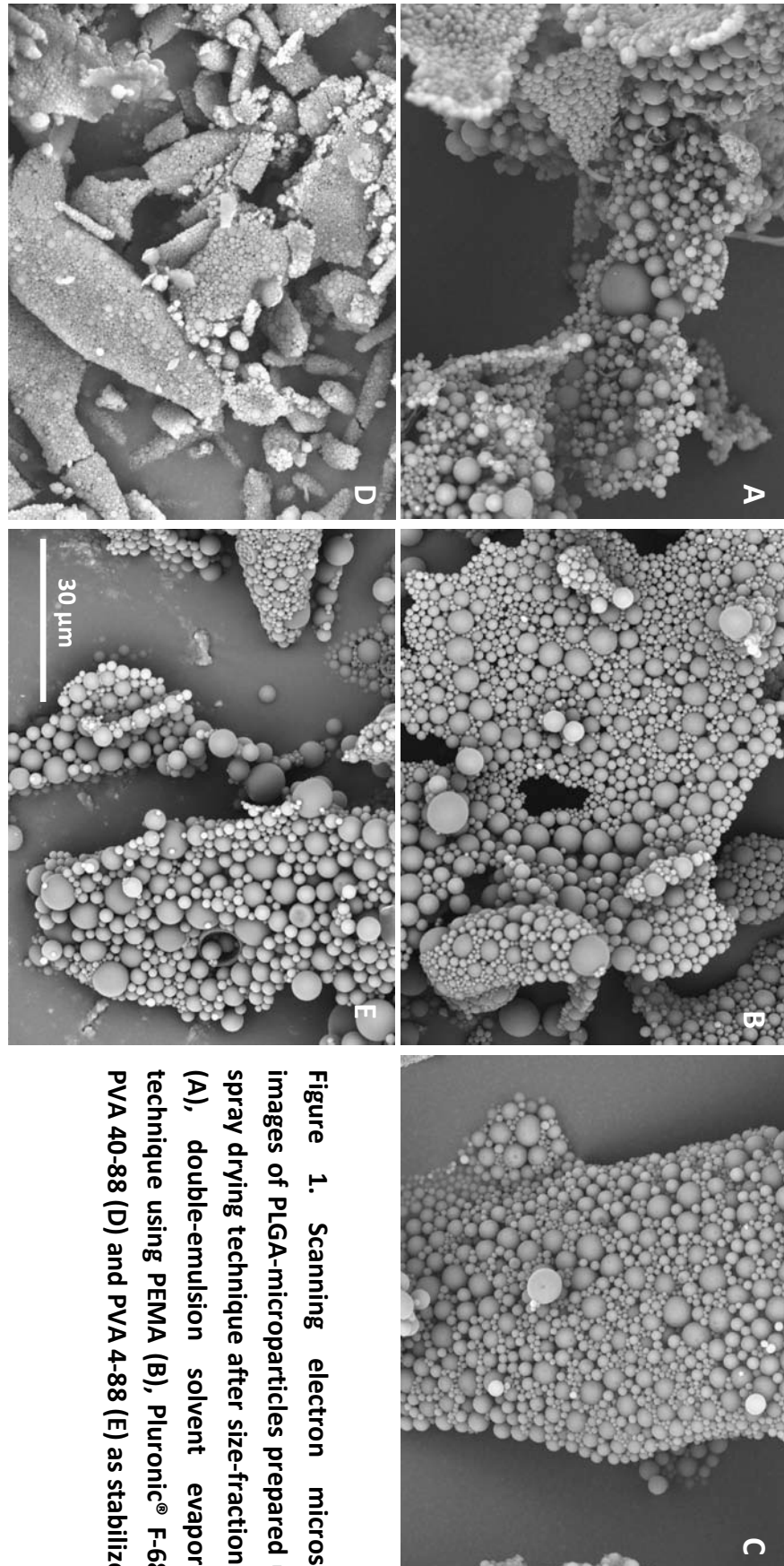
Figure 1. Scanning electron microscopic images of PLGA-microparticles prepared using spray drying technique after size-fractionation (A), double-emulsion solvent evaporation technique using PEMA (B), Pluronic® F-68 (C), PVA 40-88 (D) and PVA 4-88 (E) as stabilizer
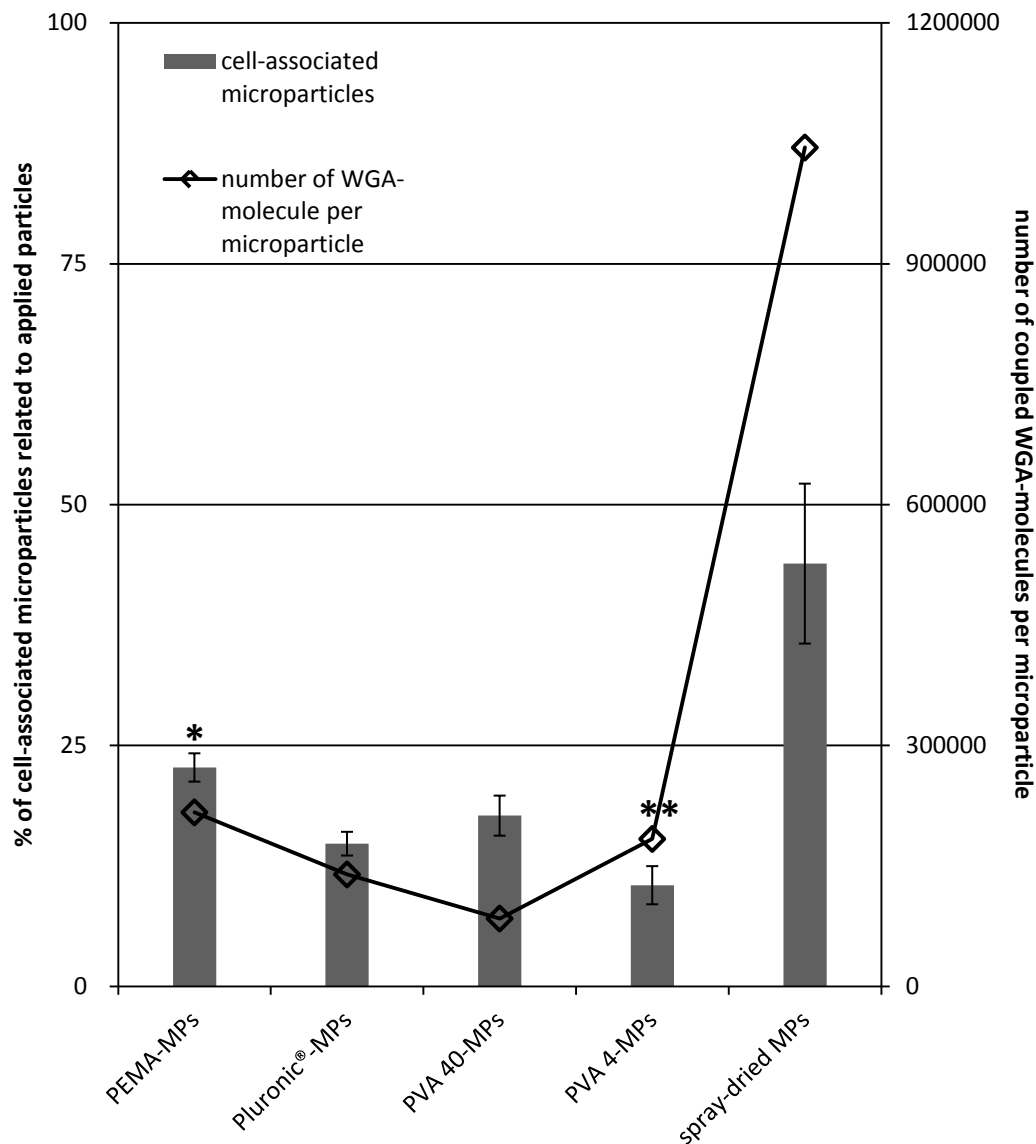
Figure 2. Cytoadhesion studies of fluorescein-labeled wheat germ agglutinin functionalized PLGA-microparticles with Caco-2 monolayers. After 30 min incubation at 4°C and removal of unbound particles, the amount of cell-associated microparticles was determined fluorimetrically. The grey columns refer to the y-axis at the left representing the percentage of the amount of cell-assiociated particles related to the amount of applied microparticles. The diamonds refer to the y-axis at the right representing the number of coupled WGA-molecules per microparticle. The significant difference of the percentage of cell-associated microparticles related to applied particles between PEMA-MPs (p<0.05) and other particles is marked with an asterisk; as well as marked with double asterisks in the case of PVA 4-MPs (p<0.01). (n=4, mean±SD)

1.2.3 Application in oral immunotherapy of allergies

Use of lectin-functionalized particles for oral immunotherapy

Susanne C Diesner[1,2], **Xue-Yan Wang**[3], Erika Jensen-Jarolim[1,4], Eva Untersmayr[1], Franz Gabor[3]

[1]Department of Pathophysiology & Allergy Research, Center of Pathophysiology, Immunology & Infectiology, Medical University of Vienna, Vienna, Austria

[2]Department of Pediatrics & Adolescent Medicine, Medical University of Vienna, Vienna, Austria

[3]Department of Pharmaceutical Technology & Biopharmaceutics, University of Vienna, Althanstrasse 14, 1090 Vienna, Austria

[4]Messerli Research Institute of the Veterinary University Vienna, the Medical University of Vienna & the University of Vienna, Vienna, Austria

R**EVIEW**

Use of lectin-functionalized particles for oral immunotherapy

Immunotherapy, in recent times, has found its application in a variety of immunologically mediated diseases. Oral immunotherapy may not only increase patient compliance but may, in particular, also induce both systemic as well as mucosal immune responses, due to mucosal application of active agents. To improve the bioavailability and to trigger strong immunological responses, recent research projects focused on the encapsulation of drugs and antigens into polymer particles. These particles protect the loaded antigen from the harsh conditions in the GI tract. Furthermore, modification of the surface of particles by the use of lectins, such as *Aleuria aurantia* lectin, wheatgerm agglutinin or *Ulex europaeus*-I, enhances the binding to epithelial cells, in particular to membranous cells, of the mucosa-associated lymphoid tissue. Membranous cell-specific targeting leads to an improved transepithelial transport of the particle carriers. Thus, enhanced uptake and presentation of the encapsulated antigen by antigen-presenting cells favor strong systemic, but also local, mucosal immune responses.

Immunotherapy is a widely accepted and applied therapeutic approach for a range of immunologically mediated diseases including autoimmunity, cancer and allergy. It aims to restore deficient functions of the immune system by the administration of biological substances, which either enhance or suppress immune responses. Although immunotherapy is often applied parenterally, the oral administration route is preferred due to higher compliance of patients and lower complication rates [1]. However, the harsh conditions of the gastrointestinal (GI) environment constitute a substantial challenge for designing immunotherapeutic drugs, which often suffer from low bioavailability when administered via the oral route. Therefore, there have been extensive research efforts to improve and optimize drugs intended for oral application. During recent years, one of these novel approaches has been the encapsulation of therapeutic agents into polymer particles within the nano- or micrometer range in size. These microparticles (MPs) or nanoparticles (NPs) display several features, which make them suitable for oral application and increase bioavailability of encapsulated substances.

Besides describing the characteristics and advantages of polymer particles for **oral immunotherapy**, we will focus on recent studies investigating **lectins** as bioactive substances for functionalizing the surface of particles to improve intestinal uptake in this review.

Preparation techniques of particle carriers for oral immunotherapy

Polymer particles used for oral immunotherapy are often made from polylactide-co-glycolide (PLGA) or polylactide (PLA) not only due to their special carrier properties, but also because of their adjuvant effects [2]. Both PLGA and PLA are characterized by high biocompatibility and biodegradability, as their degradation products are eliminated via the Krebs cycle, which is why their application in human patients has been approved by the US FDA [3–5].

Numerous studies have focused on the development and improvement of the preparation processes for vaccine-loaded particles. It has become apparent that two techniques, the double-emulsion technique and spray-drying technique, are typically being applied today.

The water-in-oil-in-water (w/o/w) or double-emulsion technique allows for entrapment of hydrophilic substances such as vaccines. A small volume of an aqueous vaccine solution is emulsified in a PLGA- or PLA-rich organic solution, for example, dichlormethane or ethyl acetate, to form the primary water-in-oil emulsion. Dispersion of this primary emulsion in an excess of a second, aqueous surfactant solution yields the w/o/w emulsion followed by formation and hardening of the particles due to evaporation or extraction of the organic solvent. The surfactants in use are mostly poly(vinyl alcohol), but also poloxamer 188 (Pluronic® F-68) and poly(ethylene-alt-maleic acid) [6–8].

Susanne C Diesner[1,2], Xue-Yan Wang[3], Erika Jensen-Jarolim[1,4], Eva Untersmayr[1] & Franz Gabor*[3]

[1]Department of Pathophysiology & Allergy Research, Center of Pathophysiology, Immunology & Infectiology, Medical University of Vienna, Vienna, Austria
[2]Department of Pediatrics & Adolescent Medicine, Medical University of Vienna, Vienna, Austria
[3]Department of Pharmaceutical Technology & Biopharmaceutics, University of Vienna, Althanstrasse 14, 1090 Vienna, Austria
[4]Messerli Research Institute of the Veterinary University Vienna, the Medical University of Vienna & the University of Vienna, Vienna, Austria
*Author for correspondence:
E-mail: franz.gabor@univie.ac.at

FUTURE SCIENCE

part of
fsg

Key Terms

Oral immunotherapy: Oral application of drugs and antigens for immunomodulation.

Lectins: (Glyco)proteins selectively binding to carbohydrate residues of epithelial cells' glycocalyx.

PLGA particles: Delivery vehicles composed of polylactic-co-glycolic acid within the micro- or nano-meter range.

Although this w/o/w method is a relatively simple and economic technique [9], the sometimes low encapsulation efficiency or payload as well as the huge initial burst release, because of the limited speed of removal of organic solvent, are disadvantageous [10]. Therefore, different modifications were investigated in order to overcome these obstacles. The solid-in-oil-in-water method differs from the double-emulsion technique in as much as the first aqueous phase is replaced by an aqueous, very fine suspension of the antigen. Since the solid state is most favorable for protein stability and, thus, bioactivity, this technique might be useful for entrapment of unstable antigens [11]. Another variation of w/o/w method is the water-in-oil-in-oil technique, also termed as coacervation method. In this, a nonsolvent is added to the primary emulsion yielding coacervate droplets, which are finally hardened by another organic solvent [12].

The spray-drying technique is a second, widely used method to prepare PLGA or PLA particles. A fine suspension or emulsion containing the vaccine and the polymer is sprayed into the air for atomization and the organic solvent is evaporated at an elevated temperature to yield solid particles. This technique allows easy tuning of particle characteristics and scale-up, but high product loss, especially in small batches, might be crucial [13].

Recently, several new methods to manufacture PLGA or PLA particles have been reported, such as the ultrasonic atomization method [14,15], the electrospray method [16], the microfluidic method [17,18], the pore-closing and thermoreversible-gel method [19,20], and the microfabrication method [21]. Although these innovative techniques are being applied rarely for the preparation of vaccine-loaded particles as of now, they still offer new possibilities for manufacturing particles with improved characteristics.

Characteristics of particles for oral immunotherapy & their fate upon ingestion

The use of particle carriers as an oral-delivery system aims to protect the encapsulated substances and deliver them in an intact form to the immunocompetent cells of the GI tract. Thus, systemic or even mucosal immune responses, when being administered via the mucosal surface, can take place. Under normal conditions, upon ingestion, proteins or carbohydrates are exposed to changing pH levels and digestive enzymes of the oral cavity, stomach, pancreas and bile as well as brush-border hydrolases during GI transit resulting in degradation [22]. Additionally, after mucosal uptake hapten drugs encounter the hepatic first-pass metabolism leading to low bioavailability of active substances [5]. Encapsulation of antigens into particle carriers protects against these harsh GI degrading conditions [23], enabling an intestinal uptake of intact antigens and drugs, and the circumvention of the hepatic first-pass metabolism due to protection of the payload by the particle matrix. Furthermore, functionalization of particles by special targeting substances can direct particle binding to specific cells and enhance the particle uptake capacity via intestinal cells.

In the intestinal mucosa, two different cell types are responsible for the uptake of particulate structures: enterocytes and 'membranous' or 'microfold' cells (M cells). M cells are part of the follicle-associated epithelium overlying the organized gut-associated lymphoid tissue, which can either be located in isolated form or within organized follicular clusters, the so-called Peyer's patches [24,25]. With the loss of brush-border enzymes, such as alkaline phosphatase, M cells show a reduced digestive function, which makes them even more interesting for drug targeting [26,27]. They are mainly responsible for the uptake of intact, particulate structures [28]. Although the proportion of M cells in follicle-associated epithelium of Peyer's patches can be high in rabbits and mini-pigs, the occurrence in rodents (10%) and humans (<5%) is much lower [29]. These cells are responsible for antigen-specific intestinal immune responses by transporting foreign material from the gut lumen to the mucosa-associated lymphatic tissue in an intact form, making them an optimal entry for antigens in oral immunotherapy. The capacity of transcytosis through the intestinal epithelial layer depends on the size, with a particle size of below 1 μm for optimal M-cell absorption [30], but also on the charge and hydrophilicity of the particle carrier [31–33]. Once bound to the apical side of M cells, macromolecules are endocytosed via clathrin-coated vesicles, thereby reaching the lysosomal compartment, from which they are exocytosed to the basolateral site to be taken up by antigen presenting cells (APCs) [34,35].

The particles' size is pivotal for stability, distribution, release of the encapsulated antigens and induction of immune responses [36,37]. Furthermore, the particles' size determines not only the uptake, but also the retention time at

M-cell sites. NPs are rapidly internalized mainly by a process that involves receptor-mediated endocytosis, and are then disseminated systemically [5,38]. In contrast, MPs greater than 5 µm remain trapped in the Peyers patches for up to 35 days [39]. The size of particles able to cross the intestinal barrier has been narrowed down to ranges between 700 nm and 10 µm [40]. In recent *in vitro* studies using the colon carcinoma cell line Caco-2 as an intestinal epithelial model, particles of different sizes from nano- to micro-meter range have been investigated for their interaction with intestinal cells and their properties for cellular uptake. NPs of 100-nm size showed a high interaction rate of more than 6000 PLGA and 200,000 polystyrene (PS) particles per Caco-2 cell. Particles with a size of 1 or 2 µm interacted in very low numbers (12 and below) with one Caco-2 cell [41]. Furthermore, while small NPs were detected intracellularly, also within the nuclei, particles bigger than 300 nm were attached to the apical membrane of Caco-2 cells. Thus, a very small difference in particle size is decisive for either sole cell-binding or even internalization [41]. Upon shuttling of NPs through intestinal epithelial cells encapsulated drugs circumvent the P-glycoprotein efflux from enterocytes and bypass liver metabolism, which enhance their oral bioavailability [42]. Additionally, slight differences of NP size have an impact on the availability of encapsulated drugs in the circulation. Particles with a size of 150 nm show a prolonged circulation time and sustained blood levels compared with particles with a size lower than 100 nm or above 200 nm, which may be taken up by the reticuloendothelial system cells. In comparison, NPs between 100 and 200 nm can escape reticuloendothelial system uptake [5,43]. A further property of PLGA and PLA particles is their negative surface charge [44–45]. As epithelial cells and mucus of the GI tract are negatively charged, the uptake of PLGA and PLA particles without surface modification may be poor. However, positively charging **PLGA particles**, for example using positively charged stabilizers, increases the epithelial penetration and systemic uptake of encapsulated, slightly soluble drugs. These favorable characteristics are not found in particulate carriers prepared with anionic stabilizers [5,46]. Therefore, the characteristics of particles, such as size and surface charge, influence the interaction, uptake and distribution by intestinal epithelial cells. The impact of particle hydrophilicity on intestinal uptake has been described very controversially in literature. Coating of PS particles with poloxamer, which increases hydrophilicity, was demonstrated to decrease the GI uptake [47]. A similar effect was shown for NPs made of polymers with different hydrophilic properties [48]. However, surface modification with poloxamer or particle preparation with different polymers influences the surface charge of the particles, which could contribute to reduced intestinal uptake [49]. A recent study by Gaumet *et al.* reported that modification of surface hydrophilicity by coating PLGA particles with chitosan, which did not affect surface charge or particle size, enhanced the interaction of particles with intestinal Caco-2 cells [49].

Therefore it is obvious that a 'fine-tuning' of particle properties and design by the choice of size and hydrophilicity is substantial for optimizing the uptake and the resulting immunological response. While the intestinal epithelial transport of particles in the nanometer range might be optimal, one has to keep in mind that nanospheres are taken up into the cells with distinct intracellular distribution, which might lead to side effects not yet known.

Immune response triggered by particles

In addition, the type and intensity of the elicited immune response are also influenced by th characteristics of the particle carrier. PLGA is not only a highly biocompatible and biodegradable material, it further affects the immune response via its adjuvant properties [50], which were hypothesized to be due to the particulate structure of the allergen carrier and due to the sustained allergen release from the particles [51]. Various studies demonstrated that the capacity of PLGA particles to act as vaccine adjuvant was high and comparable to the conventional aluminum-adsorbed vaccine formulations [52–54]. Subcutaneously applied NPs encapsulating the birch pollen allergen Bet v1 induced comparable IgG1, IgG2a and IgG2b titers in BALB/c mice as subcutaneous treatment with allergen combined with aluminum [55]. In animal studies, intraperitoneal immunization with PLGA MPs loaded with pollen extract even induced a Th1-dominant immune response including IgG2a antibodies and IFN-γ production by spleen cells [56,57]. In contrast, the widely used vaccine component aluminum hydroxide triggers a Th2-driven immune response. Therefore, the use of PLGA particles for immunomodulating purposes may be beneficial, especially in

situations where the immune system is biased towards a Th2 environment, such as in allergic diseases.

Also with regards to immune response, the particle size determines the outcome. Only MPs between 1 and 10 µm in size promote humoral responses, whereas NPs below 1 µm mainly induce cellular responses (**Figure 1**) [58]. Particle structures smaller than 5 µm are taken up by APCs, such as dendritic cells (DCs) and macrophages [59–61], and are transported directly to the lymph node [58], where the encapsulated antigen can be presented to T cells.

NPs loaded with FITC–bovine serum albumin were shown to be phagocytosed by APCs, leading to a two–threefold increase of cell size, and were then continuously endocytosed and exocytosed from the cells. Thus, only low concentrations of intracellularly released antigen could be observed over time [2]. Interestingly, immunizations with NPs containing hepatitis B surface antigen (HBsAg) led to low production of IgG, secretion of IFN-γ and upregulation of MHC-I on APCs, which indicated the induction of a cellular immune response. The uptake of NPs may result in the production and release of pro-inflammatory cytokines, such as IL-1, IL-5, IL-8, IL-10, IL-18 and TNF-α [62,63]. Semete *et al.*, however, observed no increase in cytokine production [64]. Fluorescent MPs (2–8 µm) were found to attach to the cell surface of APCs in a nonspecific manner [2]. Additionally, the encapsulated antigen is slowly and continuously released into the cell leading to enhanced antibody responses, increased production of IL-4 and upregulation of MHC-II

molecules, which in concert triggers a predominant humoral response. The high concentration of released soluble antigen leads to direct binding of the antigen to MHC-II molecules and subsequent presentation [2]. Besides the different impact on the release pattern of the entrapped antigen by hydrophobic particles in comparison to more hydrophilic carriers, the hydrophobicity of polymer microspheres and a rough surface further increase the attachment to the surface of APCs [65], and enhance the antibody response [66]. Interestingly, the capacity of phagocytosis by macrophages can be increased by coating microspheres with targeting substances, such as wheatgerm agglutinin (WGA), arginine–glycine-aspartic acid-containing peptide or mannose-polyethylene glycol$(PEG)_3$-NH_2 [67].

The uptake of NPs and the intensity of antigen presentation by APCs can be modulated by the use of substances bound to the particle surface, specifically targeting APCs, such as DC-specific intercellular adhesion molecule-3-grabbing nonintegrin (DC-SIGN) antibodies. With this DC-specific targeting approach, antigen-specific cellular responses can be stimulated at 10–100-fold lower particle concentrations than with nontargeted NPs [68]. By the incorporation of fluorescent labeled peptides and the inclusion of iron oxide, encapsulated antigens can be microscopically tracked without the loss of vaccine function. In this study, peptides loaded into NPs, which specifically targeted DC-SIGN on DCs, were found in the lysosomal compartment of DCs within 24 h and were presented to T cells despite the presence of fluorescent labels [68]. Interestingly, the surface modification with a DC-SIGN-specific antibody did not enhance uptake and presentation of MP encapsulated antigens. Recently, NPs' surface modification with an antibody against the DC lectin DEC-205 receptor induced the production of IL-10 by DCs and T cells *in vitro*. When these modified particles were intraperitoneally injected into ovalbumin (OVA) primed mice, a similar IL-10 pattern was observed, which was dependent on the density of surface modification [69]. Previous studies have shown that mannosylated particles can specifically deliver antigens and drugs to DCs and result in enhanced presentation to T cells [70]. When a dimannosyl ligand was used for liposomal vesicles targeting, which contained the Toll-like receptor (TLR)-2 ligand Pam_2CAG for strong immune stimulation and further peptide sequences of ERbB2 and Th-helper epitopes, tumors expressing

Nanoparticles   Microparticles

MHC-I   MHC-II

IFN-γ   IL-4

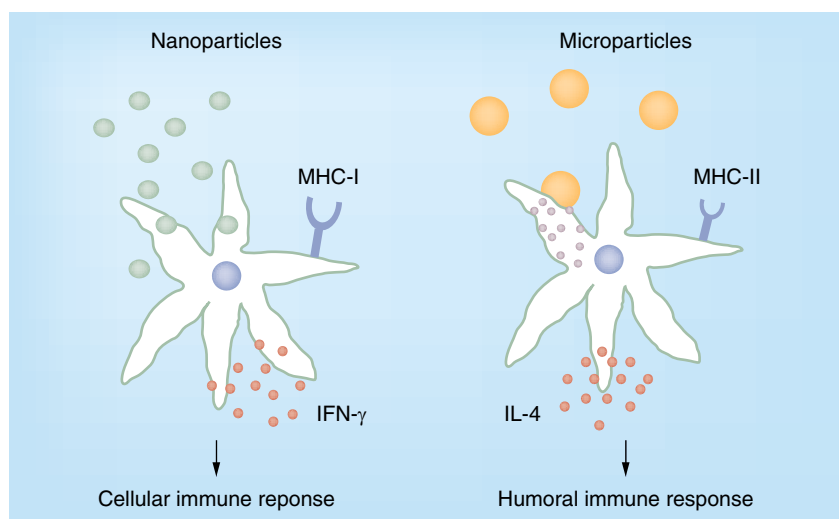Cellular immune reponse   Humoral immune response

Figure 1. Particle-induced immune response.

ErbB2 were eradicated more efficiently in an artificial mouse tumor model [71]. This combination of mannose receptor and TLR targeting beneficially affects the binding to APCs and the stimulation of cellular immune responses. Mannan or PEG coating was shown to protect against protein opsonization, enabling specific receptor-ligand binding. However, mannose coupling to microspheres initiated the phagocytosis by C-type lectin receptor, it could not stimulate DC maturation and activation toward T-cell responses [72].

After the induction of the first immune responses, the longevity of the protective effects after vaccination is determined by the induction of a memory response. The continuous release of inoculated antigens from PLGA particles after the first burst is advantageous to restimulate memory cells and responsible for a long protection time even after one vaccination [52], underlining the beneficial effects of PLGA as a carrier substance for novel vaccination approaches.

Particles for oral immunotherapy

Oral immunomodulation with polymeric particulate carriers has been investigated for a wide range of therapeutic applications, such as immunosuppressive drugs [42], viral and bacterial antigens [58,65], hormones [5,73], anticancer drugs [74], and allergens [75]. The majority of these studies focused on the investigation of PLGA particle carriers loaded with drugs or antigen but without further functionalization of the particle surface for cell targeting in the GI tract.

Recently, it was observed that the encapsulation of antigens into PLGA particles did not only protect from GI digestion, but also initiated specific immune responses by the means of IgG and IFN-γ production at very low antigen amounts [76]. In this study, encapsulation of the food allergen OVA, which was found to be degraded under physiological conditions during the GI transit [77], remained stable when entrapped within PLGA NPs. Oral application of OVA-loaded PLGA nanospheres, which were further coated with PEG to reduce particle aggregation and to enhance particulate blood circulation [78], initiated a high OVA-specific IgG response at very low allergen amounts (5 μg). However, PEGylation of glycan-modified liposomes interfered with the targeting potential to DCs, which has to be taken into consideration for designing novel formulations [79]. Moreover, very low IL-4 and significantly higher IFN-γ production of spleen cells was observed in animals immunized with particles compared with mice being fed unprotected OVA, which was even more pronounced when the β1 integrin on M cells was specifically targeted by an RGD-containing peptide [76].

In order to design PLGA particles as oral therapeutics, the size, lipophilic properties and surface charge have to be taken into consideration. However, the development of these formulations becomes even more complicated when hydrophilic drugs, such as insulin, are subject to encapsulation. This problem can be solved by the use of specific ampholytic surfactants, such as phospholipids. In a recent study, PLGA NPs loaded with insulin for oral application in diabetic rats revealed slower absorption and sustained elimination, while serum insulin concentration steadily increased over 6 h. Thus, the insulin absorption was markedly enhanced by the use of an insulin–soybean phosphatidylcholine complex loaded into PLGA NPs compared with subcutaneous insulin injection [73].

Comparing the oral route with others, a recent study focused on the encapsulation of viruses, such as rotavirus in MPs. PLA and PLGA microspheres containing rotavirus were evaluated for *in vivo* immunogenicity in mice using intranasal and oral administration as different routes of immunization. A single particle administration elicited an increase of systemic rotavirus-specific IgA and IgG antibody titers. Orally applied PLA microspheres induced a more persistent and longer-lasting serum IgA antibody response, which could be explained by the higher hydrophobicity of PLA and the slower polymer degradation. PLGA microspheres showed an improved antibody response when being applied via the intranasal route. However, it is questionable whether antibody titers in serum are significant for protection against rotaviruses as it is well known that mucosal IgA protection is most efficient [80]. Therefore, the authors hypothesized that oral immunization with these microspheres might induce a strong intestinal antibody response, although mucosal IgA levels have not been analyzed in this study [58]. This was also the subject of investigation in a murine study analyzing the systemic and mucosal immune response after oral immunization with *Helicobacter pylori* lysate-loaded PLGA NPs, in order to evaluate their potential as a novel antimicrobial treatment strategy against *H. pylori* infections. Kim *et al.* demonstrated that after two oral administrations of *H. pylori*-PLGA nanospheres, *H. plyori*-specific serum IgG1 and IgG2b levels and gut lavaged IgA were significantly elevated [81].

Another field of application is anticancer therapy with particulate carriers incorporating anticancer drugs [82–83]. It was reported that the bioavailability of chemotherapeutic drugs, such as tamoxifen or doxorubicin, encapsulated in particles significantly increased [83–84]. Furthermore, in a 7,12-dimethylbenz[a]anthracene-induced breast cancer rat model, oral administration of doxorubicin loaded PLGA NPs revealed a higher antitumor efficacy as a result of enhanced bioavailability, tumor permeation and retention effect [74]. In addition, incorporation of doxorubicin into PLGA nanospheres significantly reduced the doxorubicin-induced cardiotoxicity [74].

Targeting via surface bound lectin improves intestinal uptake of particles

While the above mentioned oral application approaches of PLGA particles seem to work appropriately in these experimental models, a further strategy to improve the quality of PLGA carriers is the functionalization of particle surface with bioactive substances. Following this approach, mucosal cells are specifically targeted, thereby improving the cellular uptake as well as transepithelial transport and inducing not only a systemic, but also a strong mucosal immune response.

Enterocytes represent the majority of epithelial cells in the intestinal tract. Thus, enterocyte-specific targeting, for example by WGA, substantially increases the transepithelial transport, which may especially be of interest for drug development where no mucosal immune response induction is needed. Enterocyte-specific targeting induces a rather systemic IgG-mediated immune response [22]. As a second group of intestinal epithelial cells that are of interest, M cells can be specifically addressed by particle functionalization. The idea of M-cell-specific uptake and the induction of subsequent immune responses derives from nature. A number of enteropathogenic microorganisms, such as *Vibrio cholerae* [85,86], *Salmonella typhimurium* [87,88], *Shigella flexneri* [89–91], *Yersinia pseudotuberculosis* and *Yersinia enterocolotica* [92–94], and reoviruses [95], but also nonenteropathogenic pathogens, such as influenza virus A [96], or human immunodeficiency virus-1 (HIV-1) [97], are primarily taken up by M cells, as reviewed by Corr *et al.* [98]. Although underlying mechanisms of the M-cell uptake are in many cases not fully understood to date, it is suspected that pathogens use specific binding approaches to surface structures on M cells to invade the human body via transmucosal transport [99]. Possible interaction partners might be M-cell expressed TLR4, platelet activating factor receptor and α5β1 integrin [100], carbohydrates and Claudin 4. The latter functions as a receptor for Clostridium perfringens enterotoxin (CPE) and has been recent focus for targeting approaches [101]. CPE30, the C-terminal 30 amino acid part of CPE, was coated to PLGA NPs, which increased the uptake by upper airways when administered intranasally or by intestinal M cells after ingestion [101]. However, in depth investigation of pathogen M-cell-binding partners has been quite difficult due to the lack of suitable *in vitro* and *in vivo* models. Due to the low number of M cells in the intestinal tract and due to the inter-species variability in surface receptors [99], results obtained in experimental animal models can only be extrapolated into the human situation when taking into account certain limitation. Furthermore, it has to be kept in mind that the distribution of surface structures on human M cells of different intestinal regions may also differ [24], which may indicate a certain local functionality. Therefore, the most convenient approach for M-cell studies might represent the human M-cell-like co-culture model, where M cells are generated by co-culturing Caco-2 cells, a colon carcinoma cell line with intestinal phenotype, together with Raji-B cells, a cell line derived from Burkitt lymphoma [102]. As this model is based on the use of carcinoma cell lines, it should be noted that epithelial glycosylation patterns in the gut are altered in colon cancer, questioning the value of this experimental model [24]. However, due to the lack of information on M-cell-specific carbohydrate residues in humans, the M-cell-like co-culture model might represent the only valuable experimental model currently available. Using this model, it has become obvious that bacterial and viral transcytosis via M cells might, in some cases, be initiated by a receptor-mediated process [99].

Numerous studies rely on the idea of specifically targeting M cells to increase the mucosal transport. Several bioactive substances, especially lectins, have been the focus of extensive research to date. Lectins are proteins that selectively bind to carbohydrate residues of epithelial cells' glycocalyx and may serve as molecules on particle surface for specifically targeting M cells [103,104].

Lectins, derived from *Ulex europaeus* (UEA-I), *Lycopersicon esculentum* (tomato lectin), *Bandeiraea simplicifolia I*, *Canavalia ensiformis*, *Triticum vulgare* (WGA) and *Aleuria aurantia* lectin (AAL) have been propagated for intestinal cell targeting, however, they differ in

their specificity for the intestinal cell type, as reviewed by Clark [105].

■ WGA for targeting enterocytes

WGA represents a dietary nontoxic lectin, which is contained in wheat flour [22]. WGA specifically binds to *N*-acetyl-D-glucosamine and sialic acid moieties of both, epithelial cells and M cells [106,107]. The usability of WGA-coated, allergen-loaded PLGA microspheres for oral immunotherapy was assessed in animal studies. After two gavages of WGA-coated microspheres, mice revealed a higher allergen-specific IgG production compared with feedings of uncoated particles [108]. However, when the efficacy of WGA-coated allergen-loaded microspheres was evaluated in birch pollen-sensitized mice, oral treatment did not induce an allergen-specific isotype switch towards IgG2a or the production of the Th1 cytokine IFN-γ in comparison to gavages of plain microspheres [74]. Additionally, WGA attached to carbopol has recently been used for surface modification of liposomes, which significantly increased the receptor mediated binding to Caco-2 cells and further enhanced the pharmacological efficacy of calcitonin, when loaded into the nanocarriers [109].

As targeting of orally applied particle carriers to epithelial cells in situations of Th2 modulation does not seem sufficient to trigger immune responses, a M-cell-specific targeting approach may increase the efficiency, because transcytosed particles reach the lymphatic tissue underlying the M cells and induce a strong mucosal, as well as systemic immune response.

■ Concanavalin A for interaction with intestinal epithelial cells & immune cells

Concanavalin A is a lectin from Canavalia ensiformis (Jack bean), which specifically recognizes glycoproteins and glycolipids containing α-D-mannosyl and α-D-glucosyl residues. Concanavalin A can not only interact with the intestinal epithelium but also with immune cells, such as macrophages, resulting in their activation and subsequent upregulation of TLRs as well as the production of NO and proinflammatory cytokines [110–112].

As the lectins listed below bind specifically to α-L-fucose, their use as targeting moieties should result in M-cell-specific adherence.

■ *Ulex europaeus* I

The lectin UEA-I has recently been used for the functionalization of HBsAg incorporating NPs

[113]. These NPs were shown to specifically bind via α-L-fucose to mouse M cells *ex vivo*. After three oral immunizations with UEA-I coated, HBsAg loaded NPs and a booster immunization after 3 weeks, mice developed HBsAg-specific serum antibody titers comparable to levels measured after intramuscular injection of HBsAg adsorbed to aluminum hydroxide. Furthermore, gavages of these UEA-I coated NPs-induced mucosal secretion of sIgA and the production of IL-2 and IFN-γ in spleens, indicating a Th1-dominant immune response [113].

Although UEA-I may be a promising targeting substance, its origin is a highly toxic plant, which makes its beneficial application in humans questionable.

■ *Lotus tetragonolobus*

The *Lotus tetragonolobus* agglutinin (LTA) from Asparagus pea represents another lectin candidate for functionalization of particles. Similar to UEA-I, LTA targets M cells specifically via α-L-fucose. Encapsulation of HBsAg in LTA-coated PLGA NPs can effectively be delivered to murine M cells. Upon oral immunization these particle carriers elicited a significantly higher sIgA response compared with uncoated nanospheres. Furthermore, mice immunized orally with these LTA-coated NPs developed a significantly higher Th1 response by means of IgG2a/IgG1 production ratio compared with intramuscular aluminum hydroxide-based HBsAg injections. This was underlined by higher levels of the Th1 cytokines IFN-γ and IL-2, suggesting the induction of cell-mediated immunity [114].

■ *Aleuria aurantia* lectin

AAL from the edible, nontoxic orange peel mushroom *Aleuria aurantia* also possesses α-L-fucose specificity and, thus, was shown to bind to murine Peyer's patches [115]. Additionally, a common *in vitro* M cell-like co-culture model of human origin was used to confirm AAL binding to human M cells. AAL coating of fluospheres resulted in an increased transcytosis of MPs by M cells compared with plain particles [115]. In the same study, AAL-coated PLGA microspheres induced a high production of the Th1 cytokines IL-2 and IFN-γ compared with only small quantities of IL-5 and IL-10 in peripheral blood mononuclear cells of allergic individuals. These data supported the suitability of AAL-coated microspheres for allergy therapy.

In subsequent studies, AAL-coated PLGA MPs were loaded with an allergen in order to

evaluate their efficacy as oral allergy immunotherapy *in vivo*. Naive BALB/c mice were orally immunized with AAL-coated, birch-pollen-loaded MPs six-times. This oral immunization regimen induced a three-times higher IgG2a antibody response compared with noncoated MPs [116]. The immunotherapeutic efficacy of these AAL functionalized MPs was further evaluated by oral treatment of birch pollen sensitized mice. Animals fed with AAL-functionalized, allergen-loaded microspheres for 15-times revealed an increase of birch pollen-specific IgG2a, whereas IgE and IgG1 were not affected, indicating the induction of a prominent Th1-biased immune response. In addition, spleen cells of animals being treated with AAL MPs via the oral route secreted significantly more T-regulatory cytokine IL-10 and Th1 cytokine IFN-γ [75]. These studies corroborate the potential of AAL functionalized MPs as a novel strategy for oral immunotherapy against Th2-biased diseases, such as allergy.

Although lectin targeting prolongs the retention time in the intestine and may, therefore, improve the mucosal uptake and the subsequent immune response, one has to keep in mind that lectins are often toxic and susceptible to proteolytic degradation in the GI tract, which renders some of them inappropriate for *in vivo* application [105,117]. Several studies have focused on novel approaches to overcome the limitations of the toxicity of lectins, such as UEA-I. The production of recombinant lectins with modified properties but with the same binding characteristics has been described for the recombinant mistletoe lectin [118]. Additionally, synthesized peptides, which mimic function and characteristics of lectins, such as size and stability, have been designed. These are promising novel interaction partners and can reduce costs. A tetragalloyl D-lysine amide construct, as the main compound of two UEA1 mimetics, leads to successful delivery of coated PS particles to mouse M cells and might specifically bind via α-L-fucose [117]. Based on this study, Misumi *et al.* have recently synthesized a tetragalloyl-D-lysine dendrimer (TGDK) and evaluated its use for M-cell binding in nonhuman primates and *in vitro* M cell-like culture model [119]. After gavage of TGDK to rhesus macaques, the dendrimer was efficiently delivered to rhesus Peyer's patches' M cells *in vivo*. Additionally, oral immunization with TGDK-conjugated multiantigens containing bovine serum albumin and a rhesus CCR5-derived

cyclopeptide, which has recently been discussed as an attractive target for mucosal HIV-1 vaccines, elicited mucosal rcDDR5-specific IgA with neutralizing activity. However, dose-finding studies need to be performed in addition to address the functional aspects of these induced autoantibodies [119].

Although these novel approaches of synthesizing lectin mimetics may be promising for future application, the question remains whether synthetic targets are superior to lectins derived from nature, which also feature characteristics suitable for oral application in humans. The targeting substances WGA [120] and AAL are nontoxic and highly resistant against gastric digestion [DIESNER SC, SCHULTZ C, WANG X-Y ET AL., UNPUBLISHED DATA] and enhance the retention time and transepithelial transport of MPs at the GI mucosa, finally resulting in improved efficacy, as reviewed by Des Rieux *et al.* [23].

Preparation of WGA & AAL microspheres

For preparation of WGA- and AAL-grafted MPs, the uncapped type of PLGA-containing terminal carboxylate groups or PLA is used as a matrix for anchorage of the lectins at the particle surface. For coupling, the carbodiimide method is applied, which represents the most popular zero-length cross-linked coupling technique [121]. Here, the carboxylic groups of PLGA or PLA react with *N*-substituted carbodiimides to yield highly reactive, but highly instable *O*-acylisourea intermediates. The latter can react with nucleophiles such as primary amino groups of the lectins to form stable amide bonds yielding isourea as a by-product. To achieve optimum coupling rates, the pH is maintained between 4.5 and 7.5. Usually, the water-soluble 1-ethyl-3-(3-dimethylaminopropyl) carbodiimide is applied, which is dissolved rapidly and used immediately to prevent extensive loss of activity. Furthermore, in presence of *N*-hydroxysuccinimide (NHS) or *N*-hydroxysulfosuccinimide the stability of the active intermediate is extended to a few hours by preventing rapid hydrolysis. Moreover, upon use of NHS, the reaction can be performed in two steps. In the first step, the carboxylic groups are activated with 1-ethyl-3-(3-dimethylaminopropyl) carbodiimide/NHS. After removing the excess coupling reagents by washing, the amine component is added and allowed to react with the active ester. The advantage of this being that the coupling of proteins, which contain

both carboxylate and amine groups, may be improved by avoiding the cross-linking of protein molecules with each other. Altogether, the addition of NHS may improve the efficiency of the reaction [122].

Current highlights & pitfalls of PLGA-based immunotherapy

Irrespective of the route of application, PLGA particles have been further developed for allergy vaccination encapsulating immunomodulatory motives. Beside the above-mentioned studies focusing on lectin-coated microspheres for allergy treatment, recent data indicated the counterbalance of Th2 responses by the use of PLGA particles co-encapsulated with the immunostimulatory TLR9 ligand oligodeoxynucleotide (CpG), protamine and phospholipase A$_2$ from bee venom [123]. Whether or not this approach may be effective in human allergic patients remains to be elucidated as especially the receptor of CpG, TLR9, is diversely expressed in mice, while in humans its expression is restricted to B-cells and plasmayctoid DCs [124], probably leading to different immunological responses.

Further novel approaches of immunomodulation in various diseases, such as infections, autoimmunity and cancer, represent the adoptive immunotherapy [125]. Antigen-specific cytotoxic T cells expand by *ex vivo* stimulation with activated APCs and are subsequently reinfused into patients. The generation and the use of APCs, however, carry the risk for infections and therefore attempts are made to replace them by novel approaches, such as artificial APC (aAPC) systems. In 2008, the concept of aAPCs using PLGA particles encapsulating IL-2 for T-cell stimulation presenting adaptor elements for recognition ligands as well as costimulatory ligands in high density was first introduced [126]. With this aAPC approach, peptide-specific cytotoxic T cells were even more efficiently activated than when using autologous cellular APCs [125]. By the coupling of different peptides and cytokines, aAPC systems based on PLGA particles might represent a promising novel approach for a number of different diseases in the future, inducing a very specific, beneficial T-cell response. Additionally, PLGA particles encapsulating tumor antigen were recently introduced for intracellular loading of DCs, which should then become efficient activators of a cytotoxic anti-tumor T-cell response [127,128].

In contrast with these recently published highlights in the development of novel immunotherapeutical approaches, one should also critically reflect on current research regarding PLGA-based immunotherapies. Due to numerous studies within recent decades, our knowledge on optimizing properties of PLGA particle carriers, such as size, functionalization or preparation methods, has extensively broadened. However, clinical trials in human patients proving the usability of PLGA particles for oral immunotherapy application are still missing, making conclusions on their efficacy and applicability impossible. Due to substantial differences of M-cell distribution and surface receptor expression between mice and men [99], data generated in animal studies might not reflect the situation in humans. The only valuable model currently available, the M cell-like co-culture model, is based on the formation of M cells from the colon cancer cell line, which is known to differently express carbohydrate residues [24]. As data on the expression of specific receptors on human M cells is lacking, the development of M-cell-specific targeting strategies, such as the coating of particles with lectins or lectin mimetics [117,119], might be more difficult than expected. It was even hypothesized that the role of M cells for luminal antigen uptake is overrated as these cells account for only a minority in the intestinal epithelium and might exert diverse functions in different intestinal regions [24], making the field of M-cell targeting even more complex.

Therefore, as long as suitable and physiological M-cell models, as well as human clinical studies are missing, conclusions on the applicability of lectin-functionalized PLGA particles for oral immunotherapy in humans have to be drawn with great caution.

Future perspective

As reviewed in this article, functionalized particles loaded with active agents to be delivered to the gut-associated lymphoid tissue, might represent a successful novel treatment strategy, especially in situations when the immune system is biased towards Th2, such as allergic diseases. Without any doubt, the murine system mirrors only partially the situation in human patients [129]. Therefore, clinical studies to prove the therapeutic efficacy of the proposed novel oral immunotherapy formulations are of paramount importance. However, additional strategies may still be improved in the future. In ongoing

current research efforts to approach the aim of successful oral immunotherapy, two functionalization strategies of particle carriers emerged, being of special interest when screening the scientific literature:

Active targeting of apical receptors on M cells as highlighted by Brayden *et al.* [130]. Since α-L-fucose is part of the sparsely mucus-coated glycocalyx of M cells, binding of active substances can be mediated by lectin-coated formulations. For oral administration, however, these certain lectins have to resist the harsh conditions during GI transit. Additional properties required are nontoxicity as well as non-immunogenicity of the carrier material, which can be achieved by synthetic modification of the carriers or by the careful choice of naturally derived targeting substances, such as WGA and AAL. Furthermore, cellular interaction is mediated by only small units of most complex structured lectin molecules. Thus, undesired effects might be avoided by designing 'neolectins', which represent exclusively the binding domain, by using phage display techniques for example. Nevertheless, one should keep in mind that cell-binding is only the first stage of a complex journey through the epithelial layer to the subjacent immune cells until an efficient immune response is elicited.

The transepithelial uptake as the second step can be enhanced by physical properties of the particulate structure. It is generally accepted that particles below 1 µm are optimally taken up by Peyer's patches and can thus, lead to sufficient antigen processing. Since the volume and, therefore, the loading capacity of MPs by far exceeds that of NPs, the usage of particles in the micrometer range seems to be most suitable in the case of encapsulating large proteins for allergen-specific immunotherapy. Thus, the combination of both targeting strategies using a biodegradable polymeric matrix with adjuvant properties might represent the deciding prerequisite for successful oral immunotherapy in the future but have to be investigated in-depth for their suitability in humans.

Acknowledgements

Executive summary

Preparation techniques of particle carriers for oral immunotherapy

- The double-emulsion technique sometimes yields low payload and huge initial burst release of particles, which might be overcome by the use of solid antigens or coacervation.
- The spray-drying technique allows fine tuning of particle characteristics and easy scaling-up. However, high product loss occurs upon processing of small batches.

Characteristics & gastrointestinal fate of particles for oral immunotherapy

- The particle matrix protects encapsulated antigens from harsh conditions in the GI tract and helps them escape the hepatic first-pass metabolism.
- Positive surface charge facilitates adhesion of particles to the negatively charged cell membrane and hydrophilicity seems to enhance the interaction with cells. Particles <1µm are taken up by M-cells as opposed to epithelial cells, whereas particles >300nm remain bound to the cell membrane and smaller ones accumulate intracellularly.

Immune response triggered by particles

- Polylactide-co-glycolide possesses adjuvant properties comparable to aluminum-adsorbed formulations. In this regard, microparticles trigger a humoral response, whereas nanoparticles elicit a cellular response.
- The sustained release of antigens restimulates memory cells.

Lectin-modified particles for oral immunotherapy

- Lectins can improve uptake and transcellular transport of particles inducing not only a systemic but also a strong mucosal response.
- Wheat-germ agglutinin-grafted microparticles interacting with both M-cells and absorptive enterocytes, induce higher IgG-levels than plain ones.
- Particles modified with α-L-fucose binding lectins such as *Ulex europaeus-I*, *Lotus tetragonolobus* agglutinin and *Aleuria aurantia* lectin induce a Th1-dominant response.

Future challenges

- (Bio)synthesis of nontoxic lectin-mimetics exhibiting gastrointestinal stability, low-molecular weight and high specificity of carbohydrate binding as targeting ligands for site-specific delivery of particles will promote progress in the field.
- Development of preclinical models with glycosylation patterns similar to that in humans and clinical trials in humans will be milestones for further advances in oral immunotherapy.

References

Papers of special note have been highlighted as:
■ of interest
■■ of considerable interest

1   Varma MV, Khandavilli S, Ashokra JY *et al.* Biopharmaceutic classification system: a scientific framework for pharmacokinetic optimization in drug research. *Curr. Drug Metab.* 5(5), 375–388 (2004).

2   Kanchan V, Panda AK. Interactions of antigen-loaded polylactide particles with macrophages and their correlation with the immune response. *Biomaterials* 28(35), 5344–5357 (2007).

3   Scholl I, Kopp T, Bohle B, Jensen-Jarolim E. Biodegradable PLGA particles for improved systemic and mucosal treatment of Type I allergy. *Immunol. Allergy Clin. North Am.* 26(2), 349–364 (2006).

4   Bala I, Hariharan S, Kumar MN. PLGA nanoparticles in drug delivery: the state of the art. *Crit. Rev. Ther. Drug Carrier Syst.* 21(5), 387–422 (2004).

5   Hariharan S, BhardwaJ. V, Bala I, Sitterberg J, Bakowsky U, Ravi Kumar MN. Design of estradiol loaded PLGA nanoparticulate formulations: a potential oral delivery system for hormone therapy. *Pharm. Res.* 23(1), 184–195 (2006).

6   Crotts G, Park TG. Preparation of porous and nonporous biodegradable polymeric hollow microspheres. *J. Control. Release* 35(2–3), 91–105 (1995).

7   Herrmann J, Bodmeier R. Biodegradable, somatostatin acetate containing microspheres prepared by various aqueous and nonaqueous solvent evaporation methods. *Eur. J. Pharm. Biopharm.* 45(1), 75–82 (1998).

8   Tamber H, Johansen P, Merkle HP, Gander B. Formulation aspects of biodegradable polymeric microspheres for antigen delivery. *Adv. Drug Deliver. Rev.* 57(3), 357–376 (2005).

■■   **Describes the different preparation techniques of polymeric formulations for antigen delivery and possible improvements thereof.**

9   Ruan G, Feng SS, Li QT. Effects of material hydrophobicity on physical properties of polymeric microspheres formed by double emulsion process. *J. Control. Release* 84(3), 151–160 (2002).

10   Ye M, Kim S, Park K. Issues in long-term protein delivery using biodegradable microparticles. *J. Control. Release* 146(2), 241–260 (2010).

■   **Describes the current status of protein microencapsulation using biodegradable materials, as well as the comparison of the characteristics of microparticles (MPs) prepared by different techniques.**

11   Castellanos IJ, Crespo R, Griebenow K. Poly(ethylene glycol) as stabilizer and emulsifying agent: a novel stabilization approach preventing aggregation and inactivation of proteins upon encapsulation in bioerodible polyester microspheres. *J. Control. Release* 88(1), 135–145 (2003).

12   Thomasin C, Ho NT, Merkle HP, Gander B. Drug microencapsulation by PLA/PLGA coacervation in the light of thermodynamics. 1. Overview and theoretical considerations. *J. Pharm. Sci.* 87(3), 259–268 (1998).

13   Ratzinger G, Fillafer C, Kerleta V, Wirth M, Gabor F. The role of surface functionalization in the design of PLGA micro- and nanoparticles. *Crit. Rev. Ther. Drug* 27(1), 1–83 (2010).

■■   **Describes current techniques of preparation, characterization and especially surface modification of polylactide-co-glycolide (PLGA) particles.**

14   Felder CH B, Blanco-Prieto MJ, Heizmann J, Merkle HP, Gander B. Ultrasonic atomization and subsequent polymer desolvation for peptide and protein microencapsulation into biodegradable polyesters. *J. Microencapsul.* 20(5), 553–567 (2003).

15   Freitas S, Rudolf B, Merkle HP, Gander B. Flow-through ultrasonic emulsification combined with static micromixing for aseptic production of microspheres by solvent extraction. *Eur. J. Pharm. Biopharm.* 61(3), 181–187 (2005).

16   Berkland C, Pack DW, Kim KK. Controlling surface nanostructure using flow-limited field-injection electrostatic spraying (FFESS) of poly(D,L-lactide-co-glycolide). *Biomaterials* 25(25), 5649–5658 (2004).

17   Hung LH, Teh SY, Jester J, Lee AP. PLGA micro/nanosphere synthesis by droplet microfluidic solvent evaporation and extraction approaches. *Lab. Chip* 10(14), 1820–1825 (2010).

18   Rhee M, Valencia PM, Rodriguez MJ, Langer R, Farokhzad OC, Karnik R. Synthesis of size-tunable polymeric nanoparticles enabled by 3D hydrodynamic flow focusing in single-layer microchannels. *Adv. Mater* 23(12), H79–H83 (2011).

19   Kim HK, Chung HJ, Park TG. Biodegradable polymeric microspheres with 'open/closed' pores for sustained release of human growth hormone. *J. Control. Release* 112(2), 167–174 (2006).

20   Leo E, Ruozi B, Tosi G, Vandelli MA. PLA-microparticles formulated by means a thermoreversible gel able to modify protein encapsulation and release without being co-encapsulated. *Int. J. Pharm.* 323(1–2), 131–138 (2006).

21   Rolland JP, Maynor BW, Euliss LE, Exner AE, Denison GM, Desimone JM. Direct fabrication and harvesting of monodisperse, shape-specific nanobiomaterials. *J. Am. Chem. Soc.* 127(28), 10096–10100 (2005).

22   Gabor F, Bogner E, Weissenboeck A, Wirth M. The lectin-cell interaction and its implications to intestinal lectin-mediated drug delivery. *Adv. Drug Deliv. Rev.* 56(4), 459–480 (2004).

■■   **Detailed description of the intracellular fate of lectins with its implications to drug delivery. Also discussed issues such as toxicity, influence of nutrients and immunogenicity.**

23   Des Rieux A, Fievez V, Garinot M, Schneider YJ, Preat V. Nanoparticles as potential oral delivery systems of proteins and vaccines: a mechanistic approach. *J. Control. Release* 116(1), 1–27 (2006).

24   Giannasca PJ, Giannasca KT, Leichtner AM, Neutra MR. Human intestinal M cells display the sialyl Lewis A antigen. *Infect. Immun.* 67(2), 946–953 (1999).

25   Jepson MA, Clark MA, Hirst BH. M cell targeting by lectins: a strategy for mucosal vaccination and drug delivery. *Adv. Drug Deliv. Rev.* 56(4), 511–525 (2004).

26   Kerneis S, Bogdanova A, Colucci-Guyon E, Kraehenbuhl JP, Pringault E. Cytosolic distribution of villin in M cells from mouse Peyer's patches correlates with the absence of a brush border. *Gastroenterology* 110(2), 515–521 (1996).

27   Tyrer P, Ruth Foxwell A, Kyd J, Harvey M, Sizer P, Cripps A. Validation and quantitation of an *in vitro* M-cell model. *Biochem. Biophys. Res. Commun.* 299(3), 377–383 (2002).

28   Davis IC, Owen RL. The immunopathology of M cells. *Springer Semin. Immunopathol.* 18(4), 421–448 (1997).

29   Buda A, Sands C, Jepson MA. Use of fluorescence imaging to investigate the structure and function of intestinal M cells. *Adv. Drug Deliv. Rev.* 57(1), 123–134 (2005).

30 Brayden DJ, Baird AW. Microparticle vaccine approaches to stimulate mucosal immunisation. *Microbes Infect.* 3(10), 867–876 (2001).

31 Mathiowitz E, Jacob JS, Jong YS *et al.* Biologically erodable microspheres as potential oral drug delivery systems. *Nature* 386(6623), 410–414 (1997).

32 Desai MP, Labhasetwar V, Walter E, Levy RJ, Amidon GL. The mechanism of uptake of biodegradable microparticles in Caco-2 cells is size dependent. *Pharm. Res.* 14(11), 1568–1573 (1997).

33 Florence AT. Nanoparticle uptake by the oral route: fulfilling its potential? *Drug Discov. Today Technol.* 2(1), 75–81 (2005).

34 Neutra MR, Phillips TL, Mayer EL, Fishkind DJ. Transport of membrane-bound macromolecules by M cells in follicle-associated epithelium of rabbit Peyer's patch. *Cell Tissue Res.* 247(3), 537–546 (1987).

35 Tuma PL, Hubbard AL. Transcytosis: crossing cellular barriers. *Physiol. Rev.* 83(3), 871–932 (2003).

36 Lamprecht A, Schafer U, Lehr CM. Size-dependent bioadhesion of micro- and nanoparticulate carriers to the inflamed colonic mucosa. *Pharm. Res.* 18(6), 788–793 (2001).

37 Shakweh M, Besnard M, Nicolas V, Fattal E. Poly (lactide-co-glycolide) particles of different physicochemical properties and their uptake by peyer's patches in mice. *Eur. J. Pharm. Biopharm.* 61(1–2), 1–13 (2005).

38 Sahana DK, Mittal G, BhardwaJ. V, Kumar MN. PLGA nanoparticles for oral delivery of hydrophobic drugs: influence of organic solvent on nanoparticle formation and release behavior *in vitro* and *in vivo* using estradiol as a model drug. *J. Pharm. Sci.* 97(4), 1530–1542 (2008).

39 Eldridge JH, Meulbroek JA, Staas JK, Tice TR, Gilley RM. Vaccine-containing biodegradable microspheres specifically enter the gut-associated lymphoid tissue following oral administration and induce a disseminated mucosal immune response. *Adv. Exp. Med. Biol.* 251, 191–202 (1989).

40 Jani P, Halbert GW, Langridge J, Florence AT. Nanoparticle uptake by the rat gastrointestinal mucosa: quantitation and particle size dependency. *J. Pharm. Pharmacol.* 42(12), 821–826 (1990).

41 Gaumet M, Gurny R, Delie F. Localization and quantification of biodegradable particles in an intestinal cell model: the influence of particle size. *Eur. J. Pharm. Sci.* 36(4–5), 465–473 (2009).

42 Italia JL, Bhatt DK, BhardwaJ. V, Tikoo K, Kumar MN. PLGA nanoparticles for oral delivery of cyclosporine: nephrotoxicity and pharmacokinetic studies in comparison to Sandimmune Neoral. *J. Control. Release* 119(2), 197–206 (2007).

43 Tian J, Yu J. Poly(lactic-co-glycolic acid) nanoparticles as candidate DNA vaccine carrier for oral immunization of Japanese flounder (*Paralichthys olivaceus*) against lymphocystis disease virus. *Fish Shellfish Immunol.* 30(1), 109–117 (2011).

44 Duncanson WJ, Figa MA, Hallock K, Zalipsky S, Hamilton JA, Wong JY. Targeted binding of PLA microparticles with lipid-PEG-tethered ligands. *Biomaterials* 28(33), 4991–4999 (2007).

45 Thomas C, Gupta V, Ahsan F. Influence of surface charge of PLGA particles of recombinant hepatitis B surface antigen in enhancing systemic and mucosal immune responses. *Int. J. Pharm.* 379(1), 41–50 (2009).

46 El-Shabouri MH. Positively charged nanoparticles for improving the oral bioavailability of cyclosporin-A. *Int. J. Pharm.* 249(1–2), 101–108 (2002).

47 Hillery AM, Florence AT. The effect of adsorbed poloxamer 188 and 407 surfactants on the intestinal uptake of 60-nm polystyrene particles after oral administration in the rat. *Int. J. Pharm.* 132(1–2), 123–130 (1996).

48 Win KY, Feng SS. Effects of particle size and surface coating on cellular uptake of polymeric nanoparticles for oral delivery of anticancer drugs. *Biomaterials* 26(15), 2713–2722 (2005).

49 Gaumet M, Gurny R, Delie F. Interaction of biodegradable nanoparticles with intestinal cells: the effect of surface hydrophilicity. *Int. J. Pharm.* 390(1), 45–52 (2010).

50 O'Hagan DT, Singh M. Microparticles as vaccine adjuvants and delivery systems. *Expert Rev. Vaccines* 2(2), 269–283 (2003).

51 Schöll I, Boltz-Nitulescu G, Jensen-Jarolim E. Review of novel particulate antigen delivery systems with special focus on treatment of type I allergy. *J. Control. Release* 104(1), 1–27 (2005).

52 Gupta RK, Chang AC, Siber GR. Biodegradable polymer microspheres as vaccine adjuvants and delivery systems. *Dev. Biol. Stand.* 92, 63–78 (1998).

53 Peyre M, Sesardic D, Merkle HP, Gander B, Johansen P. An experimental divalent vaccine based on biodegradable microspheres induces protective immunity against tetanus and diphtheria. *J. Pharm. Sci.* 92(5), 957–966 (2003).

54 Johansen P, Moon L, Tamber H, Merkle HP, Gander B, Sesardic D. Immunogenicity of single-dose diphtheria vaccines based on PLA/PLGA microspheres in guinea pigs. *Vaccine* 18(3–4), 209–215 (1999).

55 Schöll I, Weissenböck A, Förster-Waldl E *et al.* Allergen-loaded biodegradable poly(D,L-lactic-co-glucolic)acid nanoparticles down-regulate an ongoing Th2 response in the BALB/c mouse model. *Clin. Exp. Allergy* 34(2), 315–321 (2004).

56 Igartua M, Hernandez RM, Gutierro I, Gascon AR, Pedraz JL. Preliminary assessment of the immune response to *Olea europaea* pollen extracts encapsulated into PLGA microspheres. *Pharm. Dev. Technol.* 6(4), 621–627 (2001).

57 Batanero E, Barral P, Villalba M, Rodriguez R. Encapsulation of Ole e 1 in biodegradable microparticles induces Th1 response in mice: a potential vaccine for allergy. *J. Control. Release* 92(3), 395–398 (2003).

58 Nayak B, Ray AR, Panda AK, Ray P. Improved immunogenicity of biodegradable polymer particles entrapped rotavirus vaccine. *J. Biomater. Appl.* 25(5), 469–496 (2011).

59 Torche AM, Le Corre P, Albina E, Jestin A, Le Verge R. PLGA microspheres phagocytosis by pig alveolar macrophages: influence of poly(vinyl alcohol) concentration, nature of loaded-protein and copolymer nature. *J. Drug Target* 7(5), 343–354 (2000).

60 Prior S, Gander B, Blarer N *et al. In vitro* phagocytosis and monocyte-macrophage activation with poly(lactide) and poly(lactide-co-glycolide) microspheres. *Eur J. Pharm. Sci.* 15(2), 197–207 (2002).

61 Luzardo-Alvarez A, Blarer N, Peter K *et al.* Biodegradable microspheres alone do not stimulate murine macrophages *in vitro*, but prolong antigen presentation by macrophages *in vitro* and stimulate a solid immune response in mice. *J. Control. Release* 109(1–3), 62–76 (2005).

62 Chang C. The immune effects of naturally occurring and synthetic nanoparticles. *J. Autoimmun.* 34(3), J234–J246 (2010).

63 Lee HM, Shin DM, Song HM *et al.* Nanoparticles up-regulate tumor necrosis factor-alpha and CXCL8 via reactive oxygen species and mitogen-activated protein kinase activation. *Toxicol. Appl. Pharmacol.* 238(2), 160–169 (2009).

64 Semete B, Booysen Li, Kalombo L *et al. In vivo* uptake and acute immune response to orally administered chitosan and PEG coated PLGA nanoparticles. *Toxicol. Appl. Pharmacol.* 249(2), 158–165 (2010).

65 Nayak B, Panda AK, Ray P, Ray AR. Formulation, characterization and evaluation

of rotavirus encapsulated PLA and PLGA particles for oral vaccination. *J. Microencapsul.* 26(2), 154–165 (2009).

66 Raghuvanshi RR, Katare YK, Lalwani K, Ali MM, Singh O, Panda AK. Improved immune response from biodegradable polymer particles entrapping tetanus toxoid by use of different immunization protocol and adjuvants. *Int. J. Pharm.* 245(1–2), 109–121 (2002).

67 Brandhonneur N, Chevanne F, Vie V *et al.* Specific and nonspecific phagocytosis of ligand-grafted PLGA microspheres by macrophages. *Eur J. Pharm. Sci.* 36(4–5), 474–485 (2009).

68 Cruz LJ, Tacken PJ, Fokkink R *et al.* Targeted PLGA nano- but not microparticles specifically deliver antigen to human dendritic cells via DC-SIGN *in vitro. J. Control. Release* 144(2), 118–126 (2010).

69 Bandyopadhyay A, Fine RL, Demento S, Bockenstedt LK, Fahmy TM. The impact of nanoparticle ligand density on dendritic-cell targeted vaccines. *Biomaterials* 32(11), 3094–3105 (2011).

70 Taylor PR, Gordon S, Martinez-Pomares L. The mannose receptor: linking homeostasis and immunity through sugar recognition. *Trends Immunol.* 26(2), 104–110 (2005).

71 Thomann JS, Heurtault B, Weidner S *et al.* Antitumor activity of liposomal ErbB2/HER2 epitope peptide-based vaccine constructs incorporating TLR agonists and mannose receptor targeting. *Biomaterials* 32(20), 4574–4583 (2011).

72 Wattendorf U, Coullerez G, Voros J, Textor M, Merkle HP. Mannose-based molecular patterns on stealth microspheres for receptor-specific targeting of human antigen-presenting cells. *Langmuir* 24(20), 11790–11802 (2008).

73 Cui F, Shi K, Zhang L, Tao A, Kawashima Y. Biodegradable nanoparticles loaded with insulin-phospholipid complex for oral delivery: preparation, *in vitro* characterization and *in vivo* evaluation. *J. Control. Release* 114(2), 242–250 (2006).

74 Jain AK, Swarnakar NK, Das M *et al.* Augmented anticancer efficacy of doxorubicin loaded polymeric nanoparticles after oral administration in breast cancer induced animal model. *Mol. Pharm.* 8(4), 1140–1151 (2011).

75 Roth-Walter F, Scholl I, Untersmayr E *et al.* M cell targeting with *Aleuria aurantia* lectin as a novel approach for oral allergen immunotherapy. *J. Allergy Clin. Immunol.* 114(6), 1362–1368 (2004).

76 Garinot M, Fievez V, Pourcelle V *et al.* PEGylated PLGA-based nanoparticles

targeting M cells for oral vaccination. *J. Control. Release* 120(3), 195–204 (2007).

77 Diesner SC, Knittelfelder R, Krishnamurthy D *et al.* Dose-dependent food allergy induction against ovalbumin under acid-suppression: a murine food allergy model. *Immunol. Lett.* 121(1), 45–51 (2008).

78 Tang BC, Dawson M, Lai Sk *et al.* Biodegradable polymer nanoparticles that rapidly penetrate the human mucus barrier. *Proc. Natl Acad. Sci. USA* 106(46), 19268–19273 (2009).

79 Joshi MD, Unger WW, Van Beelen AJ *et al.* DC-SIGN mediated antigen-targeting using glycan-modified liposomes: formulation considerations. *Int. J. Pharm.* 416(2), 426–432 (2011).

80 Franco MA, Angel J, Greenberg HB. Immunity and correlates of protection for rotavirus vaccines. *Vaccine* 24(15), 2718–2731 (2006).

81 Kim SY, Doh HJ, Jang MH, Ha YJ, Chung SI, Park HJ. Oral immunization with *Helicobacter pylori*-loaded poly(D, L-lactide-co-glycolide) nanoparticles. *Helicobacter.* 4(1), 33–39 (1999).

82 Astete CE, Sabliov CM. Synthesis and characterization of PLGA nanoparticles. *J. Biomater. Sci. Polym. Ed.* 17(3), 247–289 (2006).

83 Kalaria DR, Sharma G, Beniwal V, Ravi Kumar MN. Design of biodegradable nanoparticles for oral delivery of doxorubicin: *in vivo* pharmacokinetics and toxicity studies in rats. *Pharm. Res.* 26(3), 492–501 (2009).

84 Jain AK, Swarnakar NK, Godugu C, Singh RP, Jain S. The effect of the oral administration of polymeric nanoparticles on the efficacy and toxicity of tamoxifen. *Biomaterials* 32(2), 503–515 (2011).

85 Owen RL, Pierce NF, Apple RT, Cray WW Jr. M cell transport of *Vibrio cholerae* from the intestinal lumen into Peyer's patches: a mechanism for antigen sampling and for microbial transepithelial migration. *J. Infect. Dis.* 153(6), 1108–1118 (1986).

86 Kerneis S, Bogdanova A, Kraehenbuhl JP, Pringault E. Conversion by Peyer's patch lymphocytes of human enterocytes into M cells that transport bacteria. *Science* 277(5328), 949–952 (1997).

87 Clark MA, Jepson MA, Simmons NL, Hirst BH. Preferential interaction of *Salmonella typhimurium* with mouse Peyer's patch M cells. *Res. Microbiol.* 145(7), 543–552 (1994).

88 Jones BD, Ghori N, Falkow S. *Salmonella typhimurium* initiates murine infection by penetrating and destroying the specialized epithelial M cells of the Peyer's patches. *J. Exp. Med.* 180(1), 15–23 (1994).

89 Siebers A, Finlay BB. M cells and the pathogenesis of mucosal and systemic infections. *Trends Microbiol.* 4(1), 22–29 (1996).

90 Gebert A, Rothkotter HJ, Pabst R. M cells in Peyer's patches of the intestine. *Int. Rev. Cytol.* 167, 91–159 (1996).

91 Jensen VB, Harty JT, Jones BD. Interactions of the invasive pathogens *Salmonella typhimurium, Listeria monocytogenes* and *Shigella flexneri* with M cells and murine Peyer's patches. *Infect. Immun.* 66(8), 3758–3766 (1998).

92 Clark MA, Hirst BH, Jepson MA. M-cell surface beta1 integrin expression and invasin-mediated targeting of *Yersinia pseudotuberculosis* to mouse Peyer's patch M cells. *Infect. Immun.* 66(3), 1237–1243 (1998).

93 Grassl GA, Bohn E, Muller Y, Buhler OT, Autenrieth IB. Interaction of *Yersinia enterocolitica* with epithelial cells: invasin beyond invasion. *Int. J. Med. Microbiol.* 293(1), 41–54 (2003).

94 Schulte R, Kerneis S, Klinke S *et al.* Translocation of *Yersinia entrocolitica* across reconstituted intestinal epithelial monolayers is triggered by *Yersinia invasin* binding to beta1 integrins apically expressed on M-like cells. *Cell Microbiol.* 2(2), 173–185 (2000).

95 Helander A, Silvey KJ, Mantis NJ. *et al.* The viral sigma1 protein and glycoconjugates containing alpha2–3-linked sialic acid are involved in type 1 reovirus adherence to M cell apical surfaces. *J. Virol.* 77(14), 7964–7977 (2003).

96 Fujimura Y, Takeda M, Ikai H *et al.* The role of M cells of human nasopharyngeal lymphoid tissue in influenza virus sampling. *Virchows Arch.* 444(1), 36–42 (2004).

97 Fotopoulos G, Harari A, Michetti P, Trono D, Pantaleo G, Kraehenbuhl JP. Transepithelial transport of HIV-1 by M cells is receptor-mediated. *Proc. Natl Acad. Sci. USA* 99(14), 9410–9414 (2002).

98 Corr SC, Gahan CC, Hill C. M-cells: origin, morphology and role in mucosal immunity and microbial pathogenesis. *FEMS Immunol. Med. Microbiol.* 52(1), 2–12 (2008).

99 Kyd JM, Cripps AW. Functional differences between M cells and enterocytes in sampling luminal antigens. *Vaccine* 26(49), 6221–6224 (2008).

100 Azizi A, Kumar A, Diaz-Mitoma F, Mestecky J. Enhancing oral vaccine potency by targeting intestinal M cells. *PLoS Pathog.* 6(11), e1001147 (2010).

101 Rajapaksa TE, Stover-Hamer M, Fernandez X, Eckelhoefer HA, Lo DD. Claudin

4-targeted protein incorporated into PLGA nanoparticles can mediate M cell targeted delivery. *J. Control. Release* 142(2), 196–205 (2010).

102 Gullberg E, Leonard M, Karlsson J. *et al.* Expression of specific markers and particle transport in a new human intestinal M-cell model. *Biochem. Biophys. Res. Commun.* 279(3), 808–813 (2000).

103 Pohlmeyer I, Jorns J, Schumacher U *et al.* Lectin histochemical investigations of the distal gut of chicks with special emphasis on the follicle-associated epithelium. *J. Vet. Med. A Physiol. Pathol. Clin. Med.* 52(3), 138–146 (2005).

104 Hathaway LJ, Kraehenbuhl JP. The role of M cells in mucosal immunity. *Cell Mol. Life Sci.* 57(2), 323–332 (2000).

105 Clark MA, Hirst BH, Jepson MA. Lectin-mediated mucosal delivery of drugs and microparticles. *Adv. Drug Deliv. Rev.* 43(2–3), 207–223 (2000).

106 Takata S, Ohtani O, Watanabe Y. Lectin binding patterns in rat nasal-associated lymphoid tissue (NALT) and the influence of various types of lectin on particle uptake in NALT. *Arch. Histol. Cytol.* 63(4), 305–312 (2000).

107 Wirth M, Hamilton G, Gabor F. Lectin-mediated drug targeting: quantification of binding and internalization of wheat germ agglutinin and *Solanum tuberosum* lectin using Caco-2 and HT-29 cells. *J. Drug Target* 6(2), 95–104 (1998).

108 Walter F, Scholl I, Untersmayr E *et al.* Functionalisation of allergen-loaded microspheres with wheat germ agglutinin for targeting enterocytes. *Biochem. Biophys. Res. Commun.* 315(2), 281–287 (2004).

■ PLGA microspheres were coated with wheatgerm agglutinin and loaded with birch pollen-induced higher levels of allergen-specific IgG after oral administration.

109 Makhlof A, Fujimoto S, Tozuka Y, Takeuchi H. *In vitro* and *in vivo* evaluation of WGA-carbopol modified liposomes as carriers for oral peptide delivery. *Eur. J. Pharm. Biopharm.* 77(2), 216–224 (2011).

110 Leon-Rodriguez L, Leiro-Vidal J, Blanco-Mendez J, Luzardo-Alvarez A. Incorporation of PVMMA to PLGA MS enhances lectin grafting and their *in vitro* activity in macrophages. *Int. J. Pharm.* 402(1–2), 165–174 (2010).

111 Andrade JL, Arruda S, Barbosa T *et al.* Lectin-induced nitric oxide production. *Cell Immunol.* 194(1), 98–102 (1999).

112 Sodhi A, Tarang S, Kesherwani V. Concanavalin A induced expression of Toll-like receptors in murine peritoneal macrophages *in vitro*. *Int. Immunopharmacol.* 7(4), 454–463 (2007).

113 Gupta PN, Khatri K, Goyal AK, Mishra N, Vyas SP. M-cell targeted biodegradable PLGA nanoparticles for oral immunization against hepatitis B. *J. Drug Target* 15(10), 701–713 (2007).

114 Mishra N, Tiwari S, Vaidya B, Agrawal GP, Vyas SP. Lectin anchored PLGA nanoparticles for oral mucosal immunization against hepatitis B. *J. Drug Target* 19(1), 67–78 (2011).

■ *Lotus tetragonolobus* agglutinin-coated PLGA nanoparticles, loaded with hepatitis B surface antigen elicited mucosal and systemic responses.

115 Roth-Walter F, Bohle B, Scholl I *et al.* Targeting antigens to murine and human M-cells with *Aleuria aurantia* lectin-functionalized microparticles. *Immunol. Lett.* 100(2), 182–188 (2005).

■■ In *in vitro* M cell-like co-culture models, MPs with *Aleuria aurantia* lectin specifically target M cells and are taken up more efficiently.

116 Roth-Walter F, Scholl I, Untersmayr E *et al.* Mucosal targeting of allergen-loaded microspheres by *Aleuria aurantia* lectin. *Vaccine* 23(21), 2703–2710 (2005).

■■ In *in vitro* M cell-like co-culture models, MPs with *Aleuria aurantia* lectin specifically target M cells and are taken up more efficiently.

117 Lambkin I, Pinilla C, Hamashin C *et al.* Toward targeted oral vaccine delivery systems: selection of lectin mimetics from combinatorial libraries. *Pharm. Res.* 20(8), 1258–1266 (2003).

118 Eck J, Langer M, Mockel B, Witthohn K, Zinke H, Lentzen H. Characterization of recombinant and plant-derived mistletoe lectin and their B-chains. *Eur. J. Biochem.* 265(2), 788–797 (1999).

119 Misumi S, Masuyama M, Takamune N *et al.* Targeted delivery of immunogen to primate M cells with tetragalloyl lysine dendrimer. *J. Immunol.* 182(10), 6061–6070 (2009).

120 Gabor F, Stangl M, Wirth M. Lectin-mediated bioadhesion: binding characteristics of plant lectins on the enterocyte-like cell lines Caco-2, HT-29 and HCT-8. *J. Control. Release* 55(2–3), 131–142 (1998).

121 Ertl B, Heigl F, Wirth M, Gabor F. Lectin-mediated bioadhesion: preparation, stability and caco-2 binding of wheat germ agglutinin-functionalized poly(D,L-lactic-co-glycolic acid)-microspheres. *J. Drug Target* 8(3), 173–184 (2000).

122 Hermanson GT. *Bioconjugate Techniques*. Academic Press, San Diego, CA, USA 170–176 (1996).

123 Martinez Gomez JM, Fischer S, Csaba N *et al.* A protective allergy vaccine based on CpG- and protamine-containing PLGA microparticles. *Pharm. Res.* 24(10), 1927–1935 (2007).

124 Duthie MS, Windish HP, Fox CB, Reed SG. Use of defined TLR ligands as adjuvants within human vaccines. *Immunol. Rev.* 239(1), 178–196 (2011).

125 Han H, Peng JR, Chen PC *et al.* A novel system of artificial antigen-presenting cells efficiently stimulates flu peptide-specific cytotoxic T cells *in vitro*. *Biochem. Biophys. Res. Commun.* 411(3), 530–535 (2011).

126 Steenblock ER, Fahmy TM. A comprehensive platform for *ex vivo* T-cell expansion based on biodegradable polymeric artificial antigen-presenting cells. *Mol. Ther.* 16(4), 765–772 (2008).

■■ Polylactide-co-glycolide particles were used as artificial antigen-presenting cells for the activation of peptide-specific T cells.

127 Hanlon DJ, Aldo PB, Devine L *et al.* Enhanced stimulation of anti-ovarian cancer CD8(+) T cells by dendritic cells loaded with nanoparticle encapsulated tumor antigen. *Am. J. Reprod. Immunol.* 65(6), 597–609 (2011).

128 Ma W, Smith T, Bogin V *et al.* Enhanced presentation of MHC class Ia, Ib and class II-restricted peptides encapsulated in biodegradable nanoparticles: a promising strategy for tumor immunotherapy. *J. Transl. Med.* 9, 34 (2011).

129 Mestas J, Hughes CC. Of mice and not men: differences between mouse and human immunology. *J. Immunol.* 172(5), 2731–2738 (2004).

130 Brayden DJ, Baird AW. Apical membrane receptors on intestinal M cells: potential targets for vaccine delivery. *Adv. Drug Deliv. Rev.* 56(6), 721–726 (2004).

2

PARTICLE-CELL INTERACTION: IMPACT OF HYDRODYNAMIC DRAG

2.1 BACKGROUND

A.T. Florence has hypothesized that hydrodynamic effects play a substantial role in the interaction between particles and cells or tissues *in vivo* [1]. However, most of the investigations dealing with the interaction between particulate systems and cells *in vitro* are commonly performed under stationary conditions. Consequently, *in vitro*, the binding of particles to the cells is due to deposition of the particles governed by sedimentation and diffusion [2]. In contrast, *in vivo* the extracellular materials such as particles are exposed to hydrodynamic flux and struggles or benefits from hydrodynamic forces. Thus, the stationary experimental set-ups run the risk of underestimation of the effects of different flow conditions in the body and reveal imprecise or probably incorrect results about interaction between particles and cells. Fortunately, nowadays more and more investigations performed that cope with this thematic area of hydrodynamic forces under physiological conditions and continuously improve our current understanding of the interaction of particles with our bodies. For instance, Hammer et al. [3, 4], Goetz et al. [5-7], and Eniola-Adefeso [8] have already published their findings in this area using different flow systems.
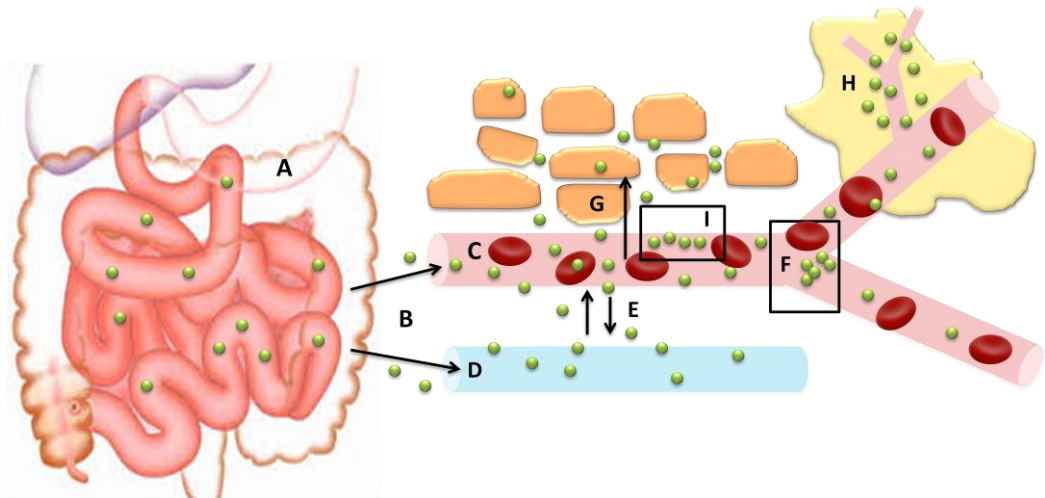

Figure 1. Schematic illustration of places of interests for particles transport in flow. A: flow in the gastrointestinal tract due to peristaltic movement; B: transport of particles to mesenteric lymph and capillaries due to binding to M-cells of Peyer's patches and enterocytes; C: blood flow in the circulatory system; D: flow in the lymph vessels; E: particle transfer between blood and lymph; F: flow characteristics at vessel bifurcations; G: extravasation of particles and flow in tissue; H: enhanced permeation and retention (EPR) effect of particles in tumor vessels; I: vascular adhesion of particles to the wall of blood vessels. [1]

Regarding flow of particles *in vivo*, several situations and processes

should be considered (Figure 1), such as (i) the flow of blood, lymph or interstitial fluid; (ii) the interaction of particles with themselves or with biological components under flow; (iii) the effect of shear forces on particle access to, interaction with and removal from receptors [1]. Among these mentioned areas of interest, the flow of particles in blood vessels is the most investigated topic.

Blood is a suspension of red blood cells (RBCs, erythrocytes), white blood cells (WBCs, leukocytes) and platelets (thrombocytes) in plasma. Since the hematocrit (volume fraction of erythrocytes) is about 40% to 45% in healthy humans, the rheological properties of blood are strongly dependent on RBCs due to their high concentration. Human erythrocytes are biconcave in shape with a mean diameter of about 8 μm and a thickness of 2 μm without nucleus. Since the RBCs are highly deformable, they can easily pass capillaries with diameters even lower than their size [9]. Within a blood vessel the erythrocytes are distributed according to the so-called 'Fahraeus Effect', which describes the accumulation of RBCs accumulate in the center of the vessel and concurrently migration off from the wall [10]. As a consequence, a cell free layer with low hematocrit is formed with varying thickness from >10 μm in capillaries to >100 μm in arterioles [11]. Leukocytes are generally spherical with a mean diameter of about 6-8 μm and less deformable than RBCs. Although the amount of WBCs is about 1000-fold lower than that of RBCs in normal blood [12, 13], leukocytes can also affect the hemodynamic properties of blood especially in the microcirculation. The mechanisms such as leukocyte deformation, entrapment of leukocytes at the entrance to or within vessels, and leukocyte adhesion to the endothelium are supposed to be involved [14-16].

The blood flow in vascular vessels of humans varies extremely. For instance, in elastic arteries the flow velocity is 300 mm s^{-1} as compared to only 0.2 mm s^{-1} in capillaries [17]. Jain et al. demonstrated that the blood flow velocity in arterioles and venules depends on the diameter of the vessels [18]. However, due to great differences between flow velocities in blood vessels, and in an effort to better compare and describe the flow of particles in blood, the shear rate and the shear stress have been introduced as two relevant and important parameters. The shear rate is defined as the rate at which the velocity of a fluid under shear changes through its cross section or the gradient of velocity in a flowing fluid with the unit of reciprocal seconds. For a Newtonian fluid flowing in a pipe, the shear rate can be roughly calculated from the 8-fold fluid velocity divided by the inner diameter of the pipe. The shear stress is calculated by multiplying the shear rate with the viscosity of the flow medium, describing the hydrodynamic forces in the system. According to its calculation, the viscosity of the

medium (*e.g.* blood) is the relevant factor [2]. Martini as well as Fahraeus and Lindaqvist observed that the blood viscosity decreases significantly when the diameter of the used tubes was smaller than 500 μm [10, 19]. Moreover, the blood viscosity is also changed upon certain diseases. For example, the blood viscosity in healthy humans is about 3 mPas, while in case of anemia it decreases to 1.5 mPas.

The endothelium constitutes the inner layer lining the blood vessels and plays an important role in vascular interactions under blood flow. It is involved in a variety of physiological and pathophysiological processes in the course of atherosclerosis [20], diabetes [21], and cancer [22]. Shear stress in blood vessels was observed to induce alteration of gene expression [23], and re-arrangement of the cytoskeletal structure of endothelial cells [24, 25]. More importantly, hydrodynamic flow strongly affects the interaction between leukocytes and endothelial cells occurring during recruitment of leukocytes in response to inflammation inside vascular walls [26].

The expression of adhesion molecules on the surface of the endothelium during inflammation plays a major role in many diseases. In this regard, the selectin group is one of the most interesting groups of adhesion molecules. They are calcium-dependent glycoproteins with an extracellular lectin-like domain and they are classified according to the site of their expression: E- selectin on activated endothelial cells, P-selectin on platelets and endothelial cells, and L-selectin on leukocytes. The 64kDa E-selectin (also known as CD62E, ELAM-1, LECAM-2) is of particular interest, since it triggers recruitment of immune cells during acute or chronic inflammation. Expression of E-selectin is stimulated by TNF-α, IL-1 or bacterial lipopolysaccharides during inflammation and the maximum expression level is reached 4 hours after cytokine stimulation. Subsequently the level drops off very quickly due to internalization by endocytosis as well as lysosomal degradation. Consequently, after 24 hours, E-selectin is no longer detectable. E-selectin interacts with leukocytes via its lectin-like domain and EGF-like domain [27].

Furthermore, the properties of particles can also strongly influence the interaction with cells under hydrodynamic conditions. One of the key parameters is the diameter, which not only determines the internalization rate of particles, but also the mechanism of internalization. Particles smaller than 500 nm or 100 nm as sometimes reported are internalized by endocytosis, while a phagocytic process is required for larger particles >1 μm, which is associated with a more complex rearrangement of the cytoskeleton [28-30]. Moreover, comparing microparticles and nanoparticles, the latter ones are relatively insensitive to effects of shear stress. Since tiny particles offer

a small contact area at the particle/cell interface, the attacking hydrodynamic forces are weak; in case of larger particles, a higher number of ligand-receptor bonds can be formed due to a larger contact area. At the same time, however, the bonds are also more vulnerable and rather broken by shear forces due to the large diameter of the particles [1, 31]. Thus, Decuzzi and Ferrari suggested that there might be an optimum size of particles for adhesion at the surface of cells under hydrodynamic conditions [32].

Another question recently under discussion is whether shape does matter. Probably due to the fact that most of the particles are spherical, the influence of shape on flow properties of particle suspension is currently underestimated [1]. However, nowadays techniques like imprinting are available that allow preparation of custom-shaped non-spherical particles but also nanocrystals [33], carbon nanotubes [34], or nano-rods [35] can possess non-spherical shape. In general, the flow properties of non-spherical particles are dependent on size and shape. These two parameters basically determine their orientation under flow but the orientation can also change over time during transport [31, 36, 37]. For example, due to the ellipsoidal structure of platelets, Mody *et al.* have suggested that, unlike rolling of leukocytes, platelets perform a flipping motion in the blood stream [38]. Therefore, ellipsoidal particles with similar shape like platelets might be interesting to simulate the flow of platelets and their adhesion to the vessel walls [1, 48]. Moreover, internalization can be influenced by the shape of particles. Mitragotri *et al.* have demonstrated that the internalization of gold nano-rods is strongly dependent on the orientation towards the cell membrane, especially by the position of the major axis that can be rectangular or parallel to the cell membrane [39]. Furthermore, the flow properties of elastic particles differ from ones. Elasticity is supposed to allow for the flow of a deformable particle inside a narrow capillary with a smaller diameter than its own [1]. All in all, the transport properties of non-spherical and non-solid particles are subject of current investigations and general principles are presently still not fully elucidated.

Additionally it should be considered that the architecture of blood vessels, especially their bifurcations, is another important issue in terms of hydrodynamics [40-42]. The behavior of particles at bifurcations is more complex than in a non-branched vessel. The particle distribution depends not only on the diameter and flexibility of particles, but also on the flow rates in different branches [1]. A classic solid particle can be trapped or hindered by obstacles and thus the rheological properties of flow would be changed. Moreover, the adsorption of particles to blood constituents or vice versa cannot be prevented. Due to the hydrophobic interactions, albumin, IgG and

fibrinogen from blood can adhere at the surface of particles [43], which is most likely to change the rheological pattern of particle flow.

In order to achieve site-specific drug delivery, surface functionalized particulates are usually investigated for active targeting. In contrast to results collected in stationary experimental set-ups, exposition to hydrodynamic forces resulting from physiological flow is supposed to basically change the interaction between decorated ligands on the surface of the particles and surface receptors of cells. A.T. Florence has predicted that some approaches towards targeted drug delivery arbitrary successful under stationary conditions will fail under flow conditions. For instance, the accelerated movement of particles under flow can offer more contact events and thus facilitate aggregation which impedes accessibility of coupled targeters. Moreover, another consequence might be the detachment of ligands from the surface of particles due to the instability of such targeters. The released ligands, however, can block with the receptors on the cell surface prior to their interaction with particles and prematurely counteract the whole approach [1].

All in all, hydrodynamic forces are an essential physiological parameter that can crucially affect bioadhesion of targeted particulate drug delivery systems to cells and tissues. Thus, development of suitable *in vitro* flow systems is a further important tessella to get a view of the whole mosaic. For this purpose, different fluidic systems have been developed to investigate the impact of hydrodynamics on bioadhesion of particles. They comprise macroscale systems such as parallel plate flow chambers [44], variable-height flow chambers [45], and variable-width linear shear stress flow chambers [46]. Moreover, microscale systems have been established such as microfluidic co-culture migration systems [47], micropatterned substrates for endothelial cell culture in microfluidic channels [48], as well as membrane devices for modeling the airways [49]. Among these versatile devices, microfluidic system based on surface acoustic waves (SAW) is a very attractive strategy, which offers a promising platform for studying the hydrodynamics especially in the human circulatory system. Due to the high potential of such a system, the properties and applications of such SAW-based chip will be discussed in detail.

Surface acoustic wave based microfluidics

A surface acoustic wave (SAW) is a wave that propagates on the surface of a solid and has been described for the first time by Lord Rayleigh in 1885 [50]. Commonly, SAW-technology is used in radio frequency communication [51], chemical and biochemical sensors [52] and optical modulators [53]. Nowadays, SAWs can be generated in a controlled
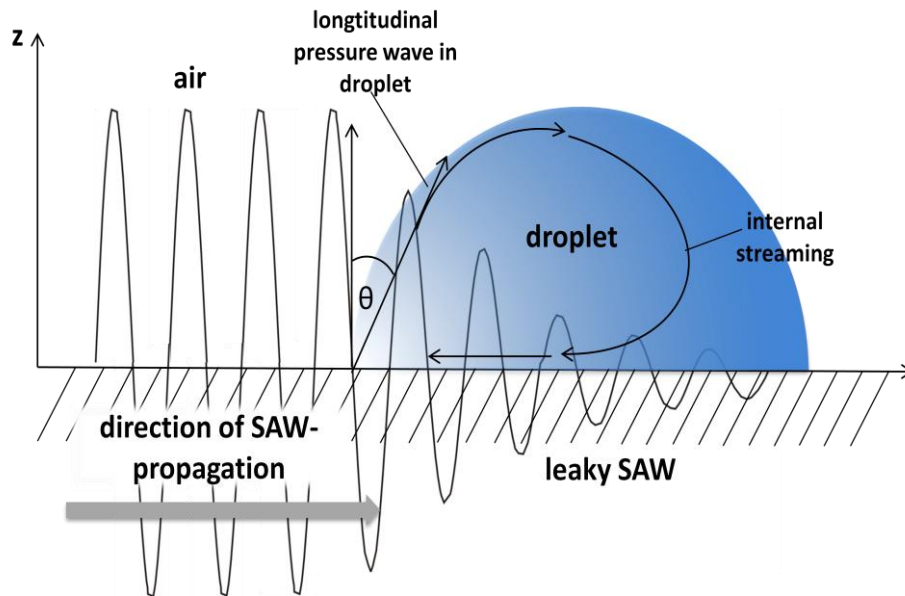
Figure 2. A schematic illustration of the acoustic streaming acting on a small droplet on the surface of a piezoelectric substrate [64, 65]. The SAW is propagating from left to right, and the acoustic energy is radiated into the fluid at the angle θ. Thus, a longitudinal sound wave travels into the fluid leading to streaming inside the droplet.

manner in the nanometer scale using chip technology [2]. For that purpose, interdigital electrodes are deposited by standard lithography and lift off/wet etching processes [54] on a piezoelectric substrate, which serves as an interdigital transducer (IDT). Exciting the interdigital electrodes are at an appropriate frequency results in high frequent deformation of the substrate and a SAW is generated at the surface. Commonly single crystal lithium niobate (LiNbO$_3$) is utilized as a piezoelectric substrate because of its high electromechanical coupling coefficient [54]. When a liquid is in contact with the IDT surface the SAW will cause a pressure difference which generates a longitudinal sound wave in the fluid [2, 55, 56]. The resulting pressure gradient acts as a pumping force and results in streaming (Figure 2). The internal flow streaming deriving from acoustic radiance pressure inside the liquid is aligned either in a clockwise direction in the case of a droplet [57], or in a counter clockwise direction in case of a liquid in a channel [58]. Such SAW-devices offer several advantages that comprise (i) strong forces, extreme accelerations, and fast operation; (ii) simple electrode network and cost-effective fabrications; (iii) simple miniaturization, high reproducibility and programmability [54, 59]. Currently there are two fields of application for SAW-based microfluidics, droplet-based and continuous-flow devices. In case of continuous-flow applications, channel structures are used to confine the liquid. At this, either open channels are fabricated by direct pattern

transfer onto a SU-8 coated substrate [60], or closed channels can be prepared from polymers, usually polydimethylsiloxan (PDMS) [61]. Continuous-flow SAW-devices are applied for micropumping [60-63] in biological test systems. Such pumping at the microscale offers the advantages of flexibility and versatility, since aggressive chemicals can be used without affecting the electrode because there is no direct contact with the liquid. Additionally, the flow can be directed by exact positioning of the IDTs, which offers versatility regarding the size of the channels [54].

The application and further development of an acoustically-driven multichannel microfluidic system will be discussed in the following section, especially parallelizing and studies focused on cytoadhesion of targeted particulate drug carrier systems in the presence of hydrodynamic drag.

REFERENCES

[1] Florence AT. Nanoparticle flow: Implications for drug delivery. In V. P. Torchilin, editor, Nanoparticles as drug carriers, pages 9–27. Imperial College Press, London, **2006.**

[2] Fillafer C. *Bioadhesion of coated particles – the impact of flow probed with acoustically-driven microfluidics* [dissertation]. University of Vienna, Vienna, Austria, **2010.**

[3] Le Ray AM, Vert M, Gautier JC, Benoit JP. Endchain radiolabeling and in vitro stability studies of radiolabeled poly(hydroxyl acid) nanoparticles. *J Pharm Sci.* **1994** 83:845-851.

[4] Eniola AO, Hammer DA. Artificial polymeric cells for targeted drug delivery. *J Control Release*. **2001** 87:15-22.

[5] Sakhalkar HS, Dalal MK, Salem AK, Ansari R, Fu J, Kiani MF, Kurjiaka DT, Hanes J, Schakesheff KM Goetz DJ. Letukocyte-inspired biodegradable particles that selectively and avidly adhere to inflamed endothelium in vitro and in vivo. *P Natl Acad Sci USA*. **2003** 100:15895-15900.

[6] Blackwll JE, Dagia NM, Dickerson JB, Berg EL, Goetz DJ. Ligand coated nanosphere adhesion to e- and p-selectin under static and flow conditions. *Ann Biomed Eng*. **2001** 29:523-33.

[7] Shinde Patil VR, Campbell CJ, Yun YH, Slack SM, Goetz DJ. Particle diameter influences adhesion under flow. *Biophys J*. **2001** 80:1733-1743.

[8] Charoenphol P, Huang RB, Eniola-Adefeso O. Potential role of size and hemodynamics in the efficacy of vascular-targeted spherical drug carriers. *Biomaterials.* **2010** 31: 1392-1402.

[9] Sugihara-Seki M, Fu BM. Blood flow and permeability in microvessel. *Fluid Dyn Res.* **2005** 37:82-132.

[10] Fahraeus R, Lindqvist T. The viscosity of the blood in narrow capillary tubes. *Am J. Physiol.* **1931** 96:562–568.

[11] Sharan M, Popel AS. A two-phase model for flow of blood in narrow tubes with increased effective viscosity near the wall. *Biorheology.* **2001** 38:415–428.

[12] Schmid-Schönbein GW, Sung KP, Tözeren H, Skalak R, Chien S. Passive mechanical properties of human leukocytes. *Biophys. J.* **1981** 36:243–256.

[13] Schmid-Schönbein GW. Leukocyte biophysics. *Cell Biophys.* **1990** 12:107–135.

[14] Eppihimer MJ, Lipowsky HH. Effects of leukocyte–capillary plugging on the resistance to flow in the microvasculature of cremaster muscle for normal and activated leukocytes. *Microvasc Res.* **1996** 51:187–201.

[15] Harris AG, Skalak TC. Leukocyte cytoskeletal structure determines capillary plugging and network resistance. *Am J Physiol*. **1993** 265:H1670–H1675.

[16] Worthen GS, Schwab B, Elson EL, Downey GP. Cellular mechanics of stimulated neutrophil: stiffening of cells induces retention in pores in vitro and lung capillaries in vivo. *Science*. **1989** 245:183–186.

[17] Welsch U. Lehrbuch Histologie. Elsevier, München, 2nd edition, **2006.**

[18] Jain RK. Delivery of molecular medicine to solid tumors: lessons from in vivo imaging of gene expression and function. *J Control Release.* **2001** 74:7-25.

[19] Martini P, Pierach A, Schreyer E. Die Stromung des Blutes in eigen Gefassen. Eine Abweichung vom Poiseuille'schne Gesetz. *Dtsch. Arch. Klin. Med.* **1930** 169:212–222.

[20] Davignon J,Ganz P. Atherosclerosis: Evolving Vascular Biology and Clinical Implications. *Circulation.* **2004** 109:27-32.

[21] Cosentino F, Luscher TF. Endothelial dysfunction in diabetes mellitus. *J. Cardiovasc. Pharmacol.* **1998** 32 Suppl 3:S54-61.

[22] Hicklin DJ, Ellis LM. Role of the vascular endothelial growth factor pathway in tumor growth and angiogenesis. *J Clin Oncol.* **2005** 23:1011-1027.

[23] Braddock M1, Schwachtgen JL, Houston P, Dickson MC, Lee MJ, Campbell CJ. Fluid Shear Stress Modulation of Gene Expression in Endothelial Cells. *News Physiol Sci.* **1998** 13:241-246.

[24] Helmke BP, Davies PF. The Cytoskeleton Under External Fluid Mechanical Forces: Hemodynamic Forces Acting on the Endothelium. *Ann Biomed Eng.* **2002** 30:284-296.

[25] Yap B, Kamm RD. Mechanical deformation of neutrophils into narrow channels induces pseudopod projection and changes in biomechanical properties. *J Appl Physiol (1985).* **2005** 98:1930-1939.

[26] Alon R, Ley K. Cells on the run: shear-regulated integrin activation in leukocyte rolling and arrest on endothelial cells. *Curr Opin Cell Biol.* **2008** 20:525-532.

[27] Jubeli E, Moine L, Vergnaud-Gauduchon J, Barratt G. E-selectin as a target for drug delivery and molecular imaging. *J Control Release.* **2012** 158:194-206.

[28] Rejman J, Oberle V, Zuhorn IS, Hoekstra D. Sizedependent internalization of particles via the pathways of clathrinand caveolae-mediated endocytosis. *Biochem J.* **2004** 377:159–169.

[29] Koval M, Preiter K, Adles C, Stahl PD, Steinberg TH. Size of IgG-Opsonized Particles Determines Macrophage Response during Internalization. *Experimental Cell Res.* **1998** 242:265–273.

[30] Herant M, Heinrich V, Dembo M. Mechanics of neutrophil phagocytosis: experiments and quantitative models. *J Cell Sci.* **2006** 119:1903–1913.

[31] Decuzzi P, Pasqualini R, Arap W, Ferrari M. Intravascular delivery of particulate systems: does geometry really matter? *Pharm Res.* **2009** 26:235-243.

[32] Decuzzi P, Ferrari M. The adhesive strength of nonspherical particles mediated by specific interactions. *Biomaterials.* **2006** 27:5307–5314.

[33] Akerman ME, Chan WC, Laakkonen P, Bhatia SN, Ruoslahti E. Nanocrystal targeting in vivo. *Proc Natl Acad Sci U S A.* **2002** 99:12617-12621.

[34] Baughman RH, Zakhidov AA, de Heer WA. Carbon nanotubes--the route toward applications. *Science.* **2002** 297:787-792.

[35] Chithrani BD, Ghazani AA, Chan WC. Determining the size and shape dependence of gold nanoparticle uptake into mammalian cells. *Nano Lett.* **2006** 6:662–668.

[36] E. Gavze, and M. Shapiro. Motion of inertial spheroidal particles in a shear flow near a solid wall with special application to aerosol transport in microgravity. *J Fluid Mech.* **1998** 371:59–79.

[37] N. Filipovic, B. Stojanovic, N. Kojic, and M. Kojic. Computer modeling in bioengineering-theoretical background. Examples and Software. J. Wiley and Sons, Wiley-Blackwell, **2008.**

[38] Vasanthi R, Bhattacharyya S, Bagchi B. Anisotropic diffusion of spheroids in liquids: Slow orientational relaxation of the oblates. *J Chem Phys.* **2002** 116:1092-1096.

[39] Champion JA, Katare YK, Mitragotri S. Making polymeric micro- and nanoparticles of complex shapes. *Proc. Natl. Acad. Sci. USA.* **2007** 104:11901–11904.

[40] Zhang Z, Kleinstreuer C, Donohue JF, Kim CS. Comparison of micro- and nano-size particle depositions in a human upper airway model. *J Aerosol Sci.* **2005** 36:211-233.

[41] Shi, H.; Kleinstreuer, C.; Zhang, Z.; Kim, C. S. Nanoparticle transport and deposition in bifurcating tubes with different inlet conditions. *Phys Fluids.* **2004** 16:2199-2213.

[42] James SC, Chrysikopoulos CV. Dense colloid transport in a bifurcating fracture. *J Colloid Interface Sci.* **2004** 270:250-254.

[43] Kim D, El-Shall H, Dennis D, Morey T. Interaction of PLGA nanoparticles with human blood constituents. *Colloids Surf B Biointerfaces.* **2005** 40:83-91.

[44] McCue S, Noria S, Langille BL. Shear-induced reorganization of endothelial cell cytoskeleton and adhesion complexes. *Trends Cardiovasc Med.* **2004**

14:143–151.

[45] Xiao Y, Truskey GA. Effect of receptor–ligand affinity on the strength of endothelial cell adhesion. *Biophys J.* **1996** 71:2869–2884.

[46] Usami S, Chen HH, Zhao YH, Chien S, Skalak R. Design and construction of a linear shear-stress flow chamber. *Ann Biomed Eng.* **1993** 21:77–83.

[47] Gutierrez E, Groisman A. Quantitative measurements of the strength of adhesion of human neutrophils to a substratum in a microfluidic device. *Anal Chem.* **2007** 79:2249–2258.

[48] Rhee WS, Taylorv AM, Tu CH, Cribbs DH, Cotman CW, Jeon NL. Patterned cell culture inside microfluidic devices. *Lab Chip.* **2005** 5:102–107.

[49] Huh D, Fujioka H, Tung YC, Futai N, Paine R, Grotberg JB, Takayama S. Gravity-driven microfluidic particle sorting device with hydrodynamic separation amplification. *Anal Chem.* **2007** 79:1369-1376.

[50] Lord Rayleigh. On waves propagated along the plane surface of an elastic solid. *P Lond Math Soc.* **1885** 17:4-11.

[51] Campbell CK. Surface Acoustic Wave Devices for Mobile and Wireless Communications. Academic Press. Inc.: Orlando, FL, USA, **1998.**

[52] Dessy R. Surface acoustic wave probe for chemical analysis. I. Introduction and instrument description. *Anal. Chem.* **1979** 51:1458-1464.

[53] Yariv A, Yeh P. Optical Waves In Crystals: Propagation And Control Of Laser Radiation; John Wiley and Sons: New York, **1984.**

[54] Luong TD, Nguyen NT. Surface acoustic wave driven microfluidics – a review. *Mater Res Soc Sym P.* **2010** 2:1876-4029.

[55] Franke TA. Wixforth A. Microfluidics for miniaturized laboratories on a chip. *Chem Phys Chem.* **2008** 9:2140-2156.

[56] Fillafer C, Ratzinger G, Neumann J, Guttenberg Z, Dissauer S, Lichtscheidl IK, Wirth M, Gabor F, Schneider MF. An acoustically-driven biochip – impact of flow on the cell-association of targeted drug carriers. *Lab chip.* **2009** 9:2782-2788.

[57] Wixforth A. Acoustically Driven Programmable Microfluidics for Biological and Chemical Applications. *JALA – J. Assoc. Lab. Auto*. **2006** 11:399-405.

[58] Nguyen NT, White RM. Acoustic streaming in micromachined flexural plate wave devices: numerical simulation and experimental verification. *IEEE Trans Ultrason Ferroelectr Freq Control.* **2000** 47:1463-1471.

[59] Yeo LY, Friend JR. Surface Acoustic Wave Microfluidics. *Annu Rev Fluid Mech.* **2014** 46:379–406.

[60] Saiki T, Okada K, Utsumi Y. In Proposal of a novel liquid flow actuator for lab-on-chips operated by surface acoustic wave. Kyoto. pp 332-333. **2007.**

[61] Fukuoka D, Utsumi Y. Fabrication of the cyclical fluid channel using the surface acoustic wave actuator and continuous fluid pumping in the cyclical fluid channel. *Microsyst Technol.* **2008** 14:1395-1398.

[62] Lindner G, Faustmann H, Fischer T, Krempel S, Munch M, Rothballer S, Schmitt M. In Acoustic surface wave induced propagation of liquids in open channels. New York. pp. 2331-2334. **2007.**

[63] Girardo S, Cecchini M, Beltram F, Cingolani R, Pisignano D. Polydimethylsiloxane-LiNbO3 surface acoustic wave micropump devices for fluid control into microchannels. *Lab Chip.* **2008** 8:1557-1563.

[64] Wixforth A. Acoustically driven planar microfluidics. *Superlattice Microst.* **2003** 33:389-396.

[65] Wixforth A. Acoustically driven programmable microfluidics for biological and chemical applications. *JALA.* **2006** 11:399-405.

2.2 SPECIFIC TOPICS

2.2.1 A multichannel microfluidic platform

A multichannel acoustically driven microfluidic chip to study particle-cell interactions

Xue - Yan Wang[1], Christian Fillafer[2], Clara Pichl[1], Stephanie Deinhammer[1], Renate Hofer-Warbinek[3], Michael Wirth[1], Franz Gabor[1]

[1]Faculty of Life Sciences, Department of Pharmaceutical Technology and Biopharmaceutics, University of Vienna, Vienna A-1090, Austria

[2]Department of Mechanical Engineering, Boston University, Boston, Massachusetts 02215, USA

[3]Department of Vascular Biology and Thrombosis Research, Center for Physiology and Pharmacology, Medical University of Vienna, Vienna A-1090, Austria

A multichannel acoustically driven microfluidic chip to study particle-cell interactions

Xue-Yan Wang,[1] Christian Fillafer,[2] Clara Pichl,[1] Stephanie Deinhammer,[1] Renate Hofer-Warbinek,[3] Michael Wirth,[1] and Franz Gabor[1,a]

[1]*Faculty of Life Sciences, Department of Pharmaceutical Technology and Biopharmaceutics, University of Vienna, Vienna A-1090, Austria*
[2]*Department of Mechanical Engineering, Boston University, Boston, Massachusetts 02215, USA*
[3]*Department of Vascular Biology and Thrombosis Research, Center for Physiology and Pharmacology, Medical University of Vienna, Vienna A-1090, Austria*

Microfluidic devices have emerged as important tools for experimental physiology. They allow to study the effects of hydrodynamic flow on physiological and pathophysiological processes, e.g., in the circulatory system of the body. Such dynamic *in vitro* test systems are essential in order to address fundamental problems in drug delivery and targeted imaging, such as the binding of particles to cells under flow. In the present work an acoustically driven microfluidic platform is presented in which four miniature flow channels can be operated in parallel at distinct flow velocities with only slight inter-experimental variations. The device can accommodate various channel architectures and is fully compatible with cell culture as well as microscopy. Moreover, the flow channels can be readily separated from the surface acoustic wave pumps and subsequently channel-associated luminescence, absorbance, and/or fluorescence can be determined with a standard microplate reader. In order to create artificial blood vessels, different coatings were evaluated for the cultivation of endothelial cells in the microchannels. It was found that 0.01% fibronectin is the most suitable coating for growth of endothelial monolayers. Finally, the microfluidic system was used to study the binding of $1 \, \mu$m polystyrene microspheres to three different types of endothelial cell monolayers (HUVEC, HUVECtert, HMEC-1) at different average shear rates. It demonstrated that average shear rates between $0.5 \, \text{s}^{-1}$ and $2.25 \, \text{s}^{-1}$ exert no significant effect on cytoadhesion of particles to all three types of endothelial monolayers. In conclusion, the multichannel microfluidic platform is a promising device to study the impact of hydrodynamic forces on cell physiology and binding of drug carriers to endothelium. © *2013 AIP Publishing LLC*. [http://dx.doi.org/10.1063/1.4819273]

I. INTRODUCTION

The endothelium constitutes the inner layer lining the blood vessels and as such is involved in a variety of physiological and pathophysiological processes, for instance, in the course of atherosclerosis,[1] diabetes,[2] and cancer.[3] Thus, from a therapeutic point of view, it would be beneficial to deliver drugs or contrast agents to dysfunctional parts of the endothelium. To reach this aim, particulate drug delivery systems, such as drug-loaded nanoparticles or liposomes, have been frequently proposed. By modifying the surface of these carriers with specific target molecules, selective adhesion to diseased cells and tissues might be possible. Several strategies have been suggested: E-selectin-binding peptide modified N-(2-hydroxypropyl) methacrylamide

---

[a]Electronic mail: franz.gabor@univie.ac.at

    7, 044127-1

(HPMA) polymer drug carriers[4] and sialyl Lewis X-conjugated liposomes for targeting inflamed vasculature,[5] anti-ICAM decorated PLGA nanocarriers[6] and RGD-conjugated HPMA copolymer particles for targeting of tumor angiogenic vasculature,[7] as well as leukocyte-mimetic anti-P-selectin and VCAM-1 grafted microparticles of iron oxide for MRI[8] are some representative examples. However, it has also been shown that coating of colloids with polymers such as polyethylene glycol (PEG) prolongs the half life of particles in the blood stream.[9] Thus, understanding the key parameters that either enhance adhesion or prolong residence in the circulatory system is of fundamental importance.

Currently, *in vitro* studies concerned with the adhesion of particles to endothelial cells are usually carried out under stationary conditions. *In vivo*, however, endothelial cells grow in a three-dimensional matrix and are constantly exposed to hydrodynamic forces caused by blood flow.[10,11] Generally, hydrodynamic flow can be regarded as an external force acting on a cell. The exposure of endothelial cells to shear stress has indeed been shown to induce alterations in gene expression[12] and cytoskeletal re-arrangement.[13,14] For instance, hydrodynamic flow strongly affects the interaction between leukocytes and endothelial cells occurring during recruitment of leukocytes in response to inflammation inside vascular walls.[15] Therefore, it would be advantageous to have *in vitro* models at hand, which allow simulation of hydrodynamic flow conditions. Microfluidic systems offer promising solutions for this purpose. By using soft lithography, channel structures can be produced in arbitrary geometries and numbers at a sub-millimeter scale. In contrast to classical flow-through chambers, only minute amounts of samples are necessary and highly reproducible experimental conditions are ensured.[16]

In the present work a multi-channel acoustically driven microfluidic system based on surface acoustic wave technology (SAW) will be described. This device will be employed to mimic physiological conditions *in vitro*. A central advantage of this setup is that quantitative analysis of cell-bound fluorescence, luminescence, and/or absorbance can be carried out by using a standard microplate reader. First, the range of flow rates that can be generated reproducibly in the system will be assessed. Second, optimized cell culture techniques, especially channel coatings with extracellular matrix components, will be described that allow cultivation of three different types of endothelial cells inside microchannels. Finally, as a proof-of-concept, the SAW-driven microfluidic device will be applied to investigate the adhesion of polymer microparticles to endothelial cell monolayers in the presence of hydrodynamic drag.

II. MATERIALS AND METHODS

A. Material

Sylgard®184 Silicone Elastomer Kit was obtained from Baltres (Baden, Austria). Yellow-green fluorescent carboxylated polystyrene particles with a diameter of 1000 nm were purchased from Polysciences Europe GmBH (Eppelheim, Germany). Human fibronectin was bought from BD Bioscience (Bedford, USA). All other chemicals were of analytical purity.

B. Fabrication of sterile microchannels

Microchannels composed of poly(dimethylsiloxane) (PDMS) were fabricated as described previously.[17] Briefly, 10 g base and 1 g curing agent were mixed by vigorous stirring. After evacuation for 30 min to remove gas bubbles, the liquid pre-polymer was poured into pre-structured aluminium molds and hardened over night at 70 °C. After peeling the PDMS replicas from the molds, they were attached to predetermined spots on a glass plate ($127 \times 85 \times 1.1$ mm, length $\times$ width $\times$ height) and fixed irreversibly by gluing with liquid pre-polymer and heating to 100 °C for 30 min.

C. Characterization of multichannel microfluidic system

Each of the four identical microchannels on the glass plate was filled with water containing $0.25\%_0$ fluorescent microparticles (3 μm, Duke Scientific Corp., California, USA).

According to Hodgson *et al.*, in order to guarantee efficient transmission of the SAWs into the microchannels, water was used as a couplant between the IDT and the glass plate.[18] The system is operated by a radio frequency generator (SMB100A, Rohde&Schwarz GmbH, Austria) connected in series to a coaxial amplifier (LZY-1, Mini Circuits, Brooklyn, USA) and a fixed attenuator (VAT-3W2+, Mini Circuits, Brooklyn, USA). The radio frequency signal is distributed to the four IDTs by a 4-way divider (D1572-102, Werlatone, Brewster, USA). The whole setup was mounted on a Zeiss Axio Observer.Z1 (Göttingen, Germany). Due to the difficulty of directly measuring the power transduced into the SAW, the input power levels given herein simply correspond to the arithmetic sum of the powers of the generator and amplifier minus loss in the splitter. The values given should not be considered as the actual power transduced into the SAW. The input power was converted from dBm to the mW-scale according to Eq. (1).

$$P = P_{ref} 10^{\frac{x}{10}},\qquad(1)$$

where P is the power in [mW], P_{ref} is the reference power (1 mW), and *x* is the power in [dBm]. The flow velocity in the microchannels was determined from the translational velocity of the fluorescent particles by microscopy. Moreover, the corresponded average shear rate was calculated according to Eq. (2),

$$\gamma = \frac{Vmax}{\frac{H}{2}},\qquad(2)$$

where γ is the average shear rate in [s^{-1}], Vmax is the flow velocity measured in a laterally as well as vertically central region of the channel, which was the highest velocity due to the character of parabolic flow, and H/2 is the half-height of the microchannel (Figure 1(D)).

D. Cultivation of endothelial cells

Three different cell types were used: (i) primary human umbilical vein endothelial cells (HUVECs) isolated from human umbilical cords by treatment with collagenase Type I, (ii) human umbilical vein endothelial cells immortalized with human telomerase reverse transcriptase (HUVECtert),[19] and (iii) immortalized human dermal microvascular endothelial cells (HMEC-1, ATCC cat no. CRL-10636).[20] The tissue culture flasks used for cultivation were coated with a 1% (w/v) aqueous solution of gelatin for 30 min prior to seeding the cells suspended in EndoPrime® Medium (EndoPrime Kit, PAA, Linz, Austria). All cells were grown in a humidified atmosphere with 5% CO_2 at 37 °C and subcultured twice a week using trypsin-EDTA solution.

The PDMS microchannels were coated with several coating solutions (see below) before seeding the endothelial cells suspended in M199 medium supplemented with growth factors, heparin, and 20% fetal bovine serum (500 μl cell suspension per channel). Confluent cell monolayers were accomplished after 1 day cultivation by seeding of 2×10^5 cells ml^{-1} in case of HUVECs and HUVECtert or after 3 days cultivation by seeding of 3×10^5 cells mL^{-1} in case of HMEC-1. The cells were used for the experiments between passage 2 to 8 (HUVECs), 21 to 28 (HUVECtert), or 30 to 38 (HMEC-1).

E. Coating of PDMS microchannels

Three different coating solutions were applied: (i) gelatin (1% w/v in phosphate buffered saline; PBS), (ii) collagen (0.14 mg ml^{-1} in PBS), and (iii) fibronectin (0.1 mg ml^{-1} in PBS). Briefly, after incubation of the autoclaved microchannels with sterile PBS (500 μl per channel) for 30 min at room temperature, 300 μl of the coating solution was added. After incubation for 1 h the coating solution was removed from the microchannels. In the case of gelatin and fibronectin, the cells were seeded immediately. In the case of collagen, the microchannels were washed twice with cell culture medium (500 μl each channel) prior to seeding of cells.
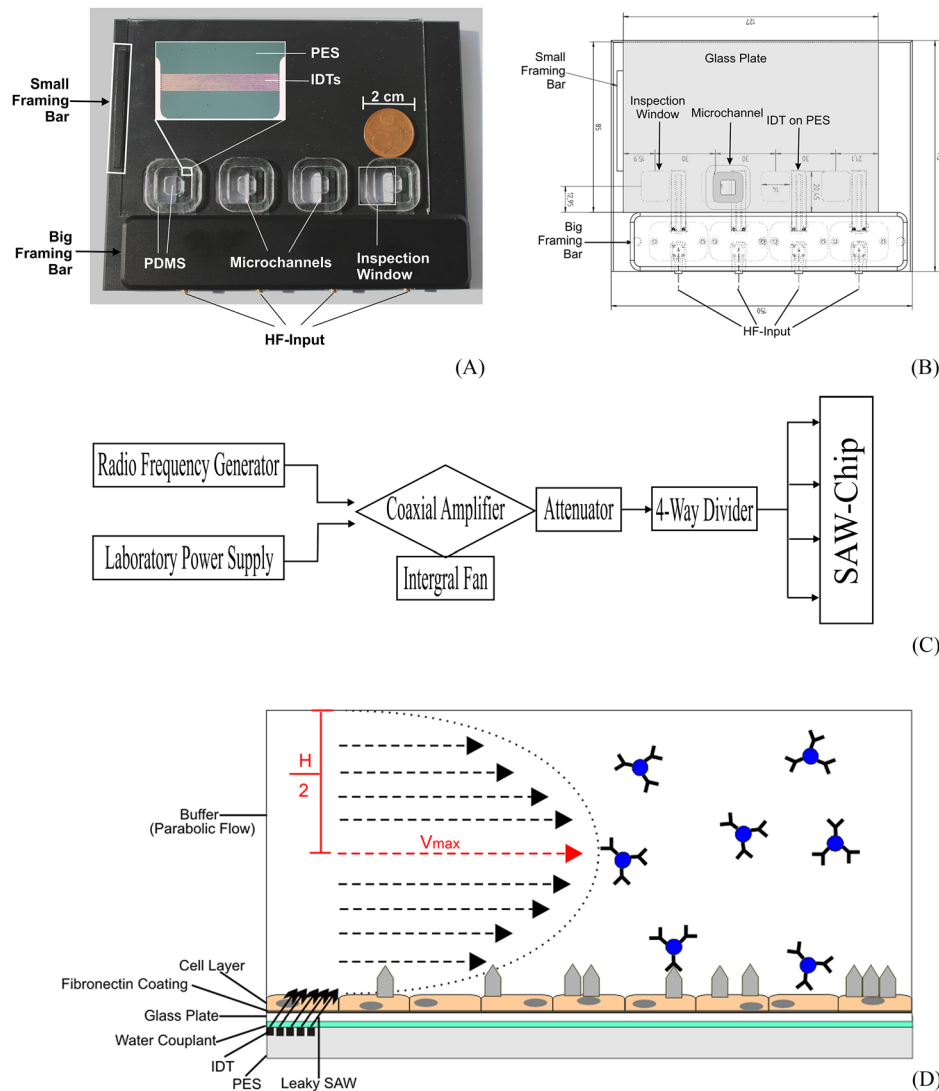
FIG. 1. Multichannel acoustically driven microfluidic platform. The SAW-chip consists of four IDTs, which are structured on a piezoelectric substrate (PES) and connected to a high frequency source (HF-input). Four microchannels for the cultivation of cells are formed by attaching poly(dimethylsiloxane) (PDMS) structures to a glass plate dimensioned $127 \times 85 \times 1.1$ mm (length $\times$ width $\times$ height). Inspection windows in the aluminum block allow for microscopic observation during experiments (A). The positioning of the microchannels on the glass plate was kept constant by a preprinted template in order to guarantee the localization of the IDTs underneath the microchannels (B). The system is operated by a radio frequency generator connected to a coaxial amplifier (operated by a laboratory power supply, with an integral fan for cooling), and a fixed attenuator. The radio frequency signal is distributed to the SAW-Chip by a 4-way divider (C). Schematic presentation of cross-section of acoustically driven microfluidic platform for the studying of interaction between particles and cells under flow condition (D).

Furthermore, composite coating with collagen/fibronectin was investigated. After collagen-coating as described above, $300\,\mu$l of fibronectin solution ($0.1\,\text{mg ml}^{-1}$ in PBS) were added and 15 min later the cells were seeded. Confluence of the cell monolayer was checked microscopically.

F. Identification of suitable buffer systems for flow experiments

Three commonly used buffer media were tested: (i) isotonic HEPES/NaOH buffer pH 7.4, (ii) PBS, and (iii) PBS supplemented with Ca^{2+}/Mg^{2+}. After filling each microchannel with $500\,\mu$l buffer, flow was induced by acoustic streaming at a power of 25 dBm (average shear

rate $\sim 2.25\,\mathrm{s}^{-1}$) for 15 min. Subsequently, the integrity of the cell monolayers was checked microscopically. M199 cell culture medium instead of buffer was used as a control.

G. Cytoadhesion of microparticles under flow conditions

To study binding of microparticles to endothelial cell monolayers, $1\,\mu\mathrm{m}$ fluorescent polystyrene microspheres were used. After removing the cell culture medium from the microchannel, and washing the monolayer once with 500 μl PBS each, 500 μl microsphere suspension ($100\,\mu\mathrm{g\,ml}^{-1}$ in PBS supplemented with $\mathrm{Ca}^{2+}/\mathrm{Mg}^{2+}$) were added and the monolayer was incubated for 15 min under flow conditions. In order to generate different flow velocities, certain input power levels from 17.5 dBm to 25 dBm corresponding to average shear rates between 0.49 and $2.25\,\mathrm{s}^{-1}$ were applied. After removal of non-bound microspheres by washing twice with 500 μl PBS supplemented with $\mathrm{Ca}^{2+}/\mathrm{Mg}^{2+}$, the cell-associated fluorescence was determined in a microplate reader (TECAN; Infinite M200; excitation: 440; emission: 485 nm). The corresponding amount of cell-bound particles was calculated from a calibration curve that has been acquired with a dilution series of microspheres in the PDMS channels.

H. Microscopy

To study the morphology and integrity of endothelial cell monolayers in microchannels, phase contrast images were acquired at defined cultivation intervals using a Zeiss Axio Observer.Z1 (Zeiss, Göttingen, Germany).

In order to visualize the distribution of microparticles on the endothelial cell surface at the end of the cytoadhesion studies and to confirm confluence of the cell monolayer even after exposure to flow, fluorescence microscopy was applied. For this purpose, the cells were fixed in ice cold methanol ($-20\,^{\circ}\mathrm{C}$) for 10 min at $-20\,^{\circ}\mathrm{C}$. After rehydration in PBS containing 1% BSA for 20 min at room temperature the cells were washed with the same buffer. Then, 300 μl polyclonal goat-anti-human VE-cadherin (C-19) antibody ($200\,\mu\mathrm{g\,ml}^{-1}$, Santa Cruz Biotechnology) in PBS containing 1% BSA was added to label vascular endothelial cadherin by incubation for 1 h at $37\,^{\circ}\mathrm{C}$. After washing with the same buffer, 300 μl of a 1:200 dilution of rhodamine-labelled rabbit-anti-goat antibody ($1\,\mathrm{mg\,ml}^{-1}$, Abcam) and 0.5 μg Hoechst 33342 in PBS containing 1% BSA were added and stored for 30 min at $37\,^{\circ}\mathrm{C}$. Finally, the cell layers were washed twice with the same buffer and fluorescence images were acquired.

I. Data analysis

Data were statistically analyzed using the Microsoft Excel® integrated analysis tool. The hypothesis test among two data sets was made by comparing two means from independent (unpaired) samples (t-test). Values of $p < 0.05$ were considered statistically significant.

III. RESULTS AND DISCUSSION

A. A multichannel acoustically driven microfluidic platform

Since hydrodynamic flow is expected to affect the adhesion of particles to cells, dynamic biopharmaceutical test systems are of highest interest especially due to the growing importance of micro- and nano-scaled drug delivery systems. It will be demonstrated that a multichannel acoustically driven microfluidic system can be used to study such hydrodynamic effects *in vitro*. SAW-induced streaming of liquids in miniature channels has already been described previously.[16,17] In brief, exciting IDTs on a piezoelectric substrate ($\mathrm{LiNbO_3}$) at an appropriate frequency generates a SAW. When this SAW couples into a liquid, it generates a pressure gradient therein that induces streaming. In contrast to classical flow systems, which rely on external pumps (e.g., syringe pumps) and tubing, acoustic streaming allows to minimize the risk of contamination. Furthermore, by eliminating the need for tubing, the system becomes simpler and avoids any dead volume. It is also possible to upgrade the device and parallelize multiple SAW pumps on a chip. In the present work, a platform was developed which can be used to

simultaneously pump liquid in four microfluidic channels (Figure 1). For this purpose, four IDTs were glued into a pre-structured aluminum block and connected with ports for cabling. As illustrated in Figure 1, a small inspection window was included for each channel which allows microscopic observation by inverted or upright microscopes during the experiment. This device holds glass plates ($127 \times 85 \times 1.1$ mm, length × width × height) on which four PDMS-microchannels with arbitrary geometry can be mounted. The dimensions of the glass plate were chosen in order to match the size of standard microplates as most plate readers allow specifying the exact location of read-out points on a microplate. Thus, the geometry of the PDMS-microchannels on the glass plate can be directly programmed into the software. Consequently, data are simply collected by reading the luminescence, absorbance or fluorescence at pre-selected points in the microchannel. All in all, the systems offers the advantages of low risk of contamination, high versatility in cultivation of cells of different origin, qualitative evaluation by microscopy and quantitative assessment of bound material by microplate reading as well as simple operation.

B. Characterization of multichannel acoustically driven microfluidic system

To assess the reproducibility and the attainable range of flow velocities with parallelized SAW-pumps, flow velocity was measured in several different microchannels. The flow velocity was determined in a laterally as well as vertically central region of the channel by measuring the translational velocity of suspended microparticles via fluorescence microscopy. As shown in Figure 2, there is a clear relation between input power and average shear rate in the channels. According to Eq. (1), the total input power, which directly operated SAW-device, ranged from 25 mW (14 dBm) to 1400 mW (31.5 dBm). Since four transducers were operated in parallel, every transducer is supplied with a fourth of the total input power. Typically, flow velocities between $0.3\,\mathrm{mm\,s^{-1}}$ and $10\,\mathrm{mm\,s^{-1}}$ were generated corresponding to average shear rates between $0.15\,\mathrm{s^{-1}}$ and $5\,\mathrm{s^{-1}}$ with the present channel geometry. It is important to mention, however, that by down-scaling of the channel dimensions (e.g., decreasing channel width and height) clearly higher average shear rates (1–2 orders of magnitude) can be attained.

As demonstrated in Figures 2(A) and 2(B), the average shear rates determined in the four microchannels are widely identical over a period of at least 30 min. This underlines that constant flow velocities and shear rates can be generated in this parallelized multichannel platform. At input powers >1400 mW (31.5 dBm), the system heats up considerably which ultimately leads to evaporation of the water couplant between the chip surface and the glass plate. This strongly reduces the coupling efficiency of the SAW into the microchannels. When operation of the SAW-chips at such high input power levels is desired, it would thus be necessary to use low-viscosity oil or similar non-aqueous coupling fluids to reduce evaporation by heating.

In order to guarantee comparable pumping levels in consecutive experiments, the localization of the IDTs underneath the microchannels has to be kept constant. This can be achieved easily by using a preprinted template for positioning of the microchannels on the glass plate (Figure 1(B)). Furthermore, two framing bars were included on the SAW-chip to allow for fixation of the glass plate and to ensure reproducible positioning of the IDTs underneath the channels (Figures 1(A) and 1(B)). If these potential pitfalls are kept in mind, only slight variations of the flow velocities will be observed (Figure 2(C)). These results collectively underline that parallelized SAW-chips can generate a considerable range of flow velocities in microchannels with satisfactory precision and reproducibility. Moreover, not only constant flow can be generated. In principle, pulsatile flow is easily attained by modulating the amplitude of the high frequency signal. The latter is a highly interesting approach to mimic the flow patterns prevalent in the circulatory system.

C. Cultivation of endothelial cells in microchannels

In order to generate artificial blood vessels, growth of endothelial cell monolayers in the microchannels would be desirable. To approach this aim, three different cell types representing large vessel and microvascular endothelial cells were tested for cultivation in PDMS microchannels:
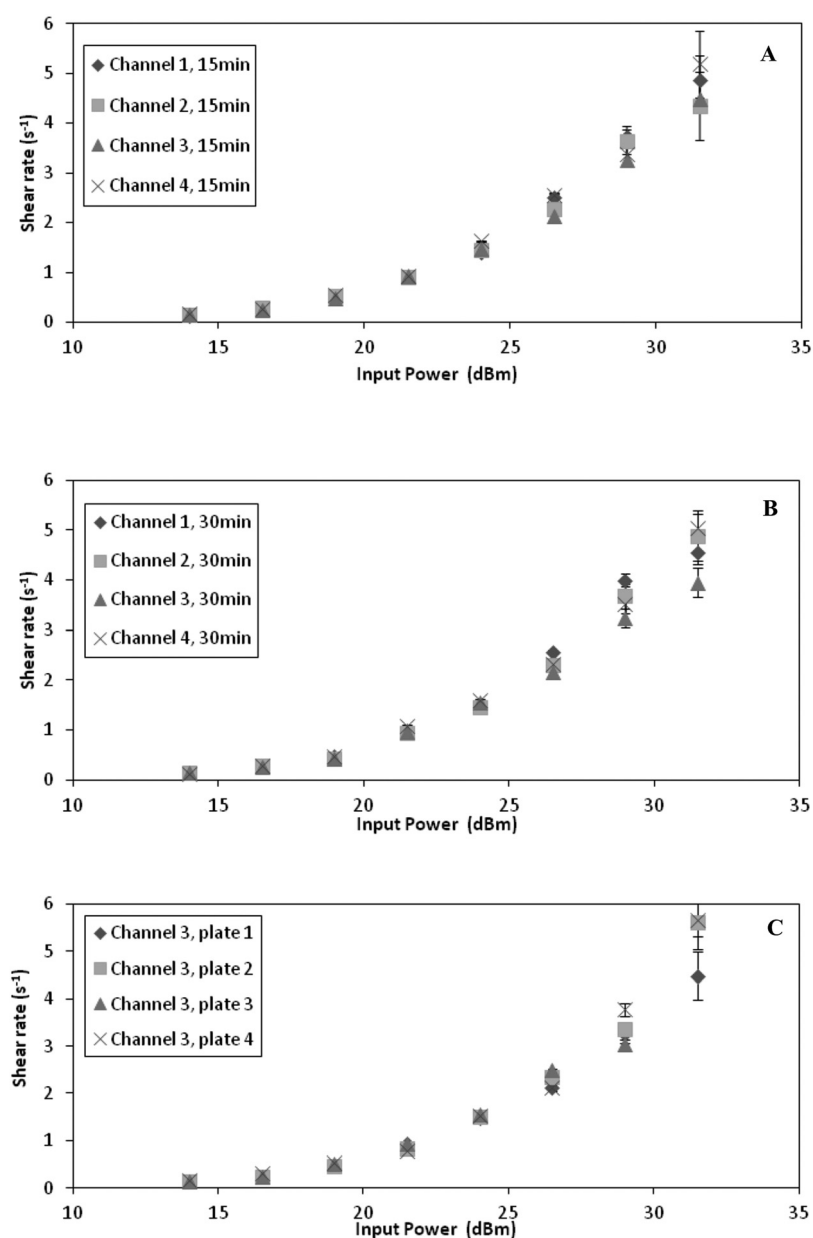
FIG. 2. Average shear rates generated by IDTs in PDMS-microchannels on microfluidic platform. Channels 1–4 represent the respective microchannels arranged on top of the four IDTs (Figure 1). Flow velocities of 10 particles per channel were determined after 15 min (A) and 30 min of operation (B), respectively. Flow velocities of 10 particles, generated by one of the four IDTs of the platform in a microchannel on four different glass plates on consecutive days, were determined after 15 min of operation (C). (SD $\leq$ 1.12, n = 10).

primary HUVECs, immortalized HUVECtert, and immortalized HMEC-1. Primary HUVECs are isolated from human umbilical cords by treatment with collagenase type I[21] and are widely used as a cell model for *in vitro* studies in flow chambers.[22] HUVECs offer the typical advantages of primary cells but they can only be cultivated for about eight passages. Retroviral infection with human telomerase reverse transcriptase (hTERT) can extend their ability to replicate and thus their lifespan.[19,23] It is supposed that immortalized HUVEC cell lines (HUVECtert) exhibit similar functional and morphogenetic characteristics like their primary parent cells. Furthermore, immortalized human dermal microvascular endothelial cells (HMEC-1) represent an interesting cell line for cultivation in flow channels since they exhibit similar morphologic, phenotypic, and functional characteristics compared to their endothelial parent cells.[20]

As endothelial cells do not adhere and proliferate on a plain glass surfaces, coating of the channel with gelatine, collagen, fibronectin, and collagen/fibronectin mixtures can facilitate adhesion. Several different techniques and protocols have been reported in the literature for one and the same adhesion molecule so that the following results only pertain to the exact protocols as described above. Although gelatin is frequently employed for the coating of tissue culture flasks for HUVECs, it was found that it is not optimal for coating PDMS-microchannels (Figure 3(A)). Similarly, coating with collagen also led to rather insular attachment of cells (Figure 3(B)). In contrast, coating with fibronectin mediated regular attachment of HUVECs to the surface inside the PDMS microchannels (Figure 3(C)). Interestingly, sequential coating of the channels with collagen and fibronectin did not result in improved cell adhesion (Figure 3(D)). Similar results as described above were also found for HUVECtert and HMEC-1 cell lines. As illustrated in Figure 4, all three types of endothelial cells formed a confluent monolayer with elongated and polygonal cells on fibronectin-coated glass. Thus, coating of PDMS microchannels with fibronectin was used in all further experiments.

D. Selection of buffers suitable for experiments with endothelial cells under flow conditions

In order to identify a suitable medium for experiments under flow conditions, the effect of three different commonly used buffer media (isotonic HEPES/NaOH buffer pH 7.4, PBS, and PBS supplemented with Ca^{2+}/Mg^{2+}) on endothelial cells were investigated. For that purpose, the cell culture medium overlying confluent endothelial cell monolayers inside PDMS microchannels was replaced by different buffers followed by incubation under flow conditions at an average shear rate of $2.25 s^{-1}$ for 15 min and microscopic images of the HUVECtert monolayers were acquired (Figure 5). As is clearly visible, the cell monolayers incubated with $PBS + Ca^{2+}/Mg^{2+}$ exhibited no morphological changes as compared to the M199 medium. Interestingly, incubation with PBS or isotonic HEPES/NaOH pH 7.4 resulted in detachment of endothelial cells from the channel surface (Figures 5(C) and 5(D)). This effect was also
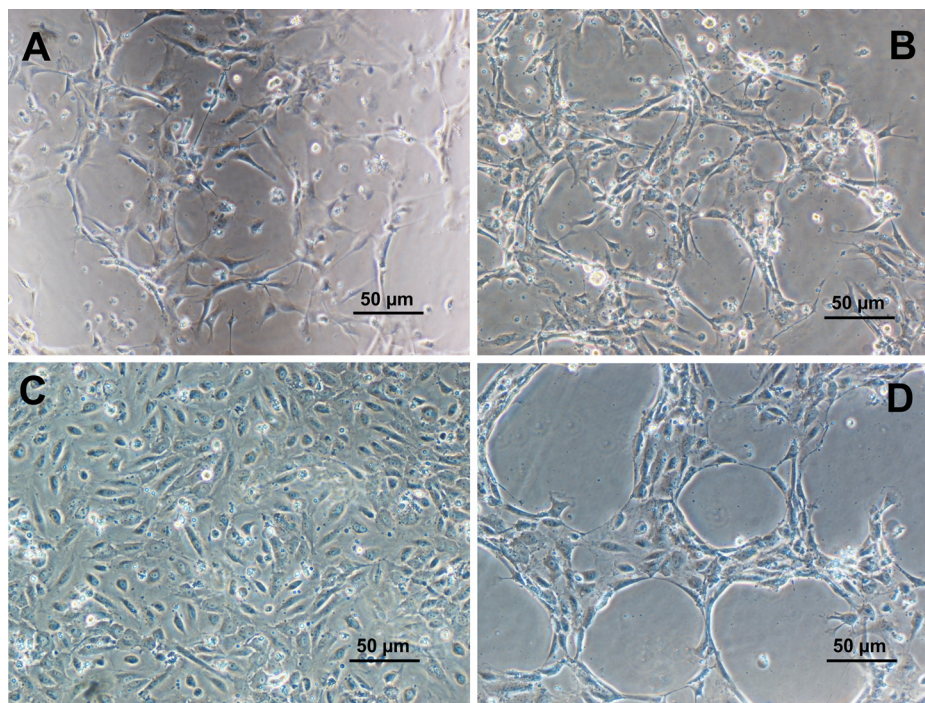

FIG. 3. Phase contrast images of primary HUVECs one day after seeding (2×10^5 cells ml^{-1}) in microchannels coated with gelatin (1%, A), collagen (0.14 mg ml^{-1}, B), fibronectin (0.1 mg ml^{-1}, C) and collagen/fibronectin (0.14 mg ml^{-1}/0.1 mg ml^{-1}, D), respectively.
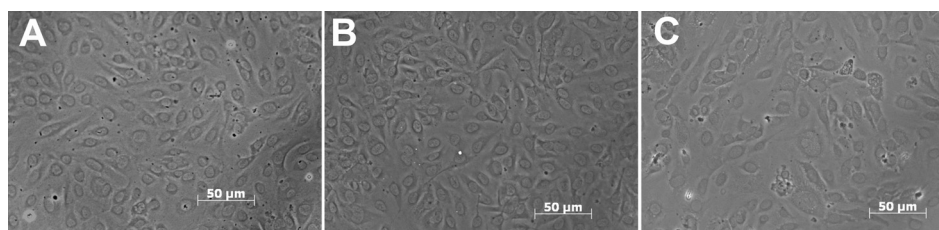
FIG. 4. Phase contrast images of primary HUVECs (A) and HUVECtert (B) one day after seeding (2×10^5 cells ml^{-1}) as well as HMEC-1 (C) four days after seeding (3×10^5 cells ml^{-1}) in microchannels coated with fibronectin (0.1 mg ml^{-1}).

observed under stationary conditions (data not shown). Most probably, the lack of Ca^{2+} and Mg^{2+} ions in these media weakens the adhesion between endothelial cells as well as that to the growth surface and reduces the monolayers' resistance against hydrodynamic stress. In addition, although the zwitter-ionic buffer HEPES is relative chemically inert[24] and is commonly used for different cell culture experiments, its stability is still not well defined and it can form aggregates that results in decreased buffering capacity.[25,26] Consequently, the instability of HEPES might contribute to monolayer detachment. Therefore, PBS $+$ Ca^{2+}/Mg^{2+} buffer was chosen as suitable medium for particle-monolayer interaction experiments.

E. Cytoadhesion of microparticles to endothelial cell monolayers under flow conditions

Finally, cytoadhesion of negatively charged 1 μm polystyrene microparticles was investigated under different flow conditions. Endothelial cell monolayers in PDMS microchannels were incubated with particles at different average shear rates between 0.49 and 2.25 s^{-1}. Non-bound colloids were removed by washing, and then each cell layer was checked for confluence under the microscope. As shown in Figure 6, most of the cell monolayers retained their confluence after flow incubation and only monolayers of full integrity were analyzed. As depicted in Figure 7, the average number of cell-bound particles decreased slightly with increasing flow velocity. Similar results were found for all three types of endothelial cells. This suggests that increasing hydrodynamic drag exerts no significant influence on the cytoadhesion of polystyrene microparticles in the rate of
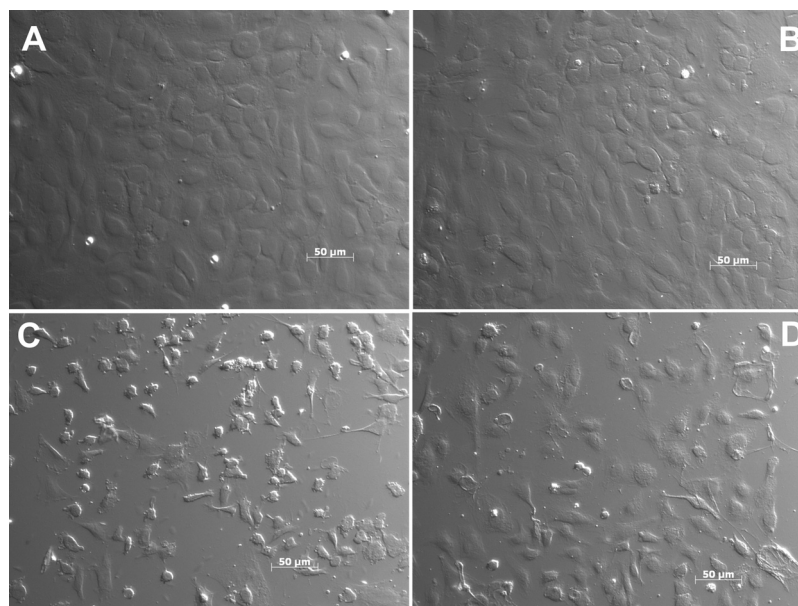

FIG. 5. Differential interference contrast images of HUVECtert after 15 min incubation with M199 medium (A), PBS $+$ Ca^{2+}/Mg^{2+} (B), PBS (C), and isotonic HEPES pH 7.4 (D) under flow conditions (average shear rate 2.25 s^{-1}).
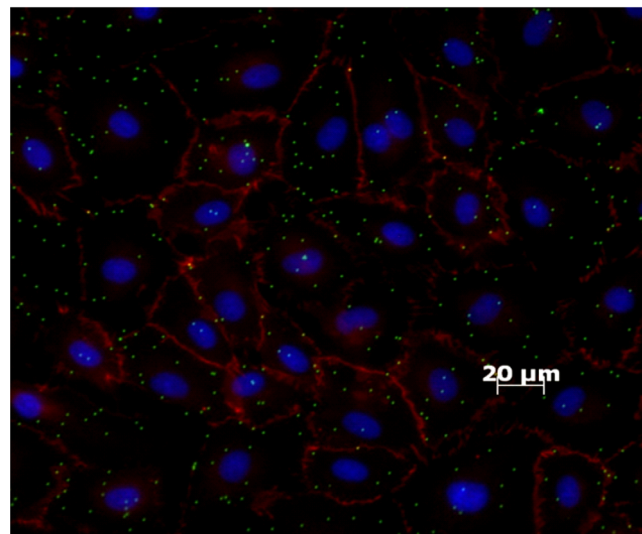
FIG. 6. Fluorescence microscopic image of cell-bound 1 μm polystyrene microparticles (green) after incubation at an average shear rate of $1.13\,\mathrm{s}^{-1}$ after two washing steps. The nuclei of HUVECs were stained in blue using Hoecht 33342 and VE-cadherin was immunostained in red.

average shear rates tested. Interestingly, similar results have been obtained for the interaction between Caco-2 cell monolayers (enterocytes) and 1 μm polystyrene microparticles coated either with wheat germ agglutinin or with poly(ethyleneimine).[27] Charoenphol *et al.*,[22] who modified the surface 0.5 and 2 μm polystyrene particles with sialyl-Lewis A to target vascular selectin, have also made comparable observations. Their cytoadhesion studies were performed in DPBS buffer using a circular parallel plate flow chamber with shear rates between $100\,\mathrm{s}^{-1}$ and $640\,\mathrm{s}^{-1}$. In accordance with our work, no significant difference in adhesion levels of particles onto endothelial monolayers was observed.[22] Interestingly, a lower binding rate of microparticles was observed in case of HMEC-1 monolayers as compared with HUVECs and HUVECtert. The latter two types of endothelial cells, however, revealed similar microparticle binding capacity. At the highest average shear rate of $2.25\,\mathrm{s}^{-1}$, the binding efficiency of particles to HMEC-1 monolayer was only about 65% of that to HUVECs monolayer; at average shear rates of 0.5, 1, and $1.5\,\mathrm{s}^{-1}$ the particle adhesion level on HMEC-1 monolayer was 79%, 73%, and 78% of that on HUVECs monolayer, respectively. This significant difference might be due to the different endothelial cell type. HUVECs were
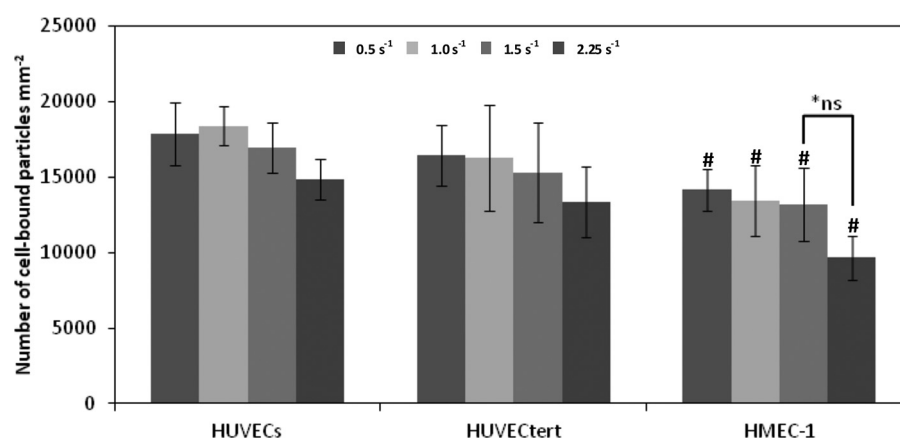

FIG. 7. Cytoadhesion of 1 μm fluorescent polystyrene microparticles on HUVECs, HUVECtert and HMEC-1 monolayers at different average shear rates between $0.5\,\mathrm{s}^{-1}$ and $2.25\,\mathrm{s}^{-1}$ in a multichannel microfluidic platform. ($n \geq 28$). Statistically significant differences were determined by student's t-test. *ns = not significantly difference. # = p < 0.01 compared to HUVECs-binding at the same average shear rate.

isolated from umbilical cords, which represent the cell type in large vessels, whereas HMEC-1 represent a microvascular cell type. According to the literature, not only the growth rate and differentiation status[20,28] but also the cell surface structures and the amounts of cell adhesion molecules expressed are different for endothelial cells derived from microvascular vessels compared to large vessels according to their different functionality.[29–32] This might be a possible reason why HUVECs exhibited higher binding of negatively charged 1 μm polystyrene particles than HMEC-1.

All in all, as a proof-of-concept, cytoadhesion studies with 1 μm negatively charged microspheres were performed in this novel multichannel microfluidic system. Three different types of endothelial cell monolayers retained their confluency under flow conditions which allows for successful mimicking of macro- and micro blood vessels. Due to the expected impact of surface properties, dimension and size of particulate drug carriers, it might be interesting to study cytoadhesive characteristics of different types of particles in further experiments. Another important parameter to be elucidated might be viscosity of the medium because the shear stress is the arithmetic product of shear rate and viscosity. Thus, further hydrodynamic studies with media of viscosity similar to blood and with suspended blood cells might bring us one step closer to physiological conditions.

IV. CONCLUSION

A.T. Florence has hypothesized that hydrodynamic effects could play a substantial role in the interaction between particles and cells or tissues *in vivo*, in particular in the circulatory system.[33] In order to shed some light on this issue, a multichannel microfluidic setup was developed and optimized that can be used to mimic physiological flow conditions in the lab. This chip-based system allows constant and pulsed flow. With the current channel geometry average shear rates up to $5\,\mathrm{s}^{-1}$ are easily generated. By integration of four identical SAW-pumps in one platform, parallelized experiments can be carried out, which greatly extends versatile applicability of this microfluidic system. In addition, the dimensions of our current setup match those of standard microplates. Thereby, channel-associated fluorescence, luminescence, and absorbance can be simply detected by using a standard microplate reader. Furthermore, the device is fully compatible with cell culture as demonstrated by successful cultivation of HUVECs, HUVECtert, and HMEC-1 monolayers inside the PDMS-microchannels. To achieve the latter, the channel surface was coated with a 0.01% solution of fibronectin. Moreover, the endothelial monolayers remained widely intact during incubation with buffers and microparticle suspensions under flow conditions. Studying the cytoadhesion of negatively charged 1 μm microparticles to endothelial cell monolayers under flow conditions revealed no significant effects of hydrodynamic drag at average shear rates between $0.5\,\mathrm{s}^{-1}$ and $2.25\,\mathrm{s}^{-1}$ for all three types of endothelial cells. However, most probably due to the differences between endothelial cells derived from large and small vessels, HUVECs and HUVECtert exhibited higher particle binding capacity as compared to HMEC-1. In conclusion, the developed multichannel microfluidic platform represents a promising device to elucidate the effect of shear forces on cell-binding of particles. Moreover, the system is not only limited to biopharmaceutical applications but is also suitable for general experiments on the effect of hydrodynamic forces in luminal compartments of the human body. Further studies with such dynamic *in vitro* test models are expected to improve our understanding of basic mechanisms in targeted drug delivery and cell physiology.

ACKNOWLEDGMENTS

[1]J. Davignon and P. Ganz, Circulation **109**, III-27 (2004).
[2]F. Cosentino and T. F. Luscher, J. Cardiovasc. Pharmacol. **32**(Suppl. 3), S54 (1998).
[3]D. J. Hicklin and L. M. Ellis, J. Clin. Oncol. **23**, 1011 (2005).
[4]Y. Shamay, D. Paulin, G. Ashkenasy, and A. David, Biomaterials **30**, 6460 (2009).
[5]J. Minaguchi, T. Oohashi, K. Inagawa, A. Ohtsuka, and Y. Ninomiya, Arch. Histol. Cytol. **71**, 195–203 (2008).

[6]S. Muro, T. Dziubla, W. Qiu, J. Leferovich, X. Cui, E. Berk, and V. R. Muzykantov, J. Pharmacol. Exp. Ther. **317**, 1161 (2006).

[7]A. Mitra, J. Mulholland, A. Nan, E. McNeill, H. Ghandehari, and B. R. Line, J. Controlled Release **102**, 191 (2005).

[8]M. A. McAteer, J. E. Schneider, Z. A. Ali, N. Warrick, C. A. Bursill, D. R. Greaves, S. Neubauer, K. M. Channon, and R. P. Choudhury, Arterioscler., Thromb., Vasc. Biol. **28**, 77 (2008).

[9]P. Decuzzi, R. Pasqualini, W. Arap, and M. Ferrari, Pharm. Res. **26**, 235 (2009).

[10]A. D. van der Meer, A. A. Poot, M. H. G. Duits, J. Feijen, and I. Vermes, J. Biomed. Biotechnol. **2009**, 1.

[11]Y.-S. Li, J. H. Haga, and S. Chien, J. Biomech. **38**, 1949 (2005).

[12]M. Braddock, J. L. Schwachtgen, P. Houston, M. C. Dickson, M. J. Lee, and C. J. Campbell, Physiology **13**(5), 241 (1998).

[13]B. P. Helmke and P. F. Davies, Ann. Biomed. Eng. **30**, 284 (2002).

[14]B. Yap and R. D. Kamm, J. Appl. Physiol. **98**, 1930 (2005).

[15]R. Alon and K. Ley, Curr. Opin. Cell Biol. **20**, 525 (2008).

[16]T. A. Franke and A. Wixforth, Chem. Phys. Chem. **9**, 2140 (2008).

[17]C. Fillafer, G. Ratzinger, J. Neumann, Z. Guttenberg, S. Dissauer, I. K. Lichtscheidl, M. Wirth, F. Gabor, and M. F. Schneider, Lab Chip **9**, 2782 (2009).

[18]R. P. Hodgson, M. Tan, L. Yeo, and J. Friend, Appl. Phys. Lett. **94**, 024102 (2009).

[19]H. B. Schiller, A. Szekeres, B. R. Binder, H. Stockinger, and V. Leksa, Mol. Biol. Cell **20**, 745 (2009).

[20]E. W. Ades, F. J. Candal, R. A. Swerlick, V. G. George, S. Summers, D. C. Bosse, and T. J. Lawley, J. Invest. Dermatol. **99**, 683 (1992).

[21]J. C. Zhang, J. Wojta, and B. R. Binder, J. Thorac. Cardiov. Sur. **109**, 1059 (1995).

[22]P. Charoenphol, R. B. Huang, and O. Eniola-Adefeso, Biomaterials **31**, 1392 (2010).

[23]J. Yang, E. Chang, A. M. Cherry, C. D. Bangs, Y. Oei, A. Bodnar, A. Bronstein, C.-P. Chiu, and G. S. Herron, J. Biol. Chem. **274**, 26141 (1999).

[24]A. T. Palasz, P. Beltran Brena, J. De la Fuente, and A. Gutierrez-Adan, Theriogenology **70**, 1461 (2008).

[25]M. T. Vasconcelos, M. A. Azenha, and O. M. Lage, Anal. Biochem. **241**, 248 (1996).

[26]R. Vespalec, M. Vlckova, and H. Horakova, J. Chromatogr. A **1051**, 75 (2004).

[27]X.-Y. Wang, C. Pichl, F. Gabor, and M. Wirth, Colloids Surf., B **102**, 849 (2013).

[28]B. R. Zetter, Diabetes **30**(Suppl. 2), 24 (1981).

[29]T. Fujimoto and S. J. Singer, J. Histochem. Cytochem. **36**, 1309 (1988).

[30]R. A. Swerlick, K. H. Lee, T. M. Wick, and T. J. Lawley, J. Immunol. **78**, 148 (1992).

[31]R. A. Swerlick, K. H. Lee, L.-J. Li, N. T. Sepp, S. W. Caughman, and T. J. Lawley, J. Immunol. **698**, 4 (1992).

[32]R. A. Swerlick, E. Garcia-Gonzalez, Y. Kubota, Y. Xu, and T. J. Lawley, J. Invest. Dermatol. **97**, 190 (1991).

[33]A. T. Florence, *Nanoparticles as Drug Carriers* (Imperial College Press, London, 2006).

2.2.1 A multichannel microfluidic platform

A novel cell-based microfluidic multichannel setup - impact of hydrodynamics and surface characteristics on the bioadhesion of polystyrene microspheres

Xue - Yan Wang, Clara Pichl, Franz Gabor, Michael Wirth

Faculty of Life Sciences, Department of Pharmaceutical Technology and Biopharmaceutics, University of Vienna, Vienna A-1090, Austria

A novel cell-based microfluidic multichannel setup—impact of hydrodynamics and surface characteristics on the bioadhesion of polystyrene microspheres

Xue-Yan Wang, Clara Pichl, Franz Gabor, Michael Wirth *

Department of Pharmaceutical Technology and Biopharmaceutics, University of Vienna, Vienna, Austria

ARTICLE INFO

ABSTRACT

Carboxylated polystyrene microspheres with 1 μm in diameter were surface-modified either by coating with poly(ethyleneimine) (PEI) as cationic polyelectrolyte leading to a conversion of the surface charge from negative to positive, or by covalent immobilization of wheat germ agglutinin (WGA) via a carbodi-imide method to obtain a carbohydrate specific biorecognitive surface. To characterize the impact of the binding mechanism on the particle–cell interaction, the binding efficiencies to Caco-2 cells were inves-tigated for both, the biorecognitive WGA-grafted particles and the positively charged PEI-microspheres, and compared to the unmodified negatively charged polystyrene particles. As a result, WGA-grafted par-ticles exhibited the highest binding rates to single cells as well as monolayers as compared to positive and negative particles under stationary conditions. Concerning ionic interactions, PEI-coated particles suffered from a critical agglomeration tendency leading to a high variance in cell binding. Further-more, in order to elucidate the bioadhesive properties under flow conditions, an acoustically-driven microfluidic multichannel system was applied. Using different setups, it could be demonstrated that the hydrodynamics exerted almost no impact on cell-bound particles with a size of 1 μm at a flow velocity of 2000 μm s^{-1}. Using this novel microfluidic system, it was thus possible to prove that the omnipresent hydrodynamic drag in vivo is mostly negligible for microparticulate drug delivery systems in the size range of 1 μm or below.

1. Introduction

Keeping path with the exciting progress of nanotechnology, micro- and nanoparticles have been intensively investigated regarding their potential application as drug delivery systems. At this, the surface of particulate drug formulations might be chemically and structurally modified to allow for prolonged residence times of micro- and nanoparticles in the body or to facilitate targeting specific cell types and tissues. Nowadays, various targets are exploited for a potential pharmaceutical application. In general, the underlying particle–cell interaction mechanisms can be divided into two different types: one is based on specific biorecognitive mechanisms, where, for exam-ple, surface immobilized antibodies [1–3], RGD [4,5], aptamers [6], and small molecules like folat [7] could be utilized; the other mechanism relies on nonspecific adhesion including hydrophobic and ionic interactions. For hydrophobic adhesion chitosan, sodium alginate, cellulose derivates such as sodium carboxylmethylcellulose and hydroxypropylmethylcellulose, as well as polyacrylates such as Carbopol® and polycarbophil are usually applied [8,9]. Moreover, nonspecific interactions might be attained by particles carrying negative or positive surface charges. At this, due to prevailing negative charges at the surface of all cell types in multicellular organisms [10], cell-binding of positively charged drug carriers might be higher due to direct ionic interactions [11,12]. In the present work two different mechanisms of adhesion were investigated using Caco-2 cells as artificial epithelial target. As to the biorecognition approach, the particles were modified with wheat germ agglutinin (WGA) representing a plant lectin which is known to interact with spe-cific carbohydrates at the surface of mammalian cells [13]. For the ionic interaction representing a nonspecific mechanism, the particles were either surface coated with poly(ethyleneimine) or left unmodified yielding negatively charged particles due to their carboxylated nature.

Furthermore, upon administration in humans, either peroral or parenteral, the flow of materials under physiological conditions and the associated hydrodynamic forces will affect the interaction of particles applied to cells and tissues. Thus, it would be interesting to investigate the impact of hydrodynamics on the cytoadhesion of particles. For experimental fact finding, different microflu-idic systems have been established, for instance, microfluidic

* Corresponding author at: Department of Pharmaceutical Technology and Bio-pharmaceutics, University of Vienna, Althanstraße 14, 1090 Vienna, Austria.
Tel.: +43 1 4277 55407; fax: +43 1 4277 9554.
E-mail address: michael.wirth@univie.ac.at (M. Wirth).

co-culture migration systems [14], micropatterned substrates for endothelial cell culture in microfluidic channels [15], as well as membrane devices for modeling the airways [16]. In the present work, a novel microfluidic system was employed to mimic physiological flow conditions recently described by Fillafer et al. [17]. This microfluidic platform is based on surface acoustic waves (SAW), which nowadays can be generated and controlled precisely in the nanometer scale using chip-technology. In the present work, the SAW-chip consisted of interdigital electrodes structured on a piezoelectric substrate (lithium niobate) and serves as an interdigital transducer (IDT), which could be excited at appropriate frequencies. Due to the resulting deformation of the substrate surface the SAW is generated. When a liquid is in contact with the IDT surface, the SAW is coupled into the liquid and the resulting pressure gradient acts as a pumping force, which provokes streaming and mixing inside the liquid. In order to confine the flow of the liquid to vessel-like structures, poly(dimethylsiloxane) (PDMS)-based channels made by replica molding were used. In an effort to allow for parallelization, four interdigital transducers (IDTs) instead of one were now operated simultaneously in a contact-free manner without the need for tubing. Upon use of Caco-2 cell monolayers, which represent a well-established model of the human intestinal epithelium and were grown in microchannels followed by combination with this SAW-chip, the impact of flow on the cytoadhesion of different modified microparticles to intestinal tissues could be investigated.

2. Materials and methods

2.1. Materials

Yellow-green fluorescent carboxylated polystyrene particles with a diameter of 1000 nm as well as poly(ethyleneimine) (PEI) (branched, MW 10 kDa) were purchased from Polysciences Europe GmBH (Eppelheim, Germany). WGA was obtained from Vector Laboratories (Burlingame, USA). Sylgard® 184 Elastomer Kit was from Baltres (Baden, Austria). All other chemicals were of analytical purity.

2.2. Preparation of PEI coated carboxylated microspheres

100 µL of a suspension of 1 µm sized polystyrene microspheres (10 mg mL^{-1}) were added dropwise to 400 µL of a PEI solution in 100 mM phosphate buffer pH 5.8 (5 mg mL^{-1}) under ultrasonication (sonifier, Bandelin electronic UW 70/HD 70; tip, MS 72/D, Berlin, Germany). After adding 1 mL phosphate buffer pH 5.8, the particle suspension was purified by centrifugation (14000 rpm, 2 min, 4 °C). Finally, after another washing step with 1500 µL of the same buffer, the particles were resuspended in 1 mL 20 mM HEPES/NaOH pH 7.4 and stored at 4 °C until use. Control particles were treated as described above but using solely buffer instead of PEI. The zeta-potential of plain and PEI coated microspheres was determined after 12.5-fold dilution of the particle suspension with HEPES/NaOH pH 7.4 using a Zetasizer Nano ZS (Malvern Instruments Ltd., UK). Additionally, the particle suspension was checked for agglomerates under fluorescence microscope just before further experiments.

2.3. Preparation of wheat germ agglutinin functionalized microspheres

Wheat germ agglutinin was coupled covalently to the surface of polystyrene microspheres via a carbodiimide method. 1 mg polystyrene microspheres was suspended in 20 mM HEPES/NaOH buffer pH 7.0 containing 0.1% Pluronic® F-68 and activated by adding 500 µL of a freshly prepared solution of

1-ethyl-3(3-dimethylaminopropyl) carbodiimide (721 mg mL^{-1}) and N-hydroxysuccinimide (30 mg mL^{-1}) in the same buffer. After end-over-end incubation for 2 h at room temperature, the microspheres were washed with 1000 µl HEPES/NaOH buffer pH 7.4 containing 0.1% Pluronic® F-68 by centrifugation (14000 rpm, 2 min, 4 °C) to remove excess reagents. After two additional washing steps with 1500 µL of the same buffer, the activated microspheres were resuspended in 500 µL HEPES/NaOH buffer pH 7.4 containing 0.1% Pluronic® F-68 and mixed with 118.6 µL of a WGA solution (5 mg mL^{-1}). After end-over-end incubation overnight at room temperature, unreacted binding sites at the particle surface were saturated by incubation with 160 µL aqueous glycine solution (100 mg mL^{-1}) for 30 min at room temperature. Subsequently, the microspheres were washed three times by centrifugation (14000 rpm, 2 min, 4 °C) as above. Finally, the particles were resuspended in 1000 µL 20 mM HEPES/NaOH buffer pH 7.4 containing 0.1% Pluronic® F-68 and stored at 4 °C until use.

2.4. Production of sterile 3D-microchannels

The applied 3D-microchannels were composed of poly(dimethylsiloxane) (PDMS). Using the Sylgard® 184 Elastomer Kit as described by Fillafer [17], a mixture of 10 g base and 1 g curing agent was vigorously stirred and evacuated for 30 min to remove gas bubbles. The liquid prepolymer was then poured into pre-shaped aluminum molds and hardened over night at 120 °C. In order to gain a hydrophilic surface, glass plates dimensioned 127 mm × 85 mm × 1.1 mm (length × width × height) were purified in piranha solution, representing a mixture of sulfuric acid and hydrogen peroxide 30% (7 + 3). After the PDMS replicas were carefully peeled off from the molds, four identical 3D-microchannels were attached to the pretreated glass plate by using the same liquid prepolymer as adhesive and a template for reproducible positioning. To guarantee proper adhesion of the PDMS to the glass, the assembly was finally heated to 100 °C for 30 min followed by disinfection in EtOH 70% and drying under laminar flow conditions prior to cell seeding.

2.5. Cell culture

The human intestinal epithelial cell line Caco-2 was purchased from the German Collection of Microorganisms and Cell Culture (DSMZ, Braunschweig, Germany). Cells were cultivated in RPMI 1640 cell culture medium containing 10% fetal bovine serum, 4 mM L-glutamine and 150 mg mL^{-1} gentamycine in humidified 5% CO_2/95% air atmosphere at 37 °C and were subcultured by TrypLE® select. All tissue culture reagents were obtained from Sigma (St. Louis, USA) and Gibco Life Technologies Ltd. (Invitrogen Corp., Carlsbad, USA). For cell culture in 3D-microchannels, each disinfected microchannel was pre-incubated for 30 min with 500 µl sterile PBS at room temperature thus allowing the PDMS to reach its final size by swelling. Then, 500 µL Caco-2 single cell suspension (1.36 × 10^5 cells mL^{-1}) were added and the cells were cultivated for 6–7 days until a confluent monolayer was formed. Cells between passage 43 and 52 were used throughout the study.

2.6. Microsphere binding to single cells

In order to determine the amount of single cell associated microparticles, 50 µL particle suspension (120 µg mL^{-1}, 60 µg mL^{-1}, and 30 µg mL^{-1} respectively) were mixed with 50 µL Caco-2 cell suspension (5 × 10^6 cells mL^{-1}) and incubated for 30 min at room temperature. Unbound or loosely associated particles were removed by centrifugation (5 min, 1000 rpm, 4 °C) and a washing step with 500 µL PBS containing 0.1% Pluronic® (PBS/Pluronic®). The cells were resuspended in 500 µL PBS and
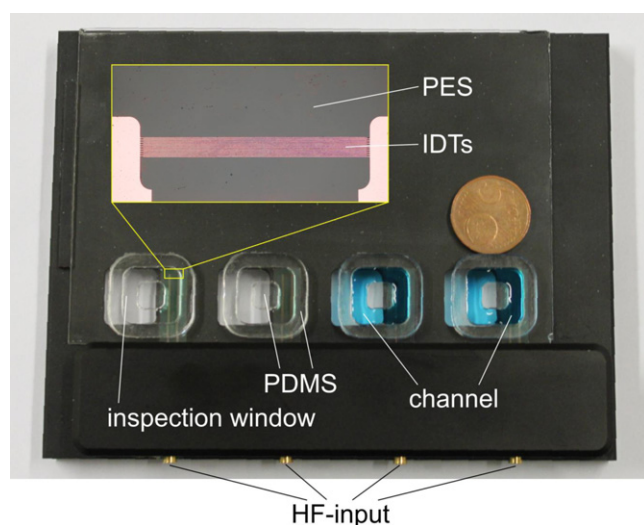
Fig. 1. Acoustically-driven microfluidic multichannel system. The surface acoustical wave (SAW)-chip consists of four parallelized interdigital electrodes, which are structured on a piezoelectric substrate (PES) and connected each with a high frequency connector (HF-input), thus serving as four identical interdigital transducers (IDTs). Four 3D-microchannels composed of poly(dimethylsiloxane) (PDMS) are attached to a glass plate dimensioned 127 mm × 85 mm × 1.1 mm (length × width × height) for the cultivation of cells. Inspection windows in the aluminum block allow microscopic observation during experiments.

analyzed on an EPICS XL-MCL analytical flow cytometer (Coulter, Miami, USA) using a forward-versus-side scatter gate for inclusion of the single-cell population and exclusion of debris and cell aggregates. Fluorescence was detected at 525 nm (10 nm bandwidth) and the mean channel number of the logarithmic intensities of individual peaks was used for further calculations. Amplification of the fluorescence signals was adjusted to put the auto fluorescence signal of unlabeled cells in the first decade of the four decade log range. Data of 3000 cells were collected for each measurement and assays were performed in triplicate.

2.7. Carbohydrate binding specificity of WGA-functionalized microspheres

To assess the carbohydrate-binding specificity of functionalized microspheres, 50 μL particle suspension (120 μg/mL) were mixed with 100 μL N,N′,N″-triacetylchitotriose solution (0, 0.05, 0.1, 0.2, 0.4, 0.8 μmol mL^{-1} in PBS/Pluronic$^{®}$) and 50 μL cell suspension (5×10^6 cells mL^{-1}). The mixture was incubated for 30 min at 4 °C and washed once with 500 μL PBS/Pluronic$^{®}$ by centrifugation (5 min, 1000 rpm, 4 °C) in order to remove unbound or loosely associated microspheres. Cells were resuspended in 500 μL PBS and analyzed by flow cytometry in triplicate as described above.

2.8. Preparation of the multichannel SAW-chip

The multichannel SAW-chip used for the present work had a similar set-up as described by Fillafer [17]. Briefly, four interdigital transducers (IDTs) were glued into a prestructured aluminum block and connected with ports for cabling. Windows in the aluminum block allow microscopic inspection with inverted or upright microscopes during experiments (Fig. 1). The system is operated via a radio frequency generator (SMB100A, Rohde&Schwarz GmbH, Austria) connected in series to a self-cooled high power amplifier (LZY-1, Mini Circuits, Brooklyn, USA) and a fixed attenuator (VAT-3W2+, Mini Circuits, Brooklyn, USA). Finally, the RF signal is distributed to the four IDTs by a 4-way divider (D1572-102, Werlatone, Brewster, USA).

2.9. Pulse-chase binding studies on Caco-2 cell monolayers at stationary and flow conditions

In order to characterize the interaction between polystyrene microparticles with different surface coatings and Caco-2 cell layers as well as the impact of flow on the adhesion, the particle suspensions were diluted in respective buffers to achieve working concentrations of 15 μg mL^{-1}, 30 μg mL^{-1}, and 60 μg mL^{-1} respectively. Prior to the experiments, the cell culture medium was removed from the 3D-microchannels and the cell monolayers were washed once with 500 μL of the respective buffer. Each microchannel was filled with 500 μL of the particle suspension and covered with a glass cover slip. Then, 200 μL of water were pipetted on each IDT as coupling medium and the glass plate was placed on the SAW-chip. The pulse-incubation was performed for 30 min at room temperature either under stationary conditions or under flow conditions with a flow velocity of 2000 μm s^{-1}. After removal of unbound or loosely adhered particles by two washing steps with 500 μL of the respective buffer per channel, the relative cell-associated fluorescence intensities were analyzed at 440/485 nm using a microplate fluorimeter (Infinite M200, Tecan, Grödig, Austria). Subsequently, the cell monolayers were further incubated for 30 min at room temperature either under stationary conditions or under flow conditions at a flow velocity of 2000 μm s^{-1} (chase-incubation). Finally, after one washing step, the relative cell-associated fluorescence intensities were assessed again as described above.

2.10. Fluorescence microscopy

To visualize the microparticle distribution on the Caco-2 cell surface at the end of the pulse-chase-experiments and to validate confluence of the cell monolayer after exposure to flow, fluorescence together with differential interference contrast (DIC) microscopy was applied. Images of the cell layers were acquired without any specific preparation immediately after fluorescence quantification using a Zeiss Axio Observer.Z1 microscopy system equipped with the LED illumination system "Colibri" and the Axio-Vision Rel. 4.8.2 software (Zeiss, Göttingen, Germany). That way, the amount of cell-associated microspheres could also be correlated to the quantified fluorescence intensities.

3. Results and discussion

3.1. Characteristics of the surface-modified polystyrene microspheres

Although the polystyrene particles used in this work are not biodegradable and consequently not suitable for administration as drug carriers, they are well suited for basic systematic studies on particulate drug formulations due to their well defined size class and the potentially functionalized surface. Since many polymers used for drug delivery purposes feature carboxyl end groups, carboxylated polystyrene microspheres were used in the present work carrying negatively charged groups at their surface. According to measurements, this results in a negative zeta potential of -85.2 ± 6.1 mV at pH 7.4. Utilizing these negative charges, cationic polyelectrolytes might thus be adsorbed onto the surface of carboxylated microspheres. A series of natural and synthetic polyelectrolytes have been employed for this purpose, including protamine [18], chitosan [19–21], Eudragit$^{®}$ RL [22], and poly(L-lysine) [5,23]. In the current study, however, low molecular weight branched PEI was used due to the high density of amino groups [24]. Following a modified protocol from Trimaille et al. [25], positive charges could be introduced at the surface of the particles as
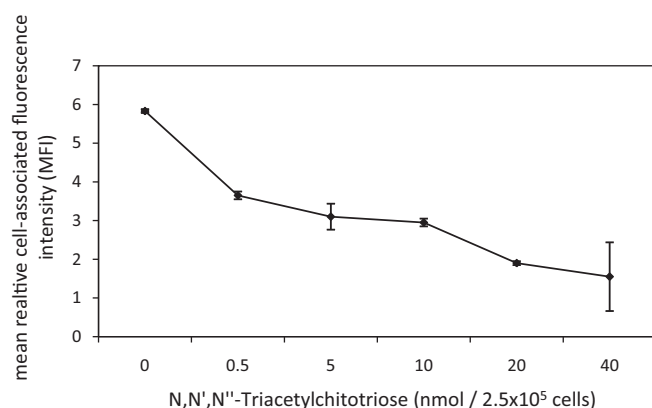
Fig. 2. Competitive inhibition of the binding of WGA-functionalized microspheres to Caco-2 single cells using N,N′,N″-triacetylchitotriose at different concentrations. Particle binding was determined by flow cytometry (mean ± S.D., n = 3).

confirmed by an inversion of the zeta potential to 71.2 ± 1.4 mV at the same pH.

Furthermore, WGA, which can specifically bind to sialic acid and N-acetyl-D-glucosamine, was covalently coupled to the surface of the microparticles using a carbodiimide method. In order to assess the binding specificity of WGA-functionalized microspheres, an inhibition test was performed. At this, the free complementary carbohydrate N,N′,N″-triacetylchitotriose competed with oligosaccharides within the glycocalyx of the Caco-2 cells for the binding to WGA-modified particles. As shown in Fig. 2, the number of cell-associated particles decreased in presence of increasing amounts of chitotriose to a minimum of 26.6% of the initial value at 40 nmol carbohydrate per 2.5×10^5 cells. This confirms that the interaction between cells and WGA-modified particles was mostly due to the lectin-coat of the microspheres representing a specific carbohydrate-binding moiety.

3.2. Binding characteristics of surface modified polystyrene microspheres to Caco-2 single cells and monolayers under stationary conditions

In order to study the impact of the different coatings, the binding rates of polystyrene microspheres either via ionic (positively, negatively charged) or biorecognitive interactions to Caco-2 single cells (Fig. 3A) as well as to Caco-2 cell monolayers (Fig. 3B) were assessed under stationary conditions. As illustrated, WGA-functionalized microparticles revealed the highest binding efficiency concerning both, single cells and monolayers.

In case of PEI-coated particles, the determined relative cell-associated fluorescence intensities showed a very high variance in both assays as indicated by the large error bars. This might be due to the strong agglomeration tendency of PEI-coated particles in PBS buffer. As shown in Fig. 4, fluorescence imaging of the particle binding to Caco-2 cells again confirmed the potential formation of large aggregates in single cell as well as in monolayer experiments for PEI-microspheres as compared to WGA-grafted or negatively charged particles.

Detailed studies on the stability of PEI-coated microspheres revealed that their agglomeration tendency was highly depending on the storage time as well as the buffer system used for the particle suspension. In order to characterize the aggregation behavior of PEI-particles, the polydispersity index (PDI) was assessed in different buffer systems. According to the literature [26–29], the PDI is a width parameter describing the size distribution of particles with a value between 0 and 1. A PDI value of <0.1 indicates monodisperse particles; a PDI between 0.1 and 0.5 represents particles with small
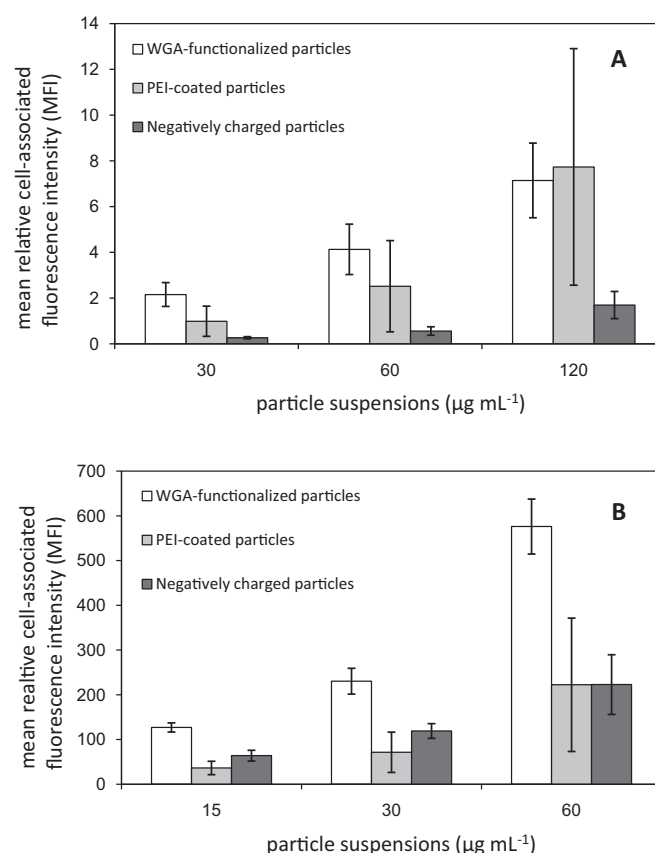

Fig. 3. Binding of polystyrene microspheres with different surface modifications to Caco-2 single cells (A) and to Caco-2 monolayers (B) (mean ± S.D., n = 3). Cells were incubated for 30 min at room temperature under stationary conditions and analyzed by flow cytometry (single cells) or fluorimetry (monolayers).

variations in size; a PDI > 0.5 signalizes a very broad size distribution rendering the suspension rather useless. As illustrated in Table 1, the PDI of PEI-microspheres rose within 30 min after coating in all buffers tested. However, using 20 mM HEPES/NaOH pH 7.4 (HEPES) the increase in PDI was only 1.8-fold as compared to the initial values immediately after coating and remained around 0.1 pointing at a narrow size-distribution. In contrast, storage in isotonic 20 mM HEPES/NaOH pH 7.4 (isoHEPES) and PBS increased the PDI 4.0-fold and 7.4-fold, respectively. However, after incubation in isoHEPES for 30 min the PDI was still below 0.5 indicating an acceptable size distribution. After storage for 30 min in PBS, broad variations in particle size were detected as represented by a PDI of almost 1 due to the presence of high amounts of agglomerated particles. The different size distributions could also be observed by fluorescence microscopy (Table 1, last row) clearly indicating different aggregation tendencies. Although the PDI was <0.5 in all three buffer systems directly after coating, PBS still exhibited the largest PDI as compared to isoHEPES and HEPES, which again confirms the larger agglomeration trend in PBS buffer. In order to avoid formation of aggregates, the microspheres were coated with PEI directly before use and stored in 20 mM HEPES/NaOH pH 7.4 which emerged to be the best storage medium. However, this buffer system could not be used for the cell-binding studies due to the restricted viability of cells in non-isotonic environment. Although the isotonisation of 20 mM HEPES/NaOH pH 7.4 also seemed to foster aggregation of PEI-coated particles, the PDI of 0.423 was within an acceptable range so that isotonic 20 mM HEPES/NaOH pH 7.4 seemed to be potentially suitable for further particle-cell experiments.

Although human cells possess a net negatively charged surface, it is difficult to conclude if positive particles actually entail
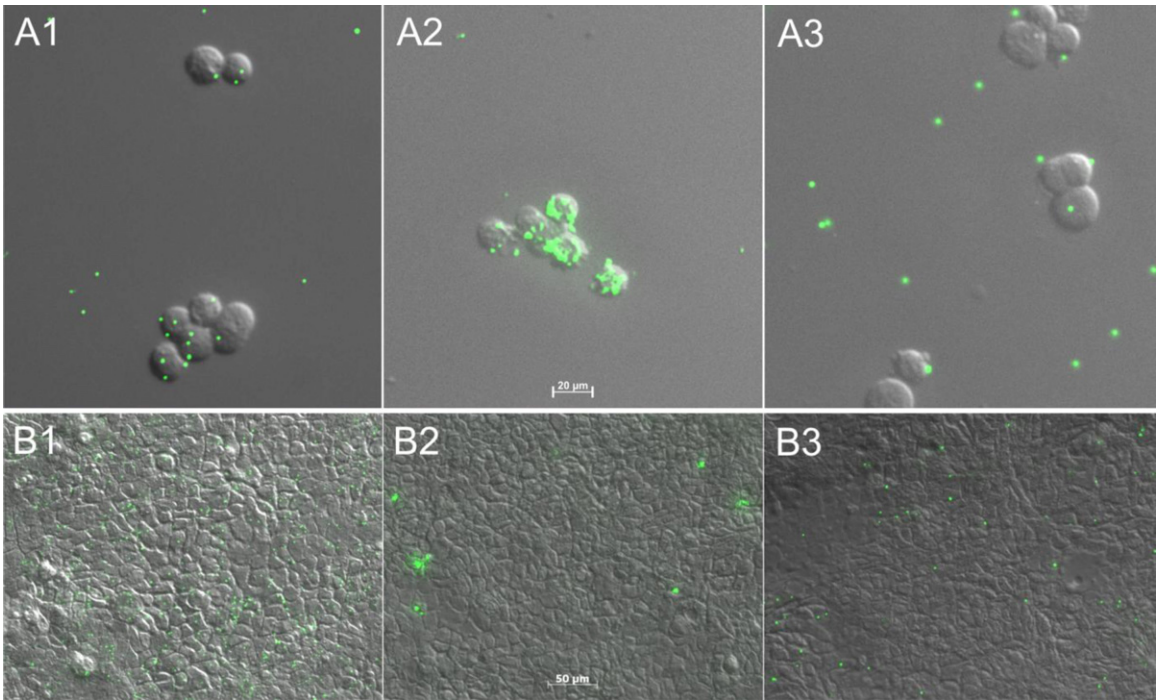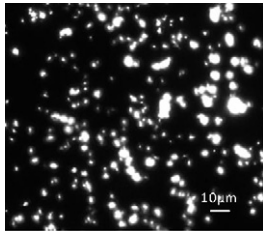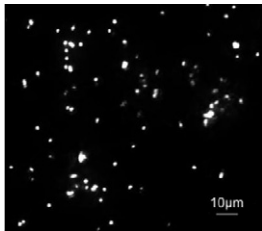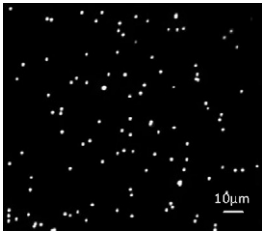
Fig. 4. Fluorescence images of the particle binding to Caco-2 single cells (A) and monolayers (B) under stationary conditions: WGA-grafted microparticles (1), PEI-coated micoparticles (2), and negatively charged microparticles (3).

Table 1
Polydispersity index of PEI-coated microspheres in different buffer systems as well as microscopic fluorescence images of these particles after storage for 30 min.

Polydispersity index (PDI)	20 mM HEPES/NaOH pH 7.4 (HEPES)	Isotonic 20 mM HEPES/NaOH pH 7.4 (isoHEPES)	Isotonic PBS
Immediately after coating	0.063	0.105	0.121
30 min after coating	0.112	0.423	0.893
Fluorescence microscopic images			

higher cell binding than negatively charged ones due to pronounced agglomeration. Nevertheless, the results clearly indicate that both ionic interactions (positive and negative particles) were characterized by a lower binding efficiency to Caco-2 cells in comparison with WGA-mediated biorecognitive interactions.

3.3. Influence of different buffers on the binding properties of surface modified microparticles

In order to evaluate the impact of cell-compatible buffers on the particle–cell interaction and to select a suitable buffer system for the upcoming experiments, binding studies on Caco-2 cell monolayers were performed with particle suspensions in PBS containing 0.1% Pluronic® F-68 (PBS/Pluronic®) as well as iso-tonic 20 mM HEPES/NaOH pH 7.4 containing 0.1% Pluronic® F-68 (isoHEPES/Pluronic®) pursuing the same protocol as described above (Section 3.2 monolayer experiments). These assays were carried out under stationary conditions with particle concentrations of 30 μg mL^{-1} for 30 min.
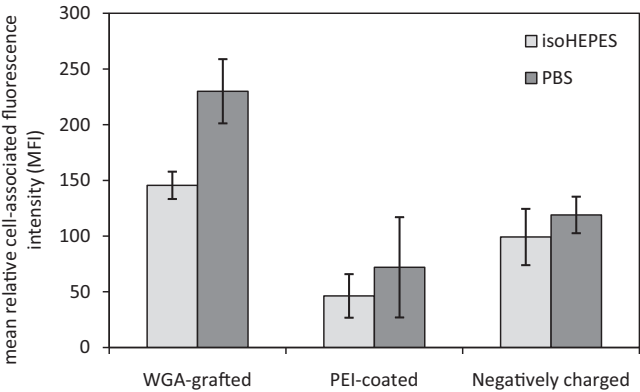

Fig. 5. Influence of the buffer system on the binding characteristics of surface modified polystyrene microspheres (30 μg mL^{-1}) to Caco-2 cell monolayers after incubation for 30 min at room temperature under stationary conditions (mean ± S.D., $n = 3$).

As illustrated in Fig. 5, the cell binding rates of WGA-grafted particles were clearly influenced by the buffer system used for the assay. Interestingly, the overlapping standard deviations indicated no distinct impact of buffer in case of positively and negatively charged particles. However, when the mean relative cell-associated fluorescence intensities of PEI-coated particles in isoHEPES/Pluronic® were compared with those in PBS/Pluronic®, the quantity of cell associated microspheres decreased by about a third at the mean. This finding is in accordance with previous studies on the PDI revealing that positive particles were more likely to agglomerate in PBS/Pluronic® than in isoHEPES/Pluronic®. Due to this pronounced agglomeration tendency of PEI-coated particles, the observed increase in cell associated fluorescence in case of PBS assays as already discussed in Section 3.2 can be explained by binding of particle clusters instead of single particles. This hypothesis is also supported by the huge standard deviations in the single cell and monolayer assays indicating a high variability in the interplay between particle aggregation and cell binding. Interestingly, according to measurements of the pH as well as the osmolarity and according to calculations the ionic strength of PBS and isoHEPES are identical. Thus, there was another impact of the buffer system on the particle–cell interaction. For that purpose, the influence of the buffers on the fluorimetric detection or alterations of the surface charge of particles and cells as well as the interactions between them were taken into consideration. According to detailed experiments, a buffer-induced alteration of fluorescence intensity is very unlikely (data not shown). However, the surface charge of cells and particles could probably be affected or altered provoking different interaction kinetics, since PBS contains multivalent ions as compared to isoHEPES. Furthermore, due to probably insufficient charge compensations at the particle surface during the PEI-coating process, locally negative and positive surface areas might be created promoting the agglomeration process.

Considering the variation of the determined MFI as shown in Fig. 5, the calculated standard deviation for the PEI-particle binding was considerably lower in case of isoHEPES. In line with the reduced tendency toward aggregation, isoHEPES/Pluronic® was thus used as standard buffer instead of PBS/Pluronic® for the binding studies in 3D-microchannels, although adhesion of WGA-modified microspheres is significantly reduced in this buffer which might lead to an underestimation of the actual binding capability of these particles. Additionally, PEI-coated particles were prepared immediately before the experiments and all particles were sonified for resuspension to exclude agglomerations as well as checked by fluorescence microscopy to guarantee proper conditions.

3.4. Pulse-chase cytoadhesion studies of modified polystyrene microspheres in a multichannel acoustically-driven microfluidic system

Upon administration in humans, either peroral or parenteral, the flow of materials under physiological conditions and the associated hydrodynamic forces will affect the binding of particles to cells and tissues. To investigate the impact of hydrodynamics on the cytoadhesion of particles a microfluidic setup similar to that described by Fillafer et al. [17] was used to characterize the cytoadhesion under flow conditions. In the present work, to improve reproducibility and to enhance versatile applicability of such acoustically-driven microfluidic techniques, a SAW platform with four identical IDTs, which were assembled on an aluminum block (Fig. 1) and could be operated in parallel, has recently been developed in our group. Moreover, the device was designed in a way that the glass plates, which serve as a support for the PDMS-channels and allow cell growth, were of the same size as standard microplates. That way, it is possible to detect plate-associated luminescence, absorbance or fluorescence with high spatiotemporal resolution in standard microplate readers.

Using this multichannel acoustically-driven microfluidic system, a series of cytoadhesion studies of surface modified particles was performed following different pulse-chase incubation setups. Throughout the experiments Caco-2 cell monolayers grown to confluence in 3D-microchannels were used. At first, the cells were incubated with all three types of polystyrene microspheres (WGA-grafted, PEI-coated and negatively charged) under stationary conditions so that both phases, the pulse- and the chase-incubation, were identical lasting for 30 min at RT each (s/s). After the pulse-incubation but prior to the fluorescence readout of the pulse-phase a washing step was performed in order to remove unbound or loosely attached particles. As illustrated in Fig. 6, at the mean, a slight difference of the cell-associated fluorescence could be observed between the pulse- and the chase step for each type of particle. The decrease in particle binding after the chase incubation was highest for the positively charged microspheres amounting to 36% of the pulse-phase value. WGA-modified particles yielded the best results with 89% of stably bound particles after the chase-phase. As these s/s assays could not reflect the impacts of flow, microsphere binding to Caco-2 cells was also assessed using an s/f setup, where a stationary pulse-incubation representing a preloading step was followed by a chase-incubation under flow conditions. That way, still loosely bound microspheres were supposed to detach from the cell monolayers due to the streaming. Interestingly, as shown in Fig. 6, almost no difference between the two phases could be observed despite exerting shear stress to the preloaded monolayers. Finally, to simulate in vivo conditions, the pulse-chase assay was performed with both incubation-steps under flow conditions (f/f). As to the s/s and s/f studies, the impact of hydrodynamic drag during the chase-phase on cell-binding of the particles was rather low. As compared to the other assay setups, however, it was interesting to note that the binding rates after the pulse-incubation in f/f studies were slightly higher for WGA-grafted and negatively charged spheres amounting to 117% and 126%, respectively. Considering the size of the polystyrene microparticles used in this work being 1 μm, only about 1% of the added particles were calculated to be deposited during 30 min of incubation. Thus, the shear stress of flow might provoke a down-drift of the microspheres, which brings more particles in close contact with the cells and results in a higher number of cell-associated particles.

All in all, the series of pulse-chase incubation studies about cytoadhesion of different types of polystyrene microspheres revealed that the impact of hydrodynamic stress on pre-bound particles at the surface of cell monolayers is rather low. Loading of the colloids under flow conditions, however, might increase the probability of access of particles to the cell surface due to additional effects of flow.

Concerning the kind of surface modification, WGA-grafted particles exhibited the highest binding rates to Caco-2 monolayers independent from the type of assay performed, exceeding that of positively and negatively charged particles 2.13–2.98-fold (Fig. 6). Hence, as also demonstrated in Section 3.2, biorecognitive interactions seem to provide a higher binding efficiency to cells than ionic interactions. Biorecognition generally comprises different binding mechanisms including electrostatic interactions, hydrogen-bonding as well as van der Waals and hydrophobic interactions [30]. As a consequence these interactions benefit from a rather high binding stability as exemplified by K_D values of about 10^{-7} for the lectin-carbohydrate interaction [31]. Another important feature of biorecognitive interactions relies on the close fit between the ligand and the binding pocket resulting in a highly specific interaction depending on 3-dimensional geometry and chemistry. In contrast, binding via ionic interactions might be impeded or at least partly shielded by electrolytes present in the
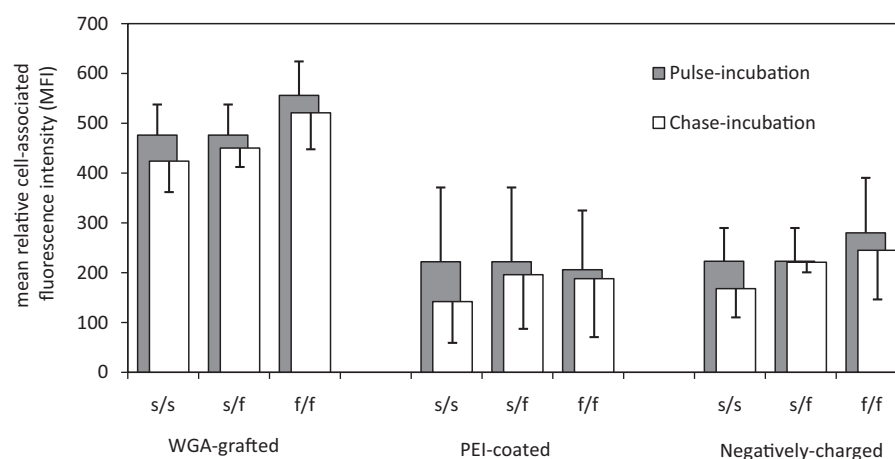
855

Fig. 6. Pulse-chase binding studies of WGA-grafted, positively and negatively charged microspheres (60 μg mL^{-1}) to Caco-2 cell monolayers at stationary and flow conditions (mean ± S.D., $n = 3$). s/s represents a setup where the incubation was identical for both phases: 30 min, room temperature, stationary conditions; s/f represents a setup with a pulse-incubation for 30 min at room temperature under stationary conditions followed by a chase-incubation for 30 min at room temperature under flow conditions. f/f represents a setup where the incubation was identical for both phases: 30 min, room temperature, flow conditions. A flow velocity of 2000 μm s^{-1} was applied for all flow conditions. After the pulse- as well as after chase-incubation but prior to fluorescence readout washing steps using isoHEPES/Pluronic® were performed.

surrounding medium. With respect to the allocation of the ionic binding partners within the cellular membrane, positive and negative charges are rather stochastically distributed over the surface, which might contribute to a rather weak local interaction.

A final comparison between the cytoadhesion efficiencies of positive and negative particles is difficult because of the high standard deviations of positively charged particles due to the fact that the storage time after modification as well as the buffer systems used further influence the results significantly. Additionally, during this work particles of only one single size (1 μm) were applied and the flow velocity was set to a constant value of 2000 μm s^{-1}. However, the dimension of the particle surface, the mass of particles, and the deposition rates vary according to the diameter of the colloids. Moreover, according to Decuzzi et al. [32] the role of particle shape should be considered for the bioadhesive behavior of particulate formulations. Hence, it might be interesting to use particles with different sizes as well as shapes at varying flow velocities in further studies. In addition, it would be interesting to perform these studies with different types of cells as the properties of the monolayer surface might also influence the interaction between particles and the cells.

4. Conclusion

Carboxylated polystyrene microspheres with 1 μm in diameter were either coated with PEI to convert the surface charge from negative to positive or modified with WGA to obtain a carbohydrate specific surface. Regarding the influence of the binding mechanism on the characteristics of particle–cell interactions, WGA-grafted particles mediating biorecognition exhibited a higher cell binding efficiency than PEI-coated or unmodified carboxylated microspheres which provoke ionic interactions. In case of positively charged PEI-particles a buffer system which provides storage stability and impedes agglomeration has to be selected. Studying the cytoadhesive properties of particles under flow conditions in an acoustically-driven microfluidic multichannel system demonstrated that the hydrodynamic drag, which is likely to occur throughout the organism during drug administration, has no negative impact on cell-bound particles at a flow velocity of 2000 μm s^{-1} independent from the type of particle preloading, but even leads to an increased probability of binding. Thus, administration of particulate drug delivery systems smaller than 1 μm might benefit from stable adhesion of the formulation to the pharmaceutical target

also in vivo. In addition, localized or targeted particulate therapy concepts relying on specific interactions with cell membrane components should be preferred provided that the size of the formulation is appropriate. Nevertheless, the impact of flow on the bioadhesive properties of different drug formulations has to be further investigated in more detail due to the ubiquitous presence of hydrodynamic forces under physiological conditions. Thus, it might be advisable to underline the current results with studies using particles of different sizes as well as shapes and under different flow velocities.

References

[1] B. Sun, B. Ranganathan, S.S. Feng, Biomaterials 29 (2008) 475.
[2] S. Acharya, F. Dilnawaz, S.K. Sahoo, Biomaterials 30 (2009) 5737.
[3] J. Lu, J.K. Jackson, M.E. Gleave, H.M. Burt, Cancer Chemother. Pharmacol. 61 (2008) 997.
[4] Z. Wang, W.K. Chui, P.C. Ho, Pharm. Res. 26 (2009) 1162.
[5] S. Faraasen, J. Voros, G. Csucs, M. Textor, H.P. Merkle, E. Walter, Pharm. Res. 20 (2003) 237.
[6] O.C. Farokhzad, J. Cheng, B.A. Teply, I. Sherifi, S. Jon, P.W. Kantoff, J.P. Richie, R.P. Langer, Proc. Natl. Acad. Sci. U.S.A. 103 (2006) 6315.
[7] A.R. Hilgenbrink, P.S. Low, J. Pharm. Sci. 94 (2005) 2135.
[8] J.D. Smart, Adv. Drug. Deliver. Rev. 57 (2005) 1556.
[9] V. Grabovac, D. Guggi, A. Bernkop-Schnuerch, Adv. Drug. Deliver. Rev. 57 (2005) 1713.
[10] J.N. Mehrishi, J. Bauer, Electrophoresis 23 (2002) 1984.
[11] L. Thiele, B. Rothen-Rutishauser, S. Jilek, H. Wunderli-Allenspach, H.P. Merkle, E.J. Walter, J. Control. Release 76 (2001) 59.
[12] L. Thiele, J.E. Diederichs, R. Reszka, H.P. Merkle, E. Walter, Biomaterials 24 (2003) 1409.
[13] C. Bies, C.-M. Lehr, J.F. Woodley, Adv. Drug. Del. Rev. 56 (2004) 425.
[14] E. Gutierrez, A. Groisman, Anal. Chem. 79 (2007) 2249.
[15] W.S. Rhee, A.M. Taylorv, C.H. Tu, D.H. Cribbs, C.W. Cotman, N.L. Jeon, Lab. Chip 5 (2005) 102.
[16] D. Huh, H. Fujioka, Y.C. Tung, N. Futai, R. Paine, J.B. Grotberg, S. Takayama, Anal. Chem. 79 (2007) 1369.
[17] C. Fillafer, G. Ratzinger, J. Neumann, Z. Guttenberg, S. Dissauer, I.K. Lichtscheidl, M. Wirth, F. Gabor, M.F. Schneider, Lab. Chip 9 (2009) 2782.
[18] J.M. Martínez Gómez, N. Csaba, S. Fischer, A. Sichelstiel, T.M. Kündig, B. Gander, P. Johansen, J. Control. Release 130 (2008) 161.
[19] A. Vila, A. Sánchez, M. Tobío, P. Calvo, M.J. Alonso, J. Control. Release 78 (2002) 15.
[20] H. Yamamoto, Y. Kuno, S. Sugimoto, H. Takeuchi, Y. Kawashima, J. Control. Release 102 (2005) 373.
[21] R. Yang, S.G. Yang, W.S. Shim, F. Cui, G. Cheng, I.W. Kim, D.D. Kim, S.J. Chung, C.K. Shim, J. Pharm. Sci. 98 (2009) 970.
[22] K. Dillen, J. Vandervoort, G. Van den Mooter, A. Ludwig, Int J. Pharm. 314 (2006) 72.
[23] M. Müller, J. Voros, G. Csucs, E. Walter, G. Danuser, H.P. Merkle, N.D. Spencer, M. Textor, J. Biomed. Mater. Res. A 66 (2003) 55.

[24] O. Boussif, F. Lezoualc'h, M.A. Zanta, M.D. Mergny, D. Scherman, B. Demeneix, J.P. Behr, Proc. Natl. Acad. Sci. U.S.A. 92 (1995) 7297.

[25] T. Trimaille, C. Pichot, T. Delair, Colloids Surf., A 221 (2003) 39.

[26] R.M. Schiffelers, J.M. Metselaar, M.H.A.M. Fens, A.P.C.A. Janssen, G. Molemay, G. Storm, Neoplasia 7 (2005) 118.

[27] M. Nidhin, R. Indumathy, K.J. Sreeram, B.U. Nair, Indian Acad. Sci. 31 (2008) 93.

[28] A.S. Lawrie, A. Albanyan, R.A. Cardigan, I.J. Mackie, P. Harrison, Vox Sang. 96 (2009) 206.

[29] R.H. Müller, R. Schuhmann, Teilchengrößenmessung in der Laborpraxis, Band 38, 1st ed., Wissenschaftliche Verlagsgesellschaft mbH, Stuttgart, 1996 (Chapter 3).

[30] D. Leckband, J. Israelachvili, Q. Rev. Biophys. 34 (2001) 105.

[31] H.-J. Gabius, The Sugar Code, Wiley-VCH Verlag GmbH&Co. KGaA, Weinheim, 2009 (Chapter 14).

[32] P. Decuzzi, R. Pasqualini, W. Arap, M. Ferrari, Pharm. Res. 26 (2009) 235.

2.2.2 Elucidation of lectin-binding to human endothelial cells and the lectin-blood cell interaction

Lectin-mediated biorecognition: Glycosylation pattern of human endothelial cells and blood cell-agglutinating effects of wheat germ agglutinin

Xue-Yan Wang[1], Martina Führinger[1], Nina Mizerovsky[1], Renate Hofer-Warbinek[2], Michael Wirth[1], Franz Gabor[1]

[1]Department of Pharmaceutical Technology & Biopharmaceutics, Althanstrasse 14, A-1090 Vienna, Austria

[2] Department of Vascular Biology and Thrombosis Research, Center for Physiology and Pharmacology, Medical University of Vienna, Vienna A-1090, Austria

Corresponding author:
Franz Gabor
Department of Pharmaceutical Technology & Biopharmaceutics
Althanstrasse 14, A-1090 Vienna, Austria
Phone: +43-1-4277-55406
Fax: +43-1-4277-9554
Email: franz.gabor@univie.ac.at

Abstract

In the present study, six fluorescein-labeled plant lectins with different carbohydrate specificity were used to elucidate the glycosylation pattern of endothelial cells before and after inflammation. Independent from the cell type the highest binding rates to endothelial monolayers were observed in case of wheat germ agglutinin (WGA) and *Ulex europaeus* isoagglutinin I indicating high numbers of accessible sialyl and fucosyl-residues at the cell surface. Upon TNF-α induced inflammation, in primary HUVEC additional sialic acid structures were disclosed as indicated by increasing WGA-binding rates. In general, the lectin binding capacity of macrovascular endothelial cells was significantly higher than that of microvascular ones. Inhibition tests with complementary sugars confirmed the specificity of lectin-binding to endothelial monolayers. Interestingly, WGA-blood cell interaction studies revealed that no agglutination of blood cells occurs up to the threshold of 15.88 µg WGA mL^{-1}. Thus, low amounts of WGA might be compatible with the circulatory system offering a promising approach towards therapeutic application of WGA-grafted drug delivery systems such as microcarriers, which might be beneficial to prolong the residence time and improve efficacy of poorly bioavailable drugs.

Keywords

Introduction

The vascular endothelium lines the entire interior surface of more than 60,000 miles of blood vessels in the human circulatory system [1]. This thin cell layer mediates a high number of physiological functions such as exchange of substances between blood and tissues, synthesis of nitric oxide, endothelin and prostacyclin for adjustment of vascular tone and blood pressure, as well as regulation of coagulation, inflammatory processes and angiogenesis. The surface of endothelial cells is coated with a glycocalyx, which contains different domains with specific carbohydrate residues [2] and is negatively charged [3]. According to electron microscopic studies with fixed samples, the glycocalyx is a fine network of different glycoproteins of 50-100 nm in thickness [4], whereas direct intravital microscopy revealed a thickness of 400-500 nm [5]. In addition, it is suggested that the glycocalyx decelerates the flow at the surface of the endothelial cells contributing to the asymmetric flow profile of blood[6-8].

The glycans decorating the surface of endothelia in different vascular beds from varying species including humans have been identified in several studies [1]. Smolkova et al demonstrated that Concanavalin A (ConA), *Lens culinaris* agglutinin (LCA), *Lycopersicon esculentum* agglutinin (LEA), *Ricinus communis* agglutinin (RCA) and wheat germ agglutinin (WGA) bound to all endothelial beds of rat microvasculature; however, *Griffonia simplicifolia* lectin I and *Helix pomatia* agglutinin interacted with certain beds [9, 10]. Lectin binding studies in early developmental chicken embryos showed that ConA, LCA and WGA specifically interact with vascular endothelium, but only LCA retained its ability to interact with endothelial cells upon further development [11]. An examination of *Ulex europaeus* isoagglutinin I (UEA-I) binding to the endothelial cells of human vasculature demonstrated that UEA-I is a specific marker for endothelial layers in human tissues as well as human tumors of endothelial origin [12-14]. Alroy et al. and Roussel et al. screened the binding of a set of lectins to 15 species including non-mammalian animals (e.g. chicken), mammalian animals (e.g. pig, goat and rabbit) and humans. The results revealed that the lectin binding pattern corresponding to the carbohydrate pattern decorating the surface of endothelial cells is a unique signature of different vascular beds and species. Additionally they ascertained an evolutionary development [15, 16].

Although several studies focused on the binding characteristics of different lectins to endothelial cells, a systematic study with human endothelium prior and after inflammation is still missing. Therefore, the aim of this work was to elucidate the binding characteristics and specificity of six plant lectins with different carbohydrate specificity. The selected plant lectins were wheat germ agglutinin (WGA) from *Triticum vulgare* binding to N-acetyl-D-glucosamine and sialic acid, the lectin from furze seeds (*Ulex europaeus isoagglutinin* I, UEA-I) interacting with α-L-fucose-containing carbohydrates, *Solanum*

tuberosum lectin (STL) from potato tubers binding to N-acetyl-D-glucosamine, lentil lectin from *Lens culinaris* (LCA) recognizing galactosaminyl-/α-mannosyl-residues, *Dolichos biflorus agglutinin* (DBA) from horse gram and peanut agglutinin (PNA) both interacting with galactosamine and its N-acetyl-derivative. Additionally, three different cell types are investigated: (i) primary human umbilical vein endothelial cells (HUVECs) isolated from human umbilical cords by treatment with collagenase Type I, (ii) human umbilical vein endothelial cells immortalized with human telomerase reverse transcriptase (HUVECtert) [17] and (iii) immortalized human dermal microvascular endothelial cells (HMEC-1) [18]. At this, primary HUVEC and HUVECtert represent macrovascular cells, whereas HMEC-1 are of microvascular origin. Moreover, another focus is set on the blood cell agglutinating activity of WGA which currently excludes this lectin from parenteral drug delivery concepts and has been already subject of some lectin-cell interaction studies [19-23]. Here, the objective was to evaluate whether it is reasonable or not to develop lectin-grafted drug delivery carriers for parenteral administration.

Materials and methods

Materials

The fluorescein-labeled lectins from *Triticum vulgare* (wheat germ agglutinin, molar ratio fluorescein/protein (F/P) = 4.5), *Solanum tuberosum* (STL; F/P = 3.2), *Ulex europaeus* (UEA-I, isoagglutinin I; F/P = 2.7), *Lens culinaris* (LCA; F/P = 3.7), *Arachis hypogaea* (PNA; F/P = 5.1) and *Dolichos biflorus* (DBA; F/P = 2.1) were purchased from Vector Laboratories (Burlingame, CA, USA). Human fibronectin was acquired from BD Bioscience (Bedford, USA). Recombinant Human TNF-α was obtained from R&D Systems (Minneapolis, MN, USA). Heparin sodium salt was from Sigma-Aldrich. All other chemicals were of analytical grade.

Cell Culture

In the present work, three different types of endothelial cells, HUVEC, HUVECtert and HMEC were used. All tissue culture flasks used for cultivation were coated with a 1% (w/v) aqueous solution of gelatin for 30 min prior to seeding the cells. All cells were cultivated in EndoPrime® Medium (EndoPrime Kit, PAA, Linz, Austria) supplemented with Bio Whittaker® Pen/Strep/Amphotericin B (final concentration 1% (v/v); Lonza, Basel, Switzerland) at 37 °C in a humidified 5% CO_2 / 95% air atmosphere and subcultured twice a week using 0.25% trypsin-EDTA solution. The cells were used for the experiments between passage 3 to 18 (HUVEC), 14 to 46 (HUVECtert) or 27 to 40 (HMEC).

For lectin binding studies and competitive sugar inhibition endothelial cell monolayers were grown in 96-well microplates. For fluorescence microscopy cell monolayers were cultivated on glass cover slips combined with the flexiPERM micro 12 system. The seeding density was for both cultivation systems 1.7×10^4 single cells/160 µL per well. Cells were cultivated under standard cell culture conditions until a confluent monolayer had been formed.

Lectin binding capacity of endothelial cells

To determine the lectin binding capacity of endothelial cells, single cells (HUVEC and HUVECtert) and monolayers (HUVEC, HUVECtert and HMEC) were investigated.

For monolayer experiments, confluent monolayers of HUVEC, HUVECtert and HMEC were washed with PBS buffer supplemented with Ca^{2+} and Mg^{2+} after removal of the culture medium. Subsequently, the cell monolayers were incubated with 50µL lectin solution (1.56 – 100 pmol, serial dilutions in the same buffer) each well for 30 minutes at 4°C. After removal of unbound lectins by three washing steps with cold buffer, the relative cell-associated fluorescence (RFI) was determined in a fluorescence microplate reader (TECAN, Infinite M200, Austria) at 485/525 nm. Monolayer samples incubated with buffer alone served as a control for autofluorescence of cells and microplates. In case of inflamed endothelial tissue (HUVEC and HUVECtert), the

monolayers were activated with TNF-α (0.5 ng/50 μL in cell culture medium) at 37°C for 4 hours. After removal of TNF-α by washing, the lectin binding capacity of inflamed endothelial cells was determined as described above for healthy cells. For comparability of the results, the read outs were related to an apparent conjugation number of 1mol fluorescein per mol lectin.

Specificity of the lectin-cell interaction

Competitive inhibition experiments using the complementary carbohydrates were performed to estimate the specificity of the lectin-cell interaction. After washing the confluent endothelial cell monolayer with cold PBS buffer supplemented with Ca^{2+} and Mg^{2+}, the cells were incubated with 25 μL of the complementary carbohydrate in buffer (see Table 2) and 25 μL of the corresponding lectin in the same buffer (12.5 pmol/well) for 30 min at 4°C. The monolayer samples were washed three times with 100 μL pre-cooled buffer and analyzed by fluorimetry. The acquired RFI values were related to control samples without carbohydrates, representing 100% lectin binding. For comparison of the data, IC_{50} values, defined as the amount of corresponding sugar necessary for 50% inhibition of lectin binding, were calculated from inhibition curves (not shown).

Cell microscopy

To visualize the cytoadhesion of different lectins in endothelial tissue, monolayer grown on slides assembled with the flexiPERM micro 12 system were incubated with 12.5 pmol lectin /50 μL PBS buffer supplemented with Ca^{2+} and Mg^{2+} per well at 4°C for 30 min. After removal of unbound lectins by three washing steps with cold buffer , the cells were fixed in ice cold methanol for 10 min at -20°C (100 μL/well). After rehydration in PBS containing 1% (v/w) BSA (100 μL/well) for 20 minutes at room temperature the monolayer were washed twice with the same buffer. Then, 100 μL solution of 0.5 μg Hoechst 3334 in PBS/ 1% BSA were added and incubated for 30 minutes at 37°C. Finally, the cells were washed twice with the same buffer and fluorescence images were acquired with a Zeiss Axio Observer.Z1 (Zeiss, Göttingen, Germany).

Evaluation of the interaction between WGA and erythrocytes from different blood groups

Blood samples were collected from healthy donors (blood groups O, A and B) using VACUETTE® blood collection tubes (3.5 mL 9NC Coagulation sodium citrate 3.2%; Greiner Bio-One GmbH, Kremsmuenster, Austria) and used immediately. To analyze the effects of WGA on erythrocyte agglutination, 19 μL blood samples were mixed with 1 μL solution of fluorescence labeled WGA (corresponding to an end concentration between 1.975-125 μg mL^{-1} in distilled water) and incubated for 10min at 37°C. For analysis within the measurement

range of the flow cytometer, the blood-lectin sample was diluted 20000-fold in two steps, first 100-fold and second 200-fold. The gates were set properly to determine single cells, cell debris, and cell aggregates. Samples without WGA served as a control and the assays were done in triplicate.

To visualize the effect of WGA on erythrocytes, the lectin-blood mixture incubated for 10 min as above was diluted 150-fold in order to avoid observation of pseudo-aggregates of erythrocytes due to the high concentrated samples. Immediately, for each concentration of the lectin at least 30 images were taken at the same magnification using a Zeiss Axio Observer.Z1 (Zeiss, Göttingen, Germany). The numbers of aggregates and single cells were counted manually and the average number of aggregates of each image was calculated. An aggregation was defined as an unarranged cluster of more than 2 cells

Inhibition experiments using chitotriose as a carbohydrate complementary to WGA were performed to verify the specificity of the lectin-binding to the erythrocyte surface. Briefly, 19 µL freshly drawn blood were mixed with 1 µL chitotriose solution (0.1 - 0.8 µmol mL^{-1}), and then with 1 µL WGA-solution (2.5mg mL^{-1}). After 10min incubation at 37°C and proper dilution the sample was analyzed by flow cytometry.

Results

Lectin binding capacity of endothelial cells

Six fluorescein-labeled plant lectins with different carbohydrate specificities were chosen to investigate the glycosylation pattern of endothelial cells. Additionally, HUVECs and HUVECtert were activated with TNF-α to estimate changes in lectin binding pattern upon inflammation. HMEC-1, however, failed to be inflamed by TNF-α treatment (data not shown). As displayed in Figure 1, independent from carbohydrate specificities of the lectins, the cell-bound fluorescence intensity increased with the lectin concentration in all three types of cells with and without TNF-α activation. The resulting binding curves leveled off between the concentrations of 12.5 and 100 pmol lectin indicating saturation of accessible carbohydrates. However, for all types of monolayers, DBA and PNA yielded very low RFIs which were scarcely higher than the autofluorescence of endothelial cells.

As demonstrated in Figure 1A and 1B, in case of HUVECs, the cell-associated fluorescence intensities followed the order: UEA-I > WGA ~ STL ~ LCA >> PNA > DBA. In contrast, in case of HUVECtert, the lectin-binding rate decreased as follows: WGA > UEA-I > STL >> LCA >> PNA > DBA. Although the lectin binding capacity was most pronounced in case of WGA and UEA-I for both cell types, the WGA binding rate to immortalized endothelial cells was higher than that of UEA-I. In contrast, UEA-I binding exceeded that of WGA in primary cells. Moreover, the cell-associated RFI of LCA was significantly lower on immortalized cells than on primary cells as indicated by only half RFI in case of HUVECtert as compared to HUVEC at 100 pmol LCA per well. Interestingly, there was an increasing LCA binding capacity of primary endothelial cells, and even saturation was not observed up to 100 pmol LCA. Furthermore, STL exhibited similar binding rates to both cell types. In contrast to primary and immortalized macrovascular endothelial cells, the HMEC-1 cell line originating from microvascular tissue showed significantly lower binding rates of the six plant lectins following the order: WGA > UEA-I ~ STL > LCA >> PNA ~ DBA. For instance, at the highest concentration of lectins the cell-associated fluorescence intensities of WGA, UEA-I and STL decreased to half of those of primary cells, and in case of LCA it decreased even to 12.5%.

Inducing inflammation of endothelial cells by pretreatment with TNF-α resulted in decreasing binding rates of most of the lectins as compared to healthy cells. In case of inflamed HUVEC at 100 pmol lectin/well the cell-associated RFI of UEA-I, STL, and LCA decreased by about 51%, 28%, and 42%, respectively (Fig. 1A and 1D); in case of immortalized HUVECtert, the binding rates of WGA, STL, and LCA decreased by about 23%, 31%, and 26%, respectively (Fig.1B and 1E). In contrast, the cell-associated fluorescence of WGA to inflamed HUVEC increased by about 24% as compared to healthy endothelial cells; thus the order of binding capacity of lectins was altered according to: WGA > UEA-I ~ STL ~ LCA >> PNA > DBA. Similarly, in case of HUVECtert a revesed ranking of WGA

and UEA-I was observed changing the lectin-binding order to UEA-I > WGA > STL > LCA >> PNA ~ DBA. At this, after activation with TNF-α, only the fluorescence of cell-associated UEA-I slightly increased by about 4% at 100 pmol per well. In order to elucidate the changes in lectin binding upon inflammation in more detail binding studies were repeated with lectins of high binding capacity at a lower concentration range from 1.56 to 12.5 pmol each well. Interestingly, no significant differences in RFI of WGA and UEA-I were detectable between inflamed and non-inflamed HUVEC and HUVECtert (Fig. 2). However, LCA-binding to HUVEC decreased slightly by about 16%.

The results of saturation analysis of lectin binding to endothelial cells were confirmed qualitatively by fluorescence microcopy (Fig. 3). Due to the strong interaction of the cell surfaces with WGA, UEA-I and STL, the apical membranes of HUVEC monolayer were intensely stained. In accordance with the rather weak interaction of PNA and DBA with the cells, fluorescent staining was not observed. Moreover, due to the temperature of pre-incubation with lectins (at 4°C), the metabolic activity of cells was minimized. Therefore, internalization of cell-bound lectins was not observed (see Figure S1C in supplementary appendix). HUVECtert and HMEC-1 yielded similar images like HUVEC (pictures not shown). Additionally, no signs of lectin mediated cytotoxicity were observed at the concentrations applied.

Specificity of the lectin-cell interaction

The specificity of the interaction between plant lectins and human endothelial cell was verified by competitive inhibition with complementary carbohydrates (Table 1). Depending on the amount of the complementary carbohydrate added, the carbohydrate binding domain of the lectin is blocked partially and inhibited from binding to the cell membrane. Due to their high binding capacity to endothelial cells WGA, UEA-I and LCA were chosen for inhibition experiments.

Generally, an increasing concentration of corresponding carbohydrate led to a decrease of lectin binding to the cell surface (Table 2). At the highest carbohydrate concentration applied, the extent of specific binding of all three lectins exceeded 80%. Whereas less than 10% of WGA and UEA-I binding to the endothelial glycocalyx was due to non-specific interactions, this extent increased to about 20% in case of LCA indicating lower specificity.

In case of microvascular HMEC-1 cells, the inhibition rates of both, WGA and UEA-I, were slightly lower than those of macrovascular HUVEC and HUVECtert exhibiting a similar level of specific binding. LCA, however, exhibited almost the same specificity of interaction with all types of endothelial cells. Inflammation of HUVEC and HUVECtert provoked no significant difference in inhibition of WGA and UEA-I binding as indicated by a mean IC_{50} of 0.0024 ± (WGA) and 0.1000 ± (UEA-I). Interestingly, after inflammation of HUVEC, the IC_{50} value of LCA decreased significantly to 24% of that of non-inflamed tissue.

Evaluation of the interaction between WGA and blood cells from different blood groups

Due to the high affinity and specificity of the interaction between WGA and endothelial cells as observed above, the effect of WGA on agglutination of blood cells was investigated. UEA-I also exhibited high affinity to endothelial cells. However, due to its blood-group specificity in contrast to WGA, which is non-specific for any blood group [24], it was excluded from the agglutination tests.

Upon incubation with increasing amounts of WGA, the percentage of aggregated blood cells of the whole population increased concurrently independent of the blood group (Fig. 4). According to flow cytometric analysis in presence of 31.25 - 125 µg WGA mL^{-1} more than 1% of the whole blood cells were aggregated. This percentage was significantly higher than that of control samples and independent from the blood group. The same results were obtained by directly counting the number of cell aggregates on microscopic images. At the highest WGA-level (125 µg mL^{-1}) huge aggregates were clearly observed (Figure 5). With decreasing amounts of WGA the size of the blood cell clumps concurrently decreased, but still several small aggregates were observed. At 31.25 µg mL^{-1} WGA, at least 2.1 aggregates were detected on each image in the case of blood groups A and O, and at least 0.5 aggregates were observed in case of blood group B (Table 3). In contrast, up to a WGA-concentration of 15.88 µg mL^{-1}, an almost constant amount of 0.13±0.06% aggregated blood cells independent from the blood group was determined. This value was not significantly different from the control samples without WGA amounting to 0.13±0.03% (Fig. 4). Moreover, microscopic analysis yielded similar results (Table 3). About 0.1±0.2 aggregates of blood cells per image were observed in presence of ≥ 15.88 µg mL^{-1} WGA as compared with 0.0±0.2 aggregates in controls without lectin.

Interestingly, on microscopic images of blood group A in presence of 15.88 µg mL^{-1} WGA a very few doublets were observed (Figure 6). However, these clumps cannot be clearly distinguished from pseudo-aggregates, which might be due to overlapping of two cells or the rouleau effect of blood cells [25]. Although the aggregation was reversible, these pseudo-aggregates were scored as aggregates to adhere to strict criteria. At the next concentration level of 7.94 µg mL^{-1} WGA no aggregation was observed like in control samples without WGA. The microscopic images of cells from blood group B and O revealed the same results (data not shown).

Discussion

In order to systematically characterize the glycosylation pattern of human endothelial cells, binding studies with a panel of lectins with different carbohydrate specificities were performed using their fluorescein-labeled analogues. For quantitative comparability of the results and to elucidate the sugar pattern of endothelial cells, it is assumed that each lectin binds only one specific carbohydrate residue. For instance, WGA is a dimeric protein containing four hevein domains as binding pockets for carbohydrates [26]. However, due to steric inaccessibility and different carbohydrate affinities [27], the molar binding ratio between WGA and glycosyl residues on the cell membrane can be limited to 1:1 even in case of cell monolayers. Additionally, the CyQuant® test assessing the cell number of the monolayer revealed no significant difference in cell numbers for all types of endothelial monolayers under investigation (supplementary appendix: Figure 2). Moreover, the RFI was related to an apparent flourescein/protein ratio of 1:1. Altogether, the ratios of detected RFI between different lectins represent the difference in glycosylation pattern of human endothelial cell monolayer.

According to the results, the glycocalyx of endothelial cells is characterized by high amounts of N-acetylglucosamine, sialic acid, fucosyl- and mannosyl residues and minor amounts of galactosamine- and N-acetyl-galactosamine-residues. These quantitative fluorimetric results are confirmed qualitatively by fluorescence microscopy (Fig. 3). The membrane of endothelial cells was intensely stained by WGA and UEA-I, followed by STL and LCA, whereas PNA and DBA-staining was almost invisible. However, the glycosylation patterns of macrovascular HUVECs and HUVECtert varied slightly probably due to immortalization. In the case of HUVECs, the carbohydrate pattern followed the order: fucose > N-acetylglucosamine and sialic acid ~ mannose >> galactosamine > N-acetyl-galactosamine. In contrast, HUVECtert contain about 5% less fucosyl residues than N-acetylglucosamine and sialic acid, as well as an approximately 46% lower amount of mannosyl structures than their primary cells. Interestingly, although WGA and STL possess similar carbohydrate specificity, the binding rate of WGA to the HUVECtert was significantly higher than that of STL. This might be due to the presence of sialic acid residues, which exclusively interact with WGA and not STL. Thus, the higher content of sialic acid residues might be due to immortalization. Comparison of the glycosylation pattern of macrovascular HUVECs and HUVECtert with HMEC-1 cell line of microvascular origin reveals a considerably lower lectin affinity to HMEC-1. HMEC-1 cells contain about 50% of fucosyl, N-acetylglucosamine and sialic acid residues, and rather less than 20% mannosyl structures at their surface as compared to HUVEC.

Nigel J. Klein postulated that inflammation by TNF-α leads to an alteration in the glycosylation pattern on the endothelial cell surface [28]. According to the increase in WGA binding and the decrease in STL

binding inflammation of primary macrovascular HUVEC provokes appearance of about 24% more sialic acid residues. However, in HUVECtert no numerical alteration of sialic acidic structures was observed. In case of UEA-I, only after TNF-α activation of HUVECtert the binding rates slightly increased by about 3.9±0.1% indicating easier accessible fucosyl residues. In HUVEC, however, the number of accessible fucosyl residues decreased by about 51% upon inflammation. Additionally, mannosylation corresponding to LCA-binding was decreased in both inflamed HUVEC and HUVECtert. At the first sight this observation is contradictory to results of increased mannose-mediated Concanavalin A (ConA)-binding after TNF-α stimulation [29-32]. However, it should be considered, although both ConA and LCA are mannose-binding legume lectins [26], that ConA possesses the strongest affinity to D-mannose at all [33]. Moreover, for a high affinity binding between LCA and glycans the presence of one fucosyl residue and two α-mannosyl residues are necessary [34]. Consequently, an increase in ConA binding not absolutely means an increase of LCA binding. Moreover, a decrease in LCA binding might not be only due to decreased mannosylation, but might also originate from reduced fucosyl residues. This additive effect might provoke the 42% decrease of LCA binding to inflamed HUVEC together with the 51% decrease of fucosylation in comparison to a 26% decrease of LCA binding to inflamed HUVECtert together with a 4% increase in fucosyl residues. In addition, although Chacko and Scott both have reported increased LCA binding to endothelial cells after TNF-α stimulation, it should be considered that human aortic endothelial cells and HUVEC purchased from ATCC were used in their studies [31, 32]. Since these two types of endothelial cells might be different from the HUVEC used in present study, which were isolated immediately after birth from the umbilical vein and represent macrovascular cells, the glycosylation patterns might differ.

According to competitive inhibition tests using complementary carbohydrates, WGA and UEA-I exhibited the highest binding specificity yielding up to 95% inhibition. In case of LCA the maximum level of inhibition was up to 83% indicating higher contribution of non-specific binding. However, the affinity of lectins to the glycocalyx on the surface of endothelial cells is quite different. According to the IC_{50} values, WGA possesses the highest binding affinity being up to 50-fold and 4000-fold higher than that of UEA-I and LCA, respectively (Table 2). Interestingly, after inflammation the binding specificity and binding affinity of WGA and UEA-I were not altered; however, in case of LCA, the IC_{50} value decreased significantly after TNF-α activation. It might be due to the decreasing of mannose structure at the cell surface after inflammation. Therefore, the needed amount of complementary sugar would be reduced for the inhibition of lectin binding to the cells.

Due to the outstanding binding rate and binding affinity of WGA to endothelial cells especially after inflammation, it might be beneficial

for therapy to develop WGA-grafted microcarriers as drug delivery systems for parenteral administration. However, Carlier, Stinissen and Peumans already discussed in 1982 [35] that wheat germ agglutinin represents a plant lectin that agglutinates human and animal erythrocytes. Nevertheless, it might be interesting to elucidate in detail the prerequisites, especially the dose of WGA necessary for red blood cell agglutination. Flow cytometry and microscopic evaluation confirmed that 15.88 µg mL^{-1} WGA is the limiting concentration for the agglutination of blood cells. Independent from the blood group no cell aggregates were observed up to this WGA concentration as compared to whole blood alone. Furthermore, Delmotte et al. reported that the minimum concentration of WGA required to agglutinate horse blood is 10 µg mL^{-1} WGA [36], which is in the range of the observed threshold of 15.88 µg mL^{-1} human blood. According to a rough calculation this limiting concentration of WGA corresponds to binding of 50000 WGA molecules per blood cell. Considering the maximum WGA-density at the surface of 3 µm PLGA-microparticles (unpublished data), agglutination of blood cells is supposed to occur only when the ratio between blood cells and microparticles exceeds 4. As administration of such extraordinary high amounts of WGA-grafted microparticles is neither reasonable nor required for efficacy, the concept of using WGA for prolonged drug delivery might be feasible. Moreover, it should be considered that this study was performed under static conditions. However, *in vivo* flow conditions are prevailing attaining shear rates up to 4000 s^{-1}, which might strongly reduce the agglutination tendency of blood cells, immediately strongly dilute the applied dose, and consequently might even increase this limiting concentration of WGA. Nevertheless, it should be also considered that factors like age and gender might affect such agglutination process.

To sum up, this study confirms that sialic acid, N-acetylglucosamine, and fucosyl residues are predominant structures in the glycocayx of endothelial cells. Especially, upon inflammation by TNF-α stimulation the increase of sialic acid structures leads to increasing WGA-binding to primary HUVEC. Moreover, the sugar inhibition study proved high specificity of the interaction between WGA and endothelial cells. In addition, up to a concentration of 15.88 µg mL^{-1} WGA exerted no agglutinating effects on blood cells. Thus, this threshold might be the maximum amount for administration of WGA for targeted drug delivery. All in all, the high binding rate and affinity of WGA to endothelial cells, as well as its rather high concentration necessary to agglutinate blood cells open new perspectives for glycotargeting in pharmaceutics.

References

[1] Scott DW, Patel RP. 2013. Endothelial heterogeneity and adhesion molecules N-glycosylation: Implications in leukocyte trafficking in inflammation. *Glycobiology* 23:622-633.

[2] Skutelsky E, Rudich Z, Danon D. 1975. Surface charge properties of the luminal front of blood vessel walls: An electron microscopical analysis. *Thromb Res.* 7:623–634.

[3] Simionescu M, Simionescu N, Palade GE. 1982. Differentiated microdomains on the luminal surface of capillary endothelium: Distribution of lectin receptors. *J Cell Biol.* 94:406–413.

[4] Squire JM, Chew M, Nneji G, Neal C, Barry J, Micheal C. 2001. Quasi-periodic substructure in the microvessel endothelial glycocalyx: a possible explanation for molecular filtering? *J. Struct. Biol.* 136:239-255.

[5] Vink H, Duling BR. 1996. Identification of distinct luminal domains for macromolecules, erythrocytes, and leukocytes within mammalian capillaries. *Circ. Res.* 79:581-589.

[6] Gao L, Lipowsky HH. 2009. Measurement of solute transport in the endothelial glycocalyx using indicator dilution techniques. *Ann. Biomed. Eng.* 37:1781-1795.

[7] Potter DR, Damiano ER. 2008. The hydrodynamically relevant endothelial cell glycocalyx observed *in vivo* is absent *in vitro*. *Circ. Res*. 102:770-776.

[8] Smith ML, Long DS, Damiano ER, Ley K. 2003. Near-wall micro-PIV reveals a hydrodynamically relevant endothelial surface layer in venules *in vivo. Biophys. J.* 85:637-645.

[9] Smolkova D, Zavadka A, Bankston P, Lutsyk A. 2001. Cellular beterogeneity of rat vascular endothelium as detected by HPA and GS I lectin-gold probes. *Med. Sci. Monit.* 7:659-668.

[10] Laitinen L. 1987. *Griffonia simplicifolia* lectins bind specifically to endothelial cells and some epithelial cells in mouse tissues. *Histochem. J.* 19:225-234.

[11] Jilani SM, Murphy TJ, Thai SN, Eichmann A, Alva JA, Iruela-Arispe ML. 2003. Selective binding of lectins to emgryonic chicken vasculature. *J. Histochem. Cytochem.* 51:597-604.

[12] Holthofer H, Virtanen I, Kariniemi AL, Hormia M, Linder E, Miettinen A. 1982. Ulex europaeus I lectin as a marker for vascular endothelium in human tissues. *Lab. Invest.* 47:60-66.

[13] Miettinen M, Holthofer H, Lehto VP, Miettinen A, Virtanen I. 1983. Ulex europaeus I lecin as a marker for tumors derived from endothlial cells. *Am. J. Clin. Pathol.* 79:32-36.

[14] Ordonez NG, Batsakis JG. 1984. Comparison of Ulex europaeus I lectin and factor VIII-related antigen in vascular lesions. *Arch. Pathol. Lab. Med.* 108:129-132.

[15] Roussel F, Dalion J. 1988. Lectins as markers of endothelial cells: Comparative study between human and animal cells. *Lab. Anim.* 22: 135-140.

[16] Alroy J, Goyal V, Skutelsky E. 1987. Lectin histochemistry of mammalian endothelium. *Histochemistry.* 86:603-607.

[17] Schiller HB, Szekeres A, Binder BR, Stockinger H, Leksa V. 2009. Mannose 6-phophate/insulin-like growth factor 2 receptor limits cell invasion by controlling alphaVbeta 3 integrin expression and proteolytic processing of urokinase-type plasminogen activator receptor. *Mol. Biol. Cell.* 20:745-756.

[18] Edes EW, Candal FJ, Swerlick RA, George VG, Summer S, Bosse DC, Lawley TJ. 1992. HMEC-1: establishment of an immortalized human microvascular endothelial cell line. *J. Invest. Dermatol.* 99:683-690.

[19] Gabor F, Stangl M, Wirth M. 1998. Lectin-mediated bioadhesion: binding characteristics of plant lectins on the enterocyte-like cell lines Caco-2, HT-29 and HCT-8. *J. Control. Rel.* 55:131-142.

[20] Gabor F, Klausegger U, Wirth M. 2001. The interaction between wheat germ agglutinin and other plant lectins with prostate cancer cells Du-145. *Int. J. Pharm.* 221:35-47.

[21] Toegel S, Harrer N, Plattner VE, Unger FM, Viernstein H, Goldring MB, Gabor F, Wirth M. 2007. Lectin binding studies on C-28/I2 and T/C-28a2 chondrocytes provide a basis for new tissue engineering and drug delivery perspectives in cartilage research. *J. Control. Release* 117:121-129.

[22] Plattner VE, Wagner M, Ratzinger G, Gabor F, Wirth M. 2008. Targeted drug delivery: Binding and uptake of plant lectins using human 5637 bladder cancer cells. *Eur. J. Pharm. Biopharm.* 70:572-576.

[23] Plattner VE, Ratzinger G, Engleder ET, Gallauner S, Gabor F, Wirth M. 2009. Alteration of the glycosylation pattern of monocytic THP-1 cells upon differentiation and its impact on lectin-mediated drug delivery. *Eur. J. Pharm. Biopharm.* 73:324-330.

[24] Debray H, Decout D, Strecker G, Spik G, Montreuil J. 1981. Specificity of Twelve Lectins Towards Oligosaccharides and Glycopeptides Related to N-Glycosylproteins. *Eur. J. Biochem.* 117:41-55.

[25] Samsel RW, Perelson AS. 1984. Kinetics of rouleau formation: II Reversible Reactions. *Biophys. J.* 45:805-824.

[26] Van Damme EJM, Peumans WJ, Pusztai A, Bardocz S. 1997. *Handbook of plant lectins: properties and biomedical applications.* 1st ed. Chichester (UK): John Wiley & Sons.

[27] Rimi JM. 1995. Lectin structure. *Annu. Rev. Biophys. Biomol. Struct.* 24:551-77.

[28] Klein NJ, Shennan GI, Heyderman RS, Levin M. 1992. Alteration in glycosaminoglycan metabolism and surface charge on human umbilical vein endothelial cells induced by cytokines, endotoxin and neutrophils. *J. Cell Sci.* 102:821-832.

[29] García-Vallejo JJ, Van Dijk W, Van Het Hof B, Van Die I, Engelse MA, Van Hinsbergh VW, Gringhuis SI. 2006. Activation of human endothelial cells by tumor necrosis factor-alpha results in profound changes in the expression of glycosylation-related genes. *J. Cell Physiol.* 206:203-10.

[30] Peng Y, Li J, Geng M. 2010. The glycan profile of endothelial cells in the present of tumor-conditioned medium and potential roles of beta-1,6-GlcNAc branching on HUVEC conformation. *Mol. Cell Biochem.* 340:143-52.

[31] Chacko BK, Scott DW, Chandler RT, Patel RP. 2011. Endothelial surface N-glycans mediate monocyte adhesion and are targets for anti-inflammatory

effects of peroxisome proliferator-activated receptor γ ligands. *J. Biol. Chem.*286:38738-47.

[32] Scott DW, Chen J, Chacko BK, Traylor JG Jr, Orr AW, Patel RP. 2012. Role of endothelial N-glycan mannose residues in monocyte recruitment during atherogenesis. *Arterioscler Thromb. Vasc. Biol.* 32:e51-9.

[33] Goldstein IJ, Poretz RD. 1986. Isolation, physicochemical characterization, and carbohydrate-binding spedificity of lectins. In: Liener IE, Sharon N, Goldstein IJ, editors. *The lectins: Properties, Functions, and Applications in Biology and Medicine.* Orlando (USA): Academic Press. p. 33-247.

[34] Kornfeld K, Reitman ML, Kornfeld R. 1981. The carbohydrate-binding specificity of pea and lentil lectins. Fucose is an important determinant. *J. Biol. Chem.* 256:6633-40.

[35] Peumans WJ, Stinissen HM, Carlier AR. 1982. A genetic basis for the origin of six different isolectins in hexaploid wheat. *Planta*. 154:562-568.

[36] Monsigny M, Roche AC, Sene C, Maget-Dana R, Delmotte F. 1980. Sugar-lectin interactions: how does wheat-germ agglutinin bind sialoglycoconjugates? *Eur. J. Biochem.* 104:147-153.
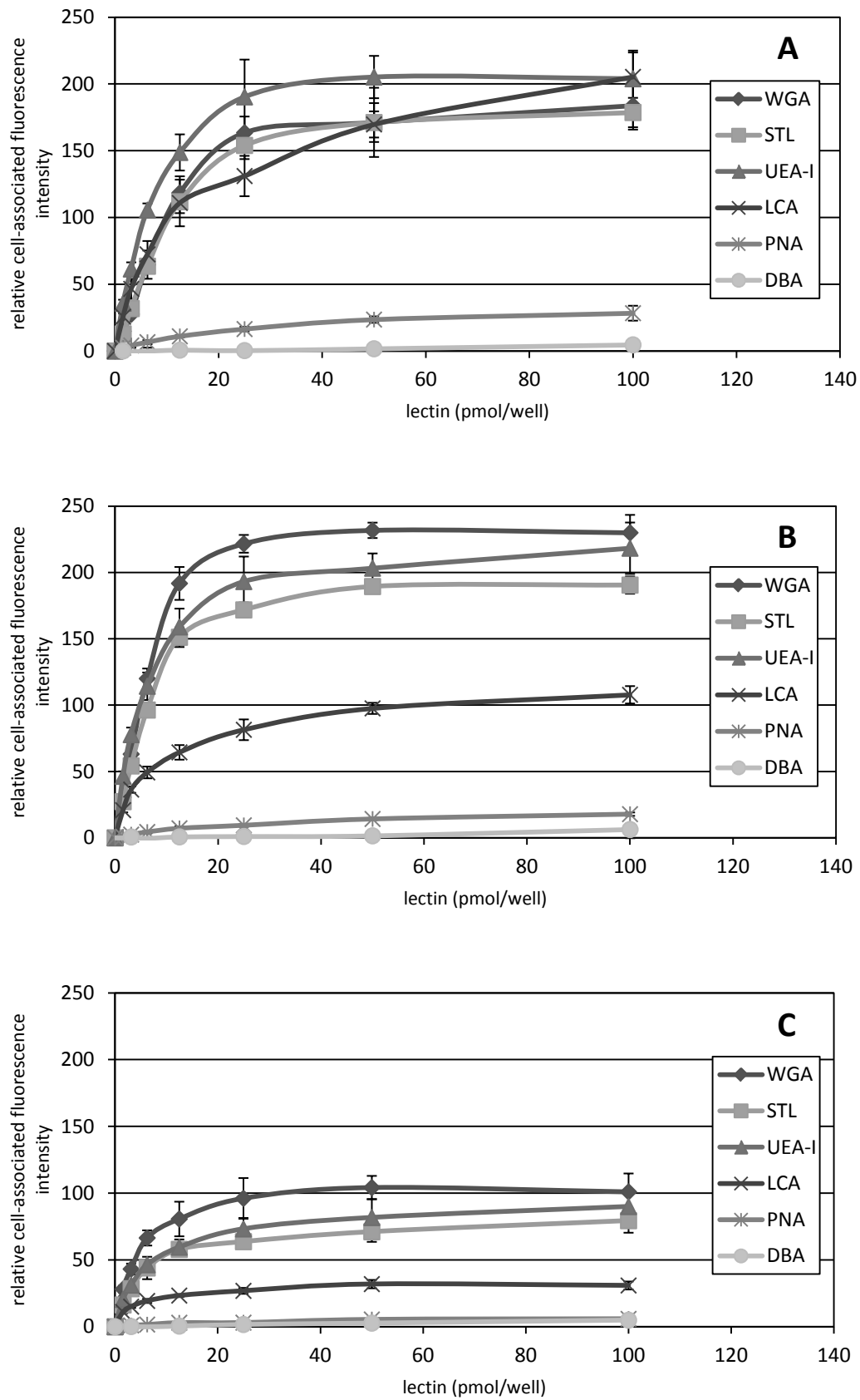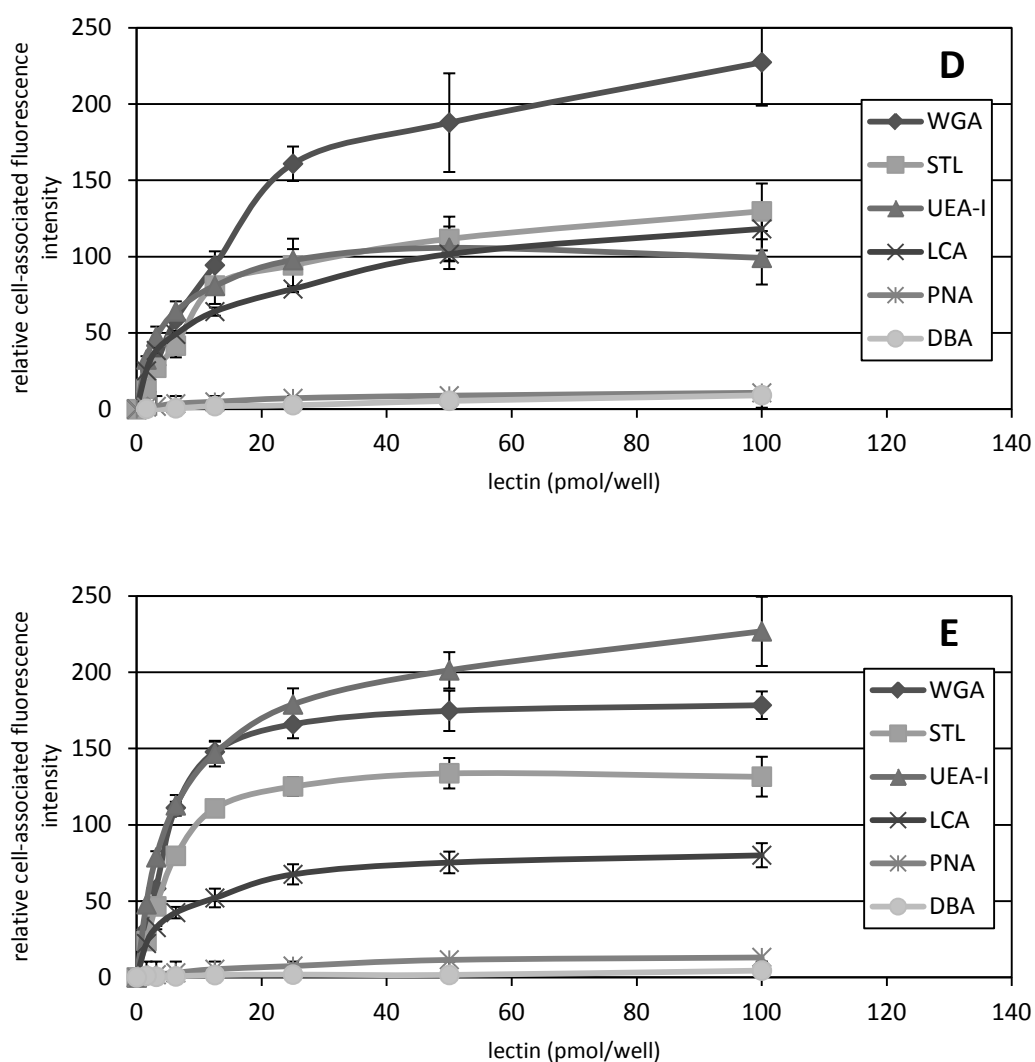
Figure 1: Lectin binding (1.56 – 100 pmol/well, serial dilutions) to endothelial monolayers at 4°C. The fluorescein-labeled lectins associated with the cell surface were related to an apparent F/P ratio of 1 (mean±SD, n=6). Monolayers of primary HUVECs(A), HUVECtert(B) and HMEC(C), as well as inflamed primary HUVECs(D) and HUVECtert(E) after TNF-α activation (0.5 ng/well over 4 hours at 37°C prior lectin binding).
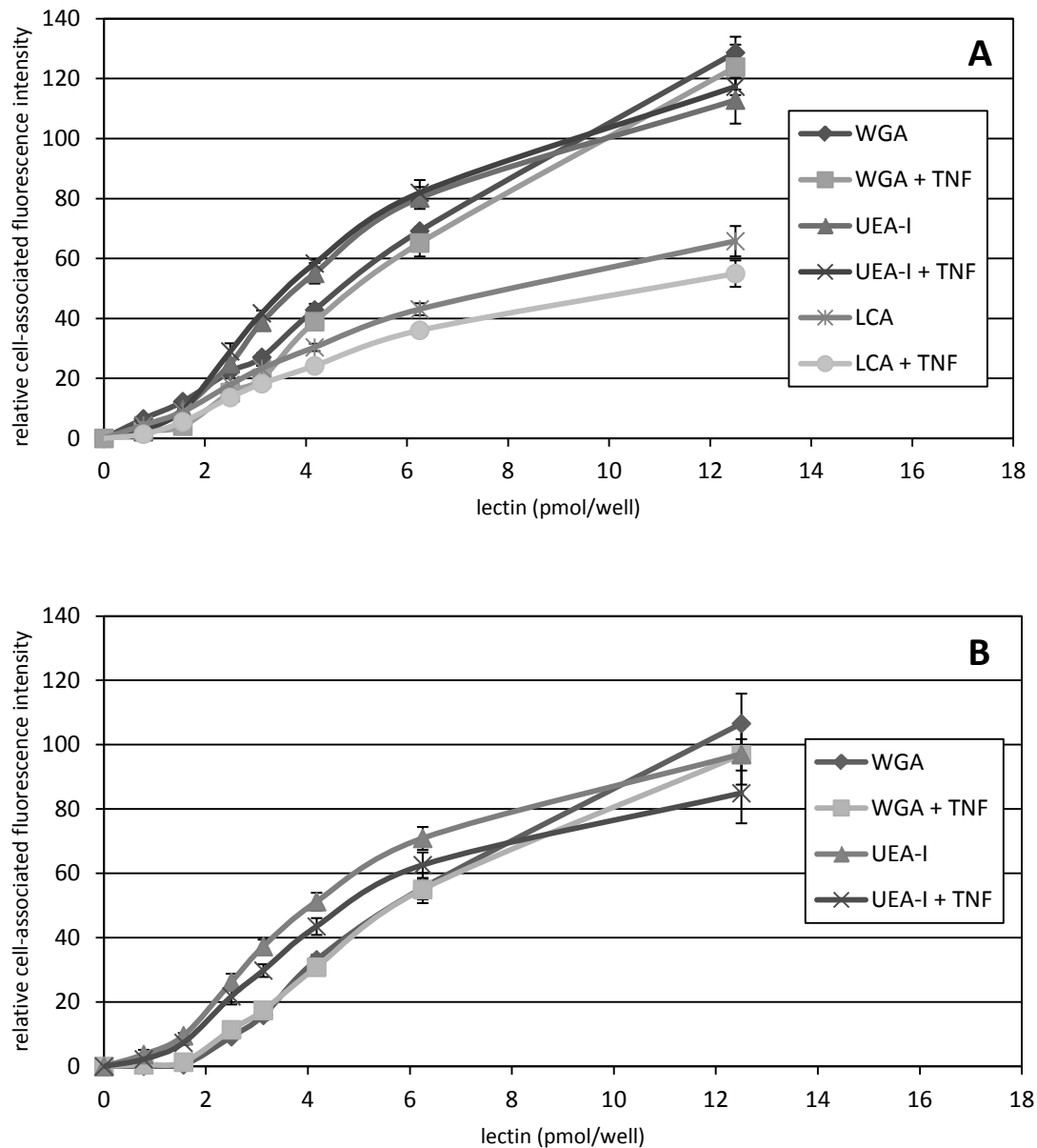
Figure 2: Lectin binding (1.56 – 12.5 pmol/well, serial dilutions) to endothelial cell monolayers at 4°C. The fluorescein-labelled lectins associated with the cell surface were related to an apparent F/P ratio of 1 (mean±SD, n=6). Monolayers of primary HUVECs(A) and HUVECtert(B) with and without TNF-α activation (0.5 ng/well over 4 hours at 37°C prior lectin binding).

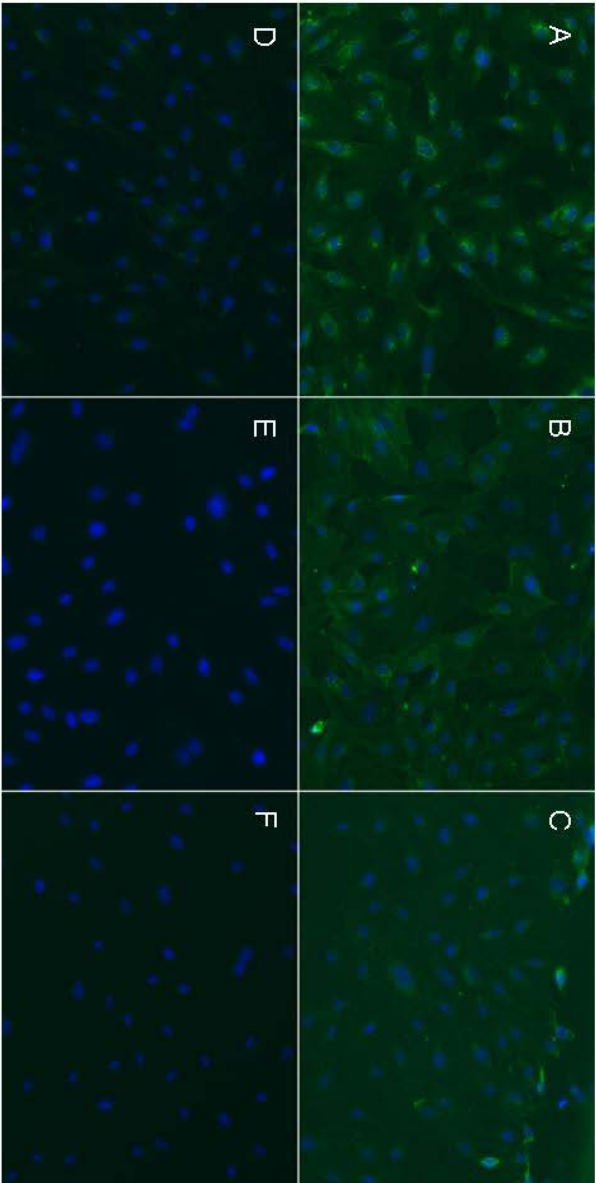**Figure 3: Fluorescence images of confluent primary HUVEC monolayer pre-incubated with fluorescein-labeled lectins (green) at 4°C for 30 min (A-F). The nuclei of cells were counterstained with Hoechst 3334 in blue. To compare fluorescence images, the length of exposure was correlated with the F/P-ratio of each lectin: WGA – 1.2sec (A), UEA – 1.7sec (B), STL – 2.0sec (C), LCA – 3.7sec (D), PNA – 5.1sec (E), DBA – 2.1sec (F).**

Figure 4: Percentage of aggregates in each sample related to the whole population including single cells, cell debris and cell aggregation determined by flow cytometry. Whole blood was incubated with WGA for 10min at 37°C before analysis of the diluted sample. The insert is a magnification of the results obtained in the range of 0 to 31.25 µg mL^{-1} WGA (n = 3).
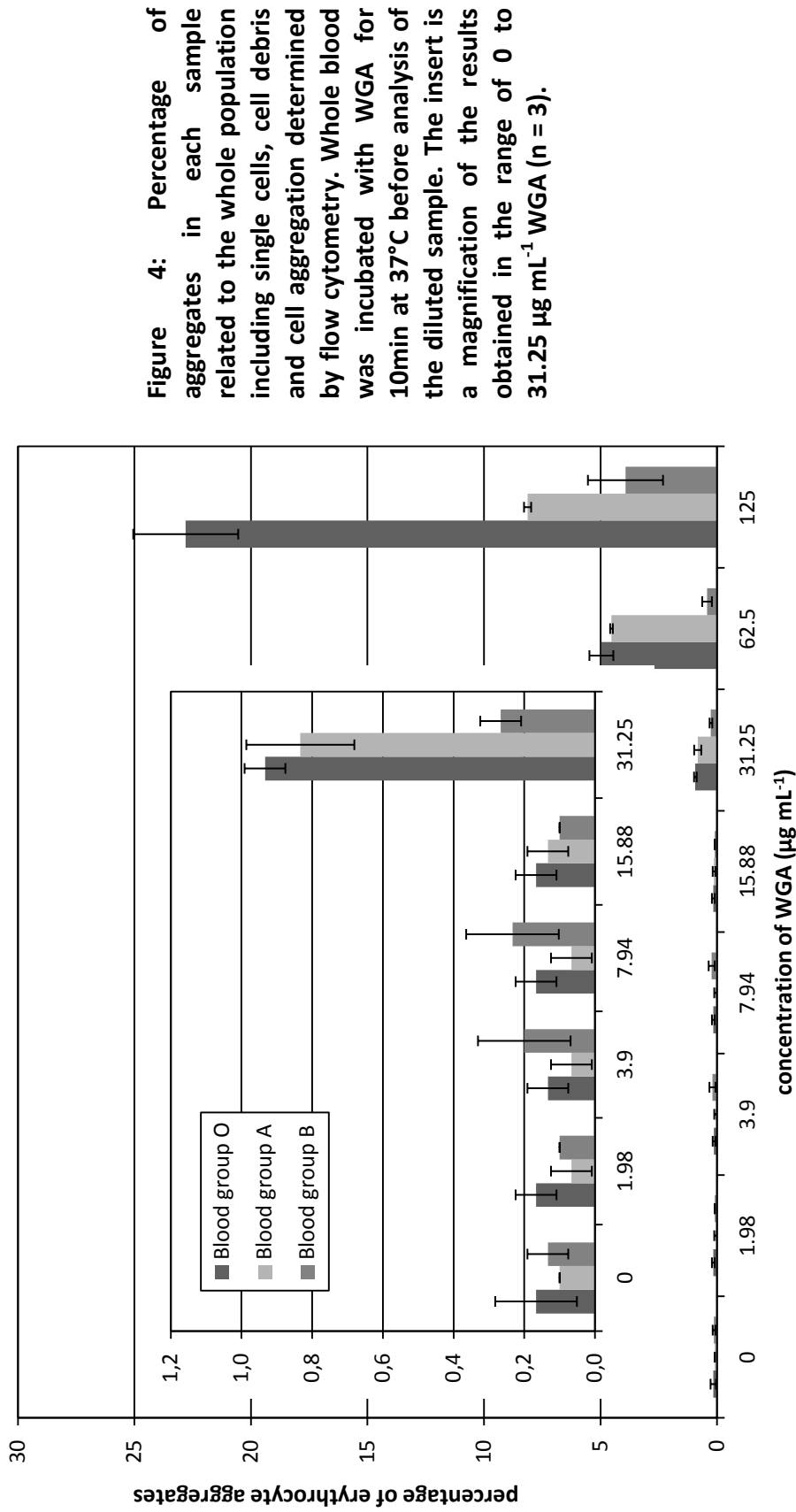
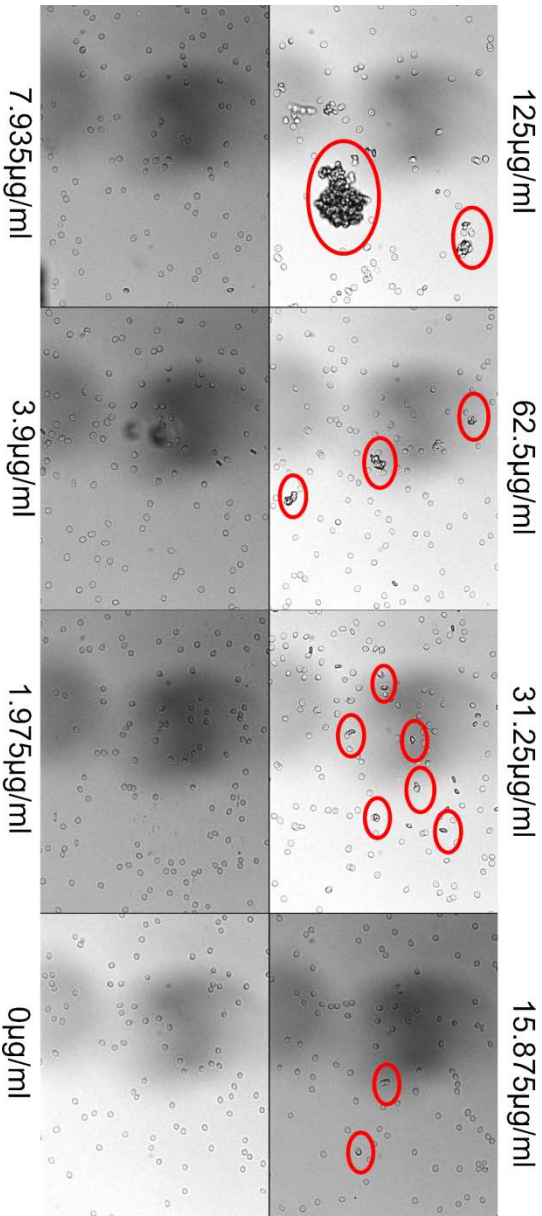**Figure 5: Microscopic images of erythrocytes from blood group A in presence of increasing amounts of WGA. Freshly drawn blood was incubated with WGA solution for 10min at 37°C. and the images were acquired after 150-fold dilution. Samples without WGA solution served as a control. Red circles indicate agglomerates of blood cells. The huge grey shadows are dirt in the light pass of microscope, and are not aggregates of cells.**
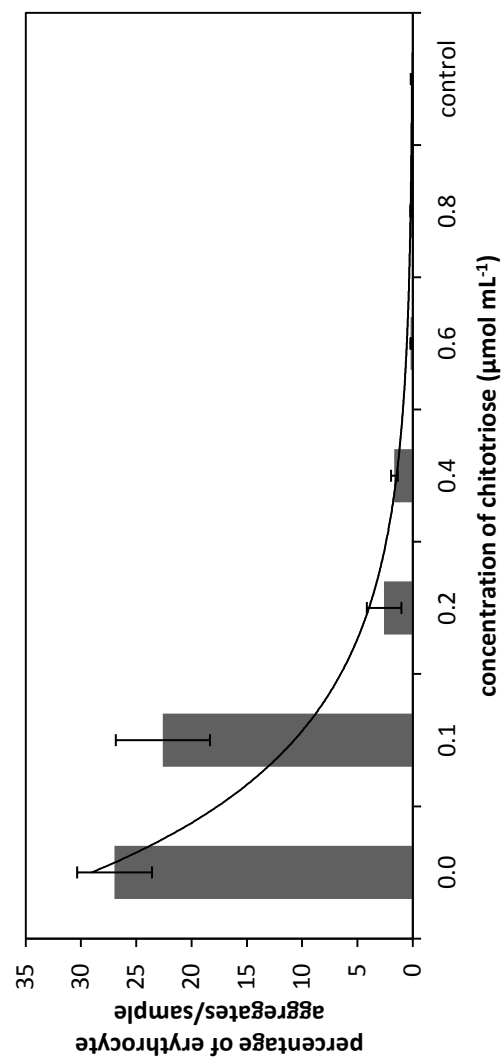
Figure 6: Competitive inhibition of WGA-binding to erythrocytes of blood group O by addition of increasing amounts of the complementary carbohydrate chitotriose. Blood samples without addition of sugar and WGA served as controls (mean ± SD, n=3).

Lectin	Molecular Weight (Da)	F/P	Carbohydrate specificity	Inhibitory sugar	Sugar added (µmol/sample)
WGA	36,000	2.9	N-acetyl-D-glucosamine, sialic acid	Chitotriose	0.0005-0.01
UEA-I	63,000	2.7	α-L-fucose	L-fucose	0.05-5
LCA	49,000	3.8	α-mannose, α-glucose, α- N-acetyl-D-glucosamine	D-mannose	0.25-30
STL	100,000	3.1	N-acetyl-D-glucosamine	Chitotriose	n.d.
PNA	110,000	5.2	β−D-galactose-N-acetyl-D-glucosamine, β−D-galactose, galactose	D-galactosamine	n.d.
DBA	120,000	2.2	α- N-acetyl-D-galactosamine, galactose	N-acetyl-D-galactosamine	n.d.

Table 1: Characteristics of plant lectins and concentrations of complementary sugars applied in the inhibition assays (F/P = fluorescein/protein ratio; n.d.= not determined).

Lectin + inhibitory sugar	Sugar (µmol/sample)	HUVEC prim	HUVEC prim + TNF-α	HUVEC tert	HUVEC tert + TNF-α	HMEC 2
				Inhibition %		
WGA + Chitotriose	0.01	95.3 ± 0.6	94.5 ± 2.7	94.1 ± 0.5	94.3 ± 1.0	91.2 ± 0.9
	0.005	83.1 ± 1.4	82.4 ± 2.8	82.2 ± 0.8	86.3 ± 1.1	73.7 ± 2.6
	0.002	41.7 ± 1.8	42.3 ± 4.1	38.6 ± 1.7	48.4 ± 5.8	27.1 ± 4.4
	0.001	23.0 ± 1.8	21.4 ± 4.1	16.7 ± 2.0	22.2 ± 3.8	14.1 ± 4.4
	0.0005	14.4 ± 3.2	16.6 ± 4.3	9.7 ± 3.1	9.2 ± 5.3	7.2 ± 6.3
	IC$_{50}$ (µmol)	0.002	0.002	0.003	0.002	0.003
UEA-I + L-Fucose	5	93.2 ± 0.2	93.8 ± 1.3	95.6 ± 1.0	94.3 ± 1.3	92.6 ± 1.1
	1	90.0 ± 1.9	91.5 ± 0.8	92.1 ± 1.2	92.2 ± 1.3	89.5 ± 0.9
	0.5	81.4 ± 2.7	81.5 ± 1.6	86.0 ± 1.7	83.3 ± 1.8	78.4 ± 2.4
	0.25	70.9 ± 1.7	66.1 ± 1.9	70.6 ± 2.8	69.5 ± 1.3	64.4 ± 3.2
	0.1	52.9 ± 3.4	47.8 ± 3.5	50.9 ± 1.9	48.0 ± 2.3	40.6 ± 2.0
	0.05	36.7 ± 5.1	30.1 ± 5.7	28.1 ± 4.1	32.4 ± 4.8	28.7 ± 3.3
	IC$_{50}$ (µmol)	0.094	0.101	0.097	0.109	0.144
LCA + D-Mannose	30	80.6 ± 0.7	81.1 ± 1.2	83.1 ± 1.1	80.4 ± 1.9	82.1 ± 1.9
	10	55.4 ± 0.9	81.3 ± 1.3	60.7 ± 1.3	60.1 ± 1.5	68.6 ± 1.6
	5	34.6 ± 1.0	71.5 ± 1.2	46.4 ± 1.1	44.5 ± 1.4	43.2 ± 3.3
	1	6.2 ± 2.1	33.6 ± 2.6	19.6 ± 2.8	9.9 ± 1.1	15.4 ± 2.0
	0.5	2.2 ± 1.2	21.7 ± 1.1	9.6 ± 1.1	7.8 ± 2.0	9.2 ± 2.4
	0.25	0.3 ± 1.8	8.6 ± 1.5	1.9 ± 2.9	1.8 ± 2.3	3.1 ± 4.2
	IC$_{50}$ (µmol)	8.345	2.005	5.946	6.381	6.024

Table 2: Competitive inhibition of lectin binding to endothelial monolayer by the addition of increasing amounts of complementary carbohydrate. Endothelial monolayers were incubated with lectin (12.5 pmol/well) and serial dilutions of complementary carbohydrate for 30min at 4°C. Data are presented as percentage of inhibition (mean±SD, n=3) in comparison to the positive control without carbohydrates, representing 100% binding or 0% inhibition. IC$_{50}$ values represent the amount of corresponding sugars needed to half-inhibit lectin binding to the cell surface.

Table 3. Number of cell aggregates in whole blood samples after WGA-incubation. Freshly drawn blood was mixed with WGA-solution and incubated for 10min at 37°C. Microscopic images were acquired immediately after 150-fold dilution. The average number of cell aggregates was calculated after manually counting (mean±SD, n=30).

Concentration of lectin ($\mu g \ mL^{-1}$)	Blood group A	Blood group B	Blood group O
	Number of cell aggregates / image		
125	14.0±3.7	10.4±5.2	2.5±1.4
62.5	8.6±3.6	6.1±1.7	0.9±0.8
31.25	2.1±0.9	2.1±1.2	0.5±0.8
15.88	0.0±0.0	0.5±0.6	0.1±0.3
7.94	0.1±0.3	0.6±0.7	0.0±0.2
3.9	0.0±0.2	0.1±0.3	0.0±0.0
1.98	0.0±0.0	0.0±0.2	0.0±0.1
control	0.0±0.0	0.0±0.0	0.0±0.2

Supplementary Appendix

Figure S1. Lectin binding studies to endothelial single cells

To study lectin binding, single cells were harvested by trypsination, collected by centrifugation and resuspended in PBS buffer supplemented with Ca^{2+} and Mg^{2+} to reach a final concentration of $5x10^6$ cells mL^{-1}. Afterwards 50 µL single cell suspension were added to 50 µL lectin solution in precooled buffer (0.8 - 6.25 pmol, serial dilutions) and incubated for 5 min. at 4°C. Unbound lectins were removed by washing twice with 400 µL cold buffer each. Finally, 100 µL cell suspension was diluted with 500 µL pre-cooled particle free buffer and the cell-bound mean fluorescence intensity (MFI) was determined flow cytometrically at 488/525 nm (Epics XL-MCL analytical flow cytometer , Beckman Coulter, Miami, USA). A forward versus side scatter gate was used to confine the analysis to the single cell population and a minimum of 5000 cells was accumulated for each analysis. For estimation of autofluorescence, control samples containing unlabelled cells were included in all experiments.

Single endothelial cells are highly sensitive and viability decreases upon external stimuli in comparison to monolayers. Thus flow cytometric analysis of lectin binding was performed only with non-activated primary HUVEC and HUVECtert in the concentration range of 0.8-6.25pmol lectin/$2.5x10^5$ cells (Figure S1, SD≤2.84, n=3). STL was excluded because of binding characteristics similar to WGA. In case of primary HUVEC single cells lectin binding was highest in case of WGA exhibiting a RFI up to 28.59±0.64, followed by UEA-I > LCA >> PNA ~ DBA (Figure S1A). In case of HUVECtert, the lectin interaction was highest in case of UEA-I in the concentration range between 0.8 to 3.125 pmol. However, at the concentration of 6.25pmol the RFI of both WGA and UEA-I was about 25, followed by LCA >> DBA ~ PNA. In contrast, UEA-I exhibited a higher binding rate to endothelial monolayers of primary HUVEC in the same concentration range (Figure 2A). This might be due to differences in accessible binding area between single cells and monolayers. While the lectins have the access to the whole cell membrane in the case of single cells, only the apical face of cell monolayers or roughly a sixth is available for the interaction with lectins.

Moreover, as demonstrated by fluorescence microscopic images of WGA-binding (12.5pmol/2.5x105 cells) to single primary HUVECs (30 min incubation-time at 4°C, Figure S1C), a homogeneous distribution of cell bound WGA throughout the entire membrane of primary HUVECs was observed. Due to the temperature level during preincubation with lectins (at 4°C), the metabolic activity of cells was minimized. Therefore, no internalization of cell-bound lectins was observed. HUVECtert and HMEC-1 revealed the similar profiles like primary HUVECs (data not shown). No sign of lectin mediated cytotoxicity was observed in the concentration tested.
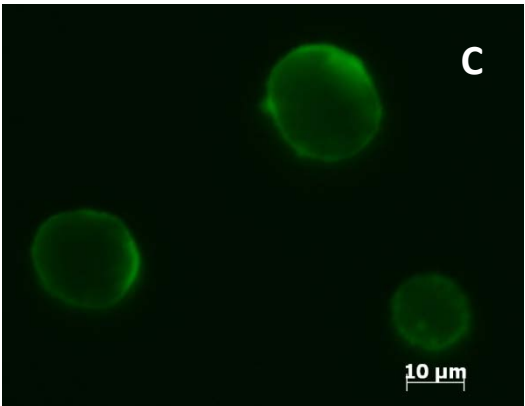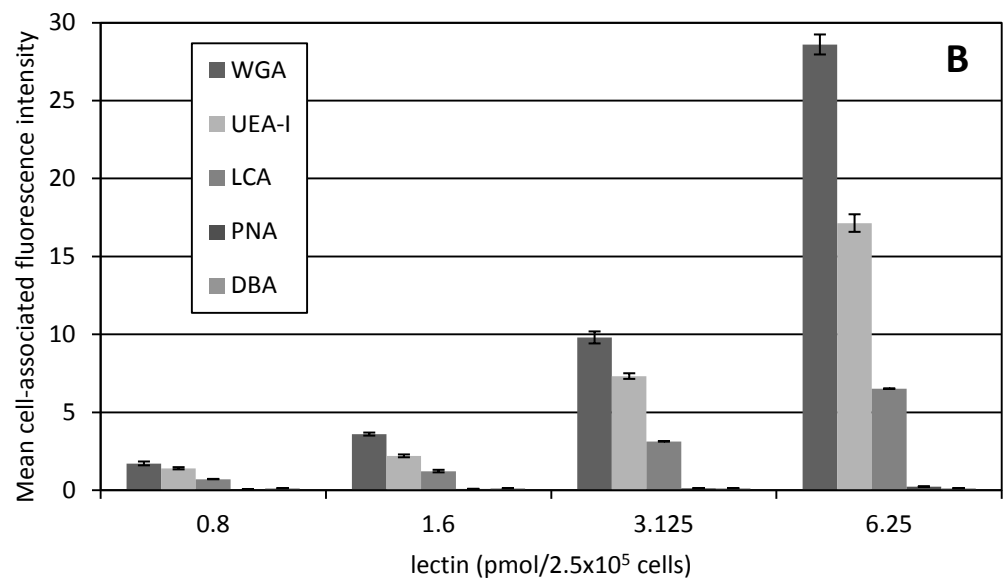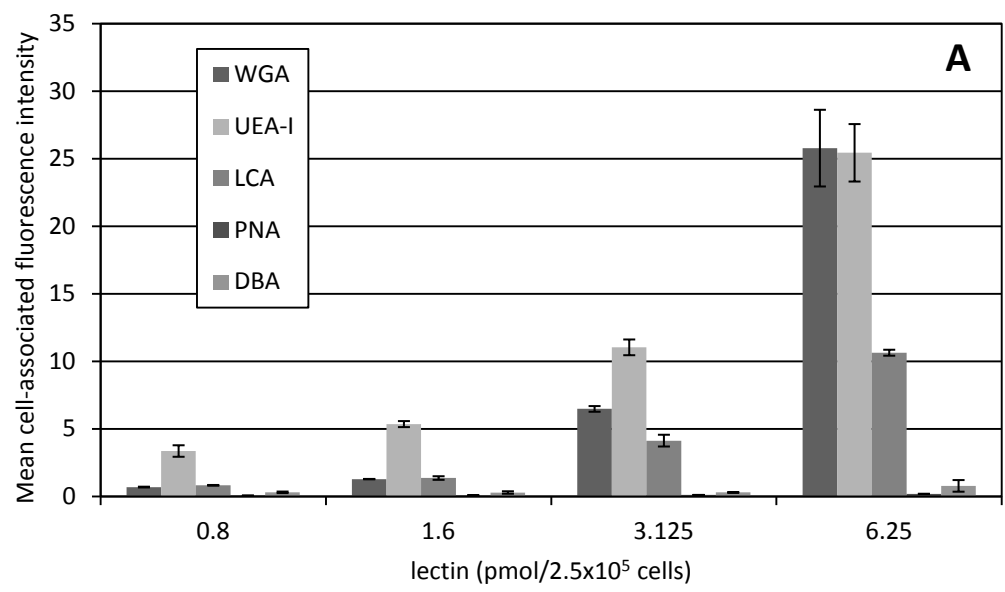
Figure S2. CyQuant® cell proliferation test

To estimate of the cell number of activated and non activated endothelial cells, a cell proliferation test (CyQuant®) was performed. For that purpose, endothelial cells were seeded in 96-well microplates at a density of 1.7×10^4 single cells/160 μL per well and cultivated at 37°C in humidified 5% CO_2 / 95% air atmosphere until confluency. After removal of the medium, 50 μL reagent I (25μL 20mM HEPES pH 7 and 25 μL Celllytic-M) were added to confluent monolayers with or without TNF-α activation. In case of inflamed cells, the monolayers were preincubated with TNF-α at a concentration of 0.5 ng/50 μL in cell culture medium for 4 hours at 37°C. After 15 min. incubation at room temperature 150 μL reagent II containing CyQuant GR (0.33%), Celllysis buffer (5.0%) and distilled water (95%) were added and the RFI was determined in a microplate reader (excitation: 485nm; emission: 535 nm). Samples of reagents without cells served as a control. As shown in figure, no significant changes in cell number during inflammation could be observed. (n=18, SD≤1544.37)
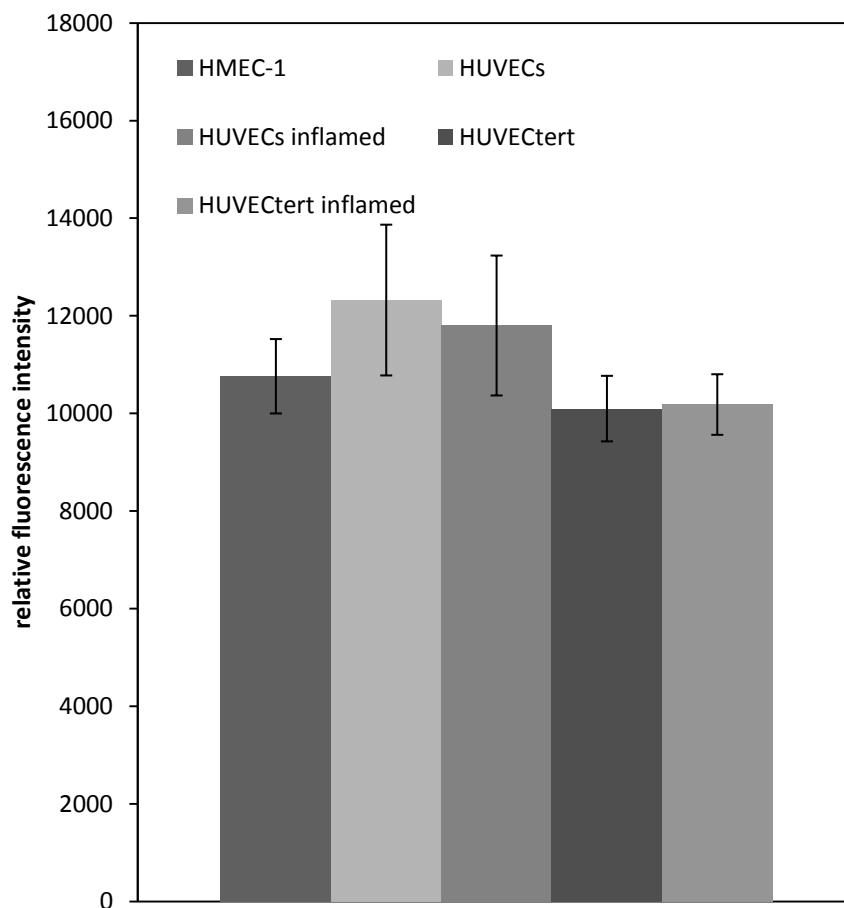
2.2.3 Metal grids as new growth support in cell-based transport studies

Permeation of nanoparticles across cell monolayers *in vitro* – Impact of growth support

Xue-Yan Wang[1#], Christian Fillafer[2#], Dietmar Pixner[1], Michael Wirth[1], and Franz Gabor[1]*

*Corresponding author: franz.gabor@univie.ac.at

[#] These authors equally contributed to this work.

[1]Faculty of Life Sciences, Department of Pharmaceutical Technology and Biopharmaceutics, University of Vienna, Vienna A-1090, Austria

[2]Department of Mechanical Engineering, Boston University, Boston, MA 02215, USA

Abstract

Background

Permeable filter supports have been widely employed for the cultivation of cell layers (*e.g.* epithelial, endothelial, etc.) and for studies of the penetration of drugs and drug carrier systems through these biological barriers. Typically, it is assumed that the characteristics of the filter membrane itself (*e.g.* filter material, pore size, pore density) do not significantly affect the outcome of the transport study. Herein, this common assumption is tested by studying the permeation of polystyrene nanoparticles through Caco-2 monolayers which had been grown on different commercially available filter membranes and stainless steel grids.

Results

Surprisingly, it was possible to cultivate Caco-2 cell monolayers on metal grids with an average pore size (~25 μm) that is larger than a cell's typical diameter (~15 μm). As indicated by immunofluorescence staining of the tight-junction associated protein ZO-1 as well as transepithelial electrical resistances of 450 Ω cm^2, these cell layers were similar as compared to their filter-supported counterparts. No permeation of nanoparticles through Caco-2 layers grown on commercially available filter membranes was detected upon incubation for 24h at 37°C. In contrast, nanoparticles clearly reach the basolateral compartment when highly porous metal grids were used as cellular growth supports. In addition, it was found that fluorescence label released from the nanoparticles during the experiment can lead to false positive particle transport results. We suggest the use of ultracentrifugation to distinguish between particle-associated and small molecule fluorescence.

Conclusion

The presented results indicate that the permeability characteristics of the filter membrane affect transport studies through artificial biological barriers. Highly porous growth materials, like the presented metal grid, might be suitable alternatives to conventional filter membranes.

Keywords

Introduction

Transport studies across cell monolayers *in vitro* are used as standard techniques for determining the permeability of drugs and prodrugs in the framework of the biopharmaceutics classification system (BCS) [1, 2]. Moreover, the same techniques are applied for studies of the cytoadhesion, internalization and transcytosis of drug delivery systems such as nano- and microparticles. Typically, such transport models consist of an apical and a basolateral compartment, which are separated by a filter membrane. At this, the filter membrane serves as a growth support for the cells, which, upon having formed a confluent layer, simulate an epithelial, endothelial or other barrier of interest. There are several commercially available transport systems, for instance Transwell™ by Costar and ThinCert™ by Greiner Bio-One. A typical device can be accommodated in microplate wells which allows automatized and parallelized operation of experiments in a medium to high-throughput manner. The filter membranes are mainly made from polymers such as polycarbonate, polyester or poly(ethylene therephthalate) and are characterized by different pore sizes and pore densities. Biopharmaceutical transport experiments usually rely on filter membranes with pore diameters ≤3 µm (mostly 0.4 µm). Several studies have also tried to clarify if nanoparticles can permeate epithelial cell barriers, for instance Caco-2 monolayers cultivated on filters with 3 µm pore size [3-5] or 0.4 µm pore size [6-8].

It seems plausible, in particular in the case of nanoparticles whose diameter approach the filter's pore size, that aside from the cell monolayer the filter itself might present a permeation barrier. If the filter membrane becomes the literal "bottleneck" for permeation, this might clearly bias the results of transport studies. To the best of our knowledge this problem has not been addressed so far.

In the present study, nanoparticle transport was studied with epithelial cell layers that had been cultivated on different commercially available filter membranes (Table 1). In addition, the suitability of a metal grid (25 µm mesh width) as an alternative highly porous growth support was investigated. Caco-2 cell monolayers, which are a widely used as an *in vitro* model for the human small intestinal epithelium [9-13], were cultivated on all of these membranes. In order to allow for their comparison, Caco-2 monolayers cultivated on filter membranes and metal grids were characterized. Subsequently, nanoparticle permeation through Caco-2 layers grown on the various growth supports were determined over a period of 24 h. Since uptake of particulate material into cells has been found to be temperature dependent [14, 15], all experiments were performed at 37°C. Fluorescent polystyrene nanoparticles with a diameter of 200 nm were used as colloids, which have been reported to cross epithelial barriers [4, 8, and 14] and which are well in the size range of potential drug carrier systems.

Material and Methods

Materials

ThinCert™ 24-well tissue culture insets for cultivation of cell monolayers (0.4 µm transparent (0.4 TP) as well as translucent (0.4 TL), 1.0 µm transparent (1.0 TP), 3.0 µm transparent (3.0 TP) as well as translucent (3.0 TL), 8.0 µm translucent (8.0 TL)) were obtained from Greiner Bio-One (Kremsmuenster, Austria). Fluoresbrite™ carboxylated yellow-green nanospheres with a diameter of 0.2 µm (2.65 % Solids-Latex, Diameter = 0.212 µm) were bought at Polysciences Europe GmbH (Eppelheim, Germany). Stainless steel tissue grid with a mesh width of 25 µm was purchased from Bueckmann GmbH (Moenchengladbach, Germany). Pluronic® F-68 was obtained from Sigma-Aldrich (Steinheim, Germany). All other chemicals used were of analytical purity.

Cell culture

The Caco-2 cell line was obtained from the German collection of microorganisms and cell cultures (DSMZ, Braunschweig, Germany). Cells were cultivated in 75 cm^2 tissue culture flasks in RPMI-1640 cell culture medium containing 10 % fetal bovine serum, 4 mM L-Glutamine and 150 µg mL^{-1} gentamycine in a humidified 5 % CO_2/95 % air atmosphere at 37°C and subcultured with TrypLE® Select (Gibco, Lofer, Austria).

Cell cultivation on filter membranes and metal grids

Caco-2 monolayers were cultivated on ThinCert™ tissue culture insets with different pore sizes and densities (Table 1). The apical compartment was filled with 120 µL cell suspension containing 1.25 x 10^4 cells while 600 µL of medium were added to the basolateral compartment. The cell culture medium in both compartments was exchanged every third day during a total cultivation period of 18 days.

For cultivation of Caco-2 cells on metal grids the filter membranes were removed from commercially available inserts. Metal grids were cut to a similar size as the original filters and were bonded to the bottom of the plastic cups (Figure 1A) with a synthetic rubber adhesive (Microset 101FF, Microset Products Ltd., Nuneaton, U.K.). Upon sterilization of these insets with ethanol for 30 min, 120 µL of cell suspension containing 1.25 x 10^4 cells was added to the apical compartment. The basolateral compartment was left empty for the first 24 h of cultivation. This step is important in order to avoid that most of the seeded cells simply sediment through the grid's mesh. If one compartment is left empty an air-water interface will be formed directly in plane of the metal grid and thus all cells will be efficiently deposited onto or close to the wires.

Characterization of cell monolayers

The cell monolayers grown on the filter membranes and metal grids were characterized regarding their confluence and electrical resistance. For localization of cells and analysis of intercellular connections the nuclei as well as tight junction associated protein ZO-1 were stained. Monolayers were fixed with ice-cold methanol (-22 °C), washed with phosphate buffered saline pH 7.4 (PBS) and rehydrated in PBS + 1% bovine serum albumin (BSA). Subsequently, a 1:100 dilution of mouse-anti-human ZO-1 antibody (BD Biosciences, Schwechat, Austria) was added followed by incubation for 1 h at 37°C. Upon washing with PBS + 1% BSA, a fluorescein isothiocyanate (FITC)-labelled goat-anti-mouse antibody (1:200) (Dako, Glostrup, Denmark) was added followed by incubation for 30 min at 37°C. Concurrent with the latter incubation step propidium iodide (2µg mL^{-1}) (Sigma Aldrich, St. Louis, USA) was added to stain the cell nuclei. After washing with PBS + 1% BSA, the samples were microscopically analyzed on a Zeiss Axio Observer.Z1 (Zeiss, Göttingen, Germany).

The transepithelial electrical resistance (TEER) of the cell monolayers was determined with an EVOMX voltmeter (World Precision Instruments, Sarasota, USA) during the 18 day cultivation period and before/after nanoparticle transport studies.

Particle transport studies

According to the stability studies of nanoparticles in transport media (supplementary materials), transport experiments of nanoparticles were performed in RPMI-1640 cell culture medium supplemented with 1% (w/v) Pluronic® F-68. For each experiment 600 µL of transport medium were added to the basolateral chamber and 120 µL of particle suspension (3 x 10^{11} particles mL^{-1}) were added to the apical compartment. The cell monolayers were incubated for 24 h at 37°C. Samples (100 µL) were drawn from the basolateral compartment after 2, 4, 6, 9, 12 and 24 h. The relative fluorescence intensity of the samples was determined using a Tecan Infinite® 200 fluorescence reader (ex/em: 440/480, Grödig, Austria) and subsequently they were retransferred to the respective well. After completion of the experiment (= after 24 h) the basolateral medium was filled into ultracentrifuge tubes (SORVALL®, Asheville, USA). Nanoparticles were spun down by ultracentrifugation with a SORVALL® Ultra Pro™ 80 (Wilmington, USA). The typical timescales necessary for centrifugation of particles can be calculated according to Eq. 1.1 [16]

$$\tau = \frac{9}{2} \frac{\eta}{(\rho_p - \rho_s)r^2\omega^2} \ln\frac{r_{max}}{r_{min}} \qquad \text{Eq. (1.1)}$$

with τ as the timescale necessary to spin down particles, η as the viscosity of the medium (water at 4°C ~0.0016 kg m^{-1} s^{-1}), ρ_p and ρ_s as the densities of polystyrene (1050 kg m^{-3}) and 1% aqueous Pluronic® F-68 solution (1000 kg m^{-3}) respectively, r [m] as the particle radius, ω [s^{-1}] as the angular frequency and r$_{max}$ [m] and r$_{min}$ [m] as parameters of

the ultracentrifuge rotor (for SORVALL® TFT-80.2 Fixed-Angle Ultracentrifuge Rotor: r_{max}=0.0601 m, r_{min}=0.0339 m). The angular frequency ω is simply obtained from Eq. 1.2

$$\omega=2\pi v_{rot} \qquad\qquad \text{Eq. (1.2)}$$

with v_{rot} [s^{-1}] as the rotation frequency.

For the polystyrene nanoparticles employed in this study, typical ultracentrifugation times of ~4 min at 60,000 rpm should be sufficient to spin down particles (in practice, the suspensions were centrifuged for 15min). The fluorescence intensity of the supernatant, which represents the contribution of released dye molecules to the total fluorescence of the acceptor medium, was then determined via fluorimetry. If all dye molecules remained bound to nanoparticles, the supernatant would not fluoresce.

Results

Characterization of cell layers on metal grids

Confluent Caco-2 cell layers were formed on stainless steel grids with a mesh width of 25 µm (Figure 1A). As illustrated by immunostaining of tight-junction associated protein ZO-1, a continuous network of intercellular connections was formed within the layer (Figure 1C). The dense occupation of the grid's pores with cell nuclei (Figure 1B) further confirmed these findings.

The formation of a tight cell layer is typically associated with an increase in the transepithelial electrical resistance (TEER) [17]. Experimentally, it was found that even empty filter membranes and metal grids contribute to TEER values. The specific resistances were rather similar amounting to ~72 Ω cm^2 for metal grids and ~68 Ω cm^2 for most commercially available filter membranes respectively (Table 1). Probably due to a smaller pore size and lower pore density, empty 0.4 TP filters are characterized by a rather high TEER of 124 Ω cm^2. After correction for these control values, the TEERs of Caco-2 monolayers typically ranged at about 449±15 Ω cm^2 (metal grids) and 471±109 Ω cm^2 (filter membranes; maximum: 665 Ω cm^2 for 8.0 TL filter, minimum: 359 Ω cm^2 for 3.0 TP filter) prior to particle transport experiments. After incubation with nanoparticles for 24 h, the TEERs of the cell layers were 438±59 Ω cm^2 (metal grids) and 506±149 Ω cm^2 (filter membranes; maximum: 709 Ω cm^2 with 8.0 TL filter, minimum: 322 Ω cm^2 with 0.4 TP filter).

Particle transport studies

Nanoparticle transport studies were performed with Caco-2 layers that had been cultivated on metal grids and on different commercially available filter membranes (Table 1). Fluorimetry was used to monitor the concentration of nanoparticles in the basolateral compartment.

<u>Nanoparticle permeation through Caco-2 monolayers on filter membranes and metal grids</u>

In course of incubation for 24 h at 37°C the mean fluorescence intensity (MFI) of the basolateral compartment increased for all types of growth supports. However, in the case of metal grids clearly higher intensities were observed (Figure 2). Initially, a relatively high rate of fluorescene accumulation was detected, which subsequently decreased after about 6-12 hours. The latter is indicative of an approach of the system towards equilibrium or saturation. Such behaviour was not observed with any of the Caco-2 monolayers cultivated on commercially available growth supports. As illustrated in Figure 2, the increase of the MFI of the basolateral compartment over time was clearly lower for these filter membranes and roughly correlated with pore size (0.4 < 1.0 < 3.0 < 8.0). At constant pore size, filter membranes with lower pore densities (transparent TP; Table 1) seemed to be associated with less transport as compared to their high-

density counterparts (translucent TL). However, this correlation was more pronounced for filter membranes with 0.4 µm pore size as compared to those with 3 µm pore size. Furthermore, the particle transport studies performed with Caco-2 layers on metal grids confirmed the tendency that higher pore density and larger pore size result in clearly increased permeation of nanoparticles. This was evidenced by the timecourse of the MFI of the basolateral medium for metal grids (Figure 2). These results suggest a more than 20-fold difference of nanoparticles transport as a consequence of the type of growth support.

Discrimination between permeation of nanoparticles and released fluorophores

Fluorimetry *per se* does not distinguish if fluorescence originates from free fluorophor or from fluorophor attached to the nanoparticle's polymer matrix. In order to clarify if the fluorescence detected in the basolateral medium was particle-associated or not, the acceptor medium was ultracentrifuged. The difference between the acceptor medium's fluorescence intensity before and after ultracentrifugation constitutes the contribution of nanoparticles to the total fluorescence. Upon ultracentrifugation, the MFIs of most basolateral media were found to be decreased by varying degrees (Figure 2). Importantly, however, in case of media from transport studies with Caco-2 monolayers grown on filter membranes, the difference was negligible. This indicates that the fluorescence detected in the basolateral compartment is almost entirely due to free fluorophore. In case of Caco-2 monolayers grown on metal grids, a distinct drop in the basolateral medium's fluorescence was observed upon ultracentrifugation (Figure 2). This result suggests that nanoparticles indeed permeated through the cell layer and the underlying metal grid.

Comparison of cell-covered and empty transport filters

In order to be able to understand the effect of the filter membrane itself on nanoparticle permeation into the basolateral compartment, the experiments as described above were performed with insets devoid of Caco-2 cell monolayers. Expectedly, in all cases studied (filters as well as metal grid) the MFI of the basolateral compartment after 24h was increased as compared to experiments in which cell layers were present. Similar MFIs were detected in the basolateral compartments of filters with pore sizes ≥3 µm (Figure 3). In contrast, in the case of filters with pore sizes ≤1 µm a relatively lower fluorescene intensity was observed. The MFI was clearly lowest in the case of 0.4 µm TP filters followed by 1.0 µm TP and 0.4 µm TL filters.

Nanoparticle permeation through Caco-2 monolayers on metal grids

It is of interest to study if the timecourse of nanoparticle permeation through Caco-2 monolayers cultivated on metal grids differs from the

timecourse of permeation of fluorophore which is obviously released from the particles (see results above). For this purpose, basolateral media were collected at several time points during the 24h incubation period and were subjected to ultracentrifugation. As illustrated in Figure 4, the concentration of particle-associated fluorescence as well as that of free fluorophore increases within the 24 h incubation period. During the first 4 hours, however, there is no significant difference between the medium's fluorescence intensity before and after ultracentrifugation. This indicates that no particles are present. After 6h, however, particle-associated fluorescence appears and increases until the end of the experiment (24h).

Discussion

The aim of the present study was to investigate the impact of different growth supports on nanoparticle permeation through Caco-2 cell layers. Usually, transport studies are performed with cell monolayers that have been cultivated on polymer filter membranes with different pore sizes and pore densities (Table 1). Transparent filters (TP) are often used if access to the cell layer by microscopy is required. In order to ensure the latter, the filters typically have lower pore densities. In contrast, translucent filters (TL) have higher pore densities and thus one expects that they impose less of a permeation barrier to nanoparticles transport. Generally, the filter's pore size seems to be less relevant for studies with low molecular weight drugs, however, it is probably important in case of drug carriers (e.g. nanoparticles, microparticles, etc.) whose size approaches the typical pore size. Generally, it should be noted that commercially available filter membranes are characterized by rather low free filtration areas. Remarkably, 85.9 - 99.7 % of a typical filter's surface is not available for permeation of nanoparticles into the basolateral compartment (Table 1). This could be considered a special limitation of *in vitro* assays. However, it also has to be pointed out that particulate drug carriers will encounter steric constraints *in vivo*, which might be similarly if not even more restrictive (e.g. basal lamina, liver sinusoids, etc.). Nevertheless, it is important to understand the limitations that arise due to choice of the assay system and as indicated by the small free filtration areas, these limitations might be drastic.

In view of these potential limitations of currently available systems, an investigation of alternative filter materials as growth supports for permeation studies seemed expedient. In the present study, a stainless steel metal grid with a mesh width of 25 μm was investigated regarding its suitability as a growth support for epithelial cell layers. The mesh structure of metal grids is highly regular and they are available in large quantities at a reasonable cost. The grid is characterized by a free filtration area of 25 %, which is almost twice that of 3 μm TL filters which are the commercially available membranes with the highest porosity. As indicated in Figure 1B, Caco-2 cells can be cultivated on these metal grids. This is remarkable, since single cells with a mean diameter of about 15 μm would be expected to pass through the pores. However, by not adding cell culture medium to the basolateral compartment for the first hours of cultivation, the cells were deposited at or near the wires and efficiently adhered there. Upon adhesion Caco-2 cells proliferated to form a confluent layer with intercellular connections as indicated by staining of the tight-junction associated protein ZO-1 (Figure 1C). Furthermore, the cell layers on the grids were characterized by transepithelial electrical resistances of 450 $\Omega\,cm^2$ similar to cell layers cultivated on filter membranes. Collectively, these results underline that the cell layers on metal grids achieve a level of "tightness" that is equivalent to that of cell layers grown on

filter membranes.

It seems intuitive to assume that the smaller a filter's pore size and density are, the more of a barrier it will present to nanoparticles. In order to test if this is indeed the case, we performed nanoparticle transport studies with "empty" filter membranes (=no cell layer present). In case of pore sizes ≥3 μm (Figure 3), no difference in the MFI of the basolateral compartment was found after 24h. This indicates that the pore sizes and densities of these filters are probably high enough to not present a barrier for equilibration between apical and basolateral. However, filter membranes with a pore size ≤1 μm affect the equilibration process. This is probably due to the filter's pore size (0.4μm) approaching the size scale of the nanoparticles, in our case nanoparticles with a diameter of ~ 200 nm. Such steric constraints, which can be further amplified by low pore densities, hinder nanoparticle permeation into the basolateral compartment. Furthermore, the considerable surface area of filter of the filter (including pores) represents a surface for adsorption of nanoparticles. In general, sequestration of nanoparticles by binding to the filter material would not be surprising [18]. It is also probable that a filter pore becomes blocked or at least narrowed if a particle adsorbs to it wall. Effectively, the latter will lead to a further decrease of the free filtration area of the membrane.

These considerations seem rather trivial, but nevertheless they have consequences for transport studies across cell monolayers. Generally, the low MFI detected in the basolateral compartments in the case of commercially available filter membranes as grown supports further exemplified this. At this, the 8 μm TL filters exhibited the highest transport rate among all types of filter membranes, and was more than 8-fold higher to 0.4 μm TP filter. In contrast, clearly higher basolateral fluorescence intensities were detected for Caco-2 layers cultivated on metal grids. After 24 h incubation, a 137-fold higher MFI as compared to 0.4 μm TP filters was observed. It seems likely that the higher permeation of particles through cell layers on metal grids is partially due to the larger free filtration areas as compared to filter membranes. This was proven by the results of comparison between particle transport with and without cell monolayers. Although the 3 μm and 8 μm filters obtained the almost same results of the permeation of fluorescent intensities for empty filters as empty metal grids, after 24 h incubation only less than 1% of the MFI in basolateral compartments in case of filters with cells to empty filters was detected. In contrast, more than 15% of the fluorescence intensity in the case of cell-covered metal grids was detected compared to the results of empty metal grids. Interestingly, it was found that the fluorescence intensity of the acceptor medium does not only increase due to transported nanoparticles, but to a large degree due to fluorophore that has been released from the colloids. This was demonstrated by ultracentrifugation experiments (Figure 2). Apparently, fluorescent

marker molecules are released from the nanoparticles in course of the experiment, permeate across the cell layer and reach the basolateral compartment. Thus, a direct inference from fluorescence intensity measurements to presence of nanoparticle is not possible. Similar reports of "false-positive" findings due to liberated fluorophore have been reported [19-21] and have to be considered for correct data interpretation. After correction for free fluorophore, no nanoparticle transport was observed for commercially available filter membranes. In contrast, the fluorescence intensity in the acceptor medium for Caco-2 monolayers on metal grids was partially due to nanoparticles. Within the first 4 hours of incubation, permeation of free fluorophore dominates (Figure 4). However, after 6 hours nanoparticles started to accumulate in the basolateral medium. Again, this result estimated that the particle transport was dependent on the free filtration area available; higher free filtration area resulted in an increased particle transport rate. Thus, according to an approximate conversion of fluorescence intensity to number of particles calculated from a calibration curve, after 24 h incubation 1.2×10^{10} nanoparticles reached the basolateral compartment across Caco-2 monolayers cultivated on a metal grid. Since 3×10^{10} nanoparticles each filter were applied corresponding to the theoretically maximal observed number of particles in the basolateral compartment (free equilibration between apical and basolateral), as consequence the percentage of experimentally observed transported nanoparticles to theoretically total particles is 40% approximately.

Conclusion

The pore size and pore density of the growth support used for the *in vitro* cultivation of biological barriers influence the outcome of particle permation studies. We demonstrated that nanoparticle transport from apical to basolateral does not only depend on the cell monolayer, but also on the free filtration area and pore size of the filter membrane. No transport of fluorescent polystyrene nanoparticles with a diameter of 200 nm was observed across Caco-2 cell monolayers cultivated on filter membranes with pore sizes up to 8 µm within 24h. Stainless steel grids with a mesh width of 25 µm were studied as a highly porous potential alternative for cell cultivation. When metal grids were used as growth supports, clearly higher nanoparticle transport rates were observed. Furthermore, it has to be highlighted that fluorimetry is - by itself - not a reliable means for particle quantification in the basolateral compartment. A combination of fluorimetry with ultracentrifugation, however, is capable of discriminating between particle-associated and free fluorophore. In conclusion, metal grids or similar materials could serve as alternative growth supports which circumvent the drawbacks of currently used filter membranes. Moreover, a standardization of the filter materials, experimental procedures as well as analytical techniques used for nanoparticle transport studies would be advantageous to improve the comparability of results between laboratories and to ultimately achieve a better understanding of nanoparticle transport.

References

[1] des Rieux A, Fievez V, Garinot M, Schneider YJ, Préat V: **Nanoparticles as potential oral delivery systems of proteins and vaccines: a mechanistic approach**. *J Control Release* 2006 **116**:1-27.

[2] Florence AT: **Nanoparticle uptake by the oral route: Fulfilling its potential?** *Drug Discov Today* 2005 **2**:75-81.

[3] des Rieux A, Fievez V, Théate I, Mast J, Préat V, Schneider YJ: **An improved in vitro model of human intestinal follicle-associated epithelium to study nanoparticle transport by M cells.** *Eur J Pharm Sci* 2007, **30**:380-391.

[4] Garinot M, Fiévez V, Pourcelle V, Stoffelbach F, des Rieux A, Plapied L, Theate I, Freichels H, Jérôme C, Marchand-Brynaert J, Schneider YJ, Préat V: **PEGylated PLGA-based nanoparticles targeting M cells for oral vaccination**. *J Control Release* 2007, **31**:195-204.

[5] Desai MP, Labhasetwar V, Walter E, Levy RJ, Amidon GL: **The mechanism of uptake of biodegradable microparticles in Caco-2 cells is size dependent.** *Pharm Res* 1997 **14**:1568-1573.

[6] Russell-Jones GJ, Arthur L, Walker H: **Vitamin B12-mediated transport of nanoparticles across Caco-2 cells.** *Int J Pharm* 1999 **15**:247-255.

[7] Cartiera MS, Johnson KM, Rajendran V, Caplan MJ, Saltzman WM: **The uptake and intracellular fate of PLGA nanoparticles in epithelial cells.** *Biomaterials* 2009 **30**:2790-2798.

[8] Behrens I, Pena AI, Alonso MJ, Kissel T: **Comparative uptake studies of bioadhesive and non-bioadhesive nanoparticles in human intestinal cell lines and rats: the effect of mucus on particle adsorption and transport.** *Pharm Res* 2002 **19**:1185-1193.

[9] Gabor F, Stangl M, Wirth M: **Lectin-mediated bioadhesion: binding characteristics of plant lectins on the enterocyte-like cell lines Caco-2, HT-29 and HCT-8**. *J Control Release* 1998 **55**:131-142.

[10] Delie F, Rubas W: **A human colonic cell line sharing similarities with enterocytes as a model to examine oral absorption: advantages and limitations of the Caco-2 model.** *Crit Rev Ther Drug Carrier Syst* 1997 **14**:221-286.

[11] Miret S, Abrahamse L, de Groene EM: **Comparison of in vitro models for the prediction of compound absorption across the human intestinal mucosa.** *J Biomol Screen* 2004 **9**:598-606.

[12] Wirth M, Kneuer C, Lehr CM, Gabor F: **Lectin-mediated drug delivery: discrimination between cytoadhesion and cytoinvasion and evidence for lysosomal accumulation of wheat germ agglutinin in the Caco-2 model**. *J Drug Target* 2002 **10**:439-448.

[13] Gabor F, Schwarzbauer A, Wirth M: **Lectin-mediated drug delivery: binding and uptake of BSA-WGA conjugates using the Caco-2 model.** *Int J Pharm* 2002 Apr **26**:227-239.

[14] des Rieux A, Ragnarsson EG, Gullberg E, Préat V, Schneider YJ, Artursson P: **Transport of nanoparticles across an in vitro model of the human intestinal follicle associated epithelium.** *Eur J Pharm Sci* 2005 **25**:455-465.

[15] Florence AT, Hussain N: T**ranscytosis of nanoparticle and dendrimer delivery systems: evolving vistas.** *Adv Drug Deliv Rev* 2001 **50 Suppl**:S69-89.

[16] Adam G, Läuger P, Stark G: **Physikalische Chemie und Biophysik.** 4th Edition. Springer, Berlin, 2007 p.309.

[17] Samstein RM, Perica K, Balderrama F, Look M, Fahmy TM: **The use of deoxycholic acid to enhance the oral bioavailability of biodegradable nanoparticles.** *Biomaterials* 2008 **29**:703-708.

[18] Lee YJ, Chung SJ, Shim CK: **The prevention of cyclosporin A adsorption to Transwell surfaces by human plasma.** *Int J Pharm* 2001 **14**:201-204.

[19] Pietzonka P, Rothen-Rutishauser B, Langguth P, Wunderli-Allenspach H, Walter E, Merkle HP: **Transfer of lipophilic markers from PLGA and polystyrene nanoparticles to caco-2 monolayers mimics particle uptake.** *Pharm Res.* 2002 **19**:595-601.

[20] Xu P, Gullotti E, Tong L, Highley CB, Errabelli DR, Hasan T, Cheng JX, Kohane DS, Yeo Y: **Intracellular drug delivery by poly(lactic-co-glycolic acid) nanoparticles, revisited.** *Mol Pharm.* 2009 **6**:190-201.

[21] Fillafer C, Friedl DS, Ilyes AK, Wirth M, Gabor F: **Bionanoprobes to study particle-cell interactions.** *J Nanosci Nanotechnol.* 2009 **9**:3239-3245.

	Pore size	Material	Pore density [a] (β)	Free filtration area [a] ($A_{filtration}$) [mm^2]	% Pore area	Transepithelial electrical resistance (TEER) in absence of cell monolayer (Ω cm^2)
Commercially available growth supports	0.4 µm transparent (0.4 TP)	PET	2×10^4	0.003	0.25	124
	0.4 µm translucent (0.4 TL)	PET	1×10^6	0.126	12.57	68
	1.0 µm transparent (1.0 TP)	PET	2×10^4	0.016	1.57	72
	3.0 µm transparent (3.0 TP)	PET	6×10^3	0.042	4.24	68
	3.0 µm translucent (3.0 TL)	PET	2×10^4	0.141	14.14	64
	8.0 µm translucent (8.0 TL)	PET	1.5×10^3	0.075	7.54	60
Metal grid	25 µm mesh width	stainless steel	4×10^2	0.25	25	72

Table 1. Comparison of commercially available growth supports for transport studies with metal grid.
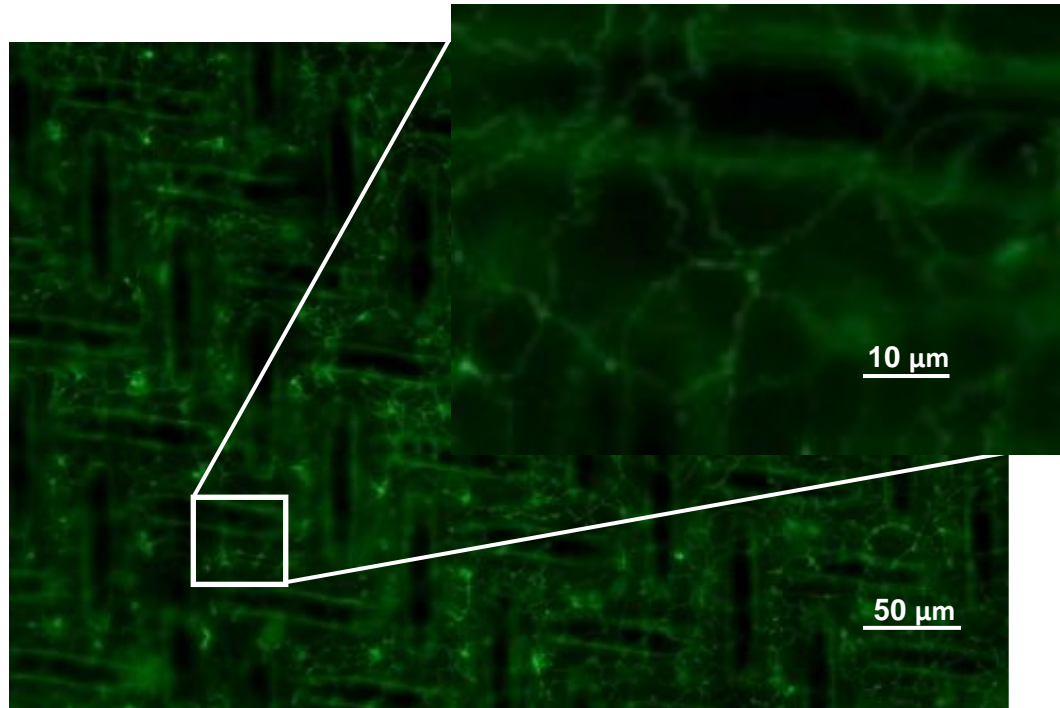
[a] per 1 mm^2 of filter material.

173
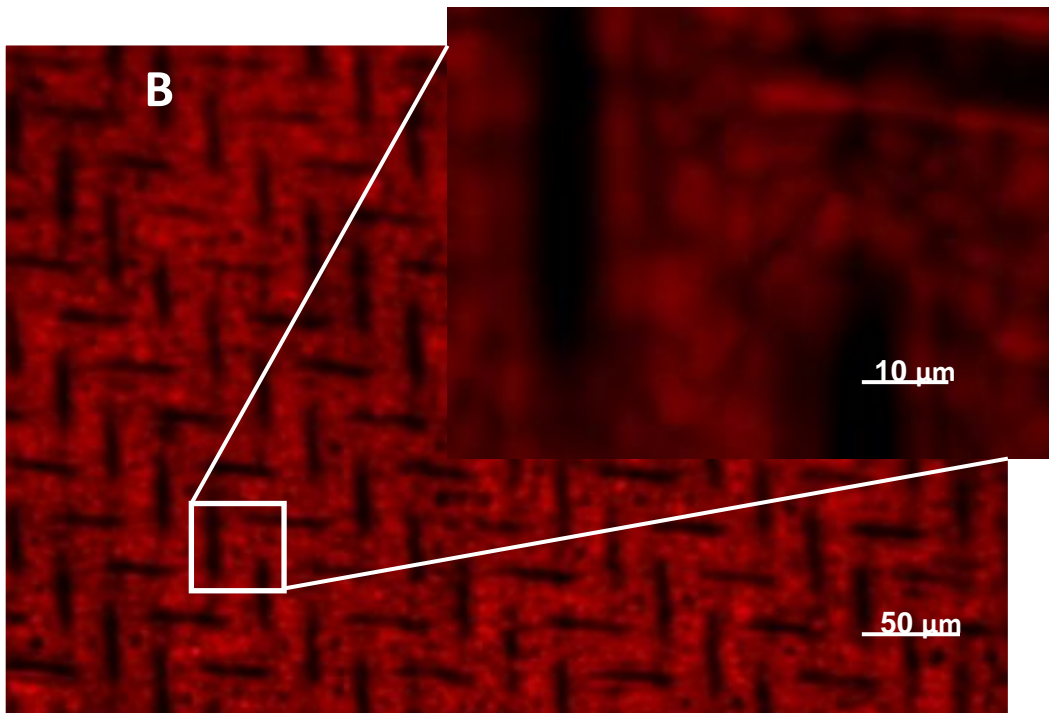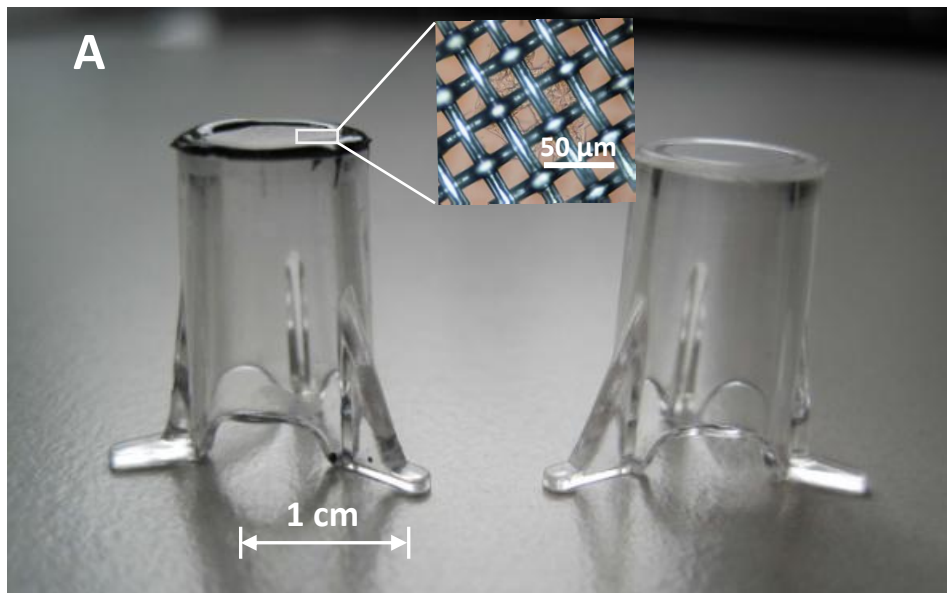
Figure 1. A: Insert with stainless steel tissue grid with a mesh width 25 μm (left) and insert with pore filter (right). B: Caco-2 cell layer cultivated on a metal grid with 25 μm mesh width. Cell nuclei stained with propidium iodide (red, B), and tight junction associated protein ZO-1 (green, C). The steel wires appear as dark structures in the background.
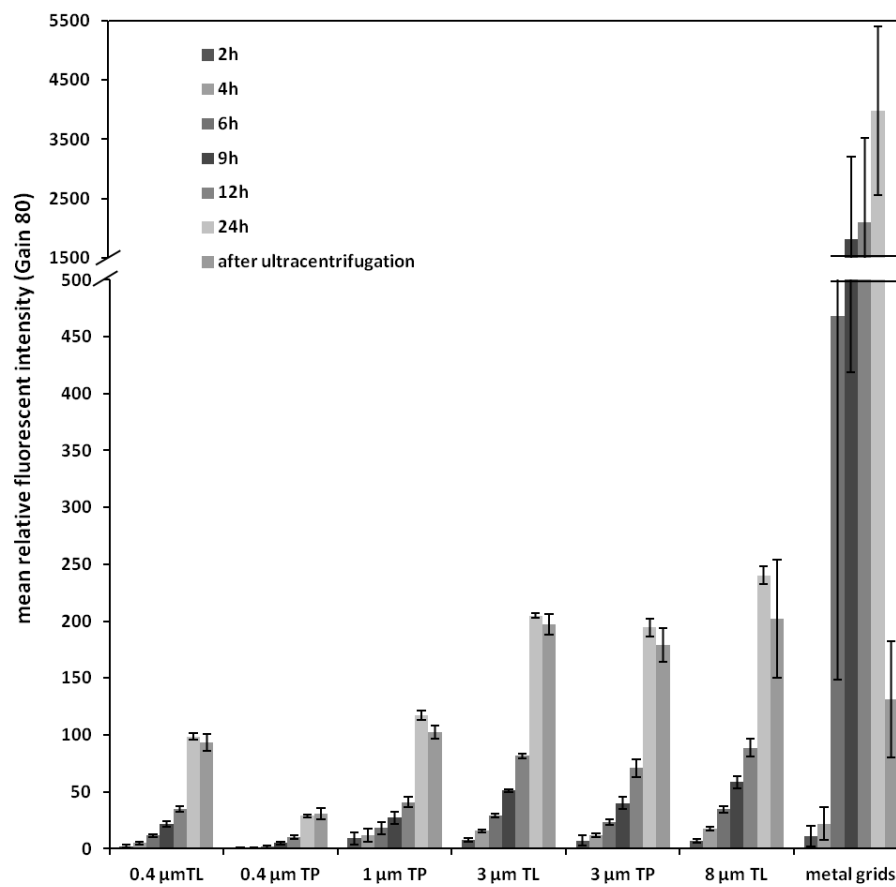
Figure 2. Mean relative fluorescent intensities detected in the basolateral compartment in course of 24h-permeation studies across Caco-2 monolayers cultivated on different commercially available filter membranes and metal grids. (n≥3, mean±SD)
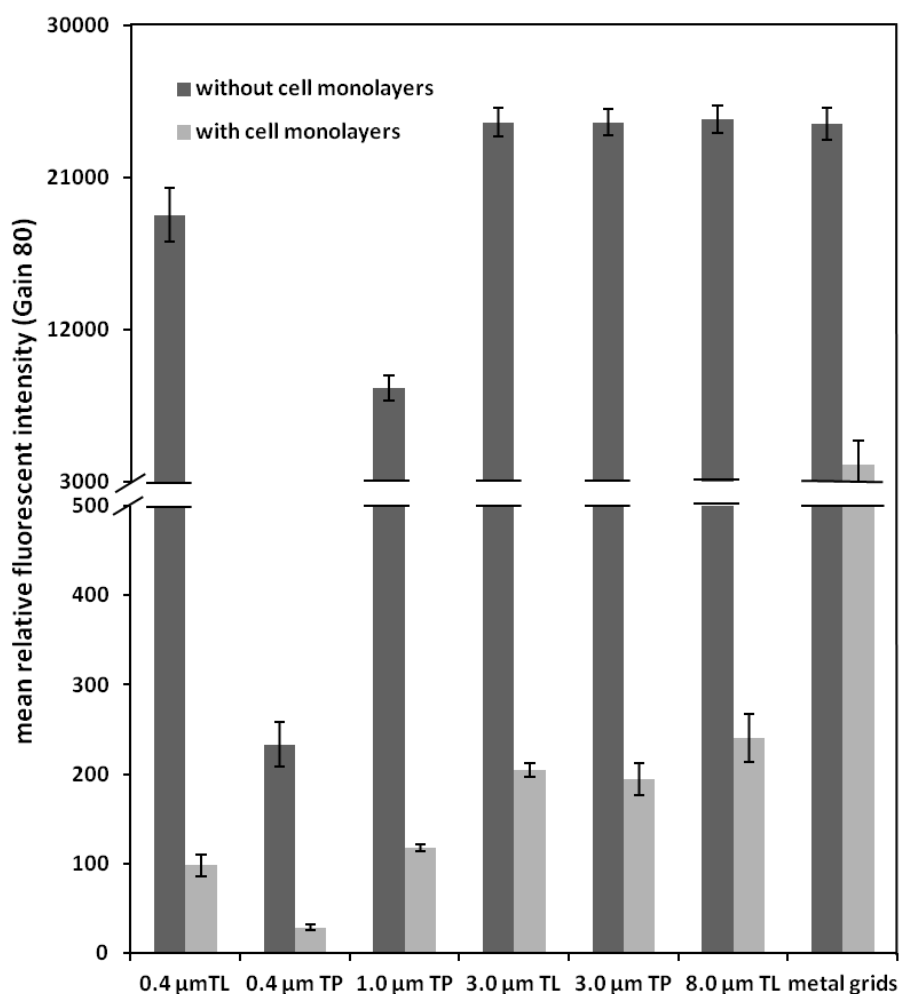
Figure 3. Comparison of mean relative fluorescent intensities detected in the basolateral compartment in course of permeation studies with and without Caco-2 monolayers cultivated on different commercially available filter membranes and metal grids after 24 h incubation. (n=3, mean±SD)
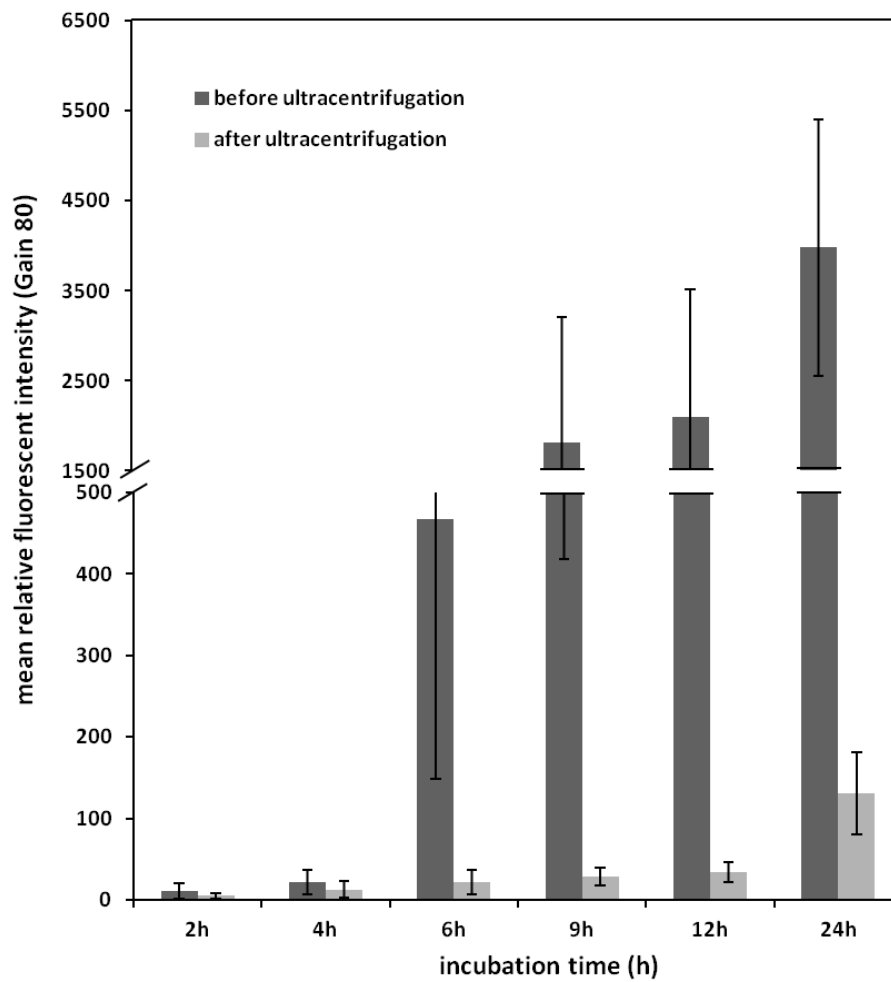
Figure 4. Comparison of mean relative fluorescent intensities in basolateral compartment before and after ultracentrifugation for metal grids. (n=8, mean±SD)

Supplementary Appendix

Table S. Nanoparticle stability in transport media

Incubation Time	Mean Particle Size (nm)/Polydispersity Index (PdI)		
	Distilled Water	RPMI+1% Pluronic® F-68	HBSS
0h	207.0 / 0.048	292.0 / 0.038	299.0 / 0.108
2h	205.0 / 0.015	288.0 / 0.002	876.0 / 0.166
4h	204.0 / 0.010	288.0 / 0.022	3479.0 / 0.453
6h	202.0 / 0.009	286.0 / 0.013	3726.0 / 0.555
9h	204.0 / 0.013	290.0 / 0.008	4471.0 / 0.357
24h	204.0 / 0.044	291.0 / 0.016	3713.0 / 0.372

To determine a suitable suspension medium for the transport studies, the stability of nanoparticles in different media was examined. While distilled water served as control, RPMI-1640 cell culture medium + 1% Pluronic® F-68 and Hank's balanced salt solution (HBSS) were used as cell culture compatible dispersants. Nanoparticle suspensions in the respective media (3×10^{11} particles mL^{-1}) were incubated end-over-end for 24h. The mean particle size and polydispersity index (PdI) of each sample were determined with a Zetasizer Nano ZS (Malvern Instruments Ltd., Worcestershire, UK) at the starting point and after 2, 4, 6, 9, and 24 h of incubation at 37°C.

According to the specifications of the manufacturer, as illustrated in Table S the mean particle size is about 207 nm in distilled water. For the incubation after 24 h at 37°C, the size of the particles remained almost unaltered with a PdI lower than 0.05, which indicated a narrow particle size distribution. When using the RPMI 1640 + 1% Pluronic® F-68 as medium, the mean size of nanoparticles was increased slightly by about 85 nm compared to the size in distilled water. However, the mean particle size did not change further in course of incubation for 24 h in the RPMI 1640 + 1% Pluronic® F-68 medium. Considering the consistently low PdIs over 24 h, it seems likely that particle aggregation in medium is not the reason for the rather spontaneous occurrence of the increase in particle size. The shift in particle size is probably due to the higher viscosity of the suspension medium which could affect the measurement result of nanoparticle size analyzed by dynamic light scattering [Fillafer C et al. Langmuir 2007 14:8699-8702.]. In contrast, nanoparticles incubated in HBSS aggregated significantly. As indicated in Table 2, the mean particle size increased immediately about 3-fold after 2 h incubation with an increase of PdI from 0.1 to 0.2. In course of

further incubation, particle agglomerations were clearly visible and confirmed by dynamic light scattering in corresponding to the increased particle size up to 4471nm. Therefore, RPMI 1640 + 1% Pluronic® F-68 was chosen as suitable medium for further experiments.

Conclusion

Colloids in the nano- and micrometer range are intensively investigated as drug delivery systems in the hope of developing efficient carriers for active pharmaceutical ingredients (APIs), especially poorly soluble or poorly absorbable substances, as well as achieving site-specific drug delivery. Nevertheless, fabrication, functionalization, and interaction of colloidal systems with cells and tissues remain challenging and require further investigations. Therefore, this thesis is aimed to contribute on some aspects of these topics for a deeper understanding of the characteristics of nano- and microparticles to finally optimize their applications as (bio-)pharmaceutical delivery systems.

Poly (D,L-lactide-*co*-glycolide) (PLGA) is a well-established polyester with excellent biocompatible and biodegradable characteristics and represents one of the most successfully applied polymers for particulate drug delivery systems. For the studies "*Lectin-coated PLGA microparticles: Thermoresponsive release and in vitro evidence for enhanced cell interation*" and "*Lectin-grafted PLGA microcarriers loaded with fluorescent model drugs: characteristics, release profiles and cytoadhesion studies*", PLGA-microparticles loaded with three different fluorescent model drugs were prepared by a modified solvent evaporation technique. Fluorescein sodium, sulforhodamine and boron-dipyrromethene (BODIPY®, BOD) are suggested to mimic hydrophilic, amphotheric, and lipophilic APIs respectively. The double-emulsion technique was chosen for encapsulation of the first two model drugs, while the single-emulsion technique was used in case of lipophilic BOD. Due to similar hydrophobicity of BOD and PLGA, BOD-entrapped microparticles yielded the smallest size with diameter of 4.1 μm and the highest encapsulation efficiency about 2.25 μg per mg PLGA. However, almost no release of encapsulated BOD was observed neither at 4°C or 37°C presumably due to strong hydrophobic interactions. In case of sulforhodamine-loaded PLGA microcarriers, the amphotheric character resulted in biggest particles and lowest drug loading, as well as no release of entrapped fluorescent dyes. The hydrophilic fluorescein-sodium entrapped PLGA-microparticles were 4.1 μm in diameter with 47% encapsulation efficiency. Interestingly, this type of microparticles exhibited thermo-responsive release kinetics, since no release was observed at 4°C or room temperature. At body temperature, however, >80% of the payload was released within 48 h. Utilizing lectin-mediated drug delivery mechanisms, the amount of model drug bound and taken up into Caco-2 cells was 5.8-fold higher than that of fluorescein in solution after incubation for 4 h at 37°C. Furthermore, fluorescence imaging also confirmed pronounced intracellular accumulation of the fluorescein payload after incubation

for 5h at 37°C. In conclusion, hydrophilicity of the particulate matrix and the encapsulated APIs determines the preparation technique as well as the characteristics of microparticles such as size, loading, and release profile. Successful encapsulation of fluorescein-sodium is a hint towards the utility of bioadhesive drug carriers for the improved delivery and absorption as well as improved storage stability of low molecular weight hydrophilic APIs. Moreover, BOD-entrapped PLGA microparticles possessing high quantum yield without any leakage represent a useful tool for the elucidation of the particle-cell interaction not only qualitatively by microscopy but also quantitatively by fluorimetry.

The development of site-specific drug carriers is one of the most important trends in pharmaceutical technology towards patient-friendly therapy. Structural modifications of the particle surface (*e.g.* grafting with biorecognitive ligands) are supposed to improve efficacy and minimize side effects due to required reduced dosage. However, the presence of stabilizers inevitably necessary for the preparation of PLGA-particles by the solvent evaporation technique counteracts the covalent surface functionalization. Thus, the influence of different surfactants on ligand density was evaluated in the study *"Influence of stabilizers and preparation procedures on ligand density of PLGA-microparticles"*. Adapting the energy input, PLGA-microparticles within a comparable size range of about 3.5 µm in terms of the surface area mean were yielded using the commonly used stabilizers polyvinylalcohol (PVA), Pluronic® F-68 (PL), and the newly introduced polymer poly(ethylene-*alt*-maleic acid) (PEMA). Although the stabilizers enabled preparation of microparticles and prevented subsequent aggregation, the adsorption of the stabilizers on the surface of the microparticles shielded the functional groups of PLGA required for modification. The calculated number of covalently immobilized wheat germ agglutinin (WGA) molecules per microparticle was significantly lower in case of PVA and PL than that of spray dried particles prepared without any stabilizer. However, the carboxylate-rich polymer PEMA exhibited enhanced modification efficiency, yielding an up to almost 3-fold higher ligand density on the surface. Although spray drying without a stabilizer was the method of first choice offering the advantage of non-restricted access for grafting, the size distribution was broad requiring size fractionation associated with high particle loss. Consequently, using PEMA as stabilizer to prepare PLGA-microparticles was found to be a better choice, since it offered sufficient stabilization during preparation as indicated by a narrow size distribution of PLGA-microparticles. Moreover, additional reactive groups are introduced by use of PEMA for immobilization of biorecognitive ligands for active targeting.

Upon the numerous applications of functionalized PLGA drug carriers, lectin-mediated biorecognition is one of the most exciting concepts for site-specific delivery. The review article "*Use of lectin-functionalized particles for oral immunotherapy*", not only summarizes the characteristics and advantages of PLGA-particles for oral immunotherapy, but also the utility of lectins as bioactive ligands for functionalization of the particle surface to improve intestinal uptake is included. Oral immunotherapy is a promising approach for the treatment of different immunologically mediated diseases, offering higher patient compliance as well as enhanced systemic and mucosal immune responses. The encapsulation of drugs and antigens within polymer particles prevents premature loss and inactivation in the gastrointestine. Furthermore, surface immobilization of lectins mediates enhanced binding to epithelial cells and mucosa-associated lymphoid tissue as well as improved cellular uptake and transport of antigen-loaded carriers. Especially, surface grafting with wheat germ agglutinin fostered the interaction with M-cells and enterocytes resulting in higher IgG-levels. In contrast, modification with *Ulex europaeus* isoagglutinin I, *Lotus tetragonolobus* agglutinin and *Aleuria aurantia* lectin induced a high Th1-dominant response.

Upon development of lectin-grafted drug delivery carriers for parenteral administration, the most fundamental prerequisite is to identify appropriate molecular targets at the surface of endothelial cells. The research article "*Lectin-mediated biorecognition: Glycosylation pattern of human endothelial cells and blood cell-agglutinating effects of wheat germ agglutinin*" summarizes the results of a study where six fluorescein-labeled plant lectins with different carbohydrate specificity were used to elucidate the glycosylation pattern of endothelial cells before and after inflammation. Both, micro- and macrovascular endothelia, predominantly exhibit sialic acid, N-acetylglucosamine, and fucosyl residues in the glycocalyx of endothelial cells corresponding to high binding of wheat germ agglutinin (WGA) and *Ulex europaeus* isoagglutinin I (UEA-I). Moreover, sugar inhibition studies revealed high specificity of the binding amounting to more than 90% for the interaction between these two lectins and endothelial cells. However, upon inflammation by stimulation with TNF-α, only the WGA-binding to primary human umbilical vein endothelial cells representing macrovascular tissue was increased which indicates an increase of sialic acid structures in the glycocalyx upon inflammation. Due to the outstanding binding rate and binding affinity of WGA to endothelial cells especially after inflammation, the dose of WGA necessary for the blood cell agglutination was elucidated in detail. Interestingly, according to flow cytometric and microscopic evaluation, the limiting concentration of

WGA for the agglutination of blood cells was about 15.88 µg mL^{-1}, since up to this concentration no cell aggregates were observed being independent from the blood group. According to a rough calculation, this limiting concentration corresponded to a ratio more than 4 between blood cells and 3 µm PLGA-microparticles considering maximum WGA-density at the particle surface. As *in vivo* administration of such extreme high amounts of microcarriers makes no sense, the concept of using WGA for parenteral drug delivery might be feasible and open new perspectives for glycotargeting.

Upon administration in humans, either peroral or parenteral, the flow of materials under physiological conditions and the associated hydrodynamic forces will affect the interaction of particles with cells and tissues. Thus, in the second part of the present experimental studies comprising the research articles *"A multichannel acoustically driven microfluidic chip to study particle-cell interactions"* and *"A novel cell-based microfluidic multichannel setup – impact of hydrodynamics and surface characteristics on the bioadhesion of polystyrene microspheres"*, a multi-channel acoustically driven microfluidic platform based on surface acoustic wave was further developed towards parallelization and employed to study the impact of hydrodynamics on the particle-cell interaction *in vitro*. The results revealed that four miniature flow channels could be operated in parallel at distinct flow velocities with only slight inter-experimental variations and average shear rates up to 5 s^{-1} were easily generated at the current channel geometry. Moreover, Caco-2 cells representing intestinal epithelial cells and three different types of endothelial cells of micro- and macrovascular origin could be successfully cultivated inside the polymer microchannels to form a confluent monolayer with or without fibronectin-precoated growth support. Furthermore, as proof-of-concept, cytoadhesion studies with 1 µm fluorescent labeled polystyrene microspheres with different surface properties such as lectin-grafted biorecognitive surface, cationic polyethylenenimine (PEI)-coated positively charged surface, and native carboxylated negatively charged surface were performed. Interestingly, at average shear rates between 0.5 s^{-1} and 2.25 s^{-1} no significant effects of hydrodynamic forces on the particle-cell interactions were observed independent from the type of surface modification, the mode of particle loading, as well as the type of cells. In conclusion, this multichannel microfluidic platform represents a promising set-up with high reproducibility and versatile utility to elucidate the effect of flow on the particle-cell interaction. Results of this *in vitro* test model sheds some light on the impact of flow and thus improved understanding of the basic mechanisms of drug carrier – cell interaction and cell physiology is expected.

Currently, commercially available filter membranes are commonly used as growth supports for the cultivation of cell layers for *in vitro* transport studies of particles across cell monolayers. It is assumed that the properties of the filter membrane itself do not significantly affect the outcome of transport studies. However, the results summarized in the study "*Permeation of nanoparticles across cell monolayers in vitro – Impact of growth support*" suggested that the filter membrane indeed influences the permeation of particles through artificial biological barriers. At this, almost no fluorescein-labeled polystyrene nanoparticles with 200 nm in diameter were transferred across Caco-2 cell monolayers cultivated on filter membranes with pore sizes up to 8 µm within 24h. This poor result was assumed to be due to the low free filtration area and the small pore size of these commercially available growth supports. In order to improve both parameters, stainless steel grids with a mesh width of 25 µm were employed as a highly porous substrate for cell cultivation. Surprisingly, the cultivation of Caco-2 cell monolayers on this metal grid was successful and tightness of the monolayer has been confirmed by immunofluorescence imaging as well as determination of transepithelial electrical resistances. As expected, the higher free filtration area and the larger pore size enabled much higher permeation of the nanoparticles across the monolayers amounting up to 40% penetration of the particles. Furthermore, it became evident that discrimination between particle-associated fluorescence and free fluorophore deriving from label leakage of the nanoparticles by ultracentrifugation of the liquid in the acceptor compartment is inevitably necessary to prevent false positive results. Thus, only by combination of ultracentrifugation and fluorimetry the nanoparticle fraction in the basolateral compartment can be determined. In conclusion, highly porous growth supports like the presented metal grid, are suitable alternatives to conventional filter membranes for transport studies to assess rather the influence of the tissue than the sieving properties of the growth support.

All in all, the results of this thesis indicate that the preparation technique and grafting method for highly efficient particulate drug carriers should be chosen according to the characteristics of the API and the matrix. Moreover, the high versatility of PLGA particles, especially with lectin-grafting, offers great potential for a wide range of administrations as site-specific drug delivery systems. Considering hydrodynamic forces as an important *in vivo* parameter also for in *in vitro* test systems will increase our understanding of the basic interaction mechanisms between particles and tissues. This contribution of some further pieces to the puzzle of site-specific drug delivery, confirms the versatility and potential utility of biorecognitive carriers as therapeutics and/or diagnostics in the foreseeable future.

Part III

APPENDIX

CURRICULUM VITAE

PERSONAL INFORMATION

Name: Xue-Yan WANG

Nationality: Chinese

Date and Place of Birth: December 9, 1984, Beijing, CHINA

EDUCATION

10/2009 - present	PhD Studies with focus on Biomaterials, Smart Drug Delivery and Microfluidic System, Supervisor: Ao. Univ.-Prof. Mag. Dr. Franz Gabor /Department of Pharmaceutical Technology and Biopharmaceuticals, University of Vienna, Vienna, Austria
02/2004 - 09/2009	Diploma Studies of Pharmacy (Title: Magistra der Pharmazie) University of Vienna, Austria
09/2003 - 02/2004	Studies of Pharmacy, School of Pharmacy, Peking University, Beijing, China
09/1997 - 07/2003	Hui-Wen High School, Beijing, China

PRACTICAL EXPERIENCE

01/2010 - present	University assistant-in-training (teaching), Department of Pharmaceutical Technology and Biopharmaceutics, University of Vienna, Vienna, Austria
10/2010 - present	Associate lecturer in the practical course on industrial pharmacy, University of Vienna, Austria
08/2007	Practice student in the food bio-safety laboratory of the institute of food safety of chinese academy of inspection and quarantine (CAIQ), Beijing, China
07/2007	Internship student in the department of scientific and regulatory affairs of Shenzhen Sanofi Pasteur Biological Products Co., Ltd. Beijing Branch, Beijing, China

HONOURS AND AWARDS

09/2010	Diploma thesis award, awarded by University of Vienna, Austria
05/2002	The second grade award National Chemistry Competition of Senior High Schools, awarded by China Chemistry Society

PEER-REVIEWED PUBLICATIONS

X.-Y. Wang, R. Koller, M. Wirth, F. Gabor. Lectin-grafted PLGA microcarriers loaded with fluorescent model drugs: characteristics, release profiles, and cytoadhesion studies. *Scientia Pharmaceutica (2014). In press.*
doi: 10.3797/scipharm.1312-08.

X.-Y. Wang, C. Fillafer, C. Pichl, S. Deinhammer, R. Hofer-Warbinek, M. Wirth, F. Gabor. A multichannel acoustically driven microfluidic chip to study particle-cell interactions. *Biomicrofluidics, 7 (2013) 044127.*

X.-Y. Wang, C. Pichl, F. Gabor, M. Wirth. A novel cell-based microfluidic multichannel setup – impact of hydrodynamics and surface characteristics on the bioadhesion of polystyrene microspheres. *Colloids and Surfaces B: Biointerfaces 102 (2013) 849-856.*

X.-Y. Wang, R. Koller, M. Wirth, F. Gabor. Lectin-coated PLGA microparticles: thermoresponsive release and in-vitro evidence for enhanced cell interaction. *International Journal of Pharmaceutics 436 (2012) 738-743.*

S. C. Diesner, **X.-Y. Wang**, E. Jensen-Jarolim, E.Untersmayr, F. Gabor. Use of lectin-functionalised particles for oral immunotherapy. *Therapeutic Delivery 3(2) (2012) 277-290.*

G. Raztinger, **X. Wang**, M. Wirth, F. Gabor. Targeted PLGA microparticles as a novel concept for treatment of lactose intolerance. *Journal of Controlled Release 147 (2010) 187–19.*

MANUSCRIPTS (to be submitted)

X.-Y. Wang, S. Kubin, M. Wirth, F. Gabor. Influence of stabilizers and preparation procedures on ligand density of PLGA-microparticles. To be submitted to Science of Advanced Materials.

X.-Y. Wang, C. Fillafer, D. Pixner, M. Wirth, F. Gabor. Permeation of nanopartiels across cell monolayers in vitro – Impact of growth support. To be submitted to Journal of Nanobiotechnolgy.

X.-Y. Wang, M. Führinger, N. Mizerovsky, R. Hofer-Warbinek, M. Wirth, F. Gabor. Lectin-mediated biorecognition: Glycosylation pattern of human endothelial cells and blood cell-agglutinating effects of wheat germ agglutinin. To be submitted to Glycobiology.

TALKS AT CONFERENCES

X.-Y. Wang, C. Fillafer, C. Pichl, R. Hofer-Warbinek, M. Wirth, F. Gabor. A multichannel acoustically-driven platform for parallelized application. *5th International Congress on Pharmaceutical Engineering, Graz, Austria, September 2011*

X.-Y. Wang, G. Ratzinger, M. Wirth, F. Gabor. Targeted PLGA-Microparticles as a Novel Concept for Treatment of Lactose Intolerance. *8th Central European Symposium on Pharmaceutical Technology, Graz, Austria, September 2010*

POSTER PRESENTATIONS

X.-Y. Wang, M. Führinger, N. Mizerovsky, R. Hofer-Warbinek, M. Wirth, F. Gabor. Lectin-mediated biorecognition: Binding characteristics of wheat germ agglutinin and other plant lectins to endothelial cells and erythrocytes. *9th World Meeting on Pharmaceutics, Biopharmaceutics and Pharmaceutical Technology, Lisbon, Portugal, April, 2014.*

X.-Y. Wang, C. Fillafer, C. Pichl, R. Hofer-Warbinek, M. Wirth, F. Gabor. Ein Akustisch-Driven Mikrofluidische Plattform für Parallelisierte Untersuchung der Partikel-Zell-Interaktionen. *47. Wissenschaftliche Fortbildungswoche für Apothekerinnen, Schladming, Austria, February, 2014.*

C. Schultz, S.C. Diesner, **X.-Y. Wang**, F. Roth-Walter, T. Eiwegger, Z. Szepfalusi, I. Pali-Schöll, E. Jensen-Jarolim, F. Gabor, E. Untersmayr. Safety evaluation of Neuraminidase as a targeting substance of allergen-loaded microparticles for oral food allergy treatment. *15th International Congress of Immunolog, Milan Italy, August 2013.*

S.C. Diesner, C. Schultz, **X.-Y. Wang**, V. Assmann, G. Ratzinger, F. Roth-Walter, P. Starkl, T. Eiwegger, A. Pollak, Z. Szepfalusi, I. Pali-Schöll, E. Jensen-Jarolim, F. Gabor, E. Untersmayr. Neuraminidase is a safe functionalization substance of allergen-loaded microparticles for oral immunotherapy of food allergy. *The European Academy of Allergy and Clinical Immunology Congress & World Allergy Organization, Milan, Italy, June 2013.*

S.C. Diesner, C. Schultz, **X.-Y. Wang**, V. Assmann, K. Kreiner, G. Ratzinger, F. Roth-Walter, P. Starkl, T. Eiwegger, A. Pollak, Z. Szepfalusi, I. Pali-Schöll, E. Jensen-Jarolim, F. Gabor, E. Untersmayr. M-cell specific targeting by Neuraminidase functionalized microparticles as a novel oral immunotherapy for food allergy. *European Congress of Immunology / Annual meeting of the Austrian Association of Allergy and Immunology, Glasgow, Scotland, September 2012.*

X.-Y. Wang, C. Fillafer, C. Pichl, R. Hofer-Warbinek, M. Wirth, F. Gabor. A novel cell-based microfluidic multichannel setup – impact of hydrodynamics and surface characteristics on the bioadhesion of polystyrene microspheres. *8th World Meeting on Pharmaceutics, Biopharmaceutics and Pharmaceutical Technolog, Istanbul, Turkey, March 2012.*

X.-Y. Wang, R. Koller, M. Wirth, F. Gabor. WGA-grafted PLGA microparticles: thermoresponsive release and enhanced cellular uptake. *8th World Meeting on Pharmaceutics, Biopharmaceutics and Pharmaceutical Technology, Istanbul, Turkey, March 2012.*

X.-Y. Wang, C. Fillafer, C. Pichl, R. Hofer-Warbinek, M. Wirth, F. Gabor. A multichannel acoustically-driven microfluidic platform: parallelized investigations of particle-cell interactions under hydrodynamic conditions. *3rd International Congress Nanotechnology in Medicine & Biology, Krems,*

Austria, March 2012.

S.C. Diesner, C. Schultz, **X. Wang**, G. Ratzinger, P. Starkl, V. Assmann, K. Kreiner, F. Roth-Walter, I. Pali, E. Jensen-Jarolim, F. Gabor, E. Untersmayr. M-cell targeting by neuraminidase functionalized microparticles for future application in oral immunotherapy. *World Allergy Congress, Cancun, Mexico, December, 2011.*

S.C. Diesner, C. Schultz, **X. Wang**, G. Ratzinger, P. Starkl, V. Assmann, K. Kreiner, F. Roth-Walter, I. Pali, E. Jensen-Jarolim, F. Gabor, E. Untersmayr. Allergen-loaded, Neuraminidase functionalized microparticles as a novel oral immunotherapy with M-cell targeting properties. *Österreiche Gesellschaft für Allergologie und Immunologie, Graz, Austria, September 2011.*